Università degli Studi di Padova

Department of Neuroscience

Padova Neuroscience Center

Ph.D. COURSE IN NEUROSCIENCE

SERIES: XXXV

COVID-19 Neuropathology: disentangling the role of SARS-CoV-2 infection in neurological manifestations and neurodegenerative diseases

Coordinator: Prof. Antonino Vallesi

Supervisor: Prof. Angelo Antonini

Co-Supervisor: Prof. Raffaele De Caro

Ph.D. Candidate: Aron Emmi

INDEX

ABSTRACT

INTRODUCTION

Part(s) of the present introduction have been previously published in:

- ***Emmi A.**, Rizzo S., Barzon S., et al. SARS-CoV-2 neuropathology: Evidence from a post-mortem autopsy series in Padova, Italy. Clinical Neuropathology, 2021.*
- ***Emmi A.**, Rizzo S., Macchi V., Sinigaglia A., Riccetti S., De Gaspari M., Carturan E., Calabrese F., Dei Tos A.P., Barzon L., Basso C., De Caro R., Porzionato A. COVID-19 Neuropathology: evidence for SARS-CoV-2 invasion of anatomically defined regions in the human CNS. Journal of Anatomy, 2021.*
- ***Emmi A.**, Sandre M., Porzionato A., Antonini A., Smell deficits in COVID-19 and possible links with Parkinson's disease. International Review of Neurobiology, 2022. doi:10.1016/bs.irn.2022.08.001*
- ***Emmi A.**, Bura I., Rader V., Matthew D., Sulzer D., Goldman J., Leta V. Covid-19, nervous system pathology, and Parkinson's disease: Bench to bedside. International Review of Neurobiology, 2022. doi:10.1016/bs.irn.2022.06.006*
- ***Emmi A.**, Rizzo S., Barzon S., et al. COVID-19 neuropathology: evidence for SARS-CoV-2 invasion of human brainstem nuclei. Nature NPJ Parkinson's Disease (under review). doi: https://doi.org/10.1101/2022.06.29.498117*
- *Porzionato A., **Emmi A.**, Barbon S., et al. (2020) Sympathetic Activation: a potential link between comorbidities and COVID-19. FEBS Journal. doi: 10.1111/febs.15481*
- *Porzionato A., **Emmi A**., Stocco E., Barbon S., et al. (2020) The role of the carotid body in COVID-19. Am J Phys. doi:10.1152/ajplung.00309.2020*
- *Porzionato A., **Emmi A.**, Contran M., Stocco E., Riccetti S., Sinigaglia A., Macchi V., Barzon L., De Caro R. The Carotid Body in COVID-19: histopathological and virological analyses of an autopsy case series. Frontiers in Immunology. doi: https://doi.org/10.3389/fimmu.2021.736529. This article is licensed under a CC BY license.*
- *Porzionato A., Stocco E., **Emmi A.**, Contran M., Macchi V., Riccetti S., Sinigaglia A., Barzon L., De Caro R. Hypopharyngeal ulcers in COVID-19: histopathological and virological analyses of an autopsy case. Frontiers in Immunology, 2021. This article is licensed under a CC BY license.*
- *Vicco A., Caccuri F., Messali S., Vitiello A., **Emmi A.**, et al. Genomic surveillance of SARS-CoV-2 in patients presenting neurological manifestations. PLOS One, 2022. doi: https://doi.org/10.1371/journal.pone.0270024. This article is licensed under a CC BY license.*

Severe Acute Respiratory Syndrome Coronavirus 2 (SARS-CoV-2) is a novel strain of the Coronavirus Family (CoV) responsible for the disease known as Coronavirus Disease 2019 (COVID19). Although manifesting primarily as a respiratory disease, neurological manifestations are common in COVID-19, either presenting as new symptoms or disorders (e.g., stroke, encephalitis, Guillain-Barré syndrome) or as the exacerbation of pre-existing symptoms of known chronic neurological conditions (Kubota & Kuroda, 2021; Ousseiran, Fares, & Chamoun, 2021). These observations, along with the detection of the virus in post-mortem tissue and cerebrospinal fluid (CSF) (Lewis et al., 2021; Mukerji & Solomon, 2021;

Tandon et al., 2021) raise the question of whether SARS-CoV-2 possesses neurotropic properties, or neurological manifestations are to be ascribed to the effects of systemic infection, ongoing cytokine storm, inflammation and hypoxia.

Viral infections of the Central Nervous System

According to the International Committee on Taxonomy of Viruses, viruses are classified into families, subfamilies, genera, and species. The family a certain virus belongs to is determined by the specific presence of an enveloping sheet, as well as the nucleic acid type (King, 2012). Recent classifications of viruses identify a wide range of viral families, however, only few can affect the human organism and seldom target the Nervous System (Peterson, 2014).

In literature, a virus that is capable of infecting the nervous system and determine neurological manifestations is referred to as Neurotropic Virus. However, for a virus to be considered neurotropic, it must be capable of invading the nervous system, an ability known as neuroinvasiveness, and consequently also lead to the development of clinical symptomatology, also known as neurovirulence (Tavčar et al., 2021).

Viruses of neurotropic nature have limited alternatives for reaching and invading the Central Nervous System (CNS). One possible pathway for accomplishing invasion of the neural tissue is through the Blood-Brain-Barrier (BBB). Once the virus undergoes an initial viral replication at the site of entry, dissemination begins. Passive leakage, or active transfer, of locally replicated virons into the blood stream is employed, a stage known as viraemia. This hematogenous spread of the virions can also be reinforced with the movement of infected leukocytes, or in some cases of systematic dissemination, as viruses can utilize a “Trojan horse” strategy by trafficking of infected monocytes.

Aside from the aforementioned pathways, viruses can also reach the central nervous system by targeting the peripheral nerve processes and deploy axonal anterograde and retrograde transport. This intracellular transport is accurate and efficient in target dissemination, continuing to spread across neurites and synapses (trans-synaptic dissemination). Once the virus replicates in a CNS site, it can further disseminate by infiltrating into the cerebrospinal fluid (CSF). This paracellular penetration of viruses involves alterations in expression or phosphorylation of tight junction proteins, as well as disruption of the basal lamina and the actin cytoskeleton (Meyding-Lamadé et al., 2019). Subsequently, after the virus enters the host cells, the viral genes are transported to the suitable intracellular structures for

transcription and replication. Viral infection of the central nervous system can lead to diverse types of inflammation, depending on the specific virus as well as the age and immune status of the target organism. On that account the inflammation can be restricted to the meninges, the gray matter, the white matter, or to both gray and white matter. Most commonly viral infections tend to cause meningeal inflammation or meningitis, with characteristic features of lymphocytic meningeal infiltrates and perivascular inflammation in the superficial cortex.
The inflammation can also be restricted to the grey matter, causing polioencephalitis or poliomyelitis, presenting with predominantly mononuclear inflammation, perivascular cuffing of blood vessels, and can be accompanied by meningitis. Neuronophagia can also be observed, marked by accumulating microglia (known as microglial nodules) and macrophages surrounding necrotic neurons. Residual clusters of microglia around the necrotic neurons are present for days and form microglial nodules.
Leukoencephalitis, for example, occurs when the inflammation is targeting the white matter of the CNS. Foci of demyelination, enlarged oligodendroglial nuclei with scant lymphocytic infiltration, multinuclear giant cells, and vacuolar myelopathy are typical pathological features in leukoencephalitis.
When the inflammation is spread in both the grey and white matter, panencephalitis or panmyelitis occurs. This pattern of disease is usually associated with mononuclear infiltration and sheets of foamy macrophages, microglial nodules in both gray and white matter, along with variable degrees of perivascular lymphocytic cuffing.

Structure and pathogenicity of SARS-CoV-2

As previously stated, SARS-CoV-2 is a member of the Coronaviridae family, a group of viruses that can infect both mammals and birds. SARS-CoV-2 has a probable zoonotic origin with bats as primary hosts (Coronaviridae Study Group of the International Committee on Taxonomy of Viruses, 2020; Zhou et al., 2020). Differently from endemic human Coronaviruses, e.g. OC43 and 229E viruses, SARS-CoV-2 not only infects the upper respiratory tract, but it can also spread to the lower tract, leading to a more severe respiratory disease (Ashour et al., 2020).
SARS-CoV-2 genome is a positive-sense single-stranded RNA that contains 14 open reading frames (ORFs). At the 5’ end of the genome, there are the leader sequence and an untranslated region (UTR). Then, the gene encoding for the viral Replicase-Transcriptase complex, which is an RNA-dependent RNA polymerase, occupies two-thirds of the genome.

This gene is made of two ORFs, ORF1a and ORF1b, that are translated together as two co-terminal polyproteins (Ziebhur, 2005). These polyproteins then auto-proteolytically cleave themselves into several products called non- structural proteins (nsp from 1 to 16) with several functions. One of the most important nsp is the nsp12 that represents the RNA-dependent RNA polymerase (RdRp). At the 3' end of the genome instead are located the genes encoding for the following structural proteins: i) the spike S glycoprotein, ii) the envelope E protein, iii) the membrane M protein, iv) the nucleocapsid N protein. Also, genes encoding for accessory proteins are located at the 3' terminal. In the viral particle, the RNA genome is tightly bound to N in a helical symmetric nucleocapsid. The viral particle is also surrounded by an envelope made of lipidic layers acquired from the host Endoplasmic Reticulum-Golgi intermediate compartment (ERGIC) and containing the viral spike (S), envelope (E) and membrane (M) proteins (Alanagreh et al., 2020).

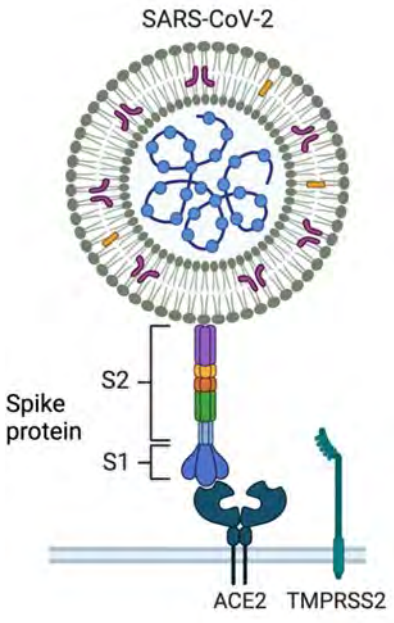

Figure 1. *SARS-CoV-2 binding to ACE2 Receptor by means of Spike Protein Subunit 1 (S1).*

Viral RNA genome is known to rapidly acquire mutations while replicating, as RNA-dependent RNA polymerases are more prone to introduce errors than DNA-dependent DNA polymerases. Interestingly, the replicase of Coronaviridae is characterized by a proofreading activity linked to the amino-terminal exoribonuclease (ExoN) domain of the Nsp14 enzyme that can correct errors inserted in the viral genome (Romano et al., 2020). Although this feature reduces the rate of sequence variability, SARS-CoV-2 can still acquire relevant mutations as it spreads worldwide. Indeed, the constant and relevant human-to-human

transmission, the natural adaptation of the virus to the new host as well as the more recent pressure of vaccination, facilitate occurrence of mutations that can be fixed in the viral population, as shown by the emergence of different variants since the beginning of the pandemic (https://www.cdc.gov/coronavirus/2019-ncov/variants/variant-classifications.html, accessed on 15th of March 2021). Currently, viral variants are classified into larger groups named lineages or clades. Different clade/lineage nomenclatures have been proposed. Among these, the Phylogenetic Assignment of Named Global Outbreak Lineages (PANGOLIN) is a software that allows a dynamic nomenclature (known as the PANGO nomenclature) of SARS-CoV-2 lineages (Alteri et al., 2021). SARS-CoV- 2 variants are grouped according to their lineage and component mutations (Tao et al., 2021). The World Health Organization (WHO) classifies some of the emerging variants as variants of concern (VOC), variants of interest (VOI) or variants under monitoring (VUM), based on their transmissibility and/or infection severity. All these variants are named with letters of the Greek alphabet (Ghosh et al., 202). Delta (B.1.617.2) and Omicron (B.A.1 and B.A.2) are the VOC currently circulating (https://www.ecdc.europa.eu/en/covid-19/variants-concern, accessed on 12th of May 2022).

Viral entry into host cells is mainly mediated by the S envelope protein, which is composed of two subunits named S1 and S2 (Harrison et al., 2020). Virus attachment to the target cells involves S1 and the host angiotensin-converting enzyme 2 (ACE-2) receptor. Following steps are allowed by the cellular proteins cathepsin L and transmembrane protease serine 2 (TMPRSS2) that, acting on the S1/S2 complex, lead to the exposure of a fusion peptide belonging to the S2 subunit (Harrison et al., 2020).

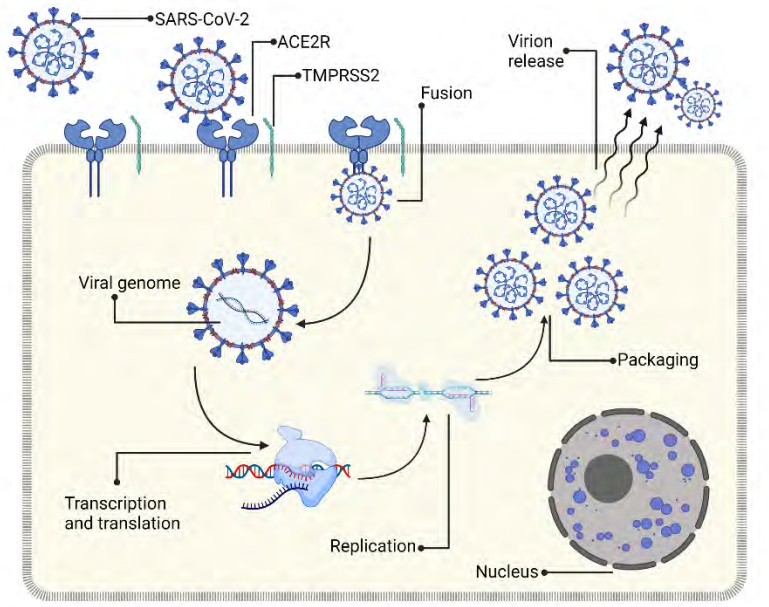

Figure 2. *Schematic diagram of SARS-CoV-2 Replication in host cells.*

Coronavirus Disease 2019 (COVID-19) is mainly a respiratory disease, but it can also involve additional organs, causing hepatic, enteric, neurological as well as psychiatric symptoms (Haidar et al., 2022). Neurological manifestations associated to COVID-19 have attracted particular attention. Among the most frequent neurological signs detected in COVID-19 patients there are headache, dizziness, nausea, confusion (Baig, 2020; Collantes et al., 2021), smell and taste disorders even at early stages of the disease (Lechien et al., 2020; Brann et al., 2020), while the most common complications are stroke, neurological damage, ataxia, delirium, brain and spinal cord inflammation (Collantes et al., 2021), encephalopathies and encephalitis (Pilotto et al., 2020; Muccioli et al., 2020). Moreover, an increased incidence of Acute Disseminated EncephaloMyelitis (ADEM) has been reported in COVID-19 patients (Paterson et al., 2020). Different respiratory viruses, including Coronaviruses, are known to infect the brain tissue (Bergmann et al., 2006; Desforges et al., 2020). For example, neuroinvasion and neurovirulence of the human coronavirus OC43 (HCoV-OC43), SARS-CoV-1 and Middle East Respiratory Syndrome (MERS)-CoV were reported in transgenic mice (Desforges et al., 2020). Importantly, ACE2 was shown to be highly expressed in neurons, astrocytes, and oligodendrocytes (Wu et al., 2020; Pujadas et al., 2021; Chen et al., 2021). The SARS-CoV-2 ability to infect the human brain has been further analyzed in human neural progenitor cells and brain organoids (Deguchi et al., 2021; Zhang et al., 2020). In addition, SARS-CoV-2 RNA was detected in brains (Matshke et al., 2020) and in the cerebrospinal fluid (CSF) of some COVID-19 patients, indicating a possible

pathophysiological involvement of the virus in the neurological symptoms (Virhammar et al., 2020). The pathogenetic mechanisms accounting for SARS-CoV-2 related neurological manifestations have been deeply analyzed in many recent studies (reviewed in Hadiar et al., 2022). Up to now, two hypotheses have been proposed to explain the COVID-19 neuropathogenesis. On the one hand, SARS-CoV-2 may enter the CNS through the olfactory bulb by binding to the ACE-2 receptor, damaging the blood brain barrier (BBB) or even exploiting leukocytes as a Trojan horse mechanism (Kumar, 2021). The neurological symptoms would be, then, a consequence of the direct viral damage to brain tissues. In this context, specific regions of the viral genome could play a role in neurotropism and/or neurovirulence. On the other hand, SARS-CoV-2 replication in the lungs, in addition of causing pulmonary dysfunctions, is known to trigger an intense and dysregulated systemic inflammatory process called cytokine storm, which is a common feature of severe COVID-19 cases. The cytokine storm has consequences for the entire organism and might affect the CNS, even without a direct invasion of the brain by the virus (Kumar, 2021; Tay et al., 2020). Finally, viral entry into the CNS may trigger a localized inflammatory response that could affect the CNS by itself, or in combination with the cytokine storm (Tay et al., 2020).

Pathways underlying SARS-CoV-2 infection and COVID-19 inflammation in the CNS

Olfactory pathways. SARS-CoV-1 enters the brain of transgenic mice via the olfactory bulb, causing neuronal death without signs of encephalitis (Netland, Meyerholz, Moore, Cassell, & Perlman, 2008), while intranasal inoculation of MERS-CoV in transgenic mice led to high levels of the virus in the CNS, particularly in the thalamus and the brainstem (Li et al., 2016). The characteristic clinical symptoms of hyposmia or anosmia in COVID-19, as well as hypogeusia or ageusia, which are quite prominent among affected patients (Guerrero et al., 2021) support the hypothesis of an involvement of the olfactory organ (Lechien et al., 2020). An increased SARS-CoV-2 viral load in the nasal epithelium have been found by RT-PCR *in situ* hybridization and immunohistochemical staining methods (Meinhardt et al., 2021). Moreover, a prospective autopsy study in Netherlands involving 21 patients who had succumbed to COVID-19 complications revealed extensive inflammation in the brain among other tissues, particularly focused in the olfactory bulbs and the medulla oblongata, although this study did not reveal virus in the brain (Schurink et al., 2020). Politi and colleagues described a case report of a COVID-19-positive woman with anosmia, who presented with subtle hyperintensities in the olfactory bulbs and the right gyrus rectus in brain magnetic

resonance imaging (MRI), although the authors highlight that this was not a consistent finding among COVID-19 patients with smell dysfunction (Politi, Salsano, & Grimaldi, 2020). A recently published paper, exploring the findings of brain scans before and after a SARS-CoV-2 infection in a large sample of UK Biobank participants, showed significant reductions in grey matter thickness and tissue-contrast in the orbitofrontal cortex and parahippocampal gyrus, along with prominent alterations in brain areas functionally connected to the primary olfactory cortex, suggestive of tissue damage (Douaud et al., 2022), although it is difficult to correlate the scan findings with cellular pathology. Furthermore, post-mortem brain MRI studies in 19 decedents of COVID-19 demonstrated an asymmetry in the olfactory bulbs in about 20% of the patients (Coolen et al., 2020). Post-mortem studies of COVID-19 patients detected the virus in the sustentacular cells of the olfactory epithelium, but not in the olfactory receptor neurons or the olfactory bulbs (Khan et al., 2021), as noted above.

Enteric pathways. With both respiratory and gastrointestinal symptoms quite common in the context of COVID-19 (Cares-Marambio et al., 2021; Groff et al., 2021) and ACE2 being highly expressed in the alveolar epithelial type II cells and the intestinal endothelial cells (Williams et al., 2021), some researchers have suggested the potential of SARS-CoV-2 entry through the intestine (Lehmann et al., 2021; Mönkemüller, Fry, & Rickes, 2020; H. Zhang et al., 2020). RNA of the SARS-CoV-2 has been identified in stool samples and rectal swabs, even in cases with negative nasopharyngeal swabs (Tang, Schmitz, Persing, & Stratton, 2020).. An autopsy study (n=21) revealed SARS-CoV-2-infected cells in the respiratory and gastrointestinal tract, among other tissues, along with extensive inflammation in the medulla oblongata, implying a potential effect on the respiratory control centre (Schurink et al., 2020). Many studies report inflammation in the medulla (see above), but the link between peripheral organs and the brain is not clear. One possible way in which systemic inflammation can influence medullary nuclei is the activation of vagal medullary afferents by inflammatory molecules. Thus, vagal endings contain receptors to IL-1 and are activated by this cytokine, subsequently activating neurons of the solitary nucleus, which then activate sympathetic output from the vagal nucleus and the nucleus ambiguous through the vagus nerve (Pavlov et al., 2012).

Vascular pathways. Non-neuronal pathways of SARS-CoV-2 that might lead to neuroinflammation must be considered, including the hematogenous route. SARS-CoV-2 can enter the blood stream and either access and damage the endothelium of brain

vasculature to cross the BBB, or trigger an inflammatory response, leading to breakdown of the BBB (Meinhardt et al., 2021; Wan et al., 2021).

Cerebrovascular disease, including ischemic and hemorrhagic strokes, constitutes a severe and common complication in COVID-19 (Tsivgoulis et al., 2020). The brains of patients who did not survive COVID-19 show acute cerebrovascular disease, including thrombotic microangiopathy and endothelial injury, without any evidence of vasculitis (Hernández-Fernández et al., 2020; Wan et al., 2021). Accumulating data suggests that COVID-19 is connected to a hypercoagulable state, which is closely related to inflammation and predisposes to macro- and microvascular thrombosis, resulting in arterial and venous infarcts (Abou-Ismail, Diamond, Kapoor, Arafah, & Nayak, 2020).

ACE2 is expressed in cells of the vasculature in the human brain, although the specific cell types have not been defined (Hamming et al., 2004). TMPRSS2 and NRP1 are also present in the endothelial cells of the vasculature (Wan et al., 2021). SARS-CoV-2 endothelitis has also been confirmed in autopsy studies concerning other human tissues (lungs, kidney, heart, liver, small intestine) (Varga et al., 2020). Moreover, Pellegrini and colleagues showed a leakage across the BBB, using a model of the human choroid plexus epithelial cells infected by SARS-CoV-2 (Pellegrini et al., 2020), although one has to consider the results of such *in vitro* studies carefully, since they may not reflect what occurs in the living brain.

On the other hand, a SARS-CoV-2 infection can cause an excessive systemic inflammatory response after triggering a cytokine storm in the periphery, resulting in a BBB disruption (David Sulzer et al., 2020). Researchers have suggested that SARS-CoV-2 may infect immune cells, using them as a “trojan horse” to invade the CNS via the impaired BBB or activate different populations of immune cells, which may infiltrate the CNS, causing a secondary cytokine storm and thus neurologic manifestations (Pezzini & Padovani, 2020; Wan et al., 2021; Williams et al., 2021).

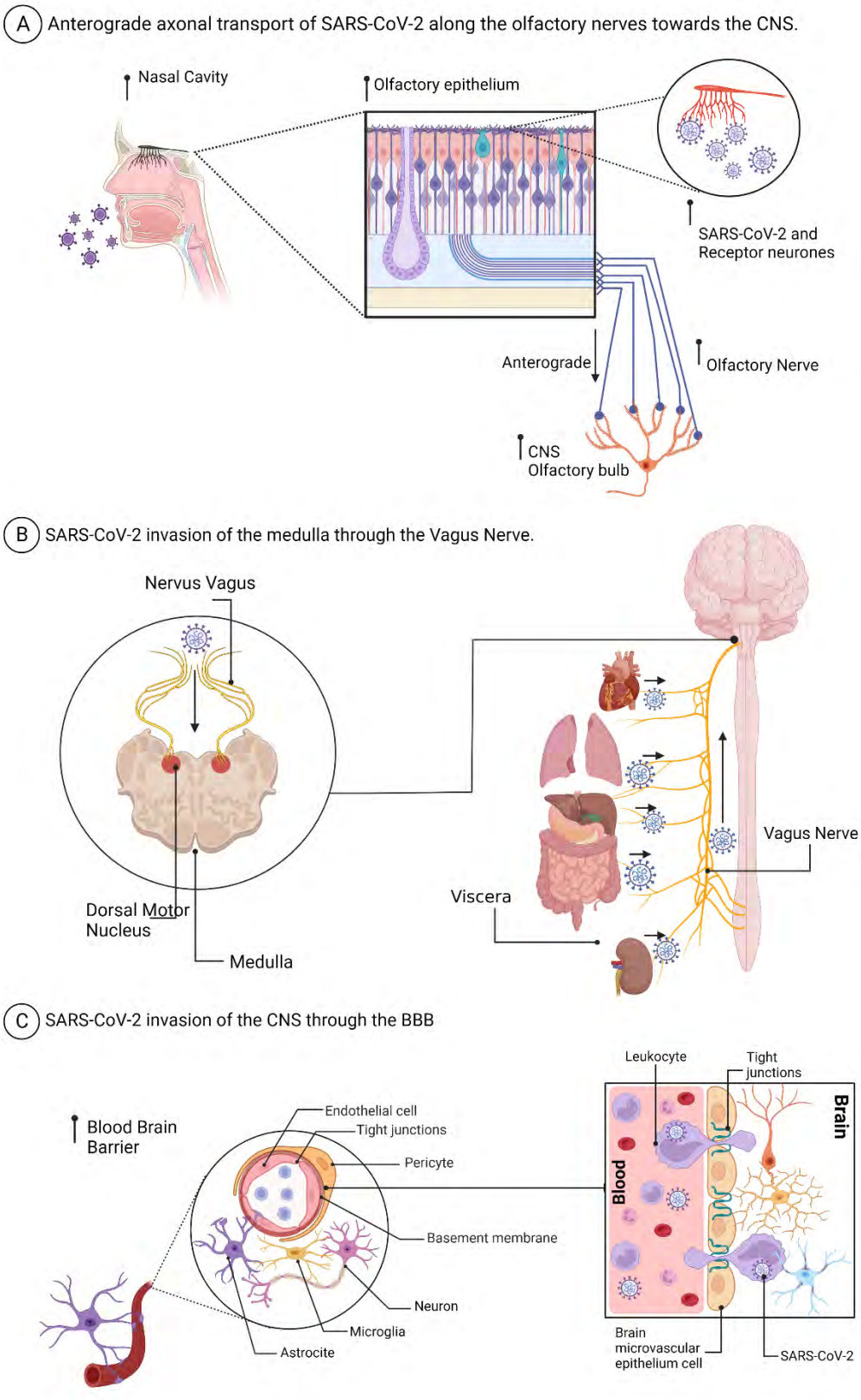

Figure 3. Pathways for SARS-CoV-2 invasion of the Central Nervous System.

COVID-19 Neuropathology

Neurological manifestations are a common finding in COVID-19. A wide spectrum of neurological manifestations, such as anosmia, ageusia, nausea and headaches are commonly reported by patients with mild manifestations of the disease, while more severe alterations, such as stroke, meningitis, encephalitis are also reported in hospitalized patients and subjects severe COVID-19 (Ellul et al., 2020; Helms et al., 2020; Iadecola et al., 2020; Mao et al., 2020; Huang et al., 2021). When investigating the neuropathological mechanisms underlying neurological manifestations in COVID-19, post-mortem studies and autopsy case series represent the most valuable source of information currently available, despite several known limitations. While animal studies allow for experimental control of numerous variables, such as virus exposure modality, infection course and duration, post-mortem studies on humans are constrained by inherent limitations, such as often ill-defined positivity interval (i.e. the time occurring between infection and death), frequent patient comorbidities, different treatment approaches, variable post-mortem interval and tissue quality conditions, which must be considered when investigating the neuropathology underlying neurological manifestations in COVID-19. Conversely, post-mortem studies present significant advantages in spatial resolution and diagnostic accuracy over commonly employed in-vivo investigation techniques, such as computed tomography (CT) and magnetic resonance imaging (MRI), allowing for the accurate evaluation of micro-scale neuropathology.

Brief timeline of major post-mortem autopsy studies in COVID-19 *(≤15 included COVID-19 subjects)*	
September 2020	Solomon et al. (2020, USA) reported the first autopsy series investigating COVID-19 related neuropathology in 18 patients (n=4 females, n=14 males; mean age 62). In all patients, SARS-CoV-2 infection was confirmed by quantitative RT-PCR analysis of oro-pharyngeal swabs. Patients were hospitalized for a median of 6 days and died 0 to 32 days after the onset of symptoms. 11 patients received mechanical ventilation. Prexisting medical conditions included diabetes mellitus (12 patients), hypertension (11) and cardiovascular disease (5), while specific neuroloigcal conditions included dementia (4 patients), prior stroke (4 patients) and anaplastic astrocytoma. SARS-CoV-2 neurotropism was investigated by the means of RT-qPCR assay for Nucleocapsid Protein and immunoperoxidase staining for Nucleocapsid Protein. Histopathological examination revealed mainly hypoxic /ischaemic alterations and did not reveal encephalitis or other specific brain changes referable to the virus. No cytoplasmic viral staining on immunohistochemical analysis was detected. However, viral RNA was detected through RT-PCR at low levels in 6 brain sections obtained from 5 patients; these levels were not consistently related to the interval from the onset of symptoms to death.
October 2020	Matschke et al. (2020, Germany) reported the largest to date brain autopsy case series in Europe. 43 patients (n=16 female, n=27 male; mean age 76 years) were included, based on positive testing for SARS-CoV-2 infection through RT-PCR of oro-pharyngeal swabs. 93% of the patients had relevant prexisting chronic medical conditions, while 30% had pre-existing neurological or neurodegenerative diseases. Neuropathological examination was conducted by evaluation of Haematoxylin and Eosin stained sections and by the means of immunohistochemistry for GFAP, Iba1, TMEM119, HLA-DR, CD68, CD8 and Sars-CoV-2 Spike and Nucleocapsid protein. Fresh territorial ischaemic lesions were identified in six (14%) patients. 37 (86%) patients had astrogliosis in all assessed regions. Activation of microglia and infiltration by cytotoxic T lymphocytes was most pronounced in the brainstem and cerebellum, and meningeal cytotoxic T lymphocyte infiltration was seen in 34 (79%) patients. Sars-CoV-2 could be detected in the brains of 21 (53%) of 40 examined patients, with Sars-CoV-2 viral proteins found in cranial nerves originating from the lower brainstem and in isolated cells of the brainstem. According to the authors, the presence of SARS-CoV-2 in the CNS was not associated with the severity of neuropathological changes.
November 2020	Meinhardt et al. (2020, Germany) investigated olfactory transmucosal SARS-CoV-2 invasion in 33 individuals (n=11 female, n=22 male, median age 71 years) with positive RT-qPCR assay for Sars-CoV-2 infection or clinical findings suggestive of COVID-19. Cases were not preselected with regard to clinical or neurological symptoms. Viral neurotropism was investigated by the means of RT-qPCR for Sars-CoV-2 RNA, Electron Microscopy, In situ hybridization for SARS-CoV-2 RNA, and immunoperoxidase and immunofluorescence for SARS-CoV-2 Spike protein at the level of the olfactory mucosa, oral mucosa, medulla oblongata, cranial nerves and cerebellum. Prominent viral load and immunohistochemical reactivity was found at the level of the olfactory mucosa. In the CNS, the authors identified

	strong upregulation of human leukocyte antigen (HLA)-DR on microglia/macrophages, arranged in microglial nodules, in 13 of 25 individuals analyzed. In 18% of the 33 individuals investigated (n = 6 of 33) a histopathological correlate of microthrombosis and subsequent acute territorial brain infarcts was detected. Immunoreactivity to SARS-CoV Spike protein in endothelial cells within these acute cerebral infarcts was also found.
Febuary 2021	Hwa-Lee et al. (2020, USA) investigated neuropathological features of COVID-19 in the brains of 18 patients (median age 50 years). 14 patients had chronic preexisting medical conditions, such as diabetes and hypertension, while 11 patients were found dead suddenly and unexpectedly. Investigation was carried out by the means of Magnetic Resonance Imaging Microscopy (11.7 Tesla MRI) and histopathological evaluation based on haematoxylin and eosin stain and multiplex fluorescence imaging. Areas of microvascular injury and fibrinogen leakage were identified in 9 patients. Minimal perivascular inflammation and no vascular occlusion was reported. Activated microglia were identified in 5 patients, suggesting neuronophagia at the level of the substantia nigra, olfactory bulb, dorsal motor nucleus of the vagus and pre-Bötzinger complex. SARS-CoV-2 was not detected by means of polymerase chain reaction with multiple primer sets, RNA sequencing of several areas of the brain, or RNA in situ hybridization and immunostaining.
August 2021	Remmelink et al. (Belgium) published a post-mortem study on 17 COVID-19 subjects, identifying several instances of hemorrhage (n=8), spongiosis (n=10) and focal necrosis (n=3). However, while immunohistochemical staining was not performed on brain sections, RT-PCR analyses revealed viral genomic sequences in nine out of eleven samples.
October 2021	Thakur et al. (USA) reported the largest autopsy-case series in the United States including 41 COVID-19 subjects (n=14 female; n=27 male; mean age 74 years). Neuropathological examination of approximately 30 brain areas was performed through haematoxylin and eosin staining, as well as multiple immunohistochemical markers (GFAP, CD68, CD3, Collagen IV, VCAM1, and IBA1). Hypoxic/ischaemic alterations were detected in all examined brains, ranging from global to focal alterations. Microglial activation with microglial nodules accompanied by neuronophagia, most prominently in the brainstem, was also a prominent finding in the cohort. To detect viral proteins and genomic sequences in fresh-frozen as well as fixed tissues, the authors performed qRT-PCR, RNAscope® and immunohistochemistry for N protein. PCR analysis revealed low to very low, but detectable, viral RNA levels in the majority of brains, although with lower cycle thresholds than nasal epithelia. RNAscope® and immunohistochemistry failed to detect viral RNA or proteins in the samples. According to the authors, these findings indicate that the levels of detectable virus in COVID-19 brains are very low and do not appear to correlate with the encountered histopathological alterations. Hence, microglial activation, microglial nodules and neuronophagia may not result from direct viral

	infection of brain parenchyma, but more likely from systemic inflammation, perhaps with synergistic contribution from hypoxia/ischaemia.
2022	Emmi et al. (2022) evaluated the neuropathological alterations of 24 COVID-19 subjects and compared these findings to a cohort of 18 non-COVID subjects who died due to other respiratory infections, pneumonia and respiratory failure. Aside from a wide spectrum of neuropathological alterations, including hypoxic / ischaemic damage, astrogliosis and lympho-monocitic infiltrations, COVID-19 subjects presented significantly higher microglial densities at the level of the medulla and midbrain compared to pneumonia subjects, and displayed a peculiar microglial phenotype characterized by the expression of both homeostatic (TMEM119) and actiavated markers (CD68, HLA-DR). In 5 COVID-19 cases, viral genomic sequences and viral antigens were detected by means of immunoperoxidase and immunofluorescent staining at the level of the neurons of the vagal nuclei and the substantia nigra, suggesting SARS-CoV-2 neurotropism. However, despite the detection of markers of viral invasion, no direct damage to neurons or glial cells was observed, with most neuropathological alterations being more likely imputable to hypoxic / ischaemic damage, neuroinflammation and the ongoing cytokine storm.

COVID-19 patients present mild-to-moderate widespread neuropathological alterations, including hypoxic / ischaemic damage, vascular pathology, small vessel thromboses and reactive astrogliosis. Hypoxic / ischaemic pathology represents a common finding in COVID-19 patients, being reported in most studies available in literature (Solomon et al., 2020; Matschke et al., 2020; Thakur et al., 2021). Alterations were mostly widespread, and both acute and subacute findings could be appreciated at the level of the cortex, basal ganglia, hippocampus and, most notably, the brainstem. Hypoxic / ischaemic damage was often associated to vascular pathology, atherosclerosis and arteriosclerosis, with numerous reported cases presenting both ischaemic and hemorrhagic infarcts (Matschke et al., 2020; Hwa-Lee et al., 2020; Remmelink et al., 2020; Thakur et al., 2021). Reactive astrogliosis in the context of hypoxic / ischaemic injuries was also one of the most common findings, prominently involving the basal ganglia and the brainstem (Matschke et al., 2020; Meinhardt et al., 2020; Thakur et al., 2021). Microvascular pathology, fibrinogen leakage and small vessel thromboses were also associated to ischaemic and vascular pathology, and represented a characteristic finding of the COVID-19 cohort (Matschke et al., 2020; Meinhardt et al., 2020; Hwa-lee et al., 2020; Schwabenland et al., 2021; Porzionato et al., 2021a,2021b). Small vessel platelet-enriched microthrombi were predominantly found in the basal ganglia, brainstem and cerebellum, and were often associated to microvascular injury

and fibrinogen leakage. Several instances of SARS-CoV-2 immunoreactive endothelial cells in the context of vascular injury were also detected (Meinhardt et al., 2021), indicating a prominent role of SARS-CoV-2 infection in determining COVID-19 associated small vessel pathology.

Neuroinflammation is prominent in COVID-19 and characterized by lympho-monocytic infiltrations, microglial activation and microglial nodules. Lympho-monocytic perivascular cuffing and infiltration were reported by most authors, with a predominance of perivascular CD68+ monocytes/macrophages and CD8+ T-cells (Matschke et al., 2020; Meinhardt et al., 2020; Hwa-lee et al., 2020; Schwabenland et al., 2021; Thakur et al., 2020). In all reported studies examining microglial cells in the context of SARS-CoV-2 infection, authors identified prominent microglial activation with upregulation of MHC-II proteins (HLA-DR) and increased lysosomal activity (CD68+), while maintaining homeostatic microglial marker TMEM119 (Matschke et al., 2020; Meinhardt et al., 2020; Deigendesch et al., 2020; Schwabenland et al., 2021, Thakur et al., 2021). Similarly, instances of neuronophagia were documented by most authors, with prominent involvement of the brainstem at the level of the medullary tegmentum, midline raphe and dorsal pons (Matschke et al., 2020; Meinhardt et al., 2020; Deigendesch et al., 2020; Schwabenland et al., 2021, Thakur et al., 2021). Microglial nodules with associated CD8+/CD3+ T-cell clusters were also a documented in most, but not all, COVID-19 patients, in contrast to non-COVID controls and ExtraCorporeal Membrane Oxygenation (ECMO) patients, which displayed no instances of microglial nodules and neuronophagia (Schwabenland et al., 2021; Thakur et al., 2021). Deep spatial profiling of the local immune response in COVID-19 brains through imaging mass spectrometry revealed significant immune activation in the medulla and olfactory bulb with a prominent role mediated by CD8+ T-cell - microglia crosstalk in the parenchyma (Schwabenland et al., 2021). Conversely, Deigendesh et al. (2021) found significant differences in HLA-DR+ activated microglia when comparing COVID-19 subjects to non-septic controls, but no differences were found with patients who had died under septic conditions; according to the authors, this may represent a histopathological correlate of critical illness-related encephalopathy, rather than a COVID-19-specific finding. Hence, while most studies seem to agree on the overall neuroinflammatory conditions occurring in COVID-19, with particular focus on microgliosis and microglia – T-cell crosstalk, disagreements on the source of inflammation are yet to be resolved. In particular, it is not clear to which extent neuroinflammatory conditions occurring in COVID-19 are determined

by the direct effects of SARS-CoV-2 invasion, rather than ongoing systemic inflammation / cytokine storm, and whether and how frequent comorbidities (i.e. hypertension, diabetes, vascular disease, neurodegenerative conditions) and hypoxic / ischaemic damage may influence microgliosis and brain inflammation.

SARS-CoV-2 neurotropism has been documented, however direct effects of neuroinvasion remain to be determined. To date, SARS-CoV-2 viral antigens and genomic sequences in the brain of COVID-19 patients have been documented only in a small subset of cases, and has not been constantly reproduced throughout available studies (Solomon et al., 2020; Matschke et al., 2020; Meinhardt et al., 2020; Hwa-lee et al., 2020; Yang et al., 2020; Schwabenland et al., 2021; Thakur et al., 2021; Emmi et al., 2022). While most studies report the detection of viral genomic sequences in the brainstem of COVID-19 subjects, viral RNA found in blood and blood vessels of investigated tissue samples can not be excluded by employed RT-PCR assays. Conversely immunoperoxidase and immunofluorescent staining, imaging mass spectrometry and in-situ hybdirization (or related techniques) allow for the spatial localization of viral proteins / RNA and can thus be employed to study SARS-CoV-2 neurotropism, but failed to consistently detect viral antigens across available studies in literature. Matschke et al. (2020) reported sparse immunoreactive cells throughout the brainstem, without specific topographic localization, but also detected distinct immunoreactivity of the glossopharyngeal and vagus nerve bundles (CN IX-X) in a subset of patients, suggesting for SARS-CoV-2 retrograde spread through these cranial nerves towards the medulla. This is also supported by the detection of SARS-CoV-2 antigen and genomic sequences in the carotid body of COVID-19 subjects (Porzionato et al., 2021b). However, no association was found with encountered neuropathological changes.
Meinhardt et al. (2020) detected viral proteins and RNA in the olfactory mucosa through immunohistochemistry, immunofluorescence and in-situ hybdirization, as well as electron microscopy. SARS-CoV-2 spike protein was found within primary olfactory neurons of the olfactory mucosa, suggesting an olfactory-transmucosal spread of the virus. This was supported by the detection of viral RNA at the level of the olfactory bulb and medulla, even though viral proteins were not detected in non-vascular cells. Conversely, SARS-CoV-2 immunoreactive endothelial cells associated with microvascular injury and microthromboses were found in a subset of COVID-19 patients at the level of the medulla, suggesting for viral spread also through the vascular compartment and the blood-brain barrier.

Schwabenland et al. (2021) detected viral antigens in ACE2-positive cells enriched in the vascular compartment. According to the authors, the presence of viral antigen was linked to vascular proximity and ACE2 expression, while also being correlated to the perivascular immune activation patterns of CD8+ and CD4+ T-cells and myeloid- and microglial-cell subsets, indicating a fundamental role of the vascular and perivascular compartment, as well as Blood-brain-barrier impairment, in mediating COVID-19 specific neuroinflammation (Schwabenland et al., 2021).

Yang et al. (2020) performed single-nucleus gene-expression profiling of frontal cortex and choroid plexus tissues from severe COVID-19 patients and detected broad perturbations, with upregulation of genes involved in innate antiviral response and inflammation, microglia activation and neurodegeneration, but no direct evidence of viral tropism was found.

Other authors did not detect viral proteins / RNA through immunohistochemistry or in-situ hybridirization, even though viral genomic sequences were detected with RT-PCR assays (Solomon et al., 2020; Hwa-lee et al., 2020; Thakur et al., 2021).

Emmi et al. (2022) detected both viral antigens (Spike and Nucleocapsid protein) via immunoperoxidase and immunofluorescent staining at the level of the vagal nuclei of the medulla and the substantia nigra in the midbrain. Findings were confirmed by concording RT-PCR analyses detecting viral genomic sequences in the same sections. However, no direct damage and / or neuronal necrotic changes (pyknosis, chromatolisis, soma shrinkage, and other morphological anomalies) were detected. While a correlation between regional brainstem microgliosis and the detection of viral antiges / genomic sequences was found, most neuropathological alteratons were to be attributed to hypoxic / ischaemic damage, neuroinflammation, systemic infection and the ongoing cytokine storm. These findings suggest that while acute fatal COVID-19 is characterized by neuropathological alterations, such as hypoxic / ischaemic damage, microthromboses and microgliosis, mediated mainly by systemic infection and the ongoing cytokine storm, SARS-CoV-2 neurotropism is a possible, yet not frequent, consequence of infection that does not appear to directly damage the brain, at least in the acute phases of the disease.

Hence, SARS-CoV-2 neurotropism remains yet to be investigated and further confirmed, with particular regard to invasion of CNS neurons and / or specific brain regions. Furthermore, more information is needed to clarify entry mechanisms and subsequent consequences of direct viral infection of the CNS, with particular regard to the link between encountered neuropathological alterations and known neurological manifestations in COVID-19 patients, as well as long-COVID patients.

SARS-CoV-2, COVID-19 and Neurodegeneration

Particularly concerning is the hypothesis that SARS-CoV-2 infection of the central nervous system may predispose, or quickly precipitate, the development of Parkinson's Disease (Beauchamp, Finkelstein, Bush, Evans, & Barnham, 2020; Bouali-Benazzouz & Benazzouz, 2021; Brundin, Nath, & Beckham, 2020). This hypothesis arises both from the 1917 Spanish flu and von Economo's encephalitis lethargica pandemics, which have seen a surge of post-encephalitic parkinsonism following the waves of the pandemic, and the known association between viral infection and the development of transient or permanent movement disorders (Jang, Boltz, Webster, & Smeyne, 2009). In fact, pathogens, and in particular respiratory viruses, have been suggested as a potential etiopathogenic factor for PD, leading to parkinsonism in subjects over the age of 50, regardless of genetic substrate (Beauchamp et al., 2020; Tanner et al., 1999). The well-established neuropathological staging of PD suggested by Braak & Braak also appears to account for neurotropic pathogens that may infect the central nervous system either through the vagus nerve (pneumo-gastric pathway) or by accessing the brain through the olfactory systems. Both the olfactory bulb and tract, as well as the medulla oblongata where the vagal nuclei are located, represent the very first sites of early PD neuropathology, and interestingly also represent the main sites of inflammation / infection encountered in COVID-19 (Hawkes, Del Tredici, & Braak, 2007; Klingelhoefer & Reichmann, 2015). Furthermore, viral-related inflammation might render the CNS susceptible to preceding or subsequent stressors (Sulzer, 2007), even in the absence of direct viral invasion; indeed, past history of infection was associated with a 20% higher risk of presenting PD in the future (Meng, Shen, & Ji, 2019). In the case of coronaviruses, higher antibodies titers against common CoV have been detected in the CSF of PD patients when compared to controls, while there was evidence of post-encephalitic parkinsonism in mice infected with a CoV strain (MHV-A59) (Fazzini, Fleming, & Fahn, 1992; Fishman et al., 1985).

In a recent study, Semerdzhiev, Fakhree, Segers-Nolten, Blum, and Claessens (2022) demonstrated that in the presence of SARS-CoV-2 Nucleocapsid protein, the onset of alpha-synuclein aggregation into amyloid fibrils is strongly accelerated, indicating that N-protein facilitates the formation of a critical nucleus for aggregation. Fibril formation does not only appear to accelerate, but also proceeds in an unusual two-step process. In cells, the presence of Nucleocapsid protein changes the distribution of alpha-synuclein over different

conformations that likely represent different functions at already short time scales. Similarly, Charnley et al. (2022) identified two peptides from the SARS-CoV-2 proteome that self-assemble into amyloid assemblies. These amyloids were shown to be highly toxic to neuronal cells and are hypothesized to trigger neurological symptoms in COVID-19. The cytotoxicity and protease-resistant structure of these assemblies may result in their persistent presence in the CNS of patients even following infection, could partially explain the lasting neurological symptoms of COVID-19, especially those that are novel in relation to other post-viral syndromes such as that following the original SARS-CoV-1. The outlook in relation to triggering of progressive neurodegenerative disease remains uncertain. Given the typically slow progress of neurodegenerative disease if such a phenomenon exists, it will most probably take some time to become evident epidemiologically. In an animal model study performed by Käufer et al. (2022), microglial activation and neuronal proteinopathy persisted even beyond viral clearance. Viral protein exposure in the nasal cavity led to pronounced microglia activation in the olfactory bulb beyond viral clearance. Cortical but not hippocampal neurons accumulated hyperphosphorylated tau and alpha-synuclein, in the absence of overt inflammation and neurodegeneration. Importantly, not all brain regions were affected, in line with the selective vulnerability hypothesis. In this animal model, despite the absence of virus in brain, neurons developed signatures of proteinopathies that may contribute to progressive neuronal dysfunction.

This is further confirmed by available neuropathological studies on COVID-19 decedents, showing very little and often conflicting evidence on SARS-CoV-2 neurotropism. On the other hand, as all available neuropathological studies are carried on subjects who died during the acute phases of the disease (Emmi et al., 2021; Matschke et al., 2020; Schwabenland et al., 2021; Solomon et al., 2020), and as such the neuropathological alterations occurring in cases of chronic infection, or in the post-infection timeframe, are yet unknown. Neurodegenerative changes induced by either direct infection or by the indirect effects mediated by neuroinflammation may not be appreciable or detectable in patients who died shortly after infection, and as most subjects in neuropathological studies already present important neurological comorbidities, it is not possible to determine which markers of neurodegeneration are directly related to COVID-19, and which are related to patient morbidity.

REFERENCES

1. Alanagreh L, Alzoughool F, Atoum M. The human coronavirus disease COVID-19: its origin, characteristics, and insights into potential drugs and its mechanisms. Pathogens. 2020;9(5):331.
2. Alteri C, et al. Genomic epidemiology of SARS-CoV-2 reveals multiple lineages and early spread of SARS-CoV-2 infections in Lombardy, Italy. Nat Commun. 2021;12(1):43.
3. Ashour HM, Elkhatib WF, Rahman M, Elshabrawy HA. Insights into the recent 2019 novel coronavirus (SARS-CoV-2) in light of past human coronavirus outbreaks. Pathogens. 2020;9(3):186.
4. Baig AM. Neurological manifestations in COVID-19 caused by SARS-CoV-2. CNS Neurosci Ther. 2020;26(5):499.
5. Beauchamp, L. C., Finkelstein, D. I., Bush, A. I., Evans, A. H., & Barnham, K. J. (2020). Parkinsonism as a Third Wave of the COVID-19 Pandemic? *Journal of Parkinson's disease, 10*(4), 1343-1353. doi:10.3233/JPD-202211
6. Bergmann CC, Lane TE, Stohlman SA. Coronavirus infection of the central nervous system: host–virus stand-off. Nat Rev Microbiol. 2006;4(2):121–132.
7. Bouali-Benazzouz, R., & Benazzouz, A. (2021). COVID-19 Infection and Parkinsonism: Is There a Link? *Mov Disord, 36*(8), 1737-1743. doi:10.1002/mds.28680
8. Brann DH, Tsukahara T, Weinreb C, Lipovsek M, Van den Berge K, Gong B, et al. Non-neuronal expression of SARS-CoV-2 entry genes in the olfactory system suggests mechanisms underlying COVID-19-associated anosmia. Sci Adv. 2020;6(31):eabc5801.
9. Brundin, P., Nath, A., & Beckham, J. D. (2020). Is COVID-19 a Perfect Storm for Parkinson's Disease? *Trends Neurosci, 43*(12), 931-933. doi:10.1016/j.tins.2020.10.009
10. C S G of the International. The species Severe acute respiratory syndrome-related coronavirus: classifying 2019-nCoV and naming it SARS-CoV-2. Nat Microbiol. 2020;5(4):536.
11. Charnley, M., Islam, S., Bindra, G. K., Engwirda, J., Ratcliffe, J., Zhou, J., . . . Reynolds, N. P. (2022). Neurotoxic amyloidogenic peptides in the proteome of SARS-COV2: potential implications for neurological symptoms in COVID-19. Nature Communications, 13(1), 3387. doi:10.1038/s41467-022-30932-1
12. Chen R, Wang K, Yu J, Howard D, French L, Chen Z, et al. The spatial and cell-type distribution of SARS-CoV-2 receptor ACE2 in the human and mouse brains. Front Neurol. 2021;11:1860.
13. Collantes M E V, Espiritu A I, Sy M C C, Anlacan V M M, Jamora R D G. Neurological manifestations in COVID-19 infection: a systematic review and meta-analysis. Can J Neurol Sci**.** 2021; 48(1), 66-76.
14. Deguchi S, Serrano-Aroca A´, Tambuwala MM, Uhal BD, Brufsky AM, Takayama K. SARS-CoV-2 research using human pluripotent stem cells and organoids. Stem Cells Transl Med. 2021;10(11):1491–1499.

15. Desforges M, Le Coupanec A, Dubeau P, Bourgouin A, Lajoie L, Dub´e M, et al. Human coronaviruses and other respiratory viruses: underestimated opportunistic pathogens of the central nervous system? Viruses. 2020;12(1):14.
16. Ellul, M. A. et al. Neurological associations of COVID-19. Lancet Neurol 19, 767-783, doi:10.1016/s1474-4422(20)30221-0 (2020).
17. Emmi, A., Rizzo, S. M. R., Barzon, L., Carturan, E., Sinigaglia, A., Riccetti, S., . . . Porzionato, A. (2021). COVID-19 Neuropathology: Evidence for SARS-CoV-2 invasion of Human Brainstem Nuclei. doi: https://doi.org/10.1101/2022.06.29.498117
18. Fazzini, E., Fleming, J., & Fahn, S. (1992). Cerebrospinal fluid antibodies to coronavirus in patients with Parkinson's disease. *Mov Disord, 7*(2), 153-158. doi:10.1002/mds.870070210
19. Fishman, P. S., Gass, J. S., Swoveland, P. T., Lavi, E., Highkin, M. K., & Weiss, S. R. (1985). Infection of the basal ganglia by a murine coronavirus. *Science (New York, N.Y.), 229*(4716), 877-879. doi:10.1126/science.2992088
20. Ghosh N, Nandi S, Saha I. A Review on evolution of emerging SARS-CoV-2 variants based on spike glycoprotein. Int Immunopharmacol. 2022;105:108565.
21. Haidar MA, Shakkour Z, Reslan MA, Al-Haj N, Chamoun P, Habashy K, et al. SARS-CoV-2 involvement in central nervous system tissue damage. Neural Regen Res. 2022;17(6):1228.
22. Harrison AG, Lin T, Wang P. Mechanisms of SARS-CoV-2 transmission and pathogenesis. Trends Immunol. 2020;41(12):1100–1115.
23. Hawkes, C. H., Del Tredici, K., & Braak, H. (2007). Parkinson's disease: a dual-hit hypothesis. *Neuropathol Appl Neurobiol, 33*(6), 599-614. doi:10.1111/j.1365-2990.2007.00874.x
24. Helms, J. et al. Neurologic Features in Severe SARS-CoV-2 Infection. N Engl J Med 382, 2268-2270, doi:10.1056/NEJMc2008597 (2020).
25. Huang, C. et al. 6-month consequences of COVID-19 in patients discharged from hospital: a cohort study. Lancet 397, 220-232, doi:10.1016/s0140-6736(20)32656-8 (2021).
26. Iadecola, C., Anrather, J. & Kamel, H. Effects of COVID-19 on the Nervous System. Cell 183, 16-27.e11, doi:10.1016/j.cell.2020.08.028 (2020).
27. Jang, H., Boltz, D. A., Webster, R. G., & Smeyne, R. J. (2009). Viral parkinsonism. *Biochim Biophys Acta, 1792*(7), 714-721. doi:10.1016/j.bbadis.2008.08.001
28. Käufer, C., Schreiber, C. S., Hartke, A.-S., Denden, I., Stanelle-Bertram, S., Beck, S., . . . Richter, F. (2022). Microgliosis and neuronal proteinopathy in brain persist beyond viral clearance in SARS-CoV-2 hamster model. eBioMedicine, 79, 103999. doi:https://doi.org/10.1016/j.ebiom.2022.103999
29. Klingelhoefer, L., & Reichmann, H. (2015). Pathogenesis of Parkinson disease--the gut-brain axis and environmental factors. *Nat Rev Neurol, 11*(11), 625-636. doi:10.1038/nrneurol.2015.197
30. Kubota, T., & Kuroda, N. (2021). Exacerbation of neurological symptoms and COVID-19 severity in patients with preexisting neurological disorders and COVID-19: A systematic review. *Clin Neurol Neurosurg, 200*, 106349. doi:10.1016/j.clineuro.2020.106349
31. Kumar A. COVID-19 Current challenges and future perspectives. Betham Books 2021. 8: 76-100.
32. Lechien JR, Chiesa-Estomba CM, De Siati DR, Horoi M, Le Bon SD, Rodriguez A, et al. Olfactory and gustatory dysfunctions as a clinical presentation of mild-to-moderate forms of the coronavirus disease (COVID-19): a multicenter European study. Eur Arch Oto-Rhino-L. 2020;277(8):2251–2261.

33. Lewis, A., Frontera, J., Placantonakis, D. G., Lighter, J., Galetta, S., Balcer, L., & Melmed, K. R. (2021). Cerebrospinal fluid in COVID-19: A systematic review of the literature. *J Neurol Sci, 421*, 117316. doi:10.1016/j.jns.2021.117316
34. Mao, L. et al. Neurologic Manifestations of Hospitalized Patients With Coronavirus Disease 2019 in Wuhan, China. JAMA neurology 77, 683-690, doi:10.1001/jamaneurol.2020.1127 (2020).
35. Matschke J, Lu¨tgehetmann M, Hagel C, Sperhake JP, Schro¨der AS, Edler C, et al. Neuropathology of patients with COVID-19 in Germany: a post-mortem case series. Lancet Neurol. 2020;19(11):919–929.
36. Muccioli L, Pensato U, Cani I, Guarino M, Cortelli P, Bisulli F. COVID-19-associated encephalopathy and cytokine-mediated neuroinflammation. Ann Neurol. 2020;88(4):860–861.
37. Mukerji, S. S., & Solomon, I. H. (2021). What can we learn from brain autopsies in COVID-19? *Neurosci Lett, 742*, 135528. doi:10.1016/j.neulet.2020.135528
38. Ousseiran, Z. H., Fares, Y., & Chamoun, W. T. (2021). Neurological manifestations of COVID-19: a systematic review and detailed comprehension. *Int J Neurosci*, 1-16. doi:10.1080/00207454.2021.1973000
39. Paterson RW, Brown RL, Benjamin L, Nortley R, Wiethoff S, Bharucha T, et al. The emerging spectrum of COVID-19 neurology: clinical, radiological and laboratory findings. Brain. 2020;143(10):3104–3120.
40. Pilotto A, Odolini S, Masciocchi S, Comelli A, Volonghi I, Gazzina S, et al. Steroid-responsive encephalitis in coronavirus disease 2019. Ann Neurol. 2020;88(2):423–427.
41. Pujadas E, Beaumont M, Shah H, Schrode N, Francoeur N, Shroff S, et al. Molecular Profiling of Coronavirus Disease 2019 (COVID-19) Autopsies Uncovers Novel Disease Mechanisms. Am J Pathol. 2021;191(12):2064–2071.
42. Romano M, Ruggiero A, Squeglia F, Maga G, Berisio R. A structural view of SARS-CoV-2 RNA replication machinery: RNA synthesis, proofreading and final capping. Cells. 2020;9(5):1267.
43. Semerdzhiev, S. A., Fakhree, M. A. A., Segers-Nolten, I., Blum, C., & Claessens, M. M. A. E. (2022). Interactions between SARS-CoV-2 N-Protein and α-Synuclein Accelerate Amyloid Formation. ACS Chemical Neuroscience, 13(1), 143-150. doi:10.1021/acschemneuro.1c00666
44. Sulzer, D. (2007). Multiple hit hypotheses for dopamine neuron loss in Parkinson's disease. *Trends Neurosci, 30*(5), 244-250.
45. Sulzer, D., Antonini, A., Leta, V., Nordvig, A., Smeyne, R. J., Goldman, J. E., . . . Ray Chaudhuri, K. (2020). COVID-19 and possible links with Parkinson's disease and parkinsonism: from bench to bedside. *npj Parkinson's Disease, 6*, 18-18. doi:10.1038/s41531-020-00123-0
46. Tandon, M., Kataria, S., Patel, J., Mehta, T. R., Daimee, M., Patel, V., . . . Sriwastava, S. (2021). A Comprehensive Systematic Review of CSF analysis that defines Neurological Manifestations of COVID-19. *Int J Infect Dis, 104*, 390-397. doi:10.1016/j.ijid.2021.01.002
47. Tanner, C. M., Ottman, R., Goldman, S. M., Ellenberg, J., Chan, P., Mayeux, R., & Langston, J. W. (1999). Parkinson disease in twins: an etiologic study. *Jama, 281*(4), 341-346. doi:10.1001/jama.281.4.341
48. Tao K, Tzou PL, Nouhin J, Gupta RK, de Oliveira T, Kosakovsky Pond SL, et al. The biological and clinical significance of emerging SARS-CoV-2 variants. Nat Rev Genet. 2021;22(12):757–773.

49. Tay MZ, Poh CM, R´enia L, MacAry PA, Ng LF. The trinity of COVID-19: immunity, inflammation and intervention. Nat Rev Immunol. 2020;20(6):363–374.
50. Virhammar J, Kumlien E, F¨allmar D, Frithiof R, Jackmann S, Sk¨old MK, et al. Acute necrotizing encephalopathy with SARS-CoV-2 RNA confirmed in cerebrospinal fluid. Neurology. 2020;95(10):445–449.
51. Wu Y, Xu X, Chen Z, Duan J, Hashimoto K, Yang L, et al. Nervous system involvement after infection with COVID-19 and other coronaviruses. Brain Behav Immun. 2020;87:18–22.
52. Zhang BZ, Chu H, Han S, Shuai H, Deng J, Hu Yf, et al. SARS-CoV-2 infects human neural progenitor cells and brain organoids. Cell Res. 2020;30(11):60131.
53. Zhou P, Yang XL, Wang XG, Hu B, Zhang L, Zhang W, et al. A pneumonia outbreak associated with a new coronavirus of probable bat origin. Nature. 2020;579(7798):270–273.
54. Ziebuhr J. The coronavirus replicase. vol. 287. Springer; 2005.

AIM AND RATIONALE OF THE STUDIES

The aim of this PhD Thesis was to evaluate the neuropathological alterations underlying neurological manifestations in COVID-19, and assess the short- and (possible) long-term consequences of COVID-19 on the nervous system. For this purpose, we present a collection of seven peer-reviewed articles which aim to define the role of SARS-CoV-2 and COVID-19 on the peripheral nervous system, on peripheral chemoreceptorial structures, and on the central nervous system. While particular focus has been given to post-mortem investigations and neuropathology underlying COVID-19, we also evaluated the link between in-vivo neurological manifestations and viral genomic variants to further characterize the disease.

The following papers, published in peer-reviewed international journals, were selected for the purpose of this thesis:

Chapter 1: Covid-19, nervous system pathology, and Parkinson's disease: Bench to bedside. International Review of Neurobiology, 2022. doi:10.1016/bs.irn.2022.06.006
Authors: Emmi A., Bura I., Rader V., Matthew D., Sulzer D., Goldman J., Leta V.
In this paper, we reviewed the literature concerning SARS-CoV-2 infection and COVID-19 neuropathology and their possible links with neurodegenerative disease, with particular regard to Parkinson’s Disease.

Chapter 2: Smell deficits in COVID-19 and possible links with Parkinson's disease. International Review of Neurobiology, 2022. doi:10.1016/bs.irn.2022.08.001**.**
Authors: Emmi A., Sandre M., Porzionato A., Antonini A.
In this paper, we evaluated the mechanisms underlying olfactory dysfunction in COVID-19 and reviewed the mechanisms underlying olfactory-transmucosal transmission towards the CNS of the coronaviridae family (SARS-CoV, SARS-CoV-2, and MERS-CoV), focusing on SARS-CoV-2 and possible implications for Parkinson’s Disease.

Chapter 3: Sympathetic Activation: a potential link between comorbidities and COVID-19. FEBS Journal. doi: 10.1111/febs.15481
Authors: Porzionato A., Emmi A., Barbon S., et al.

In this opinion paper, published at the beginning of the SARS-CoV-2 pandemic in Europe, we hypothesized the potential role of sympathetic dysfunction as a link between comorbidities and COVID-19. While initially an opinion paper, most hypotheses presented were confirmed by subsequent experimental research that also constitutes part of this thesis.

Chapter 4: Genomic surveillance of SARS-CoV-2 in patients presenting neurological manifestations. PLOS One, 2022. doi: https://doi.org/10.1371/journal.pone.0270024.
Authors: Vicco A., Caccuri F., Messali S., Vitiello A., Emmi A., et al.
In this article, we investigated SARS-CoV-2 genomic variants in relationship to neurological manifestations in hospitalized COVID-19 patients. While we detected several mutations in the viral genome of COVID-19 patients, no association was found between viral variants and neurological manifestations, suggesting that individual immune response may represent the more likely factor in mediating COVID-19 neuropathology.

Chapter 5: Neuroinflammation, SARS-CoV-2 Antigens and Viral Genomic Sequences in the Human Brainstem: implications for neurodegenerative diseases. Under Review.
Authors: Emmi A., Rizzo S., Barzon S., et al.
In this neuropathological study, we examined the brains of 24 COVID-19 patients and 18 age and sex matched control subjects who died due to other respiratory infections / pneumonia.
Our findings suggest that SARS-CoV-2 may gain access to the central nervous system in a subset of fatal COVID-19 cases, and viral antigens / genomic sequences can be detected within the anatomically defined boundaries of the vagal nuclei of the medulla and the substantia nigra of the brainstem; this is also coherent with animal models of the disease and with viral tropism of other Coronaviruses, suggesting a similar pattern of invasion. However, we did not detect neuropathological alterations directly ascribable to the presence of viral antigens, aside from increased microglial densities within affected anatomical loci. This suggest that while acute fatal COVID-19 is characterized by neuropathological alterations, such as hypoxic / ischaemic damage, microthromboses and microgliosis, mediated mainly by systemic infection and the ongoing cytokine storm, SARS-CoV-2 neurotropism is a possible, yet not frequent, consequence of infection that does not appear to directly damage the brain, at least in the acute phases of the disease.

When comparing microglial phenotypes and densities between COVID-19 patients and pneumonia subjects, we detected significantly higher microglial densities in the medulla and midbrain of COVID-19 subjects, and a peculiar phenotype with thorny morphology expressing both homeostatic (TMEM119) and activated (HLA-DR and CD68) markers. Overall, the study helps to define the neuropathology occurring in the acute phases of severe COVID-19 cases, and allows to have a realistic measure of occurring neuroinflammation by comparison with alterations found in other respiratory infections.

Chapter 6: The potential role of the carotid body in COVID-19. American Journal of Physiology - Lung. doi:10.1152/ajplung.00309.2020
Authors: Porzionato A., Emmi A., Stocco E., Barbon S., et al.
In this article, we hypothesize the possible role of peripheral chemoceptors, and in particular the Carotid Body, in COVID-19. As an opinion paper published in the first phases of the SARS-CoV-2 pandemic, we aimed to define the potential role of the carotid body, responsible for chemoception and oxygen sensing at the level of the carotid bifurcation, in COVID-19, and the possible consequences of SARS-CoV-2 infection of this structure. Subsequent experimental work allowed us to demonstrate the hypothesized phenomena described in this article.

Chapter 7: The Carotid Body in COVID-19: histopathological and virological analyses of an autopsy case series. Frontiers in Immunology. doi: https://doi.org/10.3389/fimmu.2021.736529.
Authors: Porzionato A., Emmi A., Contran M., et al.
In this article, we investigated the histopathological alterations occurring in the Carotid Body of deceased COVID-19 subjects and compared them with age matched controls. We identified instances of SARS-CoV-2 viral antigens and viral genomic sequences in the Carotid Bodies of COVID-19 subjects, accompanied by small vessel thromboses and diffuse lympho-monocytic infiltrations. These findings suggest viral infection of the Caritody Body, with subsequent disruption of peripheral chemocheption at the level of the carotid bifurcation.

Chapter 1

COVID-19, Parkinson's disease and nervous system pathology: bench to bedside

The present chapter has been previously published in: ***Emmi A.****, Bura I., Rader V., Matthew D., Sulzer D., Goldman J., Leta V. Covid-19, nervous system pathology, and Parkinson's disease: Bench to bedside. International Review of Neurobiology, 2022. doi:10.1016/bs.irn.2022.06.006*

ABSTRACT

Coronavirus disease 2019 (COVID-19) caused by Severe Acute Respiratory Syndrome Coronavirus 2 (SARS-CoV-2) infection is primarily regarded as a respiratory disease; however, multisystemic involvement accompanied by a variety of clinical manifestations, including neurological symptoms and neuroinflammatory features are commonly observed. There is, however, little evidence supporting SARS-CoV-2 infection of central nervous system cells, and neurological symptoms for the most part appear to be due to damage mediated by hypoxic/ischemic and/or inflammatory insults. In this chapter, we report evidence on candidate neuropathological mechanisms underlying neurological manifestations in COVID-19, suggesting that while there is mostly evidence against SARS-CoV-2 entry into brain parenchymal cells as a mechanism that may trigger Parkinson's disease and parkinsonism, that there are multiple means by which the virus may cause neurological symptoms.

INTRODUCTION

Severe Acute Respiratory Syndrome Coronavirus 2 (SARS-CoV-2) is a novel, highly contagious, and pathogenic strain of the Coronaviruses (CoV) family, which has caused the pandemic of coronavirus disease 2019 (COVID-19) (Hu, Guo, Zhou, & Shi, 2021; Lai, Shih, Ko, Tang, & Hsueh, 2020). Emerging in late 2019, SARS-CoV-2 has taken a toll on global morbidity and mortality as a major public health issue. Although manifesting primarily as a respiratory disease, there are numerous reports of neurological manifestations of COVID-19, either presenting as new symptoms or disorders (e.g., stroke, encephalitis, Guillain-Barré syndrome) or as the exacerbation of pre-existing symptoms of known chronic neurological conditions (Kubota & Kuroda, 2021; Ousseiran, Fares, & Chamoun, 2021). These observations, along with the detection of the virus in post-mortem tissue and cerebrospinal fluid (CSF) (Lewis et al., 2021; Mukerji & Solomon, 2021; Tandon et al., 2021) raise the question of whether SARS-CoV-2 enters the human brain or causes neurological symptoms because of the systemic illness, notably hypoxia and inflammation.

SARS-COV-2 RECEPTORS

SARS-CoV-2 shares 80% of its genome with SARS-CoV and 50% with MERS-CoV, with homologies extending to the protein spike (S), which after cleavage by the transmembrane protease serine 2 (TMPRSS2), can bind host membrane proteins acting as viral receptors.(Xu et al., 2020)(Hoffmann et al., 2020)

The main viral receptor for SARS-CoV-2 and other CoVs is angiotensin-converting enzyme 2 (ACE2), an enzyme that catalyzes the cleavage of angiotensin I into angiotensin 1-9 and angiotensin II into the vasodilator angiotensin 1-7 (Wang et al., 2020). ACE2 is a transmembrane protein that is widely expressed in human tissues, and while its expression in brain neurons and astrocytes has not been clearly demonstrated, it is expressed in brain vessels (Hamming et al., 2004) and hypoxic insult appears to upregulate its expression.(R. Zhang et al., 2009)

Similarly to MERS-CoV, virus cellular endocytosis may be alternatively mediated by sialic acid residues, which are located on plasma membrane proteins of several type of cells, including neurons (Fantini, Di Scala, Chahinian, & Yahi, 2020) or by the lectin CD209L,

which is a receptor for SARS-CoV (Jeffers et al., 2004), although such alternative receptors have not been clearly demonstrated for SARS-CoV-2.

NEUROINFLAMMATION IN POST-MORTEM COVID-19 BRAIN

Neuroinflammation is prominent in COVID-19 and characterized by lympho-monocytic infiltrations, microglial activation and microglial nodules. Lympho-monocytic perivascular cuffing and infiltration have been reported by most authors, with a predominance of perivascular CD68+ monocytes/macrophages and CD8+ T-cells (Lee et al., 2021; Matschke et al., 2020; Meinhardt et al., 2021; Schwabenland et al., 2021; Thakur et al., 2021), although lymphocyte accumulation appears mild compared to that in viral encephalitis, such as from Herpes.

In all studies examining microglial cells, authors identified prominent microglial activation with upregulation of MHC-II proteins (HLA-DR) and increased lysosomal activity (CD68+), while maintaining a homeostatic microglial marker TMEM119 (Deigendesch et al., 2020; Matschke et al., 2020; Meinhardt et al., 2021; Schwabenland et al., 2021; Thakur et al., 2021). Similarly, evidence of neuronophagia was documented by most authors with prominent involvement of the lower brainstem at the level of the medullary tegmentum, the midline raphe, inferior olivary nucleus, and the dorsal pons (Al-Dalahmah et al., 2020; Deigendesch et al., 2020; Matschke et al., 2020; Meinhardt et al., 2021; Schwabenland et al., 2021; Thakur et al., 2021). Microglial nodules with associated CD8+/ CD3+ T-cell clusters were also documented in most, but not all, COVID-19 patients, in contrast to non-COVID-19 controls and ExtraCorporeal Membrane Oxygenation (ECMO) patients, which displayed no instances of microglial nodules and neuronophagia (Schwabenland et al., 2021), although we have observed activated microglia and nodules in the brainstems of patients with severe respiratory distress (JE Goldman, P Canoll, unpublished observations). Deep spatial profiling of the local immune response in COVID-19 brains by imaging mass spectrometry revealed significant immune activation in the medulla and olfactory bulb with a prominent role mediated by CD8+ T-cell - microglia crosstalk in the parenchyma (Schwabenland et al., 2021). Conversely, Deigendesch and colleagues found significant differences in HLA-DR+ activated microglia when comparing COVID-19 subjects to non-septic controls, but no differences were found with patients who had died under septic

conditions; according to the authors, this may represent a histopathological correlate of critical illness-related encephalopathy and hypoxia, rather than a COVID-19-specific finding. Neurological symptoms of COVID-19 occur regularly without detection of SARS-CoV-2 in CSF samples, but there is evidence for autoantibody formation. In a cohort of 102 COVID-19 patients, where almost 60% presented some form of neurological symptoms, CSF anti-neuronal autoantibodies were detected in 35% of those tested (Fleischer et al., 2021). In a study of critically ill COVID-19 patients (n=11) with unexplained neurological sequelae, anti-neuronal autoantibodies were found in the CSF of all patients, as well as in their serum, suggesting that multiple autoantigens and a potential molecular mimicry to SARS-CoV-2 might mediate these symptoms, especially those related to hyperexcitability (myoclonus, seizures) (Franke et al., 2021). The above findings might guide clinicians to consider administering immunotherapy in selected patients.

Thus, while most studies are consistent on the overall neuroinflammatory conditions occurring in the context of COVID-19, with particular focus on microgliosis and microglia – T-cell crosstalk, disagreements on the source of inflammation are unresolved. In particular, it is not clear how much might be due to an ongoing systemic inflammation/cytokine storm, and whether and how frequent comorbidities, such as hypertension, diabetes, cardiovascular disease or neurodegenerative conditions, and hypoxic/ischemic damage may influence microgliosis and brain inflammation.

Little evidence of neuro-invasion in post-mortem COVID-19 cases

Neurotropism has been established for many species of the CoV family, including Middle East Respiratory Syndrome (MERS-CoV) and severe acute respiratory syndrome (SARS-CoV-1) (Zubair et al., 2020), while there have been reports for persistent chronic infections of particular CoV strains in human neuronal cell lines or in the brain of patients with neurodegenerative disorders (Arbour et al., 1999; Murray, Brown, Brian, & Cabirac, 1992). SARS-CoV-2 has been speculated to possess a neuro-invasive potential (Koyuncu, Hogue, & Enquist, 2013; Verstrepen, Baisier, & De Cauwer, 2020; Yachou, El Idrissi, Belapasov, & Ait Benali, 2020), and has been claimed in experimental models (Bullen et al., 2020). However, while there is significant evidence for neuroinflammation in the brain induced by SARS-CoV-2, as detailed here, neuropathological findings at this juncture do not support significant infection of brain cells.

To date, the presence of viral peptides in brain, determined by immunostaining, has been reported only in a small set of patients and in a few cells, and has not been constantly reproduced throughout available studies (Lee et al., 2021; Matschke et al., 2020; Meinhardt et al., 2021; Schwabenland et al., 2021; Solomon et al., 2020; Thakur et al., 2021; Yang et al., 2021). While most studies agree on the detection of low or undetectable viral RNA levels using RT-PCR analyses, detection of viral RNA in blood and blood vessels of the investigated samples cannot be excluded. In contrast, immunoperoxidase and immunofluorescent staining, imaging mass spectrometry and *in situ* hybridization that provide for the spatial localization of viral proteins/RNA have failed to consistently detect viral antigens or RNA. Matschke and colleagues found sparse immunoreactive cells throughout the brainstem, without specific topographic localization, but also detected distinct immunoreactivity of the glossopharyngeal and vagus nerve bundles (CN IX-X) in a subset of patients, and suggested SARS-CoV-2 retrograde spread through these cranial nerves towards the medulla (Matschke et al., 2020). This is also supported by the detection of SARS-CoV-2 antigen and genomic sequences in the carotid body of COVID-19 subjects (Porzionato, Emmi, et al., 2021). However, there was no apparent association between the presence of viral antigens and neuropathological changes.

Several studies have detected viral proteins and RNA in the olfactory mucosa through immunohistochemistry, immunofluorescence and in-situ hybridization, as well as electron microscopy (Meinhardt et al., 2021); Khan et al., 2021; Zazhystka et al., 2022). Meinhardt et al. observed SARS-CoV-2 spike protein in primary olfactory neurons of the olfactory mucosa, suggesting an olfactory-transmucosal spread of the virus. This was supported by the detection of viral RNA at the level of the olfactory bulb and medulla, even though viral proteins were not detected in non-vascular cells. Furthermore, SARS-CoV-2 immunoreactive endothelial cells associated with microvascular injury and micro-thromboses were found in a subset of COVID-19 patients at the level of the medulla. Conversely, two recent studies found virus in sustentacular cells of the olfactory epithelium, but not in olfactory neurons (Khan et al., 2021; Zazhystka et al., 2022). The latter detected reorganization of nuclear architecture and downregulation of olfactory receptors, as well as their signaling pathways, in the olfactory neurons, suggesting a non-cell autonomous cause of anosmia (Zazhytska et al., 2022).

Schwabenland and colleagues detected viral antigen in ACE2-positive cells enriched in the vascular compartment (Schwabenland et al., 2021). According to the authors, this finding was linked to vascular proximity and ACE2 expression, and was correlated to the

perivascular immune activation patterns of CD8+ and CD4+ T-cells and myeloid- and microglial-cell subsets, indicating a fundamental role of the vascular and perivascular compartment, as well as a blood-brain-barrier impairment in mediating COVID-19-specific neuroinflammation.

Two studies of single nucleus RNA sequencing of brains of COVID-19 patients detected broad perturbations, with upregulation of genes involved in innate antiviral response and inflammation, microglia activation and neurodegeneration, but found no direct evidence of viral RNA (Yang et al., 2021); Fullard et al., 2021). Other authors have not detected viral proteins/ RNA through immunohistochemistry or *in-situ* hybridization, even though viral genomic sequences were found with RT-PCR assays (Lee et al., 2021; Solomon et al., 2020; Thakur et al., 2021).

Hence, SARS-CoV-2 invasion of the CNS remains to be definitively shown, and much evidence points against the presence of detectable virus, although there are reports of rare instances of the presence of viral antigens in brain cells.

SARS-COV-2 AND PARKINSONISM

Understandably, the idea that neuronal infection by SARS-CoV-2 might predispose to parkinsonism has been a source of great concern (Beauchamp, Finkelstein, Bush, Evans, & Barnham, 2020; Bouali-Benazzouz & Benazzouz, 2021; Brundin, Nath, & Beckham, 2020), although, fortunately, there is little evidence supporting this response. Although there are no reports of CoV-associated parkinsonism, antibodies against common CoV have been detected in the CSF of people with Parkinson's Disease (PwP, PD) in significantly higher titers compared to controls, while there was evidence of post-encephalitic parkinsonism in mice infected with a CoV strain (MHV-A59) (Fazzini, Fleming, & Fahn, 1992; Fishman et al., 1985).

The concerns on COVID-19 influence on Parkinson's disease stem both from the 1917 Spanish flu/ von Economo's encephalitis pandemics as well an association of numerous viruses with the development of transient or permanent parkinsonism (Jang, Boltz, Webster, & Smeyne, 2009), including reports that anti-viral treatment and vaccination are associated with a decreased risk of parkinsonism in humans and animal models (Lin et al., 2019; Sadasivan, Sharp, Schultz-Cherry, & Smeyne, 2017). It has been suggested that pathogens contribute to PD pathogenesis, particularly after the age of 50 in individuals with or without

a susceptible genetic substrate (Beauchamp et al., 2020; Tanner et al., 1999). Braak and others have suggested that neurotropic pathogens may infect the CNS via the nasal or gastric pathway, both of which are sites of early pathology in PD (Hawkes, Del Tredici, & Braak, 2007; Klingelhoefer & Reichmann, 2015) and viral-related inflammation might render the CNS susceptible to preceding or subsequent stressors (D. Sulzer, 2007). Indeed, a meta-analysis demonstrated that a past history of an infection was associated with a 20% higher risk of presenting PD in the future, although this was significant only for bacterial and not viral infections (Meng, Shen, & Ji, 2019). An association between past CNS infections, particularly if multiple hospitalizations preceded, and a subsequent development of PD are described (Fang et al., 2012). Finally, epidemiological data from a large cohort of PD patients and controls indicates an increased PD frequency among occupations with a high risk for respiratory infections, such as teachers and healthcare workers, (the “clustering of PD” theory) (Tsui, Calne, Wang, Schulzer, & Marion, 1999).

While there is little evidence at this time for a role for COVID-19 in increasing PD, there could be effects particularly on peripheral catecholamine systems. L-Dopa decarboxylase (DDC), an essential enzyme in the biosynthesis of dopamine and serotonin, is the most significantly co-expressed and co-regulated gene with ACE2 in non-neuronal cell types, significantly affecting dopamine blood levels (Nataf, 2020). A SARS-CoV-2 infection of monkey cell lines was found to induce downregulation of DDC, an effect also noted with dengue and hepatitis C infections (Mpekoulis et al., 2021), pathogens associated with parkinsonism (Bopeththa & Ralapanawa, 2017; Tsai et al., 2016). DDC levels rose in nasopharyngeal tissues of asymptomatic or mild severity COVID-19 patients, while an inverse relationship was noted between SARS-CoV-2 RNA levels and DDC expression (Mpekoulis et al., 2021). Moreover, a dopamine D1 receptor agonist was found to suppress endotoxin-induced pulmonary inflammation in mice, suggesting that a potential protective role of dopamine in inflammation needs to be further explored (Bone, Liu, Pittet, & Zmijewski, 2017).

Vascular damage constitutes a recognized complication of COVID-19 (Siddiqi, Libby, & Ridker, 2021). A case of bilateral basal ganglia insult in the context of a thromboembolic encephalopathy without parkinsonism in a COVID-19 patient has been described (Haddadi, Ghasemian, & Shafizad, 2020).

Peripheral and olfactory pathways that may contribute to neuroinflammation

Olfactory pathways. SARS-CoV-1 enters the brain of transgenic mice via the olfactory bulb, causing neuronal death without signs of encephalitis (Netland, Meyerholz, Moore, Cassell, & Perlman, 2008), while intranasal inoculation of MERS-CoV in transgenic mice led to high levels of the virus in the CNS, particularly in the thalamus and the brainstem (Li et al., 2016). The characteristic clinical symptoms of hyposmia or anosmia in COVID-19, as well as hypogeusia or ageusia, which are quite prominent among affected patients (Guerrero et al., 2021) support the hypothesis of an involvement of the olfactory organ (Lechien et al., 2020). An increased SARS-CoV-2 viral load in the nasal epithelium have been found by RT-PCR *in situ* hybridization and immunohistochemical staining methods (Meinhardt et al., 2021). Moreover, a prospective autopsy study in Netherlands involving 21 patients who had succumbed to COVID-19 complications revealed extensive inflammation in the brain among other tissues, particularly focused in the olfactory bulbs and the medulla oblongata, although this study did not reveal virus in the brain (Schurink et al., 2020). Politi and colleagues described a case report of a COVID-19-positive woman with anosmia, who presented with subtle hyperintensities in the olfactory bulbs and the right gyrus rectus in brain magnetic resonance imaging (MRI), although the authors highlight that this was not a consistent finding among COVID-19 patients with smell dysfunction (Politi, Salsano, & Grimaldi, 2020). A recently published paper, exploring the findings of brain scans before and after a SARS-CoV-2 infection in a large sample of UK Biobank participants, showed significant reductions in grey matter thickness and tissue-contrast in the orbitofrontal cortex and parahippocampal gyrus, along with prominent alterations in brain areas functionally connected to the primary olfactory cortex, suggestive of tissue damage (Douaud et al., 2022), although it is difficult to correlate the scan findings with cellular pathology. Furthermore, post-mortem brain MRI studies in 19 decedents of COVID-19 demonstrated an asymmetry in the olfactory bulbs in about 20% of the patients (Coolen et al., 2020). Post-mortem studies of COVID-19 patients detected the virus in the sustentacular cells of the olfactory epithelium, but not in the olfactory receptor neurons or the olfactory bulbs (Khan et al., 2021), as noted above.

Enteric pathways. With both respiratory and gastrointestinal symptoms quite common in the context of COVID-19 (Cares-Marambio et al., 2021; Groff et al., 2021) and ACE2 being highly expressed in the alveolar epithelial type II cells and the intestinal endothelial cells (Williams et al., 2021), some researchers have suggested the potential of SARS-CoV-2

entry through the intestine (Lehmann et al., 2021; Mönkemüller, Fry, & Rickes, 2020; H. Zhang et al., 2020). RNA of the SARS-CoV-2 has been identified in stool samples and rectal swabs, even in cases with negative nasopharyngeal swabs (Tang, Schmitz, Persing, & Stratton, 2020).. An autopsy study (n=21) revealed SARS-CoV-2-infected cells in the respiratory and gastrointestinal tract, among other tissues, along with extensive inflammation in the medulla oblongata, implying a potential effect on the respiratory control centre (Schurink et al., 2020). Many studies report inflammation in the medulla (see above), but the link between peripheral organs and the brain is not clear. One possible way in which systemic inflammation can influence medullary nuclei is the activation of vagal medullary afferents by inflammatory molecules. Thus, vagal endings contain receptors to IL-1□□and are activated by this cytokine, subsequently activating neurons of the solitary nucleus, which then activate sympathetic output from the vagal nucleus and the nucleus ambiguous through the vagus nerve (Pavlov et al., 2012).

Vascular pathways. Non-neuronal pathways of SARS-CoV-2 that might lead to neuroinflammation must be considered, including the hematogenous route. SARS-CoV-2 can enter the blood stream and either access and damage the endothelium of brain vasculature to cross the BBB, or trigger an inflammatory response, leading to breakdown of the BBB (Meinhardt et al., 2021; Wan et al., 2021).

Cerebrovascular disease, including ischemic and hemorrhagic strokes, constitutes a severe and common complication in COVID-19 (Tsivgoulis et al., 2020). The brains of patients who did not survive COVID-19 show acute cerebrovascular disease, including thrombotic microangiopathy and endothelial injury, without any evidence of vasculitis (Hernández-Fernández et al., 2020; Wan et al., 2021). Accumulating data suggests that COVID-19 is connected to a hypercoagulable state, which is closely related to inflammation and predisposes to macro- and microvascular thrombosis, resulting in arterial and venous infarcts (Abou-Ismail, Diamond, Kapoor, Arafah, & Nayak, 2020).

ACE2 is expressed in cells of the vasculature in the human brain, although the specific cell types have not been defined (Hamming et al., 2004). TMPRSS2 and NRP1 are also present in the endothelial cells of the vasculature (Wan et al., 2021). SARS-CoV-2 endothelitis has also been confirmed in autopsy studies concerning other human tissues (lungs, kidney, heart, liver, small intestine) (Varga et al., 2020). Moreover, Pellegrini and colleagues showed a leakage across the BBB, using a model of the human choroid plexus epithelial cells

infected by SARS-CoV-2 (Pellegrini et al., 2020), although one has to consider the results of such *in vitro* studies carefully, since they may not reflect what occurs in the living brain.
On the other hand, a SARS-CoV-2 infection can cause an excessive systemic inflammatory response after triggering a cytokine storm in the periphery, resulting in a BBB disruption (David Sulzer et al., 2020). Researchers have suggested that SARS-CoV-2 may infect immune cells, using them as a “trojan horse” to invade the CNS via the impaired BBB or activate different populations of immune cells, which may infiltrate the CNS, causing a secondary cytokine storm and thus neurologic manifestations (Pezzini & Padovani, 2020; Wan et al., 2021; Williams et al., 2021).

Hypoxia and ischemia. Finally, hypoxic/ischemic changes of the brain due to respiratory abnormalities and hypoperfusion in the context of COVID-19 appear likely to play a crucial role in the development of secondary neurological manifestations (Sullivan & Fischer, 2021). Cases of hypoxic brain injury following Acute Respiratory Distress Syndrome (ARDS) have been described in the literature, including cases of parkinsonism, with the authors highlighting the possibility of silent hypoxia (Ayele et al., 2021; Fearon, Mikulis, & Lang, 2021; Radnis et al., 2020). However, the fact that neurological complications have been reported in the absence of any respiratory symptoms, suggest that alternative mechanisms mediate the virus-induced CNS insults (Ellul et al., 2020).
Hypoxic/ischemic pathology is particularly common in COVID-19, being reported in most studies (Matschke et al., 2020; Solomon et al., 2020; Thakur et al., 2021). Alterations were mostly widespread, and both acute and subacute findings could be appreciated at the level of the cortex, the basal ganglia, the hippocampus and, most notably, the brainstem. Hypoxic/ischemic damage can be associated with vascular pathology, with numerous reported cases presenting both ischemic and hemorrhagic infarcts (Lee et al., 2021; Matschke et al., 2020; Remmelink et al., 2020; Thakur et al., 2021), Reactive astrogliosis in the context of hypoxic/ischemic injuries was also commonly encountered, prominently involving the basal ganglia and the brainstem (Matschke et al., 2020; Meinhardt et al., 2021; Thakur et al., 2021). Microvascular pathology, fibrinogen leakage and small vessel thromboses were associated with ischemic and vascular pathology, representing a characteristic finding of the COVID-19 cohorts (Lee et al., 2021; Matschke et al., 2020; Meinhardt et al., 2021; Porzionato, Emmi, et al., 2021; Porzionato, Stocco, et al., 2021; Schwabenland et al., 2021). Small vessel platelet-enriched microthrombi were predominantly found in the basal ganglia, brainstem and cerebellum, often associated to

microvascular injury and fibrinogen leakage. Several instances of SARS-CoV-2 immunoreactive endothelial cells in the context of vascular injury were also detected (Meinhardt et al., 2021), indicating a prominent role of SARS-CoV-2 infection in determining COVID-19 associated small vessel pathology.

CONCLUSIONS

Although COVID-19 caused by SARS-CoV-2 infection is mainly regarded as a respiratory disease, a variety of clinical manifestations, including neurological symptoms, often occur. The evidence available to date suggests that COVID-19 does not significantly contribute to the incidence of Parkinson's disease and that neurological clinical manifestations observed in the context of COVID-19 are mainly secondary to an indirect damage by SARS-CoV-2 in peripheral systems, in contrast to infection of CNS neurons and astrocytes.

REFERENCES

55. Abou-Ismail, M. Y., Diamond, A., Kapoor, S., Arafah, Y., & Nayak, L. (2020). The hypercoagulable state in COVID-19: Incidence, pathophysiology, and management. *Thromb Res, 194*, 101-115. doi:10.1016/j.thromres.2020.06.029
56. Al-Dalahmah, O., Thakur, K. T., Nordvig, A. S., Prust, M. L., Roth, W., Lignelli, A., . . . Canoll, P. (2020). Neuronophagia and microglial nodules in a SARS-CoV-2 patient with cerebellar hemorrhage. *Acta Neuropathologica Communications, 8*(1), 147. doi:10.1186/s40478-020-01024-2
57. Arbour, N., Côté, G., Lachance, C., Tardieu, M., Cashman, N. R., & Talbot, P. J. (1999). Acute and persistent infection of human neural cell lines by human coronavirus OC43. *J Virol, 73*(4), 3338-3350. doi:10.1128/jvi.73.4.3338-3350.1999
58. Ayele, B. A., Demissie, H., Awraris, M., Amogne, W., Shalash, A., Ali, K., . . . Venkatasubba Rao, C. P. (2021). SARS-COV-2 induced Parkinsonism: The first case from the sub-Saharan Africa. *Clinical parkinsonism & related disorders, 5*, 100116-100116. doi:10.1016/j.prdoa.2021.100116
59. Beauchamp, L. C., Finkelstein, D. I., Bush, A. I., Evans, A. H., & Barnham, K. J. (2020). Parkinsonism as a Third Wave of the COVID-19 Pandemic? *Journal of Parkinson's disease, 10*(4), 1343-1353. doi:10.3233/JPD-202211
60. Bone, N. B., Liu, Z., Pittet, J.-F., & Zmijewski, J. W. (2017). Frontline Science: D1 dopaminergic receptor signaling activates the AMPK-bioenergetic pathway in macrophages and alveolar epithelial cells and reduces endotoxin-induced ALI. *Journal of leukocyte biology, 101*(2), 357-365. doi:10.1189/jlb.3HI0216-068RR
61. Bopeththa, B., & Ralapanawa, U. (2017). Post encephalitic parkinsonism following dengue viral infection. *BMC Res Notes, 10*(1), 655. doi:10.1186/s13104-017-2954-5
62. Bouali-Benazzouz, R., & Benazzouz, A. (2021). COVID-19 Infection and Parkinsonism: Is There a Link? *Mov Disord, 36*(8), 1737-1743. doi:10.1002/mds.28680
63. Brundin, P., Nath, A., & Beckham, J. D. (2020). Is COVID-19 a Perfect Storm for Parkinson's Disease? *Trends Neurosci, 43*(12), 931-933. doi:10.1016/j.tins.2020.10.009
64. Bullen, C. K., Hogberg, H. T., Bahadirli-Talbott, A., Bishai, W. R., Hartung, T., Keuthan, C., . . . Smirnova, L. (2020). Infectability of human BrainSphere neurons suggests neurotropism of SARS-CoV-2. *Altex, 37*(4), 665-671. doi:10.14573/altex.2006111
65. Cares-Marambio, K., Montenegro-Jiménez, Y., Torres-Castro, R., Vera-Uribe, R., Torralba, Y., Alsina-Restoy, X., . . . Vilaró, J. (2021). Prevalence of potential respiratory symptoms in survivors of hospital admission after coronavirus disease 2019 (COVID-19): A systematic review and meta-analysis. *Chron Respir Dis, 18*, 14799731211002240. doi:10.1177/14799731211002240
66. Coolen, T., Lolli, V., Sadeghi, N., Rovai, A., Trotta, N., Taccone, F. S., . . . De Tiège, X. (2020). Early postmortem brain MRI findings in COVID-19 non-survivors. *Neurology, 95*(14), e2016-e2027. doi:10.1212/wnl.0000000000010116
67. Deigendesch, N., Sironi, L., Kutza, M., Wischnewski, S., Fuchs, V., Hench, J., . . . Frank, S. (2020). Correlates of critical illness-related encephalopathy predominate postmortem COVID-19 neuropathology. *Acta Neuropathol, 140*(4), 583-586. doi:10.1007/s00401-020-02213-y
68. Douaud, G., Lee, S., Alfaro-Almagro, F., Arthofer, C., Wang, C., McCarthy, P., . . . Smith, S. M. (2022). SARS-CoV-2 is associated with changes in brain structure in UK Biobank. *Nature*. doi:10.1038/s41586-022-04569-5

69. Ellul, M. A., Benjamin, L., Singh, B., Lant, S., Michael, B. D., Easton, A., . . . Solomon, T. (2020). Neurological associations of COVID-19. *The Lancet Neurology, 19*(9), 767-783. doi:10.1016/S1474-4422(20)30221-0
70. Fang, F., Wirdefeldt, K., Jacks, A., Kamel, F., Ye, W., & Chen, H. (2012). CNS infections, sepsis and risk of Parkinson's disease. *Int J Epidemiol, 41*(4), 1042-1049. doi:10.1093/ije/dys052
71. Fantini, J., Di Scala, C., Chahinian, H., & Yahi, N. (2020). Structural and molecular modelling studies reveal a new mechanism of action of chloroquine and hydroxychloroquine against SARS-CoV-2 infection. *International Journal of Antimicrobial Agents, 55*(5), 105960. doi:https://doi.org/10.1016/j.ijantimicag.2020.105960
72. Fazzini, E., Fleming, J., & Fahn, S. (1992). Cerebrospinal fluid antibodies to coronavirus in patients with Parkinson's disease. *Mov Disord, 7*(2), 153-158. doi:10.1002/mds.870070210
73. Fearon, C., Mikulis, D. J., & Lang, A. E. (2021). Parkinsonism as a Sequela of SARS-CoV-2 Infection: Pure Hypoxic Injury or Additional COVID-19-Related Response? *Mov Disord, 36*(7), 1483-1484. doi:10.1002/mds.28656
74. Fishman, P. S., Gass, J. S., Swoveland, P. T., Lavi, E., Highkin, M. K., & Weiss, S. R. (1985). Infection of the basal ganglia by a murine coronavirus. *Science (New York, N.Y.), 229*(4716), 877-879. doi:10.1126/science.2992088
75. Fleischer, M., Köhrmann, M., Dolff, S., Szepanowski, F., Schmidt, K., Herbstreit, F., . . . Stettner, M. (2021). Observational cohort study of neurological involvement among patients with SARS-CoV-2 infection. *Ther Adv Neurol Disord, 14*, 1756286421993701. doi:10.1177/1756286421993701
76. Franke, C., Ferse, C., Kreye, J., Reincke, S. M., Sanchez-Sendin, E., Rocco, A., . . . Prüß, H. (2021). High frequency of cerebrospinal fluid autoantibodies in COVID-19 patients with neurological symptoms. *Brain, behavior, and immunity, 93*, 415-419. doi:10.1016/j.bbi.2020.12.022
77. Groff, A., Kavanaugh, M., Ramgobin, D., McClafferty, B., Aggarwal, C. S., Golamari, R., & Jain, R. (2021). Gastrointestinal Manifestations of COVID-19: A Review of What We Know. *The Ochsner journal, 21*(2), 177-180. doi:10.31486/toj.20.0086
78. Guerrero, J. I., Barragán, L. A., Martínez, J. D., Montoya, J. P., Peña, A., Sobrino, F. E., . . . Ghotme, K. A. (2021). Central and peripheral nervous system involvement by COVID-19: a systematic review of the pathophysiology, clinical manifestations, neuropathology, neuroimaging, electrophysiology, and cerebrospinal fluid findings. *BMC Infect Dis, 21*(1), 515. doi:10.1186/s12879-021-06185-6
79. Haddadi, K., Ghasemian, R., & Shafizad, M. (2020). Basal Ganglia Involvement and Altered Mental Status: A Unique Neurological Manifestation of Coronavirus Disease 2019. *Cureus, 12*(4), e7869-e7869. doi:10.7759/cureus.7869
80. Hamming, I., Timens, W., Bulthuis, M. L., Lely, A. T., Navis, G., & van Goor, H. (2004). Tissue distribution of ACE2 protein, the functional receptor for SARS coronavirus. A first step in understanding SARS pathogenesis. *J Pathol, 203*(2), 631-637. doi:10.1002/path.1570
81. Hawkes, C. H., Del Tredici, K., & Braak, H. (2007). Parkinson's disease: a dual-hit hypothesis. *Neuropathol Appl Neurobiol, 33*(6), 599-614. doi:10.1111/j.1365-2990.2007.00874.x
82. Hernández-Fernández, F., Sandoval Valencia, H., Barbella-Aponte, R. A., Collado-Jiménez, R., Ayo-Martín, Ó., Barrena, C., . . . Segura, T. (2020). Cerebrovascular

disease in patients with COVID-19: neuroimaging, histological and clinical description. *Brain, 143*(10), 3089-3103. doi:10.1093/brain/awaa239
83. Hoffmann, M., Kleine-Weber, H., Schroeder, S., Krüger, N., Herrler, T., Erichsen, S., . . . Pöhlmann, S. (2020). SARS-CoV-2 Cell Entry Depends on ACE2 and TMPRSS2 and Is Blocked by a Clinically Proven Protease Inhibitor. *Cell, 181*(2), 271-280.e278. doi:10.1016/j.cell.2020.02.052
84. Hu, B., Guo, H., Zhou, P., & Shi, Z. L. (2021). Characteristics of SARS-CoV-2 and COVID-19. *Nature reviews. Microbiology, 19*(3), 141-154. doi:10.1038/s41579-020-00459-7
85. Jang, H., Boltz, D. A., Webster, R. G., & Smeyne, R. J. (2009). Viral parkinsonism. *Biochim Biophys Acta, 1792*(7), 714-721. doi:10.1016/j.bbadis.2008.08.001
86. Jeffers, S. A., Tusell, S. M., Gillim-Ross, L., Hemmila, E. M., Achenbach, J. E., Babcock, G. J., . . . Holmes, K. V. (2004). CD209L (L-SIGN) is a receptor for severe acute respiratory syndrome coronavirus. *Proc Natl Acad Sci U S A, 101*(44), 15748-15753. doi:10.1073/pnas.0403812101
87. Khan, M., Yoo, S. J., Clijsters, M., Backaert, W., Vanstapel, A., Speleman, K., . . . Van Gerven, L. (2021). Visualizing in deceased COVID-19 patients how SARS-CoV-2 attacks the respiratory and olfactory mucosae but spares the olfactory bulb. *Cell, 184*(24), 5932-5949.e5915. doi:10.1016/j.cell.2021.10.027
88. Klingelhoefer, L., & Reichmann, H. (2015). Pathogenesis of Parkinson disease--the gut-brain axis and environmental factors. *Nat Rev Neurol, 11*(11), 625-636. doi:10.1038/nrneurol.2015.197
89. Koyuncu, O. O., Hogue, I. B., & Enquist, L. W. (2013). Virus infections in the nervous system. *Cell host & microbe, 13*(4), 379-393. doi:10.1016/j.chom.2013.03.010
90. Kubota, T., & Kuroda, N. (2021). Exacerbation of neurological symptoms and COVID-19 severity in patients with preexisting neurological disorders and COVID-19: A systematic review. *Clin Neurol Neurosurg, 200*, 106349. doi:10.1016/j.clineuro.2020.106349
91. Lai, C. C., Shih, T. P., Ko, W. C., Tang, H. J., & Hsueh, P. R. (2020). Severe acute respiratory syndrome coronavirus 2 (SARS-CoV-2) and coronavirus disease-2019 (COVID-19): The epidemic and the challenges. *Int J Antimicrob Agents, 55*(3), 105924. doi:10.1016/j.ijantimicag.2020.105924
92. Lechien, J. R., Chiesa-Estomba, C. M., De Siati, D. R., Horoi, M., Le Bon, S. D., Rodriguez, A., . . . Saussez, S. (2020). Olfactory and gustatory dysfunctions as a clinical presentation of mild-to-moderate forms of the coronavirus disease (COVID-19): a multicenter European study. *Eur Arch Otorhinolaryngol, 277*(8), 2251-2261. doi:10.1007/s00405-020-05965-1
93. Lee, M. H., Perl, D. P., Nair, G., Li, W., Maric, D., Murray, H., . . . Nath, A. (2021). Microvascular Injury in the Brains of Patients with COVID-19. *N Engl J Med, 384*(5), 481-483. doi:10.1056/NEJMc2033369
94. Lehmann, M., Allers, K., Heldt, C., Meinhardt, J., Schmidt, F., Rodriguez-Sillke, Y., . . . Siegmund, B. (2021). Human small intestinal infection by SARS-CoV-2 is characterized by a mucosal infiltration with activated CD8(+) T cells. *Mucosal Immunol, 14*(6), 1381-1392. doi:10.1038/s41385-021-00437-z
95. mukerj
96. Li, K., Wohlford-Lenane, C., Perlman, S., Zhao, J., Jewell, A. K., Reznikov, L. R., . . . McCray, P. B., Jr. (2016). Middle East Respiratory Syndrome Coronavirus Causes Multiple Organ Damage and Lethal Disease in Mice Transgenic for Human Dipeptidyl Peptidase 4. *J Infect Dis, 213*(5), 712-722. doi:10.1093/infdis/jiv499

97. Lin, W. Y., Lin, M. S., Weng, Y. H., Yeh, T. H., Lin, Y. S., Fong, P. Y., . . . Huang, Y. Z. (2019). Association of Antiviral Therapy With Risk of Parkinson Disease in Patients With Chronic Hepatitis C Virus Infection. *JAMA Neurol, 76*(9), 1019-1027. doi:10.1001/jamaneurol.2019.1368
98. Matschke, J., Lütgehetmann, M., Hagel, C., Sperhake, J. P., Schröder, A. S., Edler, C., . . . Glatzel, M. (2020). Neuropathology of patients with COVID-19 in Germany: a post-mortem case series. *The Lancet. Neurology, 19*(11), 919-929. doi:10.1016/S1474-4422(20)30308-2
99. Meinhardt, J., Radke, J., Dittmayer, C., Franz, J., Thomas, C., Mothes, R., . . . Heppner, F. L. (2021). Olfactory transmucosal SARS-CoV-2 invasion as a port of central nervous system entry in individuals with COVID-19. *Nat Neurosci, 24*(2), 168-175. doi:10.1038/s41593-020-00758-5
100. Meng, L., Shen, L., & Ji, H. F. (2019). Impact of infection on risk of Parkinson's disease: a quantitative assessment of case-control and cohort studies. *Journal of neurovirology, 25*(2), 221-228. doi:10.1007/s13365-018-0707-4
101. Mönkemüller, K., Fry, L., & Rickes, S. (2020). COVID-19, coronavirus, SARS-CoV-2 and the small bowel. *Rev Esp Enferm Dig, 112*(5), 383-388. doi:10.17235/reed.2020.7137/2020
102. Mpekoulis, G., Frakolaki, E., Taka, S., Ioannidis, A., Vassiliou, A. G., Kalliampakou, K. I., . . . Vassilaki, N. (2021). Alteration of L-Dopa decarboxylase expression in SARS-CoV-2 infection and its association with the interferon-inducible ACE2 isoform. *PLoS One, 16*(6), e0253458. doi:10.1371/journal.pone.0253458
103. Mukerji, S. S., & Solomon, I. H. (2021). What can we learn from brain autopsies in COVID-19? *Neurosci Lett, 742*, 135528. doi:10.1016/j.neulet.2020.135528
104. Murray, R. S., Brown, B., Brian, D., & Cabirac, G. F. (1992). Detection of coronavirus RNA and antigen in multiple sclerosis brain. *Ann Neurol, 31*(5), 525-533. doi:10.1002/ana.410310511
105. Nataf, S. (2020). An alteration of the dopamine synthetic pathway is possibly involved in the pathophysiology of COVID-19. *Journal of medical virology, 92*(10), 1743-1744. doi:10.1002/jmv.25826
106. Netland, J., Meyerholz, D. K., Moore, S., Cassell, M., & Perlman, S. (2008). Severe acute respiratory syndrome coronavirus infection causes neuronal death in the absence of encephalitis in mice transgenic for human ACE2. *J Virol, 82*(15), 7264-7275. doi:10.1128/jvi.00737-08
107. Ousseiran, Z. H., Fares, Y., & Chamoun, W. T. (2021). Neurological manifestations of COVID-19: a systematic review and detailed comprehension. *Int J Neurosci*, 1-16. doi:10.1080/00207454.2021.1973000
108. Pellegrini, L., Albecka, A., Mallery, D. L., Kellner, M. J., Paul, D., Carter, A. P., . . . Lancaster, M. A. (2020). SARS-CoV-2 Infects the Brain Choroid Plexus and Disrupts the Blood-CSF Barrier in Human Brain Organoids. *Cell Stem Cell, 27*(6), 951-961.e955. doi:10.1016/j.stem.2020.10.001
109. Pezzini, A., & Padovani, A. (2020). Lifting the mask on neurological manifestations of COVID-19. *Nature Reviews Neurology, 16*(11), 636-644. doi:10.1038/s41582-020-0398-3
110. Politi, L. S., Salsano, E., & Grimaldi, M. (2020). Magnetic Resonance Imaging Alteration of the Brain in a Patient With Coronavirus Disease 2019 (COVID-19) and Anosmia. *JAMA Neurol, 77*(8), 1028-1029. doi:10.1001/jamaneurol.2020.2125

111. Porzionato, A., Emmi, A., Contran, M., Stocco, E., Riccetti, S., Sinigaglia, A., . . . De Caro, R. (2021). Case Report: The Carotid Body in COVID-19: Histopathological and Virological Analyses of an Autopsy Case Series. *Front Immunol, 12*, 736529. doi:10.3389/fimmu.2021.736529
112. Porzionato, A., Stocco, E., Emmi, A., Contran, M., Macchi, V., Riccetti, S., . . . De Caro, R. (2021). Hypopharyngeal Ulcers in COVID-19: Histopathological and Virological Analyses - A Case Report. *Front Immunol, 12*, 676828. doi:10.3389/fimmu.2021.676828
113. Radnis, C., Qiu, S., Jhaveri, M., Da Silva, I., Szewka, A., & Koffman, L. (2020). Radiographic and clinical neurologic manifestations of COVID-19 related hypoxemia. *J Neurol Sci, 418*, 117119. doi:10.1016/j.jns.2020.117119
114. Remmelink, M., De Mendonça, R., D'Haene, N., De Clercq, S., Verocq, C., Lebrun, L., . . . Salmon, I. (2020). Unspecific post-mortem findings despite multiorgan viral spread in COVID-19 patients. *Critical Care, 24*(1), 495. doi:10.1186/s13054-020-03218-5
115. Sadasivan, S., Sharp, B., Schultz-Cherry, S., & Smeyne, R. J. (2017). Synergistic effects of influenza and 1-methyl-4-phenyl-1,2,3,6-tetrahydropyridine (MPTP) can be eliminated by the use of influenza therapeutics: experimental evidence for the multi-hit hypothesis. *NPJ Parkinsons Dis, 3*, 18. doi:10.1038/s41531-017-0019-z
116. Schurink, B., Roos, E., Radonic, T., Barbe, E., Bouman, C. S. C., de Boer, H. H., . . . Bugiani, M. (2020). Viral presence and immunopathology in patients with lethal COVID-19: a prospective autopsy cohort study. *The Lancet Microbe, 1*(7), e290-e299. doi:10.1016/S2666-5247(20)30144-0
117. Schwabenland, M., Salié, H., Tanevski, J., Killmer, S., Lago, M. S., Schlaak, A. E., . . . Bengsch, B. (2021). Deep spatial profiling of human COVID-19 brains reveals neuroinflammation with distinct microanatomical microglia-T-cell interactions. *Immunity, 54*(7), 1594-1610.e1511. doi:10.1016/j.immuni.2021.06.002
118. Siddiqi, H. K., Libby, P., & Ridker, P. M. (2021). COVID-19 - A vascular disease. *Trends Cardiovasc Med, 31*(1), 1-5. doi:10.1016/j.tcm.2020.10.005
119. Solomon, I. H., Normandin, E., Bhattacharyya, S., Mukerji, S. S., Keller, K., Ali, A. S., . . . Sabeti, P. (2020). Neuropathological Features of COVID-19. *N Engl J Med, 383*(10), 989-992. doi:10.1056/NEJMc2019373
120. Sullivan, B. N., & Fischer, T. (2021). Age-Associated Neurological Complications of COVID-19: A Systematic Review and Meta-Analysis. *Frontiers in aging neuroscience, 13*, 653694-653694. doi:10.3389/fnagi.2021.653694
121. Sulzer, D. (2007). Multiple hit hypotheses for dopamine neuron loss in Parkinson's disease. *Trends Neurosci, 30*(5), 244-250.
122. Sulzer, D., Antonini, A., Leta, V., Nordvig, A., Smeyne, R. J., Goldman, J. E., . . . Ray Chaudhuri, K. (2020). COVID-19 and possible links with Parkinson's disease and parkinsonism: from bench to bedside. *npj Parkinson's Disease, 6*, 18-18. doi:10.1038/s41531-020-00123-0
123. Tandon, M., Kataria, S., Patel, J., Mehta, T. R., Daimee, M., Patel, V., . . . Sriwastava, S. (2021). A Comprehensive Systematic Review of CSF analysis that defines Neurological Manifestations of COVID-19. *Int J Infect Dis, 104*, 390-397. doi:10.1016/j.ijid.2021.01.002
124. Tang, Y.-W., Schmitz, J. E., Persing, D. H., & Stratton, C. W. (2020). Laboratory Diagnosis of COVID-19: Current Issues and Challenges. *Journal of clinical microbiology, 58*(6), e00512-00520. doi:10.1128/JCM.00512-20

125. Tanner, C. M., Ottman, R., Goldman, S. M., Ellenberg, J., Chan, P., Mayeux, R., & Langston, J. W. (1999). Parkinson disease in twins: an etiologic study. *Jama, 281*(4), 341-346. doi:10.1001/jama.281.4.341
126. Thakur, K. T., Miller, E. H., Glendinning, M. D., Al-Dalahmah, O., Banu, M. A., Boehme, A. K., . . . Canoll, P. (2021). COVID-19 neuropathology at Columbia University Irving Medical Center/New York Presbyterian Hospital. *Brain, 144*(9), 2696-2708. doi:10.1093/brain/awab148
127. Tsai, H. H., Liou, H. H., Muo, C. H., Lee, C. Z., Yen, R. F., & Kao, C. H. (2016). Hepatitis C virus infection as a risk factor for Parkinson disease: A nationwide cohort study. *Neurology, 86*(9), 840-846. doi:10.1212/wnl.0000000000002307
128. Tsivgoulis, G., Palaiodimou, L., Zand, R., Lioutas, V. A., Krogias, C., Katsanos, A. H., . . . Tsiodras, S. (2020). COVID-19 and cerebrovascular diseases: a comprehensive overview. *Ther Adv Neurol Disord, 13*, 1756286420978004. doi:10.1177/1756286420978004
129. Tsui, J. K., Calne, D. B., Wang, Y., Schulzer, M., & Marion, S. A. (1999). Occupational risk factors in Parkinson's disease. *Canadian journal of public health = Revue canadienne de sante publique, 90*(5), 334-337. doi:10.1007/BF03404523
130. Varga, Z., Flammer, A. J., Steiger, P., Haberecker, M., Andermatt, R., Zinkernagel, A. S., . . . Moch, H. (2020). Endothelial cell infection and endotheliitis in COVID-19. *Lancet, 395*(10234), 1417-1418. doi:10.1016/s0140-6736(20)30937-5
131. Verstrepen, K., Baisier, L., & De Cauwer, H. (2020). Neurological manifestations of COVID-19, SARS and MERS. *Acta Neurol Belg, 120*(5), 1051-1060. doi:10.1007/s13760-020-01412-4
132. Wan, D., Du, T., Hong, W., Chen, L., Que, H., Lu, S., & Peng, X. (2021). Neurological complications and infection mechanism of SARS-COV-2. *Signal transduction and targeted therapy, 6*(1), 406-406. doi:10.1038/s41392-021-00818-7
133. Wang, Q., Zhang, Y., Wu, L., Niu, S., Song, C., Zhang, Z., . . . Qi, J. (2020). Structural and Functional Basis of SARS-CoV-2 Entry by Using Human ACE2. *Cell, 181*(4), 894-904.e899. doi:10.1016/j.cell.2020.03.045
134. Williams, A., Branscome, H., Khatkar, P., Mensah, G. A., Al Sharif, S., Pinto, D. O., . . . Kashanchi, F. (2021). A comprehensive review of COVID-19 biology, diagnostics, therapeutics, and disease impacting the central nervous system. *Journal of neurovirology, 27*(5), 667-690. doi:10.1007/s13365-021-00998-6
135. Xu, X., Chen, P., Wang, J., Feng, J., Zhou, H., Li, X., . . . Hao, P. (2020). Evolution of the novel coronavirus from the ongoing Wuhan outbreak and modeling of its spike protein for risk of human transmission. *Sci China Life Sci, 63*(3), 457-460. doi:10.1007/s11427-020-1637-5
136. Yachou, Y., El Idrissi, A., Belapasov, V., & Ait Benali, S. (2020). Neuroinvasion, neurotropic, and neuroinflammatory events of SARS-CoV-2: understanding the neurological manifestations in COVID-19 patients. *Neurological sciences : official journal of the Italian Neurological Society and of the Italian Society of Clinical Neurophysiology, 41*(10), 2657-2669. doi:10.1007/s10072-020-04575-3
137. Yang, A. C., Kern, F., Losada, P. M., Agam, M. R., Maat, C. A., Schmartz, G. P., . . . Wyss-Coray, T. (2021). Dysregulation of brain and choroid plexus cell types in severe COVID-19. *Nature, 595*(7868), 565-571. doi:10.1038/s41586-021-03710-0
138. Zazhytska, M., Kodra, A., Hoagland, D. A., Frere, J., Fullard, J. F., Shayya, H., . . . Lomvardas, S. (2022). Non-cell-autonomous disruption of nuclear

architecture as a potential cause of COVID-19-induced anosmia. *Cell, 185*(6), 1052-1064.e1012. doi:https://doi.org/10.1016/j.cell.2022.01.024
139. Zhang, H., Kang, Z., Gong, H., Xu, D., Wang, J., Li, Z., . . . Xu, H. (2020). Digestive system is a potential route of COVID-19: an analysis of single-cell coexpression pattern of key proteins in viral entry process. *Gut, 69*(6), 1010. doi:10.1136/gutjnl-2020-320953
140. Zhang, R., Wu, Y., Zhao, M., Liu, C., Zhou, L., Shen, S., . . . Wan, H. (2009). Role of HIF-1alpha in the regulation ACE and ACE2 expression in hypoxic human pulmonary artery smooth muscle cells. *Am J Physiol Lung Cell Mol Physiol, 297*(4), L631-640. doi:10.1152/ajplung.90415.2008
141. Zubair, A. S., McAlpine, L. S., Gardin, T., Farhadian, S., Kuruvilla, D. E., & Spudich, S. (2020). Neuropathogenesis and Neurologic Manifestations of the Coronaviruses in the Age of Coronavirus Disease 2019: A Review. *JAMA Neurol, 77*(8), 1018-1027. doi:10.1001/jamaneurol.2020.2065

Chapter 2

Smell deficits in COVID-19 and possible links with Parkinson's Disease

The present chapter has been previously published in: ***Emmi A.****, Sandre M., Porzionato A., Antonini A., Smell deficits in COVID-19 and possible links with Parkinson's disease. International Review of Neurobiology, 2022. doi:10.1016/bs.irn.2022.08.001*

ABSTRACT

Olfactory impairment is a common symptom in COVID-19, the disease caused by SARS-CoV-2 infection. While other viruses, such as influenza viruses, may affect the ability to smell, loss of olfactory function is often smoother and associated to various degree of nasal symptoms. In COVID-19 smell loss may appears also in absence of other symptoms, frequently with a sudden onset. However, despite great clinical interest in COVID-19 olfactory alterations, very little is known concerning the mechanisms underlying these phenomena. Moreover, olfactory dysfunction is observed in neurological conditions like Parkinson's Disease and can anticipate motor onset by many years, suggesting that viral infections, like COVID-19, and regional inflammatory responses may trigger defective protein aggregation and subsequent neurodegeneration, potentially linking COVID-19 olfactory impairment to neurodegeneration. In the following chapter, we report the neurobiological and neuropathological underpinnings of olfactory impairments encountered in COVID-19 and discuss the implications of these findings in the context of neurodegenerative disorders, with particular regard to Parkinson's Disease and alpha-synuclein pathology.

INTRODUCTION

Coronavirus Disease 2019 (COVID-19), the disease caused by Severe Acute Respiratory Syndrome – Coronavirus 2 (SARS-CoV-2), is often associated with a wide spectrum of neurological manifestations (Ellul et al., 2020; Helms et al., 2020; Huang et al., 2021; Iadecola, Anrather, & Kamel, 2020; Mao et al., 2020). Intriguingly, the COVID-19 pandemic brought to the attention of clinicians an astonishing number of patients affected by mild symptoms, the most frequent being a sudden and complete loss of olfaction, which may last for a variable period of time (Guerrero et al., 2021).

Often wrongfully regarded as an ancillary sense, olfaction covers a great role in our everyday life for its involvement in lifeguarding processes (e.g., avoiding dangerous chemicals), as well as in food evaluation. As the pleasantness of gustatory and olfactory stimuli represents an important contributor to patient quality of life, olfactory impairment is also frequently associated to anhedonia, lack of motivation and depressive symptoms in patients with COVID-19 (Athanassi, Dorado Doncel, Bath, & Mandairon, 2021; Voruz et al., 2022).

Aside of the functional impairments deriving from olfactory dysfunction, the olfactory system directly links the brain to the external environment, representing a gateway through which many viruses, such as herpesvirus-1 and 6, may access the central nervous system (Duarte et al., 2019; Harberts et al., 2011). Also, the olfactory system is involved in the pathogenesis of different neurodegenerative diseases like Parkinson's and Alzheimer's disease (Sulzer, 2007), due to its connections to the entorhinal cortex and limbic system, suggesting special care for possible long-term consequences of viral infections. In this context, olfactory transmucosal invasion of SARS-CoV-2, and the inflammatory correlates of COVID-19 at the level of the olfactory system, must be carefully considered, as they may represent possible factors for the establishment, or the precipitation, of protein aggregation and neurodegenerative phenomena.

CLINICAL FEATURES OF COVID-19 OLFACTORY IMPAIRMENT

Individual variables influencing COVID-19 olfactory impairment

During the first waves of the COVID-19 pandemic, olfactory impairment was regarded as a common clinical feature experienced by numerous patients. Early studies correlated higher propensity for acute olfactory loss with a more indolent course, but subsequent work

suggested elevated prevalence of smell loss across most COVID-19 cases, regardless of severity (Brann et al., 2020). Hornuss et al. (2020) evidenced that olfactory alterations often occur unnoticed in COVID-19 patients, and that they do not represent a predictor of severe COVID-19 manifestations. Moreover, a substantial proportion of patients with previous mild-to-moderate symptomatic COVID-19 characterized by new onset of chemosensory dysfunction, still complained on altered sense of smell or taste 1 year after the onset (Brann et al., 2020). These long term effects of COVID-19 on chemosensory functions have been investigated recently by Shelton et al. (2022), evidencing that only a restricted cluster of patients experience long-term smell loss. The authors discovered a genetic mutation in COVID-19 patients that was associated with a greater propensity for smell or taste loss. The mutation was found in two overlapping genes, called UGT2A1 and UGT2A2, encoding proteins that remove odour molecules from the nostrils after they have been detected. However, interactions between SARS-CoV-2 and the aforementioned genes remain to be clarified.

Among the main issues concerning the evaluation of individual olfactory outcomes in COVID-19, objective testing of olfactory function represents a major aspect of concern. In the case of chemical senses, two main objective tests have been developed and used over the years in the clinic, namely the Sniffin' Sticks (Hummel et al., 2009) and the University of Pennsylvania Smell Inventory Test (UPSIT) (Doty et al., 2014), while others are being developed. Their use is mandatory to have an objective evaluation of the impairment, since the subjective report is often misleading. However, they both require the direct testing of the patient, which may be difficult or impossible in the case of COVID-19 infected patients. Conversely, collecting data from patients may be of paramount importance to follow the disease, even though the utility of self-reporting about chemical sensitivity has been repeatedly questioned (Hummel et al., 2009).

SARS-CoV-2 variants and their relationship with olfactory impairment

Intriguingly, aside from intra-individual differences underlying more or less severe olfactory impairment in COVID-19, SARS-CoV-2 variants may as well affect olfactory outcome in the general populations. Coelho, Reiter, French, and Costanzo (2022) surveyed 616,318 people in the United States who had COVID-19. The authors found that, compared with those who had been infected with the original virus, people who had contracted the Alpha variant — the first variant of concern to arise — were 50% as likely to have chemosensory disruption.

This probability fell to 44% for the later Delta variant, and to 17% for the latest variant, Omicron. While this clinical data appears to be in line with a less severe clinical outcome associated with newer variants, no studies to date have examined the impact of different SARS-CoV-2 variants on the olfactory mucosa, either in animal models, nor in the neuropathological setting. Thus, the pathophysiology of olfactory impairment in new SARS-CoV-2 variants, such as the recently circulating Omicron variant, remain to be investigated.

NEUROPATHOLOGY OF COVID-19 OLFACTORY IMPAIRMENT

Other coronaviruses, such as Severe Acute Respiratory Syndrome Coronavirus 1 (SARS-CoV-1), are known to enter the brain of transgenic mice via the olfactory bulb, leading to neuronal necrosis in the absence of encephalitis (Netland, Meyerholz, Moore, Cassell, & Perlman, 2008). Similarly, high levels of viral RNA were found in the brainstem and thalamus of transgenic mice following intranasal inoculation of Middle-Eastern Respiratory Syndrome Coronavirus (MERS-CoV) (Li et al., 2016), suggesting for a common neuroinvasive potential.

As far as SARS-CoV-2 is concerned, most studies agree on the extensive inflammatory processes occurring in the olfactory mucosa and bulb of COVID-19 patients (Emmi et al., 2021; Matschke et al., 2020; Meinhardt et al., 2021; Schwabenland et al., 2021; B. Thakur et al., 2021), but often conflicting findings are reported concerning SARS-CoV-2 neurotropism. Douaud et al. (2022) investigated structural brain changes before and after a SARS-CoV-2 infection in a large sample of UK Biobank participants, revealing significant reductions in grey matter thickness and tissue-contrast in the orbitofrontal cortex and parahippocampal gyrus, along with prominent alterations in brain areas functionally connected to the primary olfactory cortex. Positron emission tomography (PET) hypometabolism in long COVID patients encompassing the olfactory gyrus and the connected limbic/paralimbic regions, extended to the brainstem and the cerebellum (Guedj et al., 2021), and in the right parahippocampal gyrus and the right thalamus (Sollini et al., 2021) were also reported.

From a neuropathological perspective, several studies identified SARS-CoV-2 viral antigens and genomic sequences through RT-PCR, immunohistochemistry, in-situ hybridization and even electron microscopy in the human olfactory system (Khan et al., 2021; Meinhardt et al., 2021; Zazhytska et al., 2022). Meinhardt et al. (2021) detected SARS-CoV-2 Spike protein in primary olfactory neurons of the olfactory mucosa in a large

sample of COVID-19 patients, suggesting an olfactory-transmucosal route of infection throughout the central nervous system, as testified also by the detection of viral RNA at the level of the olfactory bulb and the medulla oblongata.

Conversely, two recent studies found viral genomic sequences and antigens in sustentacular cells of the olfactory epithelium, but not in olfactory neurons (Khan et al., 2021; Zazhytska et al., 2022). This was associated with the reorganization of nuclear architecture and downregulation of olfactory receptors, as well as their signaling pathways, in neuronal cells of the olfactory mucosa, hinting towards a non-cell autonomous cause of anosmia (Zazhytska et al., 2022). Two studies of single nucleus RNA sequencing of brains of COVID-19 patients, focusing on the olfactory system and the choroid plexus, detected broad perturbations, with upregulation of genes involved in innate antiviral response and inflammation, microglial activation and neurodegeneration, but found no direct evidence of viral RNA in the tissue (Fullard et al., 2021; Yang et al., 2021). Similarly, authors have not detected viral proteins/ RNA through immunohistochemistry or *in-situ* hybridization, even though viral genomic sequences were found via RT-PCR assays (Lee et al., 2021; Solomon et al., 2020; K. T. Thakur et al., 2021). In concordance to these findings, animal model studies suggest that loss of smell is related to damage to the cilia and olfactory epithelium, but not infection of the olfactory neurons. For example, in an experiment where hamsters were nasally infected with SARS-CoV-2, the olfactory epithelium and cilia became very damaged, leading to anosmia, but no infection was observed in the olfactory neurons (Bryche et al., 2020). Furthermore, Brann et al. (2020) demonstrated that mouse, non-human primate and human olfactory mucosa expresses two key genes involved in SARS-CoV-2 entry, ACE2 and TMPRSS2. However, single cell sequencing revealed that ACE2 is expressed in support cells, stem cells, and perivascular cells, rather than in neurons.

Concerning neuroinflammation occurring in the olfactory system of COVID-19 patients, Schwabenland et al. (2021) performed deep spatial profiling of the local immune response through imaging mass spectrometry, revealing significant immune activation in the medulla oblongata and in the olfactory bulb, with a prominent role mediated by CD8+ T-cell - microglia crosstalk in the parenchyma. Similarly, other authors (Emmi et al., 2021; Matschke et al., 2020; Solomon et al., 2020) detected prominent astrogliosis, microglial activation and microglial nodules in the brainstem and olfactory structures of COVID-19 subjects, as seen in Figure 1. Hence, even though the detection of SARS-CoV-2 in olfactory neuronal cells has not been consistently reproduced throughout studies, most findings support marked neuroinflammation of the olfactory system in COVID-19. Combined with recent studies

indicating indirect downregulation of olfactory receptor pathways mediated by sustentacular cell infection, it appears that olfactory impairment in COVID-19 may not always be associated to direct viral invasion of olfactory neuronal cells, with subsequent olfactory-transmucosal spread of the virus throughout the CNS but can also be mediated by sustentacular cell infection and dysregulation of olfactory receptor pathways.

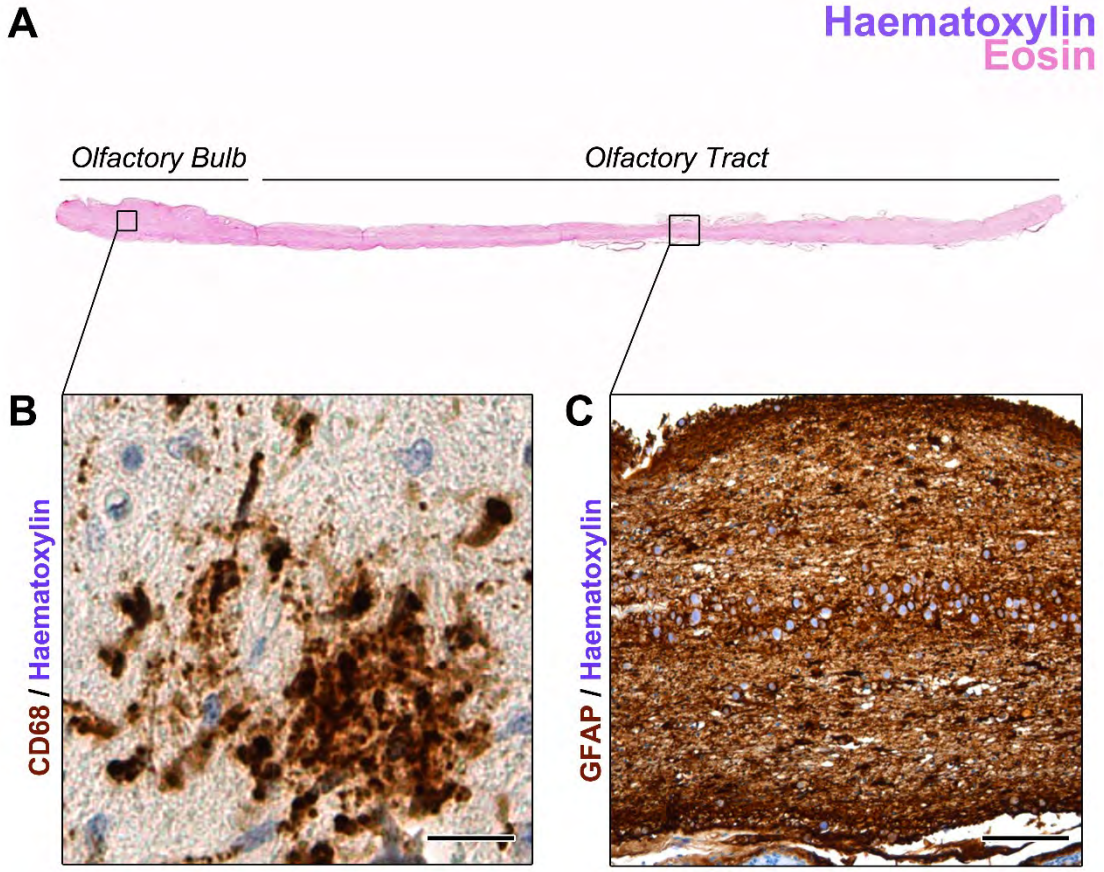

Figure 1. *A) Olfactory bulb and tract of a COVID-19 subject, Haematoxylin & Eosin staining. B) Microglial nodule at the level of the olfactory bulb, as demonstrated by CD68 immunoperoxidase staining. C) Prominent astrogliosis of the olfactory tract with numerous corpora amylacea represent a non-specific finding in COVID-19, and is often difficult to disentangle from patient comorbidities. GFAP immunoperoxidase staining.*

OLFACTORY IMPAIRMENT IN COVID-19 AND PARKINSONISM

Despite being counted as a respiratory virus, SARS-CoV-2 is associated to frequent and sometimes severe neurological manifestations, posing important interrogatives on the short and long term effects of SARS-CoV-2 infection on the central nervous system. Particularly concerning is the hypothesis that SARS-CoV-2 infection of the central nervous system may predispose, or quickly precipitate, the development of Parkinson's Disease (Beauchamp, Finkelstein, Bush, Evans, & Barnham, 2020; Bouali-Benazzouz & Benazzouz, 2021; Brundin, Nath, & Beckham, 2020). This hypothesis arises both from the 1917 Spanish flu and von Economo's encephalitis lethargica pandemics, which have seen a surge of post-encephalitic parkinsonism following the waves of the pandemic, and the known association between viral infection and the development of transient or permanent movement disorders (Jang, Boltz, Webster, & Smeyne, 2009). In fact, pathogens, and in particular respiratory viruses, have been suggested as a potential etiopathogenic factor for PD, leading to parkinsonism in subjects over the age of 50, regardless of genetic substrate (Beauchamp et al., 2020; Tanner et al., 1999). The well-established neuropathological staging of PD suggested by Braak & Braak also appears to account for neurotropic pathogens that may infect the central nervous system either through the vagus nerve (pneumo-gastric pathway) or by accessing the brain through the olfactory systems. Both the olfactory bulb and tract, as well as the medulla oblongata where the vagal nuclei are located, represent the very first sites of early PD neuropathology, and interestingly also represent the main sites of inflammation / infection encountered in COVID-19 (Hawkes, Del Tredici, & Braak, 2007; Klingelhoefer & Reichmann, 2015). Furthermore, viral-related inflammation might render the CNS susceptible to preceding or subsequent stressors (Sulzer, 2007), even in the absence of direct viral invasion; indeed, past history of infection was associated with a 20% higher risk of presenting PD in the future (Meng, Shen, & Ji, 2019). In the case of coronaviruses, higher antibodies titers against common CoV have been detected in the CSF of PD patients when compared to controls, while there was evidence of post-encephalitic parkinsonism in mice infected with a CoV strain (MHV-A59) (Fazzini, Fleming, & Fahn, 1992; Fishman et al., 1985).

In a recent study, Semerdzhiev, Fakhree, Segers-Nolten, Blum, and Claessens (2022) demonstrated that in the presence of SARS-CoV-2 Nucleocapsid protein, the onset of alpha-synuclein aggregation into amyloid fibrils is strongly accelerated, indicating that N-protein facilitates the formation of a critical nucleus for aggregation. Fibril formation does not only

appear to accelerate, but also proceeds in an unusual two-step process. In cells, the presence of Nucleocapsid protein changes the distribution of alpha-synuclein over different conformations that likely represent different functions at already short time scales. Similarly, Charnley et al. (2022) identified two peptides from the SARS-CoV-2 proteome that self-assemble into amyloid assemblies. These amyloids were shown to be highly toxic to neuronal cells and are hypothesized to trigger neurological symptoms in COVID-19. The cytotoxicity and protease-resistant structure of these assemblies may result in their persistent presence in the CNS of patients even following infection, could partially explain the lasting neurological symptoms of COVID-19, especially those that are novel in relation to other post-viral syndromes such as that following the original SARS-CoV-1. The outlook in relation to triggering of progressive neurodegenerative disease remains uncertain. Given the typically slow progress of neurodegenerative disease if such a phenomenon exists, it will most probably take some time to become evident epidemiologically. In an animal model study performed by Käufer et al. (2022), microglial activation and neuronal proteinopathy persisted even beyond viral clearance. Viral protein exposure in the nasal cavity led to pronounced microglia activation in the olfactory bulb beyond viral clearance. Cortical but not hippocampal neurons accumulated hyperphosphorylated tau and alpha-synuclein, in the absence of overt inflammation and neurodegeneration. Importantly, not all brain regions were affected, in line with the selective vulnerability hypothesis. In this animal model, despite the absence of virus in brain, neurons developed signatures of proteinopathies that may contribute to progressive neuronal dysfunction.

This is further confirmed by available neuropathological studies on COVID-19 decedents, showing very little and often conflicting evidence on SARS-CoV-2 neurotropism. On the other hand, as all available neuropathological studies are carried on subjects who died during the acute phases of the disease (Emmi et al., 2021; Matschke et al., 2020; Schwabenland et al., 2021; Solomon et al., 2020), and as such the neuropathological alterations occurring in cases of chronic infection, or in the post-infection timeframe, are yet unknown. Neurodegenerative changes induced by either direct infection or by the indirect effects mediated by neuroinflammation may not be appreciable or detectable in patients who died shortly after infection, and as most subjects in neuropathological studies already present important neurological comorbidities, it is not possible to determine which markers of neurodegeneration are directly related to COVID-19, and which are related to patient morbidity.

REFERENCES

1. Athanassi, A., Dorado Doncel, R., Bath, K. G., & Mandairon, N. (2021). Relationship between depression and olfactory sensory function: a review. Chem Senses, 46. doi:10.1093/chemse/bjab044
2. Beauchamp, L. C., Finkelstein, D. I., Bush, A. I., Evans, A. H., & Barnham, K. J. (2020). Parkinsonism as a Third Wave of the COVID-19 Pandemic? Journal of Parkinson's disease, 10(4), 1343-1353. doi:10.3233/JPD-202211
3. Bouali-Benazzouz, R., & Benazzouz, A. (2021). COVID-19 Infection and Parkinsonism: Is There a Link? Mov Disord, 36(8), 1737-1743. doi:10.1002/mds.28680
4. Brann, D. H., Tsukahara, T., Weinreb, C., Lipovsek, M., Van den Berge, K., Gong, B., . . . Datta, S. R. (2020). Non-neuronal expression of SARS-CoV-2 entry genes in the olfactory system suggests mechanisms underlying COVID-19-associated anosmia. Sci Adv, 6(31). doi:10.1126/sciadv.abc5801
5. Brundin, P., Nath, A., & Beckham, J. D. (2020). Is COVID-19 a Perfect Storm for Parkinson's Disease? Trends Neurosci, 43(12), 931-933. doi:10.1016/j.tins.2020.10.009
6. Bryche, B., St Albin, A., Murri, S., Lacôte, S., Pulido, C., Ar Gouilh, M., . . . Meunier, N. (2020). Massive transient damage of the olfactory epithelium associated with infection of sustentacular cells by SARS-CoV-2 in golden Syrian hamsters. Brain Behav Immun, 89, 579-586. doi:10.1016/j.bbi.2020.06.032
7. Charnley, M., Islam, S., Bindra, G. K., Engwirda, J., Ratcliffe, J., Zhou, J., . . . Reynolds, N. P. (2022). Neurotoxic amyloidogenic peptides in the proteome of SARS-COV2: potential implications for neurological symptoms in COVID-19. Nature Communications, 13(1), 3387. doi:10.1038/s41467-022-30932-1
8. Coelho, D. H., Reiter, E. R., French, E., & Costanzo, R. M. (2022). Decreasing Incidence of Chemosensory Changes by COVID-19 Variant. Otolaryngol Head Neck Surg, 1945998221097656. doi:10.1177/01945998221097656
9. Doty, R. L., Bayona, E. A., Leon-Ariza, D. S., Cuadros, J., Chung, I., Vazquez, B., & Leon-Sarmiento, F. E. (2014). The lateralized smell test for detecting Alzheimer's disease: failure to replicate. J Neurol Sci, 340(1-2), 170-173. doi:10.1016/j.jns.2014.03.022
10. Douaud, G., Lee, S., Alfaro-Almagro, F., Arthofer, C., Wang, C., McCarthy, P., . . . Smith, S. M. (2022). SARS-CoV-2 is associated with changes in brain structure in UK Biobank. Nature, 604(7907), 697-707. doi:10.1038/s41586-022-04569-5
11. Duarte, L. F., Farías, M. A., Álvarez, D. M., Bueno, S. M., Riedel, C. A., & González, P. A. (2019). Herpes Simplex Virus Type 1 Infection of the Central Nervous System: Insights Into Proposed Interrelationships With Neurodegenerative Disorders. Frontiers in Cellular Neuroscience, 13. doi:10.3389/fncel.2019.00046
12. Ellul, M. A., Benjamin, L., Singh, B., Lant, S., Michael, B. D., Easton, A., . . . Solomon, T. (2020). Neurological associations of COVID-19. Lancet Neurol, 19(9), 767-783. doi:10.1016/s1474-4422(20)30221-0
13. Emmi, A., Rizzo, S. M. R., Barzon, L., Carturan, E., Sinigaglia, A., Riccetti, S., . . . Porzionato, A. (2021). COVID-19 Neuropathology: Evidence for SARS-CoV-2 invasion of Human Brainstem Nuclei. doi: https://doi.org/10.1101/2022.06.29.498117
14. Fazzini, E., Fleming, J., & Fahn, S. (1992). Cerebrospinal fluid antibodies to coronavirus in patients with Parkinson's disease. Mov Disord, 7(2), 153-158. doi:10.1002/mds.870070210

15. Fishman, P. S., Gass, J. S., Swoveland, P. T., Lavi, E., Highkin, M. K., & Weiss, S. R. (1985). Infection of the basal ganglia by a murine coronavirus. Science (New York, N.Y.), 229(4716), 877-879. doi:10.1126/science.2992088
16. Fullard, J. F., Lee, H.-C., Voloudakis, G., Suo, S., Javidfar, B., Shao, Z., . . . Roussos, P. (2021). Single-nucleus transcriptome analysis of human brain immune response in patients with severe COVID-19. Genome Medicine, 13(1), 118. doi:10.1186/s13073-021-00933-8
17. Guedj, E., Campion, J. Y., Dudouet, P., Kaphan, E., Bregeon, F., Tissot-Dupont, H., . . . Eldin, C. (2021). (18)F-FDG brain PET hypometabolism in patients with long COVID. Eur J Nucl Med Mol Imaging, 48(9), 2823-2833. doi:10.1007/s00259-021-05215-4
18. Guerrero, J. I., Barragán, L. A., Martínez, J. D., Montoya, J. P., Peña, A., Sobrino, F. E., . . . Ghotme, K. A. (2021). Central and peripheral nervous system involvement by COVID-19: a systematic review of the pathophysiology, clinical manifestations, neuropathology, neuroimaging, electrophysiology, and cerebrospinal fluid findings. BMC Infect Dis, 21(1), 515. doi:10.1186/s12879-021-06185-6
19. Harberts, E., Yao, K., Wohler, J. E., Maric, D., Ohayon, J., Henkin, R., & Jacobson, S. (2011). Human herpesvirus-6 entry into the central nervous system through the olfactory pathway. Proceedings of the National Academy of Sciences, 108(33), 13734-13739. doi:doi:10.1073/pnas.1105143108
20. Hawkes, C. H., Del Tredici, K., & Braak, H. (2007). Parkinson's disease: a dual-hit hypothesis. Neuropathol Appl Neurobiol, 33(6), 599-614. doi:10.1111/j.1365-2990.2007.00874.x
21. Helms, J., Kremer, S., Merdji, H., Clere-Jehl, R., Schenck, M., Kummerlen, C., . . . Meziani, F. (2020). Neurologic Features in Severe SARS-CoV-2 Infection. N Engl J Med, 382(23), 2268-2270. doi:10.1056/NEJMc2008597
22. Hornuss, D., Lange, B., Schröter, N., Rieg, S., Kern, W. V., & Wagner, D. (2020). Anosmia in COVID-19 patients. Clinical Microbiology and Infection, 26(10), 1426-1427. doi:10.1016/j.cmi.2020.05.017
23. Huang, C., Huang, L., Wang, Y., Li, X., Ren, L., Gu, X., . . . Cao, B. (2021). 6-month consequences of COVID-19 in patients discharged from hospital: a cohort study. Lancet, 397(10270), 220-232. doi:10.1016/s0140-6736(20)32656-8
24. Hummel, T., Rissom, K., Reden, J., Hähner, A., Weidenbecher, M., & Hüttenbrink, K.-B. (2009). Effects of olfactory training in patients with olfactory loss. The Laryngoscope, 119(3), 496-499. doi:https://doi.org/10.1002/lary.20101
25. Iadecola, C., Anrather, J., & Kamel, H. (2020). Effects of COVID-19 on the Nervous System. Cell, 183(1), 16-27.e11. doi:10.1016/j.cell.2020.08.028
26. Jang, H., Boltz, D. A., Webster, R. G., & Smeyne, R. J. (2009). Viral parkinsonism. Biochim Biophys Acta, 1792(7), 714-721. doi:10.1016/j.bbadis.2008.08.001
27. Käufer, C., Schreiber, C. S., Hartke, A.-S., Denden, I., Stanelle-Bertram, S., Beck, S., . . . Richter, F. (2022). Microgliosis and neuronal proteinopathy in brain persist beyond viral clearance in SARS-CoV-2 hamster model. eBioMedicine, 79, 103999. doi:https://doi.org/10.1016/j.ebiom.2022.103999
28. Khan, M., Yoo, S.-J., Clijsters, M., Backaert, W., Vanstapel, A., Speleman, K., . . . Van Gerven, L. (2021). Visualizing in deceased COVID-19 patients how SARS-CoV-2 attacks the respiratory and olfactory mucosae but spares the olfactory bulb. Cell, 184(24), 5932-5949.e5915. doi:https://doi.org/10.1016/j.cell.2021.10.027
29. Klingelhoefer, L., & Reichmann, H. (2015). Pathogenesis of Parkinson disease--the gut-brain axis and environmental factors. Nat Rev Neurol, 11(11), 625-636. doi:10.1038/nrneurol.2015.197

30. Lee, M. H., Perl, D. P., Nair, G., Li, W., Maric, D., Murray, H., . . . Nath, A. (2021). Microvascular Injury in the Brains of Patients with COVID-19. N Engl J Med, 384(5), 481-483. doi:10.1056/NEJMc2033369
31. Li, K., Wohlford-Lenane, C., Perlman, S., Zhao, J., Jewell, A. K., Reznikov, L. R., . . . McCray, P. B., Jr. (2016). Middle East Respiratory Syndrome Coronavirus Causes Multiple Organ Damage and Lethal Disease in Mice Transgenic for Human Dipeptidyl Peptidase 4. J Infect Dis, 213(5), 712-722. doi:10.1093/infdis/jiv499
32. Mao, L., Jin, H., Wang, M., Hu, Y., Chen, S., He, Q., . . . Hu, B. (2020). Neurologic Manifestations of Hospitalized Patients With Coronavirus Disease 2019 in Wuhan, China. JAMA Neurol, 77(6), 683-690. doi:10.1001/jamaneurol.2020.1127
33. Matschke, J., Lütgehetmann, M., Hagel, C., Sperhake, J. P., Schröder, A. S., Edler, C., . . . Glatzel, M. (2020). Neuropathology of patients with COVID-19 in Germany: a post-mortem case series. The Lancet Neurology, 19(11), 919-929. doi:10.1016/S1474-4422(20)30308-2
34. Meinhardt, J., Radke, J., Dittmayer, C., Franz, J., Thomas, C., Mothes, R., . . . Heppner, F. L. (2021). Olfactory transmucosal SARS-CoV-2 invasion as a port of central nervous system entry in individuals with COVID-19. Nat Neurosci, 24(2), 168-175. doi:10.1038/s41593-020-00758-5
35. Meng, L., Shen, L., & Ji, H. F. (2019). Impact of infection on risk of Parkinson's disease: a quantitative assessment of case-control and cohort studies. Journal of neurovirology, 25(2), 221-228. doi:10.1007/s13365-018-0707-4
36. Netland, J., Meyerholz, D. K., Moore, S., Cassell, M., & Perlman, S. (2008). Severe acute respiratory syndrome coronavirus infection causes neuronal death in the absence of encephalitis in mice transgenic for human ACE2. J Virol, 82(15), 7264-7275. doi:10.1128/jvi.00737-08
37. Schwabenland, M., Salié, H., Tanevski, J., Killmer, S., Lago, M. S., Schlaak, A. E., . . . Bengsch, B. (2021). Deep spatial profiling of human COVID-19 brains reveals neuroinflammation with distinct microanatomical microglia-T-cell interactions. Immunity, 54(7), 1594-1610.e1511. doi:https://doi.org/10.1016/j.immuni.2021.06.002
38. Semerdzhiev, S. A., Fakhree, M. A. A., Segers-Nolten, I., Blum, C., & Claessens, M. M. A. E. (2022). Interactions between SARS-CoV-2 N-Protein and α-Synuclein Accelerate Amyloid Formation. ACS Chemical Neuroscience, 13(1), 143-150. doi:10.1021/acschemneuro.1c00666
39. Shelton, J. F., Shastri, A. J., Fletez-Brant, K., Auton, A., Chubb, A., Fitch, A., . . . The 23andMe, C.-T. (2022). The UGT2A1/UGT2A2 locus is associated with COVID-19-related loss of smell or taste. Nature Genetics, 54(2), 121-124. doi:10.1038/s41588-021-00986-w
40. Sollini, M., Morbelli, S., Ciccarelli, M., Cecconi, M., Aghemo, A., Morelli, P., . . . Chiti, A. (2021). Long COVID hallmarks on [18F]FDG-PET/CT: a case-control study. Eur J Nucl Med Mol Imaging, 48(10), 3187-3197. doi:10.1007/s00259-021-05294-3
41. Solomon, I. H., Normandin, E., Bhattacharyya, S., Mukerji, S. S., Keller, K., Ali, A. S., . . . Sabeti, P. (2020). Neuropathological Features of COVID-19. N Engl J Med, 383(10), 989-992. doi:10.1056/NEJMc2019373
42. Sulzer, D. (2007). Multiple hit hypotheses for dopamine neuron loss in Parkinson's disease. Trends Neurosci, 30(5), 244-250.
43. Tanner, C. M., Ottman, R., Goldman, S. M., Ellenberg, J., Chan, P., Mayeux, R., & Langston, J. W. (1999). Parkinson disease in twins: an etiologic study. Jama, 281(4), 341-346. doi:10.1001/jama.281.4.341
44. Thakur, B., Dubey, P., Benitez, J., Torres, J. P., Reddy, S., Shokar, N., . . . Dwivedi, A. K. (2021). A systematic review and meta-analysis of geographic differences in

comorbidities and associated severity and mortality among individuals with COVID-19. Scientific reports, 11(1), 8562. doi:10.1038/s41598-021-88130-w
45. Thakur, K. T., Miller, E. H., Glendinning, M. D., Al-Dalahmah, O., Banu, M. A., Boehme, A. K., . . . Canoll, P. (2021). COVID-19 neuropathology at Columbia University Irving Medical Center/New York Presbyterian Hospital. Brain, 144(9), 2696-2708. doi:10.1093/brain/awab148
46. Voruz, P., Allali, G., Benzakour, L., Nuber-Champier, A., Thomasson, M., Jacot de Alcântara, I., . . . Péron, J. A. (2022). Long COVID Neuropsychological Deficits after Severe, Moderate, or Mild Infection. Clinical and Translational Neuroscience, 6(2), 9. Retrieved from https://www.mdpi.com/2514-183X/6/2/9
47. Yang, A. C., Kern, F., Losada, P. M., Agam, M. R., Maat, C. A., Schmartz, G. P., . . . Wyss-Coray, T. (2021). Dysregulation of brain and choroid plexus cell types in severe COVID-19. Nature, 595(7868), 565-571. doi:10.1038/s41586-021-03710-0
48. Zazhytska, M., Kodra, A., Hoagland, D. A., Frere, J., Fullard, J. F., Shayya, H., . . . Lomvardas, S. (2022). Non-cell-autonomous disruption of nuclear architecture as a potential cause of COVID-19-induced anosmia. Cell, 185(6), 1052-1064.e1012. doi:https://doi.org/10.1016/j.cell.2022.01.024

Chapter 3

Sympathetic activation: a potential link between comorbidities and COVID-19

*The present chapter has been previously published in: Porzionato A., **Emmi A.**, Barbon S., et al. (2020) Sympathetic Activation: a potential link between comorbidities and COVID-19. FEBS Journal. doi: 10.1111/febs.15481*

ABSTRACT

In Coronavirus Disease 2019 (COVID-19), higher morbidity and mortality are associated with age, male gender and comorbidities, such as chronic lung diseases, cardiovascular pathologies, hypertension, kidney diseases, diabetes mellitus and obesity. All the above conditions are characterized by increased sympathetic discharge, which may exert significant detrimental effects on COVID-19 patients, through actions on lungs, heart, vessels, kidneys, metabolism and/or immune system. In turn, COVID-19 may also furtherly increase sympathetic discharge, through changes in blood gases (chronic intermittent hypoxia, hyperpnea), Angiotensin-Converting Enzyme (ACE)1/ACE2 imbalance, immune/inflammatory factors or emotional distress. Nevertheless, the potential role of the sympathetic nervous system has not yet been considered in the pathophysiology of COVID-19. In our opinion, sympathetic overactivation could represent a so far undervalued mechanism for a vicious circle between COVID-19 and comorbidities.

INTRODUCTION

In Coronavirus Disease 2019 (COVID-19), higher morbidity and mortality are associated with comorbidities, such as chronic lung disease, cardiovascular pathologies, hypertension, kidney diseases, diabetes mellitus and obesity (e.g., 1-3). Conversely, COVID-19 deaths are frequently caused by a final homeostasis dysregulation caused not only by pulmonary damage but also by cardiac, circulatory, renal and/or metabolic effects. Attention has been focused on the mechanisms involved in the comorbidity-induced increase in morbidity/mortality but the potential role of the sympathetic nervous system has not yet been considered, despite sympathetic activation represents one of the specific characteristics of most above comorbidities and it could play a detrimental effect on COVID19 patients.

All comorbidities associated with increased morbidity/mortality in COVID-19 are characterized by sympathetic overactivation

It is widely known that increased sympathetic discharge is associated with chronic obstructive pulmonary disease, obstructive sleep apnea syndrome, cardiovascular diseases (hypertension, heart failure), renal pathologies and metabolic disturbances (diabetes, obesity, metabolic syndrome). Increase in peripheral hypoxic chemosensitivity is a common mechanism stimulating sympathetic activation in the above conditions (4-9) but other stimulatory mechanisms are present.

Chronic obstructive pulmonary disease and obstructive sleep apnea syndrome increase sympathetic activation mainly through chronic intermittent hypoxia, which acts by increasing the peripheral chemosensory response (10-11).

In heart failure, the increased sympathetic outflow correlates with disease progression and poor prognosis (12-13). It has been ascribed to decreased arterial/cardiopulmonary baroreflex, increased chemosensitivity, increased metabolic reflexes or progression of correlated renal insufficiency or sleep apnea syndrome (14-16).

Renal damage (for instance, experimental models of renal ischemia-reperfusion) is also associated with sympathetic activation, due to activation of the renal afferents and brain renin-angiotensin system. Conversely, in a positive feedback loop, sympathetic overactivity stimulates tubular Na+/H2O reabsorption, decreases renal blood flow and stimulates renin-angiotensin system. It also aggravates ischemia/reperfusion-induced renal damage through pro-inflammatory mechanisms (reviewed in 17).

In obesity, diabetes and metabolic syndrome, sympathetic overactivity has been ascribed to high levels of circulating insulin and leptin, which stimulate the sympathetic outflow both centrally and peripherally, and/or to chronic intermittent hypoxia due to obstructive sleep apnea (e.g., 18-19). Sympathetic overactivation in turn increases insulin resistance, maintaining a positive feedback loop (20).

The effects of smoking on COVID-19 are still highly controversial and conflicting data are present in literature. Epidemiological studies and meta-analyses report unexpectedly low prevalence of smoking among COVID-19 hospitalized patients (e.g., 21). Conversely, other authors observed significant associations of smoking with clinical progression and mortality of hospitalized COVID-19 patients, consistently with the well-known detrimental effects of smoking on lung function (e.g., 22-23). The potential role of autonomic effects could also warrant an evaluation, as cigarette smoking results in increased sympathetic discharge and decreased baroreflex activity (24-28).

Sympathetic overactivity may exert significant detrimental effects on COVID-19 patients

In COVID-19, the comorbidity-induced increase in sympathetic activity may show negative effects on pulmonary, cardiovascular, renal, metabolic, and immune/inflammatory homeostasis.

In COVID-19, cardiovascular complications frequently occur, including arrhythmias, myocarditis, heart failure and myocardial infarction (e.g., 29). All these conditions are negatively affected by sympathetic overactivation and could represent a way through which comorbidity-induced sympathoactivation may increase COVID-19 morbidity/mortality. In some reports, myocardial injury has been reported in 20-40% of hospitalized cases (30-33). Cases of Takotsubo syndrome have also been reported in COVID-19 (34-37). In this kind of stress-related cardiomyopathy, myocardial injury is probably mediated by catecholamine-induced vascular spasm and/or direct catecholamine action on myocytes. In particular, catecholamine release in response to cytokine storm, or metabolic and emotional distress has been proposed to play a role in COVID-19-related Takotsubo syndromes (34-37), consistently with our hypothesis.

Acute kidney injury has been reported in >20% of severe or deceased COVID-19 patients and chronic kidney diseases are also significantly associated with severe COVID-19 (2). Moreover, the above mechanisms involved in the vicious cycle between sympathetic overactivity and renal function also show detrimental effects on the cardiocirculatory (e.g.,

38-39) and lung (e.g., 40) functions. Thus, it appears reasonable that sympathetic activation in comorbidities may exert negative homeostasis effects in COVID-19 also through renal effects. Moreover, liver injuries have also been reported in COVID-19 patients (e.g., 41) and sympathetic activation may also be detrimental for liver function (42).

The autonomic system also exerts a modulatory role on the immune system and its potential role in the complex immunological situation of COVID-19 is all to be studied. Sympathetic nerve fibres innervate most lymphoid organs, including bone marrow (43) and adrenergic receptors are present in many different immune cell types (44). The effects of sympathetic system on immune system are quite complex and depend on the differentiation state of the immune cells. However, evidence is available about a pro-inflammatory effect at least in some tissues and experimental or pathological conditions. For instance, in a mouse model of angiotensin (Ang) II-mediated hypertension, sympathetic stimulation produces noradrenaline-mediated T cell activation and vascular inflammation (45). Bilateral ablation of renal sympathetic nerves prevents immune activation and renal inflammation in a murine model of AngII-induced hypertension (46). Catheter-based renal denervation has been demonstrated to reduce monocyte activation and inflammation markers in hypertensive patients (47). In an experimental mouse model of chronic stress, hematopoietic stem cell proliferation and increased output of neutrophils and inflammatory monocytes have been reported, in response to noradrenaline release by sympathetic nerve fibers (48). Increased sympathetic discharge through the splenic nerve has also been reported to increase cytokine release by splenocytes (49). Conversely, the vagal nerve has an inhibitory effect on tumor necrosis factor-α (TNFα) release by macrophages (50-51). The anti-inflammatory effects of the parasympathetic vagal system have been observed also with reference to intestinal diseases (52-54) and arthritis (55). These potential immune/inflammatory effects of a sympathetic/parasympathetic imbalance seem particularly intriguing in the patho-physiology of COVID-19, which led to homeostasis derangement also through a ‘cytokine storm’.

Apart from the above effets on systemic homeostasis, increased sympathetic activity may have specific detrimental effects on the respiratory system. Sympathetic overactivation and the correlated renin-angiotensin system overflow play a pivotal role in progression of pulmonary hypertension (e.g., 56-58). It has been pointed out that angiotensin-converting enzyme (ACE)1/ACE2 imbalance may contribute to progression to acute respiratory distress syndrome (ARDS) in COVID-19 patients through pulmonary vasoconstriction, inflammation and oxidative and fibrotic damage (e.g., 29). Sympathetic innervation is known to increase

pulmonary capillary leakage and favour ARDS (59-62). Restrictive lung function has been associated with increased sympathetic nerve activity in heart failure, possibly due to interstitial pulmonary edema or changes in alveolar capillary units (63).

Aging and male gender are also associated with sympatho-activation

Risks of severe COVID-19 and related mortality increase with advancing age and male gender, as also sympathetic activation. In fact, muscle sympathetic nerve activity (MSNA) has been reported to increase with age in non-obese normotensive men and women, the latter showing lower values for age <50 years (64). Conversely, children are known to be protect by severe disease; various mechanisms are probably involved (developmental changes in immunity, lower prevalence of comorbidities, higher lung regenerative potential) but a possible role of the quite complex maturation of the sympathetic/parasympathetic balance may not be excluded. For instance, plasma norepinephrine, which is mainly derived from sympathetic nerve endings, increases with advancing puberty in males (65). Relevant gender differences are present in obesity-induced increase in sympathetic activity. For instance, resting MSNA is positively correlated with body mass index in men but not in women (66-67). This gender-based difference is partly explained by correlation of sympathetic overactivation with abdominal fat, more than subcutaneous one (68). Thus, increased sympathetic activation could (at least partially) contribute to the pathophysiologic association of aging and male gender with COVID-19 morbidity/mortality.

COVID-19 may furtherly increase sympathetic output in a vicious circle

The sympathetic nervous system is activated by the hypoxic and hypercapnic stimuli which characterize respiratory dysfunctions. In particular, a large amount of studies has stressed that chronic intermittent hypoxia increases sympathetic output through increased carotid body sensitivity. Thus, COVID-19-induced alterations of the respiratory function may furtherly aggravate sympathetic overactivity.

COVID-19 may also activate the sympathetic system through increased production and release of AngII. The cellular receptor for Severe Acute Respiratory Syndrome – Coronavirus (SARS-CoV) and SARS-CoV2 is ACE2, a usually membrane-bound homologue of angiotensin-converting enzyme. ACE2 is widely expressed not only in lungs but also in other organs, such as heart, brain, kidney and intestine. ACE1 and ACE2 have different enzymatic functions and produce different effects: ACE1 converts AngI in AngII; ACE2 converts AngI in Ang(1-9), which is then converted in Ang(1-7), and may also convert

AngII in Ang(1-7). Thus, in the different tissues, a balance between the two pathways (ACE1/AngII/AT1-R and ACE2/Ang(1-7)/MasR) is present, which can be affected in various clinical conditions. As a consequence ACE2 decreases the production of AngII in favour of Ang(1-7). AngII mediates vasoconstriction, fibrosis, hypertrophy and inflammation through AT1-R binding; Ang(1-7) mediates vasodilation, anti-fibrosis, anti-growth, and anti-inflammation through MasR binding (e.g., 4). Apart from the above effects, AngII mediates sympatho-excitation whereas Ang(1-7) mediates sympatho-inhibition. Internalization of SARS-CoV2 causes inhibition of ACE2 activity and progressive depletion of membrane-bound ACE2 (69-73), with ACE1/ACE2 imbalance and increase in AngII.

Circulating AngII may increase the sympathetic output both centrally, at the level of the circumventricular organs (area postrema and subfornical organ) (58), and peripherally, by acting on the carotid body (e.g., 58, 74). Thus, COVID-19-induced increase in AngII (proportional to the viral load) (75) may represent an additional way to furtherly worsen sympatho-activation in comorbidities.

Moreover, the brainstem, and particularly the solitary tract nucleus, is directly invaded by different types of coronaviruses, so that neuroinvasion by SARS-CoV2 has also been hypothesized (76). ACE2 is also expressed in the solitary tract nucleus and carotid body so that sympathetic activation may be furtherly increased by local ACE1/ACE2 imbalance and AngII stimulation.

In the COVID-19 severe patients, the occurrence of a ‘cytokine storm’ (IL6, IL10, and TNFα) has been reported (e.g., 77). AngII may also activate macrophages and other immune cells to produce inflammatory cytokines, such as IL6, TNFα and others (78-80). Circulating cytokines mainly activate the parasympathetic system, through the so-called inflammatory reflex pathway, but in certain conditions stimulation of the sympathetic output has also been reported (e.g., 81).

In the discussion of cardiovascular implications of COVID-19, Guzik et al. (29) have recently recalled that the activation of the sympathetic nervous system is associated with viral infections themselves and even with social isolation (82-83).

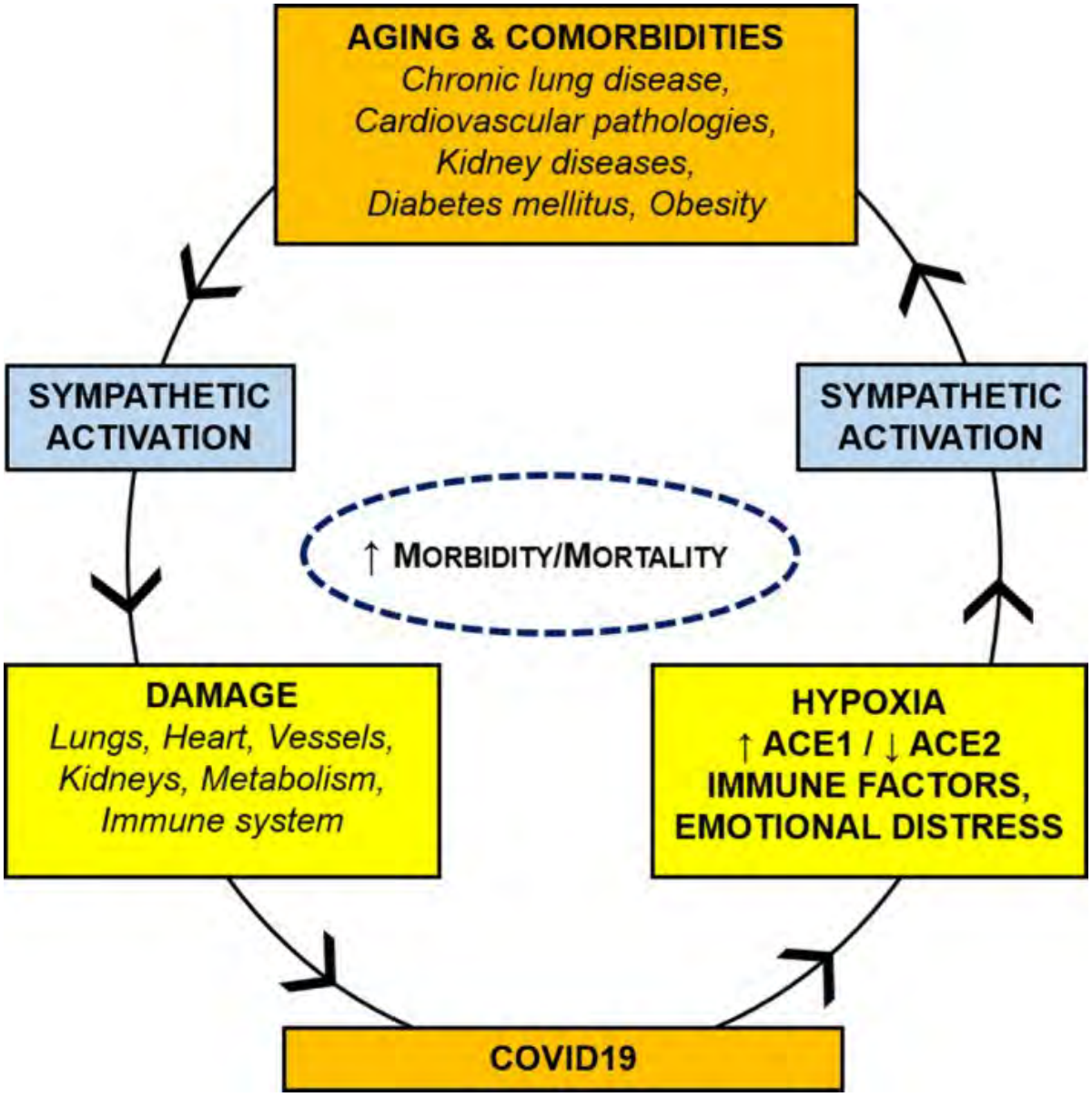

Figure 1. *Vicious circle between COVID-19 and comorbidities. Aging and comorbidities (lung, cardiovascular, kidney, and metabolic diseases) are characterized by sympathetic overactivity, which may exert detrimental effects on lungs, heart, vessels, kidney, metabolism, and/or immune system of COVID-19 patients. COVID-19 may furtherly increase sympathetic discharge, through hypoxia, ACE1/ACE2 imbalance, immune/inflammatory factors, and emotional distress.*

CONCLUSIONS

In conclusion, all comorbidities associated with increased morbidity/mortality in COVID-19 are characterized by sympathetic overactivation, similarly to aging and male gender. Sympathetic overactivity may exert significant detrimental effect on COVID-19 patients through its actions on lungs, heart, vessels, kidney, metabolism and/or immune system. In turn, COVID-19 may also furtherly increase sympathetic discharge through change in blood gases (chronic intermittent hypoxia, hyperpnea), ACE1/ACE2 imbalance or cytokine release. Thus, sympathetic overactivation could represent a so-far undervalued mechanism at the basis of the vicious circle between COVID-19 and comorbidities. Finally, it must be kept in mind that the clinical course of COVID-19 is characterized by different evolutionary phases and heterogeneous individual responses, so that the potential role of the sympathetic nervous system will have to be investigated consistently with this pathophysiological and clinical complexity.

Author contributions: Conceptualization, A.P., A.E., R.D.C.; data curation, A.P., A.E., S.B., R.B.B., C.S., E.S., V.M., R.D.C.; writing – original draft preparation, A.P.; writing – review and editing, A.P., A.E., S.B., R.B.B., C.S., E.S., V.M., R.D.C.; supervision, A.P., R.D.C.

Funding: No funding for this work.

Conflicts of interest: The authors declare no conflict of interest.

REFERENCES

1. Zhou F, Yu T, Du R, Fan G, Liu Y, Liu Z, Xiang J, Wang Y, Song B, Gu X, Guan L, Wei Y, Li H, Wu X, Xu J, Tu S, Zhang Y, Chen H, Cao B. Clinical course and risk factors for mortality of adult inpatients with COVID-19 in Wuhan, China: a retrospective cohort study. *Lancet.* 2020;395(10229):1054-1062.
2. Sardu C, Gambardella J, Morelli MB, Wang X, Marfella R, Santulli G. Hypertension, Thrombosis, Kidney Failure, and Diabetes: Is COVID-19 an Endothelial Disease? A Comprehensive Evaluation of Clinical and Basic Evidence. *J Clin Med.* 2020;9(5):E1417.
3. Garg S, Kim L, Whitaker M, O'Halloran A, Cummings C, Holstein R, Prill M, Chai SJ, Kirley PD, Alden NB, Kawasaki B, Yousey-Hindes K, Niccolai L, Anderson EJ, Openo KP, Weigel A, Monroe ML, Ryan P, Henderson J, Kim S, Como-Sabetti K, Lynfield R, Sosin D, Torres S, Muse A, Bennett NM, Billing L, Sutton M, West N, Schaffner W, Talbot HK, Aquino C, George A, Budd A, Brammer L, Langley G, Hall AJ, Fry A. Hospitalization Rates and Characteristics of Patients Hospitalized with Laboratory-Confirmed Coronavirus Disease 2019 - COVID-NET, 14 States, March 1-30, 2020. *MMWR Morb Mortal Wkly Rep.* 2020;69(15):458-464.
4. Patel KP, Schultz HD. Angiotensin peptides and nitric oxide in cardiovascular disease. *Antioxid Redox Signal.* 2013;19(10):1121-1132.
5. Conde SV, Sacramento JF, Guarino MP, Gonzalez C, Obeso A, Diogo LN, Monteiro EC, Ribeiro MJ. Carotid body, insulin, and metabolic diseases: unraveling the links. *Front Physiol.* 2014;5:418.
6. Conde SV, Sacramento JF, Guarino MP. Carotid body: a metabolic sensor implicated in insulin resistance. *Physiol Genomics.* 2018;50(3):208-214.
7. Paton JF, Sobotka PA, Fudim M, Engelman ZJ, Hart EC, McBryde FD, Abdala AP, Marina N, Gourine AV, Lobo M, Patel N, Burchell A, Ratcliffe L, Nightingale A. The carotid body as a therapeutic target for the treatment of sympathetically mediated diseases. *Hypertension.* 2013;61(1):5-13.
8. Porzionato A, Macchi V, De Caro R. Role of the carotid body in obesity-related sympathoactivation. *Hypertension.* 2013;61(6):e57.
9. Cunha-Guimaraes JP, Guarino MP, Timóteo AT, Caires I, Sacramento JF, Ribeiro MJ, Selas M, Santiago JCP, Mota-Carmo M, Conde SV. Carotid body chemosensitivity: early biomarker of dysmetabolism in humans. *Eur J Endocrinol.* 2020;182(6):549-557.
10. Rey S, Del Rio R, Alcayaga J, Iturriaga R. Chronic intermittent hypoxia enhances cat chemosensory and ventilatory responses to hypoxia. *J Physiol.* 2004;560(Pt2):577-586.
11. Prabhakar NR, Peng YJ, Jacono FJ, Kumar GK, Dick TE. Cardiovascular alterations by chronic intermittent hypoxia: importance of carotid body chemoreflexes. *Clin Exp Pharmacol Physiol.* 2005;32(5-6):447-449.
12. Cohn JN, Levine TB, Olivari MT, Garberg V, Lura D, Francis GS, Simon AB, Rector T. Plasma norepinephrine as a guide to prognosis in patients with chronic congestive heart failure. *N Engl J Med.* 1984;311(13):819-823.
13. Barretto AC, Santos AC, Munhoz R, Rondon MU, Franco FG, Trombetta IC, Roveda F, de Matos LN, Braga AM, Middlekauff HR, Negrão CE. Increased muscle sympathetic nerve activity predicts mortality in heart failure patients. *Int J Cardiol.* 2009;135(3):302-307.
14. Ueno H, Asanoi H, Yamada K, Oda Y, Takagawa J, Kameyama T, Hirai T, Nozawa T, Takashima S, Inoue H. Attenuated respiratory modulation of chemoreflex-

mediated sympathoexcitation in patients with chronic heart failure. *J Card Fail.* 2004;10(3):236-243.
15. Floras JS. Sympathetic nervous system activation in human heart failure: clinical implications of an updated model. *J Am Coll Cardiol.* 2009;54(5):375-385.
16. Oda Y, Joho S, Harada D, Hirai T, Asanoi H, Inoue H. Renal insufficiency coexisting with heart failure is related to elevated sympathetic nerve activity. *Auton Neurosci.* 2010;155(1-2):104-108.
17. Grisk O. The sympathetic nervous system in acute kidney injury. *Acta Physiol.* 2020;228(2):e13404.
18. Fu Q. Sex differences in sympathetic activity in obesity and its related hypertension. *Ann N Y Acad Sci.* 2019;1454(1):31-41.
19. Shi Z, Wong J, Brooks VL. Obesity: sex and sympathetics. *Biol Sex Differ.* 2020;11(1):10.
20. Ribeiro MJ, Sacramento JF, Gonzalez C, Guarino MP, Monteiro EC, Conde SV. Carotid body denervation prevents the development of insulin resistance and hypertension induced by hypercaloric diets. *Diabetes.* 2013;62(8):2905-2916.
21. Farsalinos K, Barbouni A, Niaura R. Systematic review of the prevalence of current smoking among hospitalized COVID-19 patients in China: could nicotine be a therapeutic option? Intern Emerg Med. 2020:1-8.
22. Patanavanich R, Glantz SA. Smoking is Associated with COVID-19 Progression: A Meta-Analysis. Nicotine Tob Res. [published online May 13, 2020].
23. Karanasos A, Aznaouridis K, Latsios G, Synetos A, Plitaria S, Tousoulis D, Toutouzas K. Impact of smoking status on disease severity and mortality of hospitalized patients with COVID-19 infection: a systematic review and meta-analysis. Nicotine Tob Res. 2020:ntaa107.
24. Kotamäki M. Smoking induced differences in autonomic responses in military pilot candidates. Clin Auton Res. 1995;5(1):31-36.
25. Narkiewicz K, van de Borne PJ, Hausberg M, Cooley RL, Winniford MD, Davison DE, Somers VK. Cigarette smoking increases sympathetic outflow in humans. Circulation. 1998;98(6):528-534.
26. Gerhardt U, Vorneweg P, Riedasch M, Hohage H. Acute and persistant effects of smoking on the baroreceptor function. J Auton Pharmacol. 1999;19(2):105-108.
27. Arosio E, De Marchi S, Rigoni A, Prior M, Lechi A. Effects of smoking on cardiopulmonary baroreceptor activation and peripheral vascular resistance. Eur J Clin Invest. 2006;36(5):320-325.
28. Manzano BM, Vanderlei LC, Ramos EM, Ramos D. Acute effects of smoking on autonomic modulation: analysis by Poincaré plot. Arq Bras Cardiol. 2011;96(2):154-160.
29. Matsushita K, Marchandot B, Jesel L, Ohlmann P, Morel O. Impact of COVID-19 on the Cardiovascular System: A Review. *J Clin Med.* 2020;9(5):E1407.
30. Ruan Q, Yang K, Wang W, Jiang L, Song J. Clinical predictors of mortality due to COVID-19 based on an analysis of data of 150 patients from Wuhan, China. *Intensive Care Med.* 2020;46(5):846-848.
31. Xu Z, Shi L, Wang Y, Zhang J, Huang L, Zhang C, Liu S, Zhao P, Liu H, Zhu L, Tai Y, Bai C, Gao T, Song J, Xia P, Dong J, Zhao J, Wang FS. Pathological findings of COVID-19 associated with acute respiratory distress syndrome. *Lancet Respir Med.* 2020;8(4):420-422.
32. Shi S, Qin M, Shen B, Cai Y, Liu T, Yang F, Gong W, Liu X, Liang J, Zhao Q, Huang H, Yang B, Huang C. Association of Cardiac Injury With Mortality in Hospitalized

Patients With COVID-19 in Wuhan, China [published online March 25, 2020]. *JAMA Cardiol.*
33. Huang I, Lim MA, Pranata R. Diabetes mellitus is associated with increased mortality and severity of disease in COVID-19 pneumonia - A systematic review, meta-analysis, and meta-regression. *Diabetes Metab Syndr.* 2020;14(4):395-403.
34. Minhas AS, Scheel P, Garibaldi B, Liu G, Horton M, Jennings M, Jones SR, Michos ED, Hays AG. Takotsubo Syndrome in the Setting of COVID-19 Infection. JACC Case Rep. [published online May 1, 2020].
35. Pasqualetto MC, Secco E, Nizzetto M, Scevola M, Altafini L, Cester A, Rigo F. Stress Cardiomyopathy in COVID-19 Disease. Eur J Case Rep Intern Med. 2020;7(6):001718.
36. Giustino G, Croft LB, Oates CP, Rahman K, Lerakis S, Reddy VY, Goldman M. Takotsubo Cardiomyopathy in Males with COVID-19. J Am Coll Cardiol. 2020:S0735-1097(20)35551-0.
37. Taza F, Zulty M, Kanwal A, Grove D. Takotsubo cardiomyopathy triggered by SARS-CoV-2 infection in a critically ill patient. BMJ Case Rep. 2020;13(6):e236561.
38. Schiller AM, Pellegrino PR, Zucker IH. The renal nerves in chronic heart failure: efferent and afferent mechanisms. *Front Physiol.* 2015;6:224.
39. Kiuchi MG, Ho JK, Nolde JM, Gavidia LML, Carnagarin R, Matthews VB, Schlaich MP. Sympathetic Activation in Hypertensive Chronic Kidney Disease - A Stimulus for Cardiac Arrhythmias and Sudden Cardiac Death? *Front Physiol.* 2020;10:1546.
40. Sorino C, Scichilone N, Pedone C, Negri S, Visca D, Spanevello A. When kidneys and lungs suffer together. *J Nephrol.* 2019;32(5):699-707.
41. Kukla M, Skonieczna-Żydecka K, Kotfis K, Maciejewska D, Łoniewski I, Lara LF, Pazgan-Simon M, Stachowska E, Kaczmarczyk M, Koulaouzidis A, Marlicz W. COVID-19, MERS and SARS with Concomitant Liver Injury-Systematic Review of the Existing Literature. J Clin Med. 2020;9(5):E1420.
42. Joung JY, Cho JH, Kim YH, Choi SH, Son CG. A literature review for the mechanisms of stress-induced liver injury. *Brain Behav.* 2019;9(3):e01235.
43. Felten DL, Felten SY, Carlson SL, Olschowka JA, Livnat S. Noradrenergic and peptidergic innervation of lymphoid tissue. *J Immunol.* 1985;135(2 Suppl):755s-765s.
44. Brodde OE, Engel G, Hoyer D, Bock KD, Weber F. The beta-adrenergic receptor in human lymphocytes: subclassification by the use of a new radio-ligand, (+/-)-125 Iodocyanopindolol. *Life Sci.* 1981;29(21):2189-2198.
45. Marvar PJ, Thabet SR, Guzik TJ, Lob HE, McCann LA, Weyand C, Gordon FJ, Harrison DG. Central and peripheral mechanisms of T-lymphocyte activation and vascular inflammation produced by angiotensin II-induced hypertension. *Circ Res.* 2010;107(2):263-270.
46. Xiao L, Kirabo A, Wu J, Saleh MA, Zhu L, Wang F, Takahashi T, Loperena R, Foss JD, Mernaugh RL, Chen W, Roberts J 2nd, Osborn JW, Itani HA, Harrison DG. Renal Denervation Prevents Immune Cell Activation and Renal Inflammation in Angiotensin II-Induced Hypertension. *Circ Res.* 2015;117(6):547-557.
47. Zaldivia MT, Rivera J, Hering D, Marusic P, Sata Y, Lim B, Eikelis N, Lee R, Lambert GW, Esler MD, Htun NM, Duval J, Hammond L, Eisenhardt SU, Flierl U, Schlaich MP, Peter K. Renal Denervation Reduces Monocyte Activation and Monocyte-Platelet Aggregate Formation: An Anti-Inflammatory Effect Relevant for Cardiovascular Risk. *Hypertension.* 2017;69(2):323-331.
48. Heidt T, Sager HB, Courties G, Dutta P, Iwamoto Y, Zaltsman A, von Zur Muhlen C, Bode C, Fricchione GL, Denninger J, Lin CP, Vinegoni C, Libby P, Swirski FK,

Weissleder R, Nahrendorf M. Chronic variable stress activates hematopoietic stem cells. *Nat Med.* 2014;20(7):754-758.
49. Ganta CK, Lu N, Helwig BG, Blecha F, Ganta RR, Zheng L, Ross CR, Musch TI, Fels RJ, Kenney MJ. Central angiotensin II-enhanced splenic cytokine gene expression is mediated by the sympathetic nervous system. *Am J Physiol Heart Circ Physiol.* 2005;289(4):H1683-1691.
50. Wang H, Yu M, Ochani M, Amella CA, Tanovic M, Susarla S, Li JH, Wang H, Yang H, Ulloa L, Al-Abed Y, Czura CJ, Tracey KJ. Nicotinic acetylcholine receptor alpha7 subunit is an essential regulator of inflammation. *Nature.* 2003;421(6921):384-388.
51. Huston JM, Ochani M, Rosas-Ballina M, Liao H, Ochani K, Pavlov VA, Gallowitsch-Puerta M, Ashok M, Czura CJ, Foxwell B, Tracey KJ, Ulloa L. Splenectomy inactivates the cholinergic antiinflammatory pathway during lethal endotoxemia and polymicrobial sepsis. *J Exp Med.* 2006;203(7):1623-1628.
52. Ghia JE, Blennerhassett P, Kumar-Ondiveeran H, Verdu EF, Collins SM. The vagus nerve: a tonic inhibitory influence associated with inflammatory bowel disease in a murine model. *Gastroenterology.* 2006;131(4):1122-1130.
53. Sun P, Zhou K, Wang S, Li P, Chen S, Lin G, Zhao Y, Wang T. Involvement of MAPK/NF-κB signaling in the activation of the cholinergic anti-inflammatory pathway in experimental colitis by chronic vagus nerve stimulation. *PLoS One.* 2013;8(8):e69424.
54. Goverse G, Stakenborg M, Matteoli G. The intestinal cholinergic anti-inflammatory pathway. *J Physiol.* 2016;594(20):5771-5780.
55. McAllen RM, Cook AD, Khiew HW, Martelli D, Hamilton JA. The interface between cholinergic pathways and the immune system and its relevance to arthritis. *Arthritis Res Ther.* 2015;17:87.
56. Shirai M, Tsuchimochi H, Nagai H, Gray E, Pearson JT, Sonobe T, Yoshimoto M, Inagaki T, Fujii Y, Umetani K, Kuwahira I, Schwenke DO. Pulmonary vascular tone is dependent on the central modulation of sympathetic nerve activity following chronic intermittent hypoxia. *Basic Res Cardiol.* 2014;109(5):432.
57. Vaillancourt M, Chia P, Sarji S, Nguyen J, Hoftman N, Ruffenach G, Eghbali M, Mahajan A, Umar S. Autonomic nervous system involvement in pulmonary arterial hypertension. *Respir Res.* 2017;18(1):201.
58. Iturriaga R, Castillo-Galán S. Potential Contribution of Carotid Body-Induced Sympathetic and Renin-Angiotensin System Overflow to Pulmonary Hypertension in Intermittent Hypoxia. *Curr Hypertens Rep.* 2019;21(11):89.
59. Bilodeau MS, Leiter JC. Angiotensin 1-7 in the rostro-ventrolateral medulla increases blood pressure and splanchnic sympathetic nerve activity in anesthetized rats. *Respir Physiol Neurobiol.* 2018;247:103-111.
60. Cure E, Cumhur Cure M. Angiotensin-converting enzyme inhibitors and angiotensin receptor blockers may be harmful in patients with diabetes during COVID-19 pandemic. *Diabetes Metab Syndr.* 2020;14(4):349-350.
61. Cure E, Cumhur Cure M. Comment on "Should COVID-19 Concern Nephrologists? Why and to What Extent? The Emerging Impasse of Angiotensin Blockade" [published online April 20, 2020]. *Nephron.*
62. Al-Dhahir MA, M Das J, Sharma S. Neurogenic Pulmonary Edema. *StatPearls*. Treasure Island (FL): StatPearls Publishing; 2020 Jan-2020 Mar 28.
63. Joho S, Ushijima R, Akabane T, Hirai T, Inoue H. Restrictive Lung Function Is Related to Sympathetic Hyperactivity in Patients With Heart Failure. *J Card Fail.* 2017;23(2):96-103.

64. Matsukawa T, Sugiyama Y, Watanabe T, Kobayashi F, Mano T. Gender difference in age-related changes in muscle sympathetic nerve activity in healthy subjects. *Am J Physiol.* 1998;275(5):R1600-1604.
65. Weise M, Eisenhofer G, Merke DP. Pubertal and gender-related changes in the sympathoadrenal system in healthy children. *J Clin Endocrinol Metab.* 2002;87(11):5038-5043.
66. Lambert E, Straznicky N, Eikelis N, Esler M, Dawood T, Masuo K, Schlaich M, Lambert G. Gender differences in sympathetic nervous activity: influence of body mass and blood pressure. *J Hypertens.* 2007;25(7):1411-1419.
67. Tank J, Heusser K, Diedrich A, Hering D, Luft FC, Busjahn A, Narkiewicz K, Jordan J. Influences of gender on the interaction between sympathetic nerve traffic and central adiposity. *J Clin Endocrinol Metab.* 2008;93(12):4974-4978.
68. Alvarez GE, Beske SD, Ballard TP, Davy KP. Sympathetic neural activation in visceral obesity. *Circulation.* 2002;106(20):2533-2536.
69. Kuba K, Imai Y, Rao S, Gao H, Guo F, Guan B, Huan Y, Yang P, Zhang Y, Deng W, Bao L, Zhang B, Liu G, Wang Z, Chappell M, Liu Y, Zheng D, Leibbrandt A, Wada T, Slutsky AS, Liu D, Qin C, Jiang C, Penninger JM. A crucial role of angiotensin converting enzyme 2 (ACE2) in SARS coronavirus-induced lung injury. *Nat Med.* 2005;11(8):875-879.
70. Haga S, Yamamoto N, Nakai-Murakami C, Osawa Y, Tokunaga K, Sata T, Yamamoto N, Sasazuki T, Ishizaka Y. Modulation of TNF-alpha-converting enzyme by the spike protein of SARS-CoV and ACE2 induces TNF-alpha production and facilitates viral entry. *Proc Natl Acad Sci USA.* 2008;105(22):7809-7814.
71. Glowacka I, Bertram S, Herzog P, Pfefferle S, Steffen I, Muench MO, Simmons G, Hofmann H, Kuri T, Weber F, Eichler J, Drosten C, Pöhlmann S. Differential downregulation of ACE2 by the spike proteins of severe acute respiratory syndrome coronavirus and human coronavirus NL63. *J Virol.* 2010;84(2):1198-1205.
72. Zhang H, Penninger JM, Li Y, Zhong N, Slutsky AS. Angiotensin-converting enzyme 2 (ACE2) as a SARS-CoV-2 receptor: molecular mechanisms and potential therapeutic target. *Intensive Care Med.* 2020;46(4):586-590.
73. Gurwitz D. Angiotensin receptor blockers as tentative SARS-CoV-2 therapeutics [published online March 4, 2020]. *Drug Dev Res.*
74. Fung ML. The role of local renin-angiotensin system in arterial chemoreceptors in sleep-breathing disorders. *Front Physiol.* 2014;5:336.
75. Liu Y, Yang Y, Zhang C, Huang F, Wang F, Yuan J, Wang Z, Li J, Li J, Feng C, Zhang Z, Wang L, Peng L, Chen L, Qin Y, Zhao D, Tan S, Yin L, Xu J, Zhou C, Jiang C, Liu L. Clinical and biochemical indexes from 2019-nCoV infected patients linked to viral loads and lung injury. *Sci China Life Sci* 2020;63(3):364-374.
76. Li YC, Bai WZ, Hashikawa T. The neuroinvasive potential of SARS-CoV2 may play a role in the respiratory failure of COVID-19 patients [published online February 27, 2020]. *J Med Virol.*
77. Pedersen SF, Ho YC. SARS-CoV-2: a storm is raging [published online April 13, 2020]. *J Clin Invest.*
78. Lee YB, Nagai A, Kim SU. Cytokines, chemokines, and cytokine receptors in human microglia. *J Neurosci Res.* 2002;69(1):94-103.
79. Recinos A 3rd, LeJeune WS, Sun H, Lee CY, Tieu BC, Lu M, Hou T, Boldogh I, Tilton RG, Brasier AR. Angiotensin II induces IL-6 expression and the Jak-STAT3 pathway in aortic adventitia of LDL receptor-deficient mice. *Atherosclerosis.* 2007;194(1):125-133.

80. Yamamoto S, Yancey PG, Zuo Y, Ma LJ, Kaseda R, Fogo AB, Ichikawa I, Linton MF, Fazio S, Kon V. Macrophage polarization by angiotensin II-type 1 receptor aggravates renal injury-acceleration of atherosclerosis. *Arterioscler Thromb Vasc Biol.* 2011;31(12):2856-2864.
81. Lu P, Liang LW, Xu AL, Sun YY, Jiang SJ, Shi Z. Pro-inflammatory cytokines in the paraventricular nucleus mediate the adipose afferent reflex in rats. *Pflugers Arch*. 2020;472(3):343-354.
82. Custaud MA, Belin de Chantemele E, Larina IM, Nichiporuk IA, Grigoriev A, Duvareille M, Gharib C, Gauquelin-Koch G. Hormonal changes during long-term isolation. *Eur J Appl Physiol.* 2004;91(5-6):508-515.
83. Xia N, Li H. Loneliness, Social Isolation, and Cardiovascular Health. *Antioxid Redox Signal.* 2018;28(9):837-851.

Chapter 4

Genomic surveillance of SARS-CoV-2 in patients presenting neurological manifestations

*The present chapter has been previously published in: Vicco A., Caccuri F., Messali S., Vitiello A., **Emmi A.**, et al. Genomic surveillance of SARS-CoV-2 in patients presenting neurological manifestations. PLOS One, 2022. doi: https://doi.org/10.1371/journal.pone.0270024. This article is licensed under a CC BY license.*

ABSTRACT

During the first wave of infections, neurological symptoms in Coronavirus Disease 2019 (COVID-19) patients raised particular concern, suggesting that, in a subset of patients, the severe acute respiratory syndrome coronavirus 2 (SARS-CoV-2) could invade and damage cells of the central nervous system (CNS). Indeed, up to date several in vitro and in vivo studies have shown the ability of SARS-CoV-2 to reach the CNS. Both viral and/or host related features could explain why this occurs only in certain individuals and not in all the infected population. The aim of the present study was to evaluate if onset of neurological manifestations in COVID-19 patients was related to specific viral genomic signatures. To this end, viral genome was extracted directly from nasopharyngeal swabs of selected SARS-CoV-2 positive patients presenting a spectrum of neurological symptoms related to COVID-19, ranging from anosmia/ageusia to more severe symptoms. By adopting a whole genome sequences approach, here we describe a panel of known as well as unknown mutations detected in the analyzed SARS-CoV-2 genomes. While some of the found mutations were already associated with an improved viral fitness, no common signatures were detected when comparing viral sequences belonging to specific groups of patients. In conclusion, our data support the notion that COVID-19 neurological manifestations are mainly linked to patient-specific features more than to virus genomic peculiarities.

INTRODUCTION

The severe acute respiratory syndrome coronavirus 2 (SARS-CoV-2) is a member of the Coronaviridae family, a group of viruses that can infect both mammals and birds. SARS-CoV-2 has a probable zoonotic origin with bat as primary host [1,2]. Differently from endemic human Coronaviruses, e.g. OC43 and 229E viruses, SARS-CoV-2 not only infects the upper respiratory tract, but it can also spread to the lower tract, leading to a more severe respiratory disease [3].

SARS-CoV-2 genome is a positive-sense single-stranded RNA that contains 14 open reading frames (ORFs). At the 5' end of the genome, there are the leader sequence and an untranslated region (UTR). Then, the gene encoding for the viral Replicase-Transcriptase complex, which is an RNA-dependent RNA polymerase, occupies two-thirds of the genome. This gene is made of two ORFs, ORF1a and ORF1b, that are translated together as two co-terminal polyproteins [4]. These polyproteins then auto-proteolytically cleave themselves into several products called non- structural proteins (nsp from 1 to 16) with several functions. One of the most important nsp is the nsp12 that represents the RNA-dependent RNA polymerase (RdRp). At the 3' end of the genome instead are located the genes encoding for the following structural proteins: i) the spike S glycoprotein, ii) the envelope E protein, iii) the membrane M protein, iv) the nucleocapsid N protein. Also, genes encoding for accessory proteins are located at the 3' terminal. In the viral particle, the RNA genome is tightly bound to N in a helical symmetric nucleocapsid. The viral particle is also surrounded by an envelope made of lipidic layers acquired from the host Endoplasmic Reticulum-Golgi intermediate compartment (ERGIC) and containing the viral spike (S), envelope (E) and membrane (M) proteins [5]. Viral RNA genome is known to rapidly acquire mutations while replicating, as RNA-dependent RNA polymerases are more prone to introduce errors than DNA-dependent DNA polymerases. Interestingly, the replicase of Coronaviridae is characterized by a proofreading activity linked to the amino-terminal exoribonuclease (ExoN) domain of the Nsp14 enzyme that can correct errors inserted in the viral genome [6]. Although this feature reduces the rate of sequence variability, SARS-CoV-2 can still acquire relevant mutations as it spreads worldwide. Indeed, the constant and relevant human-to-human transmission, the natural adaptation of the virus to the new host as well as the more recent pressure of vaccination, facilitate occurrence of mutations that can be fixed in the viral population, as shown by the emergence of different variants since the beginning of the pandemic (https://www.cdc.gov/coronavirus/2019-ncov/variants/variant-classifications.html, accessed

on 15th of March 2021). Currently, viral variants are classified into larger groups named lineages or clades. Different clade/lineage nomenclatures have been proposed. Among these, the Phylogenetic Assignment of Named Global Outbreak Lineages (PANGOLIN) is a software that allows a dynamic nomenclature (known as the PANGO nomenclature) of SARS-CoV-2 lineages [7]. SARS-CoV- 2 variants are grouped according to their lineage and component mutations [8]. The World Health Organization (WHO) classifies some of the emerging variants as variants of concern (VOC), variants of interest (VOI) or variants under monitoring (VUM), based on their transmissibility and/or infection severity. All these variants are named with letters of the Greek alphabet [9]. Delta (B.1.617.2) and Omicron (B.A.1 and B.A.2) are the VOC currently circulating (https://www.ecdc.europa.eu/en/covid-19/variants-concern, accessed on 12th of May 2022).

Viral entry into host cells is mainly mediated by the S envelope protein, which is composed of two subunits named S1 and S2 [10]. Virus attachment to the target cells involves S1 and the host angiotensin-converting enzyme 2 (ACE-2) receptor. Following steps are allowed by the cellular proteins cathepsin L and transmembrane protease serine 2 (TMPRSS2) that, acting on the S1/S2 complex, lead to the exposure of a fusion peptide belonging to the S2 subunit [10].

Coronavirus Disease 2019 (COVID-19) is mainly a respiratory disease, but it can also involve additional organs, causing hepatic, enteric, neurological as well as psychiatric symptoms [11]. Neurological manifestations associated to COVID-19 have attracted particular attention. Among the most frequent neurological signs detected in COVID-19 patients there are headache, dizziness, nausea, confusion [12, 13], smell and taste disorders even at early stages of the disease [14, 15], while the most common complications are stroke, neurological damage, ataxia, delirium, brain and spinal cord inflammation [13], encephalopathies and encephalitis [16, 17]. Moreover, an increased incidence of Acute Disseminated EncephaloMyelitis (ADEM) has been reported in COVID-19 patients [18]. Different respiratory viruses, including Coronaviruses, are known to infect the brain tissue [19, 20]. For example, neuroinvasion and neurovirulence of the human coronavirus OC43 (HCoV-OC43), SARS-CoV-1 and Middle East Respiratory Syndrome (MERS)-CoV were reported in transgenic mice [20]. Importantly, ACE2 was shown to be highly expressed in neurons, astrocytes, and oligodendrocytes [22, 23]. The SARS-CoV-2 ability to infect the human brain has been further analyzed in human neural progenitor cells and brain organoids [24, 25]. In addition, SARS-CoV-2 RNA was detected in brains [26] and in the cerebrospinal fluid (CSF) of some COVID-19 patients, indicating a possible pathophysiological

involvement of the virus in the neurological symptoms [27]. The pathogenetic mechanisms accounting for SARS-CoV-2 related neurological manifestations have been deeply analyzed in many recent studies (reviewed in [11]). Up to now, two hypotheses have been proposed to explain the COVID-19 neuropathogenesis. On the one hand, SARS-CoV-2 may enter the CNS through the olfactory bulb by binding to the ACE-2 receptor, damaging the blood brain barrier (BBB) or even exploiting leukocytes as a Trojan horse mechanisms [28]. The neurological symptoms would be, then, a consequence of the direct viral damage to brain tissues. In this context, specific regions of the viral genome could play a role in neurotropism and/or neurovirulence. On the other hand, SARS-CoV-2 replication in the lungs, in addition of causing pulmonary dysfunctions, is known to trigger an intense and dysregulated systemic inflammatory process called cytokine storm, which is a common feature of severe COVID-19 cases. The cytokine storm has consequences for the entire organism and might affect the CNS, even without a direct invasion of the brain by the virus [28, 29]. Finally, viral entry into the CNS may trigger a localized inflammatory response that could affect the CNS by itself, or in combination with the cytokine storm [11, 29].

Here we investigated whether viral genomes obtained from selected patients displayed peculiar mutations associated to the degree of severity of the neurological symptoms. To avoid artifacts due to the high viral mutation rates in vitro, we avoided virus amplification in cell culture and directly sequenced the viral genomic RNA obtained from the nasopharyngeal swabs of the enrolled individuals. First, we focused our attention on two SARS-CoV-2 envelope proteins: i) the spike glycoprotein, which is responsible for the viral tropism and the viral entry into target cells, ii) the E protein, that is linked to the modulation of the inflammatory responses in several Coronaviruses. Second, a whole genome analysis was performed to detect mutations that might be related to neurovirulence. Overall our data indicate that no mutations can be found associated to specific neurological symptoms or to their severity, thus supporting the notion that CNS manifestations in COVID-19 patients are mainly linked to the individual inflammatory response, more than to peculiar viral features.

MATERIALS AND METHODS

Study design

The study was approved by the Padua Hospital Research Ethics Committee (Protocol 056881). A group of patients displaying SARS-CoV-2 related neurological symptoms with different degrees of severity was selected, as shown in Table 2 (Results section). All enrolled

subjects underwent Magnetic Resonance Imaging (MRI). Informed consent was obtained from all participants.

Nasopharyngeal swabs were handled, following standard procedure to inactivate the virus. Viral RNA was directly extracted by an automatic nucleic acids extractor (MagNA Pure by Roche), following the manufacturer's instructions. Obtained samples were coded with letters from A to G, according to chronological order of the extraction date. In particular, viral extract from patient A was obtained on March 27, those from patients B, C, D, E and F were collected between March 4 and 12, while the viral RNA from patient G was extracted on November 23, 2020. Following analyses were conducted in blind, meaning that no information on symptoms were known until the overall sequencing results were analyzed.

Sanger sequencing

First, genes of interest (E and S) were retro-transcribed from total RNA viral extracts by the AgPath-IDT One-Step RT-PCR kit (Thermofisher), following the manufacturer's instructions. The adopted oligonucleotides sequences and position within the target are reported in Table 1 and in Figure 1, respectively. Briefly, for the E sequence adopted oligonucleotides mapped at the 3' and 5' ends of the gene; while three pairs of primers were designed to reverse-transcribe the large S gene into three fragments of similar length (Figure 1).

Next, to obtain a sufficient amount of cDNA, an additional PCR amplification step was carried on by using the same primers described above along with the high-fidelity DNA-dependent polymerase Phusion Hot Start II High-Fidelity DNA Polymerase (Invitrogen). The PCR products were purified by NucleoSpin Gel and PCR Clean-up kit (Macherey-Nagel), and 6.4 pmoles were dried at 65°C for a few minutes. Sanger sequencing of the PCR products was performed by BMR Genomics (Padua, Italy), by adopting the same pairs of oligonucleotides reported in Table 1 and Figure 1.

Primer name	Primer sequence 5'-3'
Primer E forward	ATGTACTCATTCGTTTCGGA
Primer E reverse	TTAGACCAGAAGATCAGGA
Primer S forward	ATGTTTGTTTTTCTTGTTTTATTGCCACTA
Primer S reverse	GCTCAAAGGAGTCAAATTACATTACACATA
Primer S1 reverse	GGGCAAACTGGAAAGATTGCTG
Primer S2 forward	GCAAACTGGAAAGATTGCTGATTATA
Primer S2 reverse	TCTACTTTTCAACAAAGTGACACTTG
Primer S3 forward	TTTCAACAAAGTGACACTTGCAGAT

Table 1. Sequences of primers adopted for Sanger sequencing of E and S genes. *The table displays the sequences of the oligonucleotides adopted for reverse-transcription and amplification of the S and E genes performed in order to Sanger sequence these viral genomic regions.*

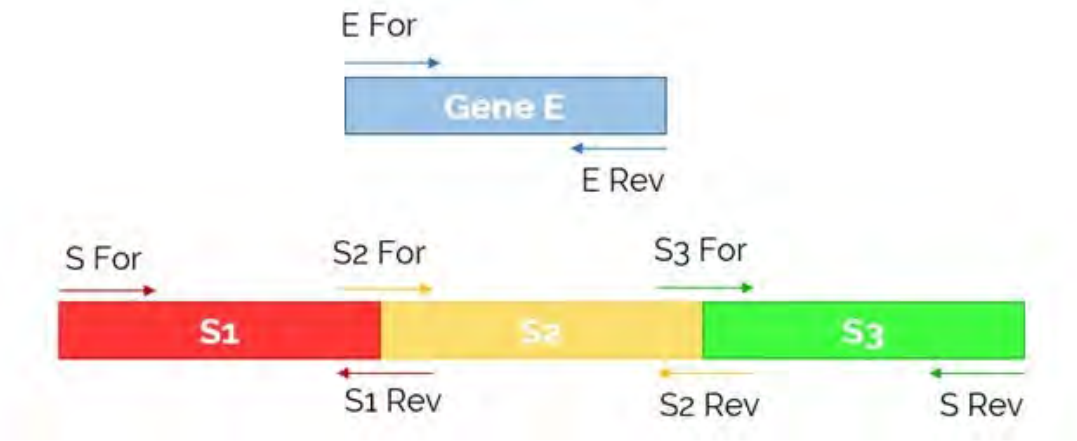

Figure 1. Primer position within the gene of interest. *The figure schematically display where primers adopted for reverse-transcription, amplification and sequencing of the E (light blue) and S (red, yellow and green) genes map within the viral regions of interest. While a single pair of oligonucleotides were designed to amplify and sequence the entire E gene, one couple of external primers along with two additional pair of internal primers were used in the case of the S gene. "E For" stands for primer E forward ; "E Rev" for primer E reverse, "S For" for primer S forward; "S1 Rev" for primer S1 reverse; "S2 For" for primer S2 forward; "S2 Rev" for primer S2 reverse, "S3 For" for primer S3 forward; "S Rev" for primer S reverse.*

Whole genome sequencing

For the whole genome sequencing, an amplicon-based approach, targeting 343 partially overlapping subgenomic regions, that cover the entire SARS-CoV-2 genome, was used.

Virus genomes were generated using Paragon Genomics' CleanPlex multiplex PCR Research and Surveillance Panel, according to the manufacturer's protocol [30, 31]. Briefly, similar amounts of RNA were reverse transcribed with random primers and the resulting cDNA, magnetically purified, was used as template in a 10 µl-multiplex PCR performed with two pooled-primer mixtures. Samples were treated with 2 µl of CleanPlex digestion reagent at 37°C for 10 min to remove non-specific PCR products. After magnetic bead purification, PCR products were subjected to further 25 rounds of amplification in a secondary PCR where indexed primers allow to generate the amplicons library. Subsequently, purified libraries were quantified with the Qubit DNA HS Assay Kit (Thermo Fisher Scientific). Amplicon libraries were loaded in a 300-cycle sequencing cartridge and deep sequencing was performed on MiSeq platform (Illumina, San Diego, CA, USA). Sequencing raw data were checked for quality using FastQC (https://www.bioinformatics.babraham.ac.uk/projects/fastqc) and then analyzed with software SOPHiA GENETICS' SARS-CoV-2 Panel (SOPHiA GENETICS, Lausanne, Switzerland). To confirm data analyses, the paired-end reads were trimmed with Trimmomatic ver. 0.38 for quality (Q score > 25) and length (> 36 bp) and assayed by the Geneious® software (version 11.1.5) (Biomatters Ltd, New Zealand). The consensus sequence was reconstructed by mapping the reads to the SARS-CoV-2 reference sequence NC_045512 using Bowtie2 in sensitive-local mode with consensus threshold at 65%. The variant calling was carried out by the Variant Finder Tool (Geneious) filtering out variants with a p-value greater than 0, using a minimum variant frequency of 0 and default parameters for Maximum Variant p-value (10^{-6}).

Sequence alignment and classification of viral sequences into SARS-CoV-2 lineages and clades

The pool of sequences obtained by NGS was aligned with those reported in the GISAID online database (https://www.gisaid.org/ accessed on March 15th 2021). Specifically, mutation analysis was performed exploiting the CoVsurver application of GISAID (https://www.gisaid.org/epiflu-applications/covsurver-mutations-app/ accessed on the 15th of March 2021). Classification into clades was performed through Nextstrain (https://nextstrain.org/SARS-CoV-2/ accessed on the 15th of March 2021), while lineage assessment was conducted using the Phylogenetic Assignment of Named Global Outbreak LINeages (PANGOLIN) tool available at https://github.com/hCoV-2019/pangolin [32] (accessed on the 15th of March 2021) .

Phylogenetic analysis

Public SARS-CoV-2 complete genome sequences (>29 Kb), available in the GISAID repository until December 2021 were retrieved. Low-quality genomes and nearly identical sequences (genetic similarity > 99.99%) were excluded, obtaining a global dataset of 2463 public genomes plus 7 genomes reported in this study. The global datasets of 2470 whole genome sequences were aligned by MAFFT (FF-NS-2 algorithm) using default parameters [33]. The alignment was manually curated using Aliview [34] to remove artifacts at the ends. Phylogenetic analysis was performed using IQ-TREE (version 1.6.10) under the best fit model according to Bayesian Information Criterion (BIC) indicated by the Model Finder application implemented in IQ-TREE [35]. The statistical robustness of individual nodes was determined using 1000 bootstrap replicates.

RESULTS

The S and E proteins shared a conserved sequence among the SARS-CoV-2 genomes under study

Patients enrolled in this study were all SARS-CoV-2 positive subjects belonging to one of the following three groups based on their neurological symptoms: symptomatic, mild-symptomatic, asymptomatic. Patients were coded with letters from A to G, according to chronological order of viral RNA extraction date. In this manuscript, for clarity reasons, these capital letters are followed by the lower case letters “s”, “m” or “a”, representing the relative neurological symptomatology (symptomatic, mild-symptomatic, asymptomatic, respectively). In more details:

- Patients As, Fs and Gs were severely symptomatic (s), displaying neurological signs already reported as associated to COVID-19, i.e. generalized seizures and encephalopathy. In addition to these common manifestations, patient Fs had also a stroke. As, Fs, Gs were hospitalized and displayed severe respiratory symptoms, requiring intubation.
- Patients Cm and Em were mildly symptomatic (m), showing smell deficit, that was full recovered only by patient Em.
- Patients Ba and Da were the negative controls, as they were SARS-CoV-2 positive but display neither neurological nor non-neurological symptoms [asymptomatic (a)].

None of the patients reported relevant comorbidities. Main information on the enrolled individuals is summarized in Table 2.

Total viral RNA was recovered directly from nasopharyngeal swabs of the selected patients, to avoid possible accumulation of mutations during SARS-CoV-2 amplification in cell culture. Next, the S and E envelope genes were Sanger sequenced. In the case of the S gene, all sequences were sharing the same A to G substitution with respect to the Wuhan-Hu-1 reference sequence (NCBI Reference Sequence: NC_045512.2), at position 23403 of genomic RNA. This nucleotide variation corresponds to a predicted amino acidic substitution of an aspartic acid (D) to a glycine (G) in the amino acidic position 614. The D614G is well known as it represents the most significant characteristic of an early SARS-CoV-2 variant [36] that rapidly spread in Europe and USA, becoming responsible for the greatest number of infections, by May 2020. Our data show that this variant was circulating in Italy (Veneto Region), since early March 2020. In the case of the E gene, all sequences were identical to the one of the Wuhan reference strain.

In conclusion, from viral genomes deriving from a specific group of patients no peculiar and common sequence signature were detected in the S or E genes, at least with the Sanger sequencing.

Code	Age	Sex	Clinical symptoms	Imaging	Outcome
As	55	M	Encephalopathy, generalized seizures and interstitial pneumonia	MRI negative	Full recovery
Ba	29	M	Asymptomatic	MRI negative	Full recovery
Cm	26	F	Smell deficit	MRI negative	Smell dysfunction after 6 months
Da	30	F	Asymptomatic	MRI negative	Full recovery
Em	31	F	Smell deficit	MRI negative	Full recovery
Fs	74	M	Encephalopathy, seizures, stroke and interstitial pneumonia	Lesions related to stroke	Hemiparesis, cognitive disturbances
Gs	77	F	Encephalopathy, generalized seizures and interstitial pneumonia	MRI negative	Full recovery

Table 2. Characteristics of the enrolled COVID-19 patients relevant for the study. *The Table reports main information of COVID-19 patients enrolled in this study. Patients were coded with capital letter from A to G. In this manuscript, additional lower case letters were associated to each patient in relation to her/his neurological symptoms as follows: s=symptomatic, m = mild-symptomatic, a =asymptomatic. Each patient underwent magnetic resonance imaging (MRI).*

Whole genome sequencing highlighted several known mutations present in the viral extracts but none common and unique of SARS-CoV-2 genomes retrieved from neurological symptomatic patients

Despite the finding that all viral genomes under evaluation shared identical E and S genes, peculiar features associated with neurological symptoms could not be ruled out in other SARS-CoV-2 genomic regions. Thus, a whole-genome analysis by next generation sequencing was carried out starting from the same viral RNA extracts adopted for the E and S Sanger sequencing. Specifically, the Illumina MiSeq platform was applied on 343 partially overlapping subgenomic regions, obtained by an amplicon-based approach to cover the entire SARS-CoV-2 genome. Obtained sequences were aligned with the Wuhan-Hu-1 reference sequence (NCBI Reference Sequence: NC_045512.2). The Geneious Find Variations/SNPs program, used to evaluate the presence of mutations in our samples, finds variants above a minimum threshold to screen out disagreements due to read errors. The tool calculates p-values for variations and filters only the single-nucleotide variations (SNVs) with a specified maximum P-Value. The lower the p-value, the more likely the variation at the given position represents a real variant. For this reason, we decided to filter out variants with a maximum p value of 10^{-6}, with 0.001% probability to see variant by chance. We selected stringent parameters, together with a minimum coverage of 10 reads, to have the possibility to find all the SNVs present in patient's samples. Nevertheless, almost all of the identified mutations have a depth of more than 100 reads with a variant frequency >70%.

Found mutations are reported in Table 3. Among the most significant ones, 4 mutations (genomic positions 241, 3037, 14408 and 23403 of the RNA letter code), characteristic of lineage B.1, were found in all the analyzed viral genomes. Another set was shared between the viral extract obtained from 1 mild symptomatic patient (Cm) and 1 asymptomatic subject (Ba). This was a variation of 3 nucleotides at position 28881-2-3, which is a main feature of most sequences belonging to Lineage B.1.1.

Among patients characterized by the most severe clinical situation, the viral RNA extracted from patients Fs and Gs shared C28932T substitution in the RNA sequence. This mutation causes the change of an alanine (A) to an amino acid of similar properties, valine (V), in position 220 of the amino acidic sequence (A220V). The A220V non-synonymous mutation is located within the viral nucleocapsid N protein. The alignment with sequences present in the Global Initiative on Sharing All Influenza Data (GISAID) repository until the 15th of March 2021 showed that the A220V mutation has a frequency of roughly 16% (Table 4). A220V has been reported in viral genomes from 81 Countries, with the first one reported in January 2020 in the Netherlands, and predominant in Spain during summer 2020. Interestingly, A220V displays a distribution pattern similar to the one of the A222V of the S glycoprotein [37]. In fact, both mutations are generally associated in the 20A.EU1 clade. However, both Fs and Gs viral extracts lack the A222V change. Interestingly, while the Fs nasopharyngeal swab was performed in early March 2020, the Gs was obtained in November of the same year. Of note, the third severely symptomatic patient (As) lacks the A220V polymorphism.
In addition to known mutations, viral genomes obtained from patients As (symptomatic), Ba (asymptomatic) and Cm (mild-symptomatic) displayed “extra” polymorphisms that are less studied. When sequences were aligned with those reported in the online GISAID database until the 15th of March 2021 (Table 4) these extra polymorphisms were characterized, in general, by a frequency below 1%, with the nucleotide substitution G25459T (patient Ba), approaching 1%, and the T11652C (patient As), approaching 0%. Among the mutations reported in Table 4 the most interesting are the following:

- C25433T in ORF3a of viral extract As: in the amino acidic code this mutation is translated into T14I, with a reported frequency of around 0.19%. This mutation was shared by 758 sequences present in the GISAID database, reported in 23 Countries with the first sequence dating back March 2020. This substitution changes a polar amino acid, threonine (T), to a non-polar one, isoleucine (I).
- T29568C in ORF10 of viral extract As: it leads to an amino acidic substitution from a non-polar amino acid, isoleucine (I), to a polar one, threonine (T), i.e. I4T. GISAID analysis did not find sequences with such a mutation reported in the database. However, it is likely that, in a genome 29.9 kb-long, a mutation located in position 29600 is in a non-coding region.
- G25459T in ORF3a of viral extract Ba: it is translated in an amino acid change from a non-polar amino acid, alanine (A) to a polar one, serine (S), and named A23S. It

has a frequency of 0.91% and has been reported in 241 sequences of 23 Countries, with the first sequence deposited in March 2020 in Russia.

- T18417C in ORF1ab of viral extract As: it is the only synonymous mutation reported in patient A. This mutation is located in the nsp14, the protein responsible for the proof-reading activity of the polymerase. This mutation has been reported in only a few sequences between May and June 2020.

It must be noted that there were no sequences reported in the online database with 100% similarity to the sequences obtained from patients As, Ba and Cm.

Classification of the identified SARS-CoV-2 genomes into clades and lineages and phylogenetic analysis

Based on the NGS analysis, viral sequences were classified in their corresponding lineages by adopting the Phylogenetic Assignment of Named Global Outbreak LINeages (PANGOLIN) tool. In more details, the results showed that viral sequences from patients As, Da and Em belonged to B.1 lineage, while the ones from patients Fs and Gs belonged to lineage B.1.177. In addition, the viral sequences from patients Cm and Ba were classified into lineage B.1.1.

Furthermore, a clade classification by Nextstrain was also obtained. The results showed that the viral sequences from patients As, Da, Em, Fs and Gs were all associated to clade 20A, while Ba and Cm belonged to clade 20B. The mutation shared between patients Fs and Gs was observed in both a branch of clade 20B as well as in clade 20E.EU1. However, it must be noted that the latter clade is defined by the presence of A222V amino acidic variation in the spike protein, that, as already mentioned, was absent in these patients. In conclusion, there was no association between a specific viral lineage/clade and a specific patient group.

Finally, in order to accurately assess possible evolutionary relationships on a global scale among these seven Italian SARS-CoV-2 sequences, a maximum likelihood (ML) tree was implemented. The dataset utilized in this analysis consists of 2463 global sequences collected from the beginning of pandemic until December 2021 and belonging to different lineages: A, B, B.1, B.1.1, B.1.177. As shown in Fig 2, the two sequences found in patients Fs and Gs, two of the severely symptomatic ones, gave rise to the B.1.177 cluster, while the remaining sequences from the other patients were located in accordance with their lineage but are scattered across the phylogenetic tree. Interestingly, phylogenetic analysis revealed that the GISAID sequences EPI_ISL_539548 and EPI_ISL_3716577, located at the

beginning of B.1.177 branch before patients Fs and Gs, derived from symptomatic and hospitalized patients.

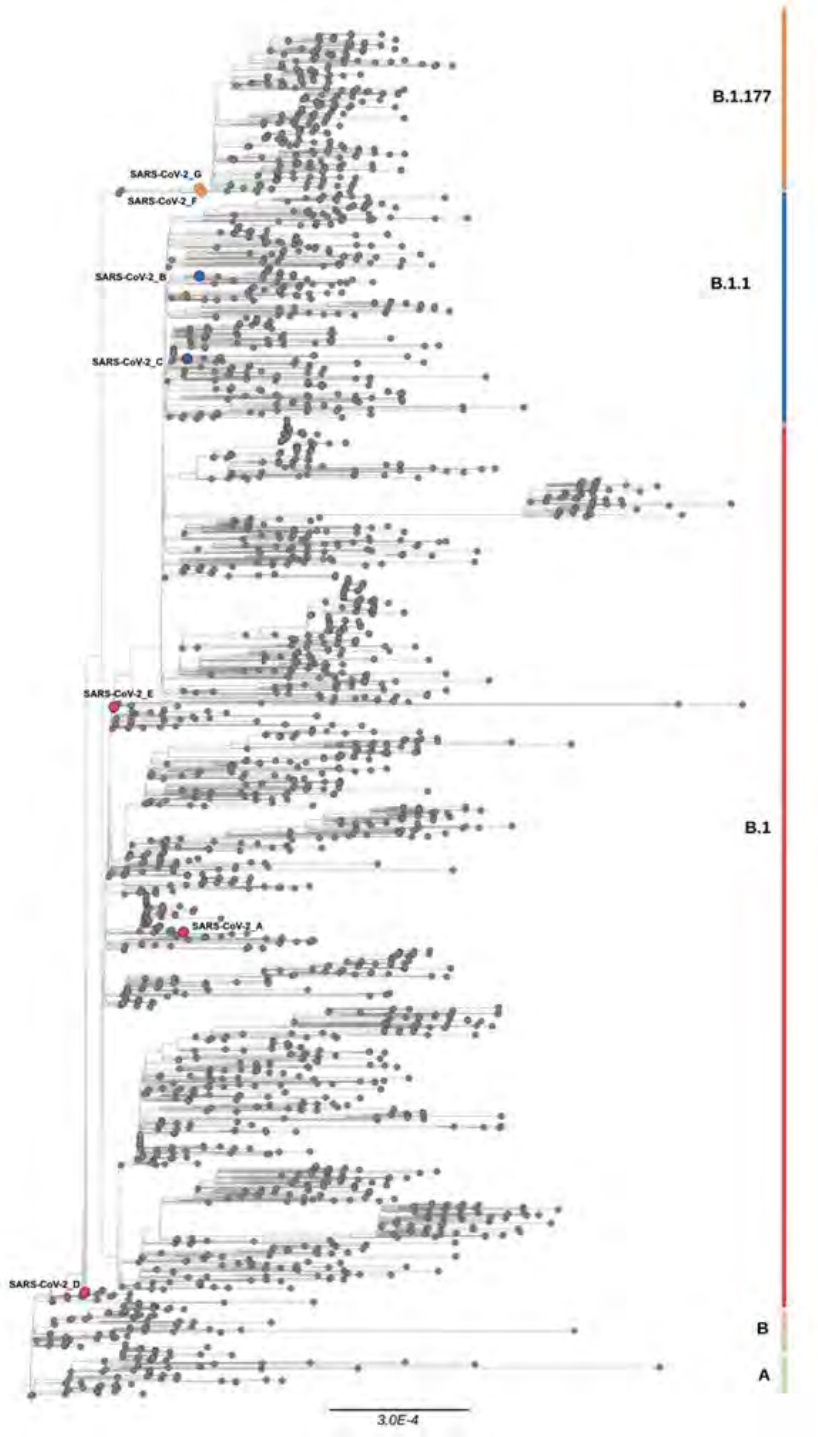

Figure 2. Maximum-likelihood (ML) tree of SARS-CoV-2 sequences. *The ML tree includes 2463 SARS-CoV-2 sequences retrieved globally from GISAID database until December 2021 and 7 SARS-CoV-2*

sequences evaluated in this study represented as dots. SARS-CoV-2 sequences of this study are coloured by lineages: B.1 in red; B.1.1 in blue; B.1.177 in orange; all the other world sequences in black.

Pos	Ref	Mut	Gene	Protein	Type	As	Ba	Cm	Da	Em	Fs	Gs
41	C	T	5'UTR			T	T	T	T	T	T	T
626	G	T	ORF1ab	Leader	Non-syn	WT	V121F	WT	WT	WT	WT	WT
3037	C	T	ORF1ab	nsp3	Syn	F924	F924	F924	F924	F924	F924	F924
8334	C	T	ORF1ab	nsp3	Non-syn	A2690V	WT	WT	WT	WT	WT	WT
11652	T	C	ORF1ab	nsp6	Non-syn	L3796P	WT	WT	WT	WT	WT	WT
12153	C	T	ORF1ab	nsp8	Non-syn	WT	WT	A3963V	WT	WT	WT	WT
14408	C	T	ORF1ab	RdRp	Non-syn	P4715L	P4715L	P4715L	P4715L	P4715L	P4715L	P4715L
18417	T	C	ORF1ab	nsp14	Syn	D6051	WT	WT	WT	WT	WT	WT
23403	A	G	S	S	Non-syn	D614G	D614G	D614G	D614G	D614G	D614G	D614G
25433	C	T	ORF3a		Non-syn	T14I	WT	WT	WT	WT	WT	WT
25459	G	T	ORF3a		Non-syn	WT	A23S	WT	WT	WT	WT	WT
28881	G	A	N	N	Non-syn	WT	R203K	R203K	WT	WT	WT	WT
28882	G	A	N	N	Non-syn	WT	R203K	R203K	WT	WT	WT	WT
28883	G	C	N	N	Non-syn	WT	G204R	G204R	WT	WT	WT	WT
28932	C	T	N	N	Non-syn	WT	WT	WT	WT	WT	A220V	A220V
29568	T	C	ORF10		Non-syn	I4T	WT	WT	WT	WT	WT	WT

Table 3. Summary of the mutations retrieved in each extract by whole genome analysis. *The table reports in the first column the position (Pos) of the mutated nucleotide within the viral genome. Ref stands for the nucleotide located in Pos within the reference sequence, Mut for the mutated nucleotide, Gene and Protein for the gene and the protein where the mutation is located respectively, Type for the type of mutation, Syn for synonymous mutation, Non-syn for non-synonymous mutation, WT for wild-type when identical to the reference sequence, mut for mutated when compared to the reference sequence, From column #7 to column #13 the amino acidic changes are reported when appropriate.*

Pt	Nt	Gene	Protein	Type	aa change	Freq	N_seq	N_Countries	First Country	Date (2020)
As	C8334T	ORF1ab	nsp3	Non-syn	A2690V	0.04%	152	20	Portugal	March
As	T11652C	ORF1ab	nsp6	Non-syn	L3796P	0.00%	6	5	Netherlands	April
As	T18417C	ORF1ab	nsp14	Syn	D6051	/	10	/	Netherlands	May
As	C25433T	ORF3a	Nnsp	Non-syn	T14I	0.19%	758	23	Netherlands	March
As	T29568C	ORF10	Nsp	Non-syn	I4T	NC	/	/	/	/
Ba	G626T	ORF1ab	leader	Non-syn	V121F	0.01%	22	10	China	February
Ba	G25459T	ORF3a	Nsp	Non-syn	A23S	0.91%	241	23	Russia	March
Cm	C12153T	ORF1ab	nsp8	Non-syn	A3963V	0.02%	75	13	Italy	March
Fs+Gs	C28932T	N	N	Non-syn	A220V	15.59%	137527	81	Netherlands	January

Table 4. Highlights on the results of the sequence alignment with those retrieved in the GISAID repository. *The Table reports some of the results obtained by the alignment of the sequences obtained in this study with those present in the GISAID repository until the 15th of March 2021. In particular, the table focuses on those mutations highlighted by the sequencing alignment that were not previously described in literature. Pt stands for patient, nt for the mutated nucleotide, Gene and Protein for the gene and the protein where the mutation is located, respectively, Type for the type of mutation (i.e. Non-syn for non-synonymous, Syn for synonymous), aa change for the amino acidic mutation, N_seq for the number of sequences with the mutation, N_Countries corresponds to the number of Countries that had reported the mutation, and the first to report it (First Country), Date stands for date of database entry, NC (non-classified), "/" (not specified).*

DISCUSSION

COVID-19 is mainly a respiratory syndrome. However, since the beginning of the disease in a subset of individuals extra-respiratory symptoms/complications could arise. Among those, neurological manifestations, ranging from olfactory dysfunction to any neurologic manifestation, with the most common being encephalopathy, have been of great concern since the beginning of the pandemic [11, 38]. The mechanisms accounting for the onset of neurological symptoms/complications in certain COVID-19 patients is still matter of study, especially in terms of the role directly played by the virus [11, 28, 38, 39].

The aim of this study was to analyze whether SARS-CoV-2 genomes directly retrieved from the nasopharyngeal swabs of patients characterized by severe CNS manifestations displayed specific and common signatures not shared with the ones obtained from asymptomatic/mild symptomatic subjects. In particular, seven SARS-CoV-2 positive individuals were enrolled between March and November 2020. These patients were either fully asymptomatic or experienced variable neurological manifestations, including three subjects admitted to the intensive care unit of the Padua Hospital due to severe encephalopathy. In this cohort of patients, four were between 25 and 35 years old, one around 55 and two above 70 years old. Neurological symptoms and complications displayed by the selected subjects are reported in the literature among the most frequent COVID19-related neurological manifestations [13, 39]. All patients in the most severe neurological conditions presented important respiratory symptoms, such as interstitial pneumonia, and were intubated. This finding supports the notion that patients with severe disease are more likely to develop neurological disorders [40, 41]. Finally, and not surprisingly [42, 43], the three hospitalized patients were also the oldest of this cohort and two out of three were males.

Data demonstrate that SARS-CoV-2 can access the CNS and can potentially damage the brain tissues by directly lysing infected cells and by triggering a localized inflammatory response [11, 28]. On the other hand, SARS-CoV-2 replication in the lungs stimulates a cytokine storm that could also affect the CNS, even in the absence of a direct brain invasion by the virus [28, 29]. The two SARS-CoV-2 envelope proteins S and E could play a role in both these neuro-pathogenetic mechanisms. Indeed, while the S protein is the main viral tropism determinant [10, 11], the E protein is involved in different steps of viral replication and in regulating viral/cell host interactions [44]. Studies focused on SARS-CoV-1, in particular, have shown that E protein is a virulence factor involved in the activation of various

inflammatory pathways [45]. Of note, the E genes of SARS-CoV-1 and SARS-CoV-2 are highly identical. Based on these evidence, we started by Sanger sequencing the S and E genes of SARS-CoV-2 genomes directly extracted from the nasopharyngeal swabs of the enrolled cohort. However, with the exception of the well-known and expected D614G mutation [36], present in the S gene and common to all the analyzed sequences, no other mutations were detected in either the S or E genes.

Next, the same viral RNA extracts underwent whole genome analysis, obtaining a classification of the SARS-CoV-2s under investigation into three different lineages: B.1, B.1.177 and B1.1. More specifically, viral sequences obtained from patients As, Da and Em were linked to the B.1 lineage, which has been circulating since mid-January 2020, and is characterized by 4 predominant mutations. These mutations include D614G and P323L that have been observed in all the analyzed patients. The B.1 lineage was the most prevalent lineage in Europe during 2020 (Pangolin Cov-lineages: https://cov-lineages.org/resources/pangolin.html accessed on the 15th of March 2021). The viral sequences from patients Fs and Gs were linked to the B.1.177 lineage, which is a sub-lineage of the B.1 lineage. These sequences shared the same 4 mutations as before, but with the addition of A220V in the nucleocapsid N protein. The B.1.177 lineage had spread mainly in Europe during summer 2020 and is slowly disappearing (Pangolin Cov-lineages: https://cov-lineages.org/resources/pangolin.html).

The viral genomes sequenced from patients Cm and Ba were associated to the B.1.1 lineage, which derives from lineage B.1. These viral sequences were characterized by the additional presence of 3 consecutive SNVs at position 28881-2-3. This lineage was also prevalent in Europe, specifically in England, circulating since mid-February (Pangolin Cov-lineages: https://cov-lineages.org/resources/pangolin.html). The Nextstrain classification into clades showed that the viral sequences from patients As and Da, together with patients Em, Fs and Gs were all classified into clade 20A, while those from patients Ba and Cm were classified into clade 20B. The 4 most common mutations shared by the B.1, B.1.177, B.1.1 lineages were 4 SNVs: C241T, C3037T, C14408T, A23403G. These 4 SNVs that have been widely described in literature [46, 47], appeared when the virus started circulating outside of China, and are widely distributed in Europe and in the USA. Indeed, since the beginning of March 2020, when, according to the databases, these mutations were present in 10% of the analyzed sequences, their frequency increased exponentially, reaching 78% by the end of May 2020 [48] and overall constituted the dominant haplotype in Europe during year 2020. Indeed, these mutations, which are located far apart from each other in the genome, have

a strong allelic association, likely due to different factors, as a founder effect or a gain in viral fitness [49].

C241T is a non-coding mutation located in the 5' UTR, and even if it does not cause changes in the amino acid sequence, it could still lead to a relevant change in the secondary structure of the RNA or/and modify the repertoire of interactions with viral and cellular proteins, thus affecting the RNA replication or the speed of the infection cycle [28]. C3037T is a single nucleotide substitution in position 3037 of the RNA genome, located in the nsp3 gene. It is a silent, synonymous, mutation named F924; it is located in the nsp3 protein, which is a phosphodiesterase. Although silent, this mutation may affect the RNA secondary structure, and therefore the interaction with other proteins [36].

C14408T is a non-synonymous mutation in the nsp12, which is the RNA-dependent RNA-polymerase [50]. This single nucleotide variation leads to an amino acid substitution from a proline (P) to a leucine (L), in position 323 of the nsp12, which in turn is a P4715L substitution in the ORF1ab. This mutation is located outside the catalytic site, specifically at the interface domain of the protein, that is responsible for the interaction with other proteins [51]. According to literature, this mutation could have multiple effects. Not only it could cause an increased interaction with the SARS-CoV-2 non-structural protein nsp8, which is a processivity factor; but it could also alter the interaction with the viral nsp14, an exonuclease responsible for the proof-reading activity of the polymerase. This way, it could affect the fidelity of replication and be responsible for a higher mutational rate [50]. Furthermore, given its hydrophobicity, leucine tends to remain inside the secondary structure, rather than being exposed to the outside, as proline does; thus, the substitution could cause the loss of one of the nsp12 epitopes leading to antibodies escape [52].

A23403G single nucleotide variation is in the spike-encoding gene. This SNV causes an amino acid change from a hydrophilic and negatively charged aspartic acid (D) to hydrophobic and uncharged glycine (G), therefore it is called D614G. In literature, this mutation is reported to be associated with increased virus infectivity and transmissibility [48, 53]. However, the reason for this increase remains to be answered. On the one hand, it is thought to be related to an increased affinity for the angiotensin converting enzyme 2 (ACE2) receptor which, in turns, increases the entry efficiency of the virus [54]. On the other hand, it seems to be related to a more efficient incorporation of the spike in the newly formed virions, due to its greater stability and reduced shedding of the S1 subunit upon cleavage [55]. It must be noted that, overall, this set of four mutations was not linked to either a greater

disease severity, in terms of hospitalization rate, nor to a reduced antibody neutralization [48].

Viral sequences from the asymptomatic patient Ba and the mild symptomatic patient Cm were characterized not only by the four mutations described above, but also by a variation of three nucleotides at position 28881-2-3 [56]. This three-nucleotide variation from GGG to AAC is located within the gene encoding for the viral nucleocapsid N protein. These three SNVs have a strong allelic association and lead to an amino acid change at position 50-51 from arginine-glycine to lysin-arginine, thus bringing together two basic and polar amino acids, which could create a stronger binding between the N protein and the viral RNA. These mutations are expected to affect viral infectivity, due to the replacement of an arginine-glycine by a lysine-arginine in a serine-rich motif of the nucleoprotein [57]. This triplet characterizes most of the sequences deposited in GISAID belonging to the B.1.1 lineage first reported in late February 2020. This lineage was predominant until June 2020, when it started rapidly decreasing in its frequency [37]. Indeed, there was a reversion of this mutated triplet into the original one, and a parallel spread of a new variant characterized by 2 spike mutations associated with an A220V mutation of the nucleocapsid N protein. However, the mutated triplet reappeared in the most recent variants, and it can be found also in sequences belonging to the Omicron variant (https://www.gisaid.org/ accessed on March 15th 2021).

Of those patients with the most severe symptoms, the viral RNA obtained from patients Fs and Gs showed the A220V amino acid change of the N protein. This mutation has a similar distribution pattern to the A222V spike mutation; these two mutations are generally associated and define the 20A.EU1 clade. This variant dated back to summer 2020 when it appeared in the Netherlands and then in Spain and spread throughout Europe, and with a lower frequency in the rest of the world [37, 56]. The A220V in N protein propagated rapidly, associated with two spike mutations (L18F and A222V), in the second wave of the pandemic. However, in our cohort, these two spike mutations were absent in all analysed patients. On the one hand, the A220V variation was only present in two severely symptomatic patients and neither in the controls, nor in the mild symptomatic patients. On the other hand, the A220V mutation was not shared by the third severely symptomatic patient As. Of note, the same mutation was found in two GISAID sequences (EPI_ISL_539548 and EPI_ISL_3716577) obtained from symptomatic patients.

The symptomatic patient As, asymptomatic Ba and mild-symptomatic Cm had unique mutations in their viral sequence. The alignment with sequences in the database showed that all these mutations were rare, with a frequency below 1% and none of them was

phenotypically characterized. Therefore, if the frequency of these non-synonymous mutations will increase, it could be important to evaluate whether they may affect the corresponding protein function. On the other side, none of these “novel” mutations was shared between the three patients.

In conclusion, while interesting mutations were found in the viral genome under study, from the overall analysis no correlation is evident between symptoms and viral sequence features. Furthermore, the MRI performed on the patients excludes the possibility of a brain localised inflammatory response. In fact, the MRI of each patient was always negative, with exception of one patient (Fs), where there was a concomitant ischaemic episode. Hence, overall, our data support the notion that COVID-19 neurological manifestations are linked to the individual inflammatory response, rather than to specific signature of the viral genome [58]. The main limit of this pilot study is surely the small number of enrolled patients. However, on one hand, and as mentioned before, these data are worth of attention, as they have been obtained by whole genome sequencing performed on viral RNA directly extracted from the nasopharyngeal swabs of the enrolled patients, without viral amplification in cell culture. This procedure is recommended by the WHO to avoid accumulation of extra mutations not reflecting the in vivo situation [59]. On the other hand, the sampled population is heterogeneous in terms, for instance, of age and sex. Indeed, despite the limited number of patients, we found an association between neurological and severe respiratory symptoms and between symptom severity in general, and age and sex, as reported in the literature [42, 60]. Thus, the reported results are worth of attention and deserve further validation in larger cohorts of patients.

Acknowledgements

This study was funded by the grant COVID-CNS of Fondazione Cassa di Risparmio di Padova e Rovigo (CARIPARO).

REFERENCES

1. C S G of the International. The species Severe acute respiratory syndrome-related coronavirus: classifying 2019-nCoV and naming it SARS-CoV-2. Nat Microbiol. 2020;5(4):536.

2. Zhou P, Yang XL, Wang XG, Hu B, Zhang L, Zhang W, et al. A pneumonia outbreak associated with a new coronavirus of probable bat origin. Nature. 2020;579(7798):270–273.
3. Ashour HM, Elkhatib WF, Rahman M, Elshabrawy HA. Insights into the recent 2019 novel coronavirus (SARS-CoV-2) in light of past human coronavirus outbreaks. Pathogens. 2020;9(3):186.
4. Ziebuhr J. The coronavirus replicase. vol. 287. Springer; 2005.
5. Alanagreh L, Alzoughool F, Atoum M. The human coronavirus disease COVID-19: its origin, characteristics, and insights into potential drugs and its mechanisms. Pathogens. 2020;9(5):331.
6. Romano M, Ruggiero A, Squeglia F, Maga G, Berisio R. A structural view of SARS-CoV-2 RNA replication machinery: RNA synthesis, proofreading and final capping. Cells. 2020;9(5):1267.
7. Alteri C, et al. Genomic epidemiology of SARS-CoV-2 reveals multiple lineages and early spread of SARS-CoV-2 infections in Lombardy, Italy. Nat Commun. 2021;12(1):43.
8. Tao K, Tzou PL, Nouhin J, Gupta RK, de Oliveira T, Kosakovsky Pond SL, et al. The biological and clinical significance of emerging SARS-CoV-2 variants. Nat Rev Genet. 2021;22(12):757–773.
9. Ghosh N, Nandi S, Saha I. A Review on evolution of emerging SARS-CoV-2 variants based on spike glycoprotein. Int Immunopharmacol. 2022;105:108565.
10. Harrison AG, Lin T, Wang P. Mechanisms of SARS-CoV-2 transmission and pathogenesis. Trends Immunol. 2020;41(12):1100–1115.
11. Haidar MA, Shakkour Z, Reslan MA, Al-Haj N, Chamoun P, Habashy K, et al. SARS-CoV-2 involvement in central nervous system tissue damage. Neural Regen Res. 2022;17(6):1228.
12. Baig AM. Neurological manifestations in COVID-19 caused by SARS-CoV-2. CNS Neurosci Ther. 2020;26(5):499.
13. Collantes M E V, Espiritu A I, Sy M C C, Anlacan V M M, Jamora R D G. Neurological manifestations in COVID-19 infection: a systematic review and meta-analysis. Can J Neurol Sci**.** 2021; 48(1), 66-76.
14. Lechien JR, Chiesa-Estomba CM, De Siati DR, Horoi M, Le Bon SD, Rodriguez A, et al. Olfactory and gustatory dysfunctions as a clinical presentation of mild-to-moderate forms of the coronavirus disease (COVID-19): a multicenter European study. Eur Arch Oto-Rhino-L. 2020;277(8):2251–2261.
15. Brann DH, Tsukahara T, Weinreb C, Lipovsek M, Van den Berge K, Gong B, et al. Non-neuronal expression of SARS-CoV-2 entry genes in the olfactory system suggests mechanisms underlying COVID-19-associated anosmia. Sci Adv. 2020;6(31):eabc5801.
16. Pilotto A, Odolini S, Masciocchi S, Comelli A, Volonghi I, Gazzina S, et al. Steroid-responsive encephalitis in coronavirus disease 2019. Ann Neurol. 2020;88(2):423–427.
17. Muccioli L, Pensato U, Cani I, Guarino M, Cortelli P, Bisulli F. COVID-19-associated encephalopathy and cytokine-mediated neuroinflammation. Ann Neurol. 2020;88(4):860–861.
18. Paterson RW, Brown RL, Benjamin L, Nortley R, Wiethoff S, Bharucha T, et al. The emerging spectrum of COVID-19 neurology: clinical, radiological and laboratory findings. Brain. 2020;143(10):3104–3120.
19. Bergmann CC, Lane TE, Stohlman SA. Coronavirus infection of the central nervous system: host–virus stand-off. Nat Rev Microbiol. 2006;4(2):121–132.

20. Desforges M, Le Coupanec A, Dubeau P, Bourgouin A, Lajoie L, Dub´e M, et al. Human coronaviruses and other respiratory viruses: underestimated opportunistic pathogens of the central nervous system? Viruses. 2020;12(1):14.
21. Wu Y, Xu X, Chen Z, Duan J, Hashimoto K, Yang L, et al. Nervous system involvement after infection with COVID-19 and other coronaviruses. Brain Behav Immun. 2020;87:18–22.
22. Pujadas E, Beaumont M, Shah H, Schrode N, Francoeur N, Shroff S, et al. Molecular Profiling of Coronavirus Disease 2019 (COVID-19) Autopsies Uncovers Novel Disease Mechanisms. Am J Pathol. 2021;191(12):2064–2071.
23. Chen R, Wang K, Yu J, Howard D, French L, Chen Z, et al. The spatial and cell-type distribution of SARS-CoV-2 receptor ACE2 in the human and mouse brains. Front Neurol. 2021;11:1860.
24. Deguchi S, Serrano-Aroca A´, Tambuwala MM, Uhal BD, Brufsky AM, Takayama K. SARS-CoV-2 research using human pluripotent stem cells and organoids. Stem Cells Transl Med. 2021;10(11):1491–1499.
25. Zhang BZ, Chu H, Han S, Shuai H, Deng J, Hu Yf, et al. SARS-CoV-2 infects human neural progenitor cells and brain organoids. Cell Res. 2020;30(11):60131.
26. Matschke J, Lu¨tgehetmann M, Hagel C, Sperhake JP, Schro¨der AS, Edler C, et al. Neuropathology of patients with COVID-19 in Germany: a post-mortem case series. Lancet Neurol. 2020;19(11):919–929.
27. Virhammar J, Kumlien E, F¨allmar D, Frithiof R, Jackmann S, Sk¨old MK, et al. Acute necrotizing encephalopathy with SARS-CoV-2 RNA confirmed in cerebrospinal fluid. Neurology. 2020;95(10):445–449.
28. Kumar A. COVID-19 Current challenges and future perspectives. Betham Books 2021. 8: 76-100.
29. Tay MZ, Poh CM, R´enia L, MacAry PA, Ng LF. The trinity of COVID-19: immunity, inflammation and intervention. Nat Rev Immunol. 2020;20(6):363–374.
30. Li C, et al. Highly sensitive and full-genome interrogation of SARS-CoV-2 using multiplexed PCR enrichment followed by next-generation sequencing. BioRxiv. 2020; Forthcoming.
31. Al Khatib HA, Benslimane FM, Elbashir IE, Coyle PV, Al Maslamani MA, Al-Khal A, et al. Within-host diversity of SARS-CoV-2 in COVID-19 patients with variable disease severities. Front Cell Infect Microbiol. 2020; 534.
32. Rambaut A, Holmes EC, O'Toole A´, Hill V, McCrone JT, Ruis C, et al. A dynamic nomenclature proposal for SARS-CoV-2 lineages to assist genomic epidemiology. Nat Microbiol. 2020;5(11):1403–1407.
33. Katoh K, Rozewicki J, Yamada KD. MAFFT online service: multiple sequence alignment, interactive sequence choice and visualization. Brief Bioinformatics. 2019;20(4):1160–1166.
34. Larsson A. AliView: a fast and lightweight alignment viewer and editor for large datasets. Bioinformatics. 2014;30(22):3276–3278.
35. Nguyen LT, Schmidt HA, Von Haeseler A, Minh BQ. IQ-TREE: a fast and effective stochastic algorithm for estimating maximum-likelihood phylogenies. Mol Biol Evol. 2015;32(1):268–274.
36. Mercatelli D, Giorgi FM. Geographic and genomic distribution of SARS-CoV-2 mutations. Front Microbiol. 2020; 1800.
37. Vilar S, Isom DG. One year of SARS-CoV-2: how much has the virus changed? Biology. 2021;10(2):91.
38. Hingorani K S, Bhadola S, Cervantes-Arslanian A M. COVID-19 and the Brain. Trends cardiovasc. Med. 2022; https://doi.org/10.1016/j.tcm.2022.04.004 .

39. Xu Y, Zhuang Y, Kang L. A review of neurological involvement in patients with SARS-CoV-2 infection. Med. Sci. Monit. 2021; 27: e932962-1.
40. Mao L et al. Neurological manifestations of hospitalized patients with COVID-19 in Wuhan, China: A retrospective case series study (February 24, 2020). JAMA Neurol. 2020; 77(6): 1–9.
41. Aghagoli G, Gallo Marin B, Katchur N J, Chaves-Sell F, Asaad W F, Murphy S A. Neurological involvement in COVID-19 and potential mechanisms: a review. Neurocritical care. 2021; 34(3): 1062-1071.
42. Tazerji SS et al. Global data analysis and risk factors associated with morbidity and mortality of COVID-19. Gene Rep. 2022; 26: 101505.
43. Ellul M A et al. Neurological associations of COVID-19. The Lancet Neurology, 2020; 19(9): 767-783.
44. Zhu Y et al. Interactions of Severe Acute Respiratory Syndrome Coronavirus 2 Protein E With Cell Junctions and Polarity PSD-95/Dlg/ZO-1-Containing Proteins. Front Microbiol. 2022; 13 :829094.
45. Morales L, Oliveros JC, Enjuanes L, Sola I. Contribution of Host miRNA-223-3p to SARS-CoV-Induced Lung Inflammatory Pathology. mBio. 2022; 13(2): e0313521.
46. Weber S, Ramirez C, Doerfler W. Signal hotspot mutations in SARS-CoV-2 genomes evolve as the virus spreads and actively replicates in different parts of the world. Virus Res. 2020;289:198170.
47. Yang HC, Chen Ch, Wang JH, Liao HC, Yang CT, Chen CW, et al. Analysis of genomic distributions of SARS-CoV-2 reveals a dominant strain type with strong allelic associations. Proc Natl Acad Sci USA. 2020;117(48):30679–30686.
48. Korber B, Fischer WM, Gnanakaran S, Yoon H, Theiler J, Abfalterer W, et al. Tracking changes in SARS-CoV-2 spike: evidence that D614G increases infectivity of the COVID-19 virus. Cell. 2020;182(4):812–827.
49. van Dorp L, Richard D, Tan C, Shaw LP, Acman M, Balloux F. No evidence for increased transmissibility from recurrent mutations in SARS-CoV-2. Nat Commun. 2020;11(1):5986.
50. Pachetti M, Marini B, Benedetti F, Giudici F, Mauro E, Storici P, et al. Emerging SARS-CoV-2 mutation hot spots include a novel RNA-dependent-RNA polymerase variant. J Transl Med. 2020;18(1):179.
51. Kannan SR, Spratt AN, Quinn TP, Heng X, Lorson CL, S¨onnerborg A, et al. Infectivity of SARS-CoV-2: there is something more than D614G? J Neuroimmune Pharmacol. 2020;15(4):574–577.
52. Gupta AM, Chakrabarti J, Mandal S. Non-synonymous mutations of SARS-CoV-2 leads epitope loss and segregates its variants. Microbes Infect. 2020;22(10):598–607.
53. Plante JA, Liu Y, Liu J, Xia H, Johnson BA, Lokugamage KG, et al. Spike mutation D614G alters SARS-CoV-2 fitness. Nature. 2021;592(7852):116–121.
54. Ozono S, Zhang Y, Ode H, Sano K, Tan TS, Imai K, et al. SARS-CoV-2 D614G spike mutation increases entry efficiency with enhanced ACE2-binding affinity. Nat Commun. 2021;12(1):848.
55. Zhang L, Jackson CB, Mou H, Ojha A, Peng H, Quinlan BD, et al. SARS-CoV-2 spike-protein D614G mutation increases virion spike density and infectivity. Nat Commun. 2020;11(1):1–9.
56. Hodcroft EB, Zuber M, Nadeau S, Vaughan TG, Crawford KH, Althaus CL, et al. Spread of a SARS-CoV-2 variant through Europe in the summer of 2020. Nature. 2021;595(7869):707–712.

57. Ayub M, et al. Reporting two SARS-CoV-2 strains based on a unique trinucleotide-bloc mutation and their potential pathogenic difference. Preprintsorg. 2020; Forthcoming.
58. Sulzer D, Antonini A, Leta V, Nordvig A, Smeyne RJ, Goldman JE, et al. COVID-19 and possible links with Parkinson's disease and parkinsonism: from bench to bedside. NPJ Parkinson's Dis. 2020;6(1):1–10.
59. World Health Organization, Genomic Sequencing of SARS-CoV-2: A Guide to Implementation for Maximum Impact on Public Health. Geneva 2021.
60. Pijls BG et al. Temporal trends of sex differences for COVID-19 infection, hospitalisation, severe disease, intensive care unit (ICU) admission and death: a meta-analysis of 229 studies covering over 10M patients. F1000Res. 2022; 11(5): 5.

Author contributions statement

A.V., F.C., equally contributed in carrying out the sequencing experiments and analysis of the data as well as in writing the manuscript. S.M. carried out the sequencing experiments and analysis of the data. A.V. helped in the interpretation of the results and in writing the manuscript. A.E. helped with patients' enrolment and clinical data acquisition; C.D.V. collected viral RNA samples and helped in writing the manuscript; A.R. helped with Sanger sequencing experiments and in revising the manuscript; A.C. helped in the interpretation of the results; G.O. helped with patients' enrolment and in clinical data acquisition; C.M. contributed to the study design and writing the manuscript. C.P. contributed to the study design; A.A. and A.C. equally contributed to the study design, interpretation of the results, writing of the manuscript. All authors have reviewed the final version of the article.

Data availability

Genomic data reported in this study are available at Global Initiative on Sharing All Influenza Data (GISAID). Accession numbers:

EPI_ISL_9616211 (hCoV-19/Italy/LOM-UNIBS-MM65-A/2020)

EPI_ISL_9616280 (hCoV-19/Italy/LOM-UNIBS-LP91-B/2020)

EPI_ISL_9616612 (hCoV-19/Italy/LOM-UNIBS-BC94-C/2020)

EPI_ISL_9617639 (hCoV-19/Italy/LOM-UNIBS-GMF90-D/2020)

EPI_ISL_9617936 (hCoV-19/Italy/LOM-UNIBS-MP89-E/2020)

EPI_ISL_9618235 (hCoV-19/Italy/LOM-UNIBS-RR46-F/2020)

EPI_ISL_9618359 (hCoV-19/Italy/LOM-UNIBS-ADA43-G/2020)

Chapter 5

Neuroinflammation, SARS-CoV-2 Antigens and Viral Genomic Sequences in the Human Brainstem: implications for neurodegenerative diseases

Part(s) of the present chapter have been previously published in:

- ***Emmi A.**, Rizzo S., Barzon S., et al. SARS-CoV-2 neuropathology: Evidence from a post-mortem autopsy series in Padova, Italy. Clinical Neuropathology, 2021.*
- ***Emmi A.**, Rizzo S., Macchi V., Sinigaglia A., Riccetti S., De Gaspari M., Carturan E., Calabrese F., Dei Tos A.P., Barzon L., Basso C., De Caro R., Porzionato A. COVID-19 Neuropathology: evidence for SARS-CoV-2 invasion of anatomically defined regions in the human CNS. Journal of Anatomy, 2021.*
- ***Emmi A.**, Rizzo S., Barzon S., et al. COVID-19 neuropathology: evidence for SARS-CoV-2 invasion of human brainstem nuclei. Nature NPJ Parkinson's Disease (under review). doi: https://doi.org/10.1101/2022.06.29.498117*

ABSTRACT

Neurological manifestations are common in COVID-19, the disease caused by SARS-CoV-2. Despite reports of SARS-CoV-2 detection in the brain and cerebrospinal fluid of COVID-19 patients, it's still unclear whether the virus can infect the central nervous system, and which neuropathological alterations can be ascribed to viral tropism, rather than immune-mediated mechanisms.

Here, we assess neuropathological alterations in 24 COVID-19 patients and 18 matched controls who died due to pneumonia / respiratory failure. Aside from a wide spectrum of neuropathological alterations, SARS-CoV-2-immunoreactive neurons were detected in the dorsal medulla and in the substantia nigra of 5 COVID-19 subjects. Viral RNA was also detected by real-time RT-PCR. Quantification of reactive microglia revealed an anatomically segregated pattern of inflammation within affected brainstem regions, and was higher when compared to controls. While the results of this study support the neuroinvasive potential of SARS-CoV-2 and characterize the role of brainstem inflammation in COVID-19, its potential implications for neurodegeneration, especially in Parkinson's disease, require further investigations.

INTRODUCTION

Neurological manifestations are common in coronavirus disease 19 (COVID-19), the disease caused by severe acute respiratory syndrome coronavirus-2 (SARS-CoV-2)[1-5]. Symptoms range from anosmia, ageusia, dizziness and headache, which are commonly reported by patients with mild disease, to altered mental status, neuropsychiatric disorders, stroke, and, rarely, meningitis, encephalitis, and polyneuritis, which occur in hospitalized patients with severe disease[1,5]. Between 10 to 30% of people with SARS-CoV-2 infection experience long-term sequelae, referred as "long COVID", including neurological manifestations such as hyposmia, hypogeusia, headaches, fatigue, sleep disorders, pain, and cognitive impairment[3]. Despite some reports of detection of SARS-CoV-2 in the brain and cerebrospinal fluid of patients with COVID-19[2,3,6], it is still unclear whether the virus can infect the central nervous system (CNS). In particular, it still remains to be elucidated whether neurological manifestations and neuronal damage are a direct consequence of viral invasion of the CNS, are due to post-infectious immune-mediated disease, or are the result of systemic disease[1,6,7]. Studies on human neural cell cultures and brain organoids report conflicting data on SARS-CoV-2 neurotropism[8]. Overall, they suggest that SARS-CoV-2 does not infect and replicate efficiently in human neural cells, while it can replicate at high rates in choroid plexus epithelial cells[9-11]. At variance, intranasal inoculation of SARS-CoV-2 in transgenic mice overexpressing human ACE2 under the K18 promoter resulted in brain invasion and widespread infection of neurons, radial glia and neuronal progenitor cells[12,13]. Other coronaviruses, such as SARS-CoV and MERS-CoV, appear to be able to infect the CNS in both humans and animal models[14].

Data deriving from large autopsy studies in patients who died from COVID-19 suggest for the neuroinvasive potential of SARS-CoV-2 in the CNS[14-16], even though infection appears to be limited to sparse cells in the brainstem and not associated with encephalitis or other specific changes referable to the virus[16]. Conversely, other studies failed to detect SARS-CoV-2 antigens or genomic sequences in brain tissues of COVID-19 patients[7,14,17-19]. In numerous instances, neuropathological changes in the brains of COVID-19 patients were moderate and mainly represented by ischaemic lesions, astrogliosis, microglial nodules, and cytotoxic T lymphocyte infiltrates, most pronounced in the brainstem, cerebellum, and meninges[7,15-17,20]. While diffuse to focal hypoxic / ischaemic damage was a common finding in COVID-19 patients across studies, no direct link between encountered neuropathological alterations and direct viral invasion could be established, with systemic inflammation and

hypoxia playing a likely major role in mediating brain immune response[18]. Single-nucleus gene-expression profiling of frontal cortex and choroid plexus tissues from severe COVID-19 patients showed broad perturbations, with upregulation of genes involved in innate antiviral response and inflammation, microglia activation and neurodegeneration[21], but no direct evidence of viral tropism was found; similarly, Fullard et al.[19] were unable to detect viral transcripts and S proteins in different brain regions of COVID-19 subjects. Deep spatial profiling of the local immune response in COVID-19 brains through imaging mass spectrometry revealed significant immune activation in the CNS with pronounced neuropathological changes (astrocytosis, axonal damage, and blood-brain-barrier leakage) and detected viral antigen in ACE2-positive cells enriched in the vascular compartment[18]. Hence SARS-CoV-2 infection of CNS seems to be limited to isolated cells within the perivascular compartment of the brainstem and olfactory bulb, and have been reported in a subset of cases in the various autopsy series, while widespread neuropathological sequelae (such as astrogliosis, microgliosis, lymphocyte infiltration, microvascular injury, fibrinogen leakage) have been documented in most examined specimens. The possibility of direct viral invasion, and eventual associated long-term sequelae of infection, remain to be investigated. This appears to be particularly concerning for elderly subjects, with known susceptibility for COVID-19, and for patients vulnerable to - or already suffering from - neurodegenerative diseases, such as Parkinson's Disease. Indeed, the hypothesis that viral infections, such as COVID-19, may trigger or precipitate neurological manifestations and neurodegeneration, either through direct invasion or indirectly via neuroinflammation, requires particular attention in future post-pandemic scenarios. As the clinical burden of post-infectious syndromes, i.e long COVID, appears to be continuously increasing, particular care must be taken to investigate yet unknown factors underlying potentially severe long-term sequelae in COVID-19.

In the present study, we assess the neuropathological changes of 24 patients who died following a diagnosis of SARS-CoV-2 infection in Italy during the COVID-19 pandemic (from March 2020 to May 2021) and 18 age-matched controls with comparable medical conditions who died due to pneumonia and / or respiratory failure.

MATERIALS AND METHODS

Hospitalized patients who died following a diagnosis of SARS-CoV-2 infection in the Veneto Region, Italy, during the peak incidence of COVID-19 (from March 2020 to May 2021) were autopsied according to established COVID-19 infection security protocols. Inclusion criteria for the study were: a) diagnosis of SARS-CoV-2 infection confirmed by molecular testing of rhino-pharyngeal swabs and b) high-quality brain tissue samples available for histopathological and immunohistochemical analysis. Tissue quality was determined by Post-Mortem Interval (PMI) ≤5 days, absence of tissue maceration, fixation time ≤ 3 weeks and adequate formalin penetration within the tissue. A total of 24 COVID-19 patients were included in the study.
18 age- and sex-matched subjects with comparable general medical conditions, predating the COVID-19 pandemic in Italy, were included as controls.

Clinical information. Available clinical data for COVID-19 subjects and controls were examined, including ante-mortem medical history, neurological and neuroradiological findings, hospitalization time, ICU and oxygen therapy status, and prescribed medication. However, as most subjects died during the sanitary emergency of the first wave of the COVID-19 pandemic in Italy, ante-mortem clinical data were at times limited, especially when concerning post-hospitalization neurological status. This represents one of the main limitations of our study, determining significant constrains to the association between ante-mortem neurological findings and encountered neuropathological alterations, which is often not unequivocal.

Sampling and fixation procedures. Sampled brains were immersion fixed in 4% phosphate-buffered formalin solution following autopsy (mean PMI: 3 days; Range 0-5 days; average fixation time: 2-3 weeks) and subsequently sectioned for histopathological and immunohistochemical analysis. Samples of the cerebral cortex, basal ganglia, hippocampus, cerebellar cortex, deep cerebellar nuclei, choroid plexuses and meninges were obtained, while the brainstem was isolated at the level of the rostral extremity of the midbrain and extensively sampled in its whole cranio-caudal extent. The 12 cranial nerves, where available, including the olfactory bulb, tract and bifurcation, were also sampled. To preserve antigen quality, a slow dehydration and clearing protocol was performed prior to paraffin embedding (24h mean tissue processing time).

Histochemical and immunoperoxidase staining. Haematoxylin and Eosin staining was employed for routine histopathological evaluation. Immunoperoxidase staining was performed on a Dako EnVision Autostainer (Dako Denmark A/S, Glostrup, Denmark) according to manufacturer recommendations. Antibodies for CD3 (Polyclonal Rabbit Anti-Human, Citrate Buffer HIER, dilution 1:200, Dako Omnis, Code Number: GA503), CD20 (Monoclonal Mouse Anti-Human, Citrate Buffer HIER, dilution 1:200 Clone KP1, Dako Omnis, Code Number: M0814) and CD68 (Monoclonal Mouse Anti-Human, EDTA Buffer HIER, IHC dilution 1:5000, IF dilution 1:500, Clone L26, Dako Omnis, Code Number: M0756) were employed to characterize lympho-monocytic infiltrations. Microglial Activation was assessed using both CD68 (as above), HLA-DR Antibody (Monoclonal Rabbit Anti-Human, Citrate Buffer HIER, dilution 1:50 Clone: LN-3, Invitrogen, Thermo Fisher Scientific, Waltham, MA, USA), TMEM119 (Rabbit Anti-Human, Citrate Buffer HIER, dilution 1:250, Abcam, Code Number: ab185333), while microglial proliferation was assessed using anti-Ki-67 immunohistochemistry (Mouse Anti-Human, EDTA Buffer HIER, dilution 1:200, Spring Bioscience, Code number: M3060). Anti-GFAP immunohistochemistry (Polyclonal Rabbit Anti-Human, Proteinase K enzymatic antigen retrieval, dilution 1:1000, DAKO Omnis, Code Number: GA524) was employed to assess reactive astrogliosis. Anti-CD61 immunohistochemistry (Monoclonal Mouse Anti-Human, Citrate Buffer HIER, dilution 1:75, Clone Y2/51, Dako Omnis, Code Number: M0753) was also employed to evaluate the presence of platelet-enriched microthrombi.
Anti-SARS-CoV-2 nucleocapsid (Rabbit Anti-Human, Citrate Buffer HIER, dilution 1:7000, Sino Biologicals, 40143-R001) and -Spike Subunit 1 Antibody (Monoclonal Rabbit Anti-Human, Citrate Buffer HIER, dilution 1:100, Clone 007, Sino Biological, Code Number: 40150-R007) immunostainings were employed to evaluate viral antigens within the tissue. The expression of ACE2 Receptor protein (Rabbit Anti-Human Polyclonal, Citrate Buffer HIER, dilution 1:2000, Abcam, Code Number: ab15348) and TMPRSS-2 protein (Rabbit Anti-Human Monoclonal, Citrate Buffer HIER, dilution 1:2500, Abcam, Code Number: ab242384) was assessed within the brainstem and cerebellum, and in all sections with positive findings for viral proteins.
Anti-nucleocapsid and anti-spike antibodies were validated through SARS-CoV-2 infected Vero E6 cells and autopsy-derived lung tissue from SARS-CoV-2 infected patients as positive controls; non-infected cells and lung sections deriving from autopsy cases predating COVID-19 pandemic (2017) were used as negative controls (Supplementary Figure 1). Peroxidase reactions were repeated at least three times to ensure reaction consistency.

Immunofluorescent staining and confocal microscopy. Fluorescent immunohistochemistry was performed manually. Antigen retrieval was performed on de-paraffinized tissue sections using Dako EnVision PTLink station according to manufacturer recommendations. Following antigen retrieval, autofluorescence was quenched with a 50 mM NH_4Cl solution for 10 minutes. Sections were treated with permeabilization and blocking solution (15% vol/vol Goat Serum, 2% wt/vol BSA, 0.25% wt/vol gelatin, 0.2% wt/vol glycine in PBS) containing 0.5% Triton X-100 for 90 minutes before primary antibody incubation. The following antibodies were employed: CD68 (#M0756; 1:500); TMEM119 (#ab185333; 1:200); Ki-67 (#M3060; 1:200); β-III Tubulin (#T8578; 1:300); Tyrosine Hydroxylase (#T2928; 1:6000); SARS-CoV-2 Nucleocapsid Protein (#40143-R001; 1:3000); SARS-CoV-2 Spike Subunit 1 Protein (#40150-R007; 1:100); ACE2 Receptor Protein (#ab15348; 1:500) and TMPRSS-2 (#ab242384; 1:1000). Primary antibodies were diluted in blocking solution and incubated at 4°C overnight. Alexa-Fluor plus 488 Goat anti-Mouse secondary antibody (Code number: A32723) and Alexa-Fluor plus 568 anti-Rabbit secondary antibody (Code number: A-11011) were diluted 1:200 in blocking solution as above and incubated for 60 minutes at room temperature. To further avoid background signal and tissue autofluorescence, slides were incubated for 10 minutes in 0.5% Sudan Black B solution in 70% ethanol at room temperature and abundantly washed with PBS, followed by Hoechst 33258 nuclear staining (Invitrogen, dilution: 1:10000 in PBS) for 10 minutes. Slides were mounted and coverslipped with Mowiol solution (prepared with Mowiol 4-88 reagent, MerckMillipore, Code number: 475904-100GM). Confocal immunofluorescence z-stack images were acquired on a Leica SP5 Laser Scanning Confocal Microscope using a HC PL FLUOTAR 20x/0.50 Dry or HCX PL APO lambda blue 40X/1.40 Oil objectives. Images were acquired at a 16-bit intensity resolution over 2048 × 2048 pixels. Z-stacks images were converted into digital maximum intensity z-projections, processed, and analyzed using ImageJ software.

RT-PCR analyses. Viral RNA analysis was performed on 20μm thick paraffin-embedded sections collected in sterile 2ml Eppendorf vials; disposable microtome blades and tongs were changed for each section to reduce contamination risk. Real-time RT-PCR analyses were performed to detect SARS-CoV-2 genome sequences. Briefly, total RNA was purified from selected material using a RecoverAll™ Total Nucleic Acid Isolation kit (Thermo Fisher Scientific) following the manufacturer's instructions. One-step real-time RT-PCR assays targeting SARS-CoV-2 nucleocapsid (N) coding region and subgenomic RNA were run on

ABI 7900HT Sequence Detection Systems (Thermo Fisher Scientific), as previously reported[25].

Histopathological and morphometrical evaluation. Slides were examined by three independent histopathologists and morphologists blind to patient clinical findings and COVID-19 status. Disagreements were resolved by consensus. The degree of brainstem hypoxic / ischaemic damage, astrogliosis and microgliosis were classified using a four-tiered semi-quantitative approach for each evaluated section, while microglial density and activation was assessed by the means of digitally-assisted immunoreactivity quantification by three independent evaluators.

Quantification of Activated Microglia. The degree of microgliosis was assessed through a digitally-assisted quantification approach at the level of the medulla, pons and mesencephalon. For each subject, standard sections passing through the area postrema (medulla), locus coeruleus (pons) and decussation of the superior cerebellar peduncles or red nucleus (midbrain) underwent TMEM119 immunoperoxidase staining and TMEM119 / CD68 double fluorescent immunohistochemistry. TMEM119+ structures with visible nucleus and microglial-compatible morphology were classified as microglial cells, while TMEM119- / CD68+ elements with compatible morphology were classified as monocyte/macrophages. Ramifications and cell processes without a visible nucleus were excluded from our analysis in order to avoid overestimation of cell densities by including neighboring structures belonging to adjacent sections. Morphometrical evaluation occurred within six counting fields (fields of view, FOV) spanning across the dorsal-to-ventral axis of the sections; FOV boundaries and anatomical landmarks are summarized in Supplementary Table 1 for each level of sectioning. The number of immunoreactivities per mm^2 was calculated for each counting field and assigned to one anatomical compartment (i.e. tegmentum, tectum and basis), based on their topography according to Mai and Paxinos[25]. Comparisons and statistical evaluations were conducted per individual counting field, anatomical compartment and level of section (medulla, pons, midbrain). To assess the degree of lysosomal-activity as a marker for microglia phagocytic activity, CD68 immunoreactive area (expressed as percentage of CD68+ immunoreactive area within a counting field, or A%) for 5 randomly selected counting fields at each level of sectioning was computed through particle analysis of the green fluorescent channel on ImageJ software.

Statistical Analyses. Statistical analyses and visualizations were performed using GraphPad Prism 9. Differences in microglial densities (microglia / mm^2) within subgroups of the COVID-19 cohort in figures 4A, 5A and 6A were analyzed by t tests with Welch's correction. Microglial density between individual counting fields (FOVs) in COVID-19 subjects (Figures 4D, 5D, and 6D), as well as differences between anatomical compartments in COVID-19 subgroups (Figures 4B and 5B) and in COVID-19 versus controls (Figures 2E, 4C, 5B, 6E) were determined by Welch one-way ANOVA tests corrected for Dunnett's multiple comparisons. Correlation matrices in Figures 4E and 7G were computed as Spearman's rho for continuous variables and as point-biserial correlations for nominal – continuous variables. Spearman's rho and linear regression was performed in figure 2F. Further statistical details for each plot can be found in the corresponding figure legend. Throughout the manuscript * indicates $p < 0.05$, ** $p < 0.01$, *** $p < 0.001$ and **** $p < 0.0001$.

ETHICAL APPROVAL

All procedures were carried out in accordance to the Declaration of Helsinki. Samples were anonymous to the investigators and used in accordance with the directives of the Committee of the Ministers of EU member states on the use of samples of human origin for research. Donor subjects gave their written informed consent prior to death according to regulations of the Body Donation Program of the Institute of Human Anatomy, Department of Neuroscience, University of Padova.

RESULTS

The main cause of death in COVID-19 subjects was diffuse alveolar damage. Twenty-four COVID-19 patients were included in our study. In all patients, SARS-CoV-2 RNA was detected by molecular testing in rhino-pharyngeal swabs. Eleven were females, while 13 were males. The mean age of the included subjects was 73±13.7 years. Most included subjects were affected by preexisting chronic medical conditions. Eleven patients (7 female, 4 male) were affected by neurological or neurodegenerative disease prior to SARS-CoV-2 infection. Twenty-three patients were hospitalized prior to death. Patients were hospitalized for 14.5±11.3 days and died 1 to 34 days following admission. Eleven subjects were admitted to the ICU during hospitalization and received intensive oxygen therapy (IOT) (i.e. the administration of supplemental oxygen via nasal cannulae, face masks, or tracheal intubation). Fifteen subjects received antithrombotic therapy during hospitalization and were

treated with corticosteroid medication. The available clinical data for our cohort is reported in Table 1.

The main cause of death of the control cohort was respiratory failure and pneumonia, aside from other relevant comorbidities. Eighteen age- and sex-matched subjects with comparable ante-mortem medical conditions were included as controls. All patients were negative for SARS-CoV-2 infection or died prior to the COVID-19 pandemic in Italy. Eight were female, while 10 were male. The mean age of included controls was 72±12 years. The mean hospitalization time was 20±15.6 days. Thirteen patients died due to pneumonia, while the remaining subjects died due to respiratory insufficiency, multiorgan failure or ischaemic heart disease. One patient died due to septic shock. Five patients had a clinical diagnosis of cognitive decline. The available clinical data for the control group are reported in Table 2.

ID	Age	Sex	Hospitalization (days)	ICU	Intensive Oxygen Therapy	Anti-thrombotic medication	Steroid Medication	Hypertension	PMI	Antemortem Head CT	Neurological signs	Neuropathological evaluation	Brainstem Hypoxic Damage	Microthrombosis (NON-CNS)	Cause of Death
#1	87	F	2	N	N	Y	Y	Y	4	NA	Cognitive decline	AD neuropathological changes, CAA	Mild	Lungs, liver	Diffuse alveolar damage
#2	92	F	5	N	N	N	Y	N	1	NA	Cognitive decline, Alzheimer type	AD neuropathological changes, CAA	Mild	Lungs	Diffuse aveolar damage, intestinal infarction
#3	83	M	8	N	N	Y	Y	Y	2	Cerebral and cerebellar atrophy, chronic ischemic vascular disease	Frontoparietal ischemic insult (old) episodes of hepatic encephalopathy (HCV+)	Multi-infarct dementia, arteriosclerosis	Moderate	No	Diffuse alveolar damage, hepatic cyrrhosis
#4	97	F	9	N	N	Y	Y	Y	5	NA	Vascular dementia	Vascular dementia, arterioscelrosis, diffuse hypoxic/ischaemic damage	Mild	Lungs	Diffuse alveolar damage, cardiac amyloidosis
#5	78	F	15	N	N	Y	Y	Y	5	NA	NA	Early AD neuropathological changes, diffuse hypoxic/ischaemic damage	Mild	Liver	pneumonia, aspergillus bronchopneumonia
#6	74	M	13	Y	Y	Y	Y	Y	4	Vascular calcification, expansive lesion of the right frontal lobe and right cerebellar hemisphere in patient with pulmonary neoplasia	NA	Small cell metastasic lung carcinoma with right cerebellar and frontal metastases	Mild	No	Small cell metastatic lung carcinoma, diffuse alveolar damage
#7	58	F	11	Y	Y	Y	N	N	2	Extensive ischaemic lesion of the territory of the right PCA, occulsion of the PCA	NA	Medial temporal lobe infarction	Moderate	No	Acute myocardial infarction, cardiogenic shock
#8	50	M	1	N	N	N	N	N	3	NA	NA	Arteriosclerosis, diffuse hypoxic/ischaemic damage	No detectable changes	No	Coronary atherosclerosis and myocardiosclerosis
#9	81	F	30	N	N	N	N	Y	3	Ischaemic regions in the MCA territory and diffuse cerebral and cerebellar atrophy due to chronic ischaemic vascular disease.	Soporous status	Mixed dementia with AD neuropathological changes, CAA and chronic ischemic vascular disease	Moderate	Lungs, liver	Atherosclerotic aortic aneurysm, pneumonia.
#10	60	M	30	Y	Y	Y	Y	N	3	NA	NA	Diffuse hypoxic/ischaemic damage	Mild	Heart	Pneumonia with emphysema.
#11	55	M	15	Y	Y	Y	Y	N	2	NA	NA	CNS microthromboses, haemorragic injury in the territory of the right MCA	Moderate	No	Pulmonary thromboembolism with infarcts.
#12	62	M	27	Y	Y	Y	Y	N	2	NA	NA	Arteriosclerosis, diffuse hypoxic/ischaemic damage	Mild	Lungs	Pneumonia with hemorrhages. Intestinal and hepatic infarcts.
#13	73	M	21	Y	Y	Y	Y	Y	2	NA	NA	Diffuse hypoxic/ischaemic damage	Moderate	No	Pneumothorax, Pneumonia, right pleurodesis,
#14	58	F	24	Y	Y	Y	Y	Y	1	Right anisocoria	No relevant signs	Diffuse hypoxic/ischaemic damage	Mild	Lungs	Pneumonia. Necrotic-haemorragic pancreatitis. Multiorgan failure.
#15	49	F	3	Y	Y	Y	N	N	2	Confusion and hallucinations; CSF Streptococcus Pneumoniae +	NA	Acute purulent meningitis, post-anoxic pathology	Moderate	No	Acute purulent meningitis. Post-anoxic cerebral death.
#16	72	M	10	Y	Y	Y	Y	Y	4	Hypostenia, dizziness, anosmia. Sudden fall.	NA	Diffuse hypoxic/ischaemic damage	Severe	No	Consolidative pneumonia. Hypertensive heart disease.
#17	72	M	38	N	N	N	Y	N	1	NA	NA	CNS microthromboses, extensive haemorragic injury of the right cerebellar hemisphere, ischaemic vascular disease	Mild	No	Multivascular obstructive coronary atherosclerosis. Left pulmonary infarct.

#18	82	M	6	N	N	N	Y	Y	3	Acute neurological event: Anisocoria, non responding	NA	CNS microthromboses, ischemic vascular disease	Mild	No	Lobar pneumonia
#19	40	F	1	N	N	NA	NA	Y	ND	NA	NA	CNS microthromboses, diffuse hypoxic/ischaemic damage	Moderate (medulla not sampled)	NA	Diffuse alveolar damage
#20	68	M	NA	N	N	NA	NA	Y	ND	NA	NA	CNS microthromboses, diffuse hypoxic/ischaemic damage	Severe (medulla not sampled)	NA	Diffuse alveolar damage
#21	73	M	5	Y	Y	Y	Y	N	5	NA	NA	CNS microthromboses, cortical and subcortical haemorrages, global ischaemia	Moderate	Lungs	Diffuse alveolar damage, Platelet/fibrin microthrombosis
#22	77	F	34	N	N	N	N	Y	5	No signs	NA	CNS microthromboses, ischemic vascular disease	Moderate to severe	Lungs	Chronic emphysema, diffuse alveolar damage and platelet/fibrin microthromboses.
#23	84	M	12	Y	Y	Y	Y	Y	4	Chronic ischaemic vascular disease	Cognitive decline	AD neuropathological changes, Parkinson's Disease, CNS microthromboses, ischemic vascular disease	Moderate	Lungs	Chronic emphysema, bacterial pneumonia, diffuse alveolar damage lung platelet/fibrin microthrombosis.
#24	89	F	1	N	N	N	N	Y	5	Chronic ischaemic vascular disease, territorial ischaemic injury (right occipital lobe, caudate nucleus and cerebellum)	Cognitive decline	AD neuropathological changes, CNS microthromboses, diffuse hypoxic/ischaemic damage	Moderate	Lungs	Chronic emphysema, diffuse alveolar damage and platelet/fibrin microthromboses

Table 1. *COVID-19 patients clinical data.*

ID	Age	Sex	Hospitalization (days)	Hypertension	PMI	Antemortem Head CT	Neurological signs	Neuropathological evaluation	Brainstem Hypoxic damage	Microthrombosis (NON-CNS)	Cause of Death
#1	83	M	10	Y	5	Cerebral atrophy, Chronic ischaemic vascular disease	Cognitive decline	Mixed dementia with AD neuropathological changes ad chronic ischaemic vascular disease	Moderate	No	Pneumonia, respiratory insufficiency, ischaemic heart disease
#2	74	M	2	Y	4	Vascular calcification, ischaemic heart disease	NA	Chronic ischaemic vascular disease, diffuse hypoxic/ischaemic damage	Mild	No	Ischaemic heart disease.
#3	40	M	1	N	4	No signs	No signs	Diffuse hypoxic/ischaemic damage	No detectable microscopical changes	No	Haemorragic Shock
#4	79	F	31	Y	3	Cerebral atrophy, Chronic ischaemic vascular disease	Cognitive decline, Alzheimer type	AD neuropathological changes, CAA, ischemic vascular disease	Mild	No	Pentalobar pneumonia, respiratory insufficiency
#5	62	M	22	Y	5	NA	NA	Diffuse hypoxic/ischaemic damage	Mild	No	Pneumonia, respiratory insufficiency
#6	76	M	15	Y	6	NA	NA	Ischaemic vascular disease, diffuse hypoxic/ischaemic damage	Mild	No	Pneumonia, chronic ischaemic vascular disease
#7	75	M	12	Y	4	NA	NA	Diffuse hypoxic/ischaemic damage	Mild	No	Pneumonia, ischaemic heart disease
#8	78	F	8	Y	3	No	NA	Diffuse hypoxic/ischaemic damage	Mild	No	Pneumonia, ischaemic heart disease
#9	71	F	40	Y	3	NA	NA	Diffuse hypoxic/ischaemic damage	Moderate to severe	No	Acute respiratory failure, septic shock, peritonitis
#10	46	F	15	N	4	No signs	No signs	Diffuse hypoxic/ischaemic damage	No detectable microscopical changes	No	Respiratory insufficiency, multiorgan failure, cervical neoplasia
#11	75	F	20	Y	5	Chronic Ischaemic Vascular disease, Cerebral atrophy	NA	Vascular dementia, ischaemic vascular disease, diffuse hypoxic/ischaemic damage	Moderate	No	Pneumonia, acute respiratory failure, candidosis
#12	80	F	8	Y	4	Cerebral atrophy	Cognitive decline, Alzheimer type	AD neuropathological changes, diffuse hypoxic/ischaemic damage	Moderate	No	Pentalobar pneumonia, respiratory insufficiency
#13	81	F	NA	Y	3	NA	NA	Diffuse hypoxic/ischaemic damage	Mild	No	Pneumonia, acute respiratory failure
#14	63	F	NA	N	3	No signs	No signs	Diffuse hypoxic/ischaemic damage	Mild	No	Ischaemic heart disease
#15	70	M	38	Y	5	Chronic ischaemic vascular disease	NA	Ischaemic vascular disease, diffuse hypoxic/ischaemic damage	Moderate	No	Bilateral pneumonia, respiratory insufficiency.
#16	81	M	10	Y	4	Cerebral atrophy	Cognitive decline, Alzheimer type	Mixed AD neuropathological changes and Lewy Body pathology, diffuse hypoxic/ischaemic damage	Moderate	No	Pneumonia, respiratory insufficiency
#17	75	M	58	Y	6	Cerebral atrophy	NA	Vascular dementia, ischaemic vascular disease, diffuse hypoxic/ischaemic damage	Moderate	No	Pneumonia, respiratory insufficiency.
#18	87	M	30	Y	6	Cerebral atrophy	Cognitive decline	AD neuropathological changes, diffuse hypoxic/ischaemic damage	Moderate	No	Pneumonia, multiorgan failure.

Table 2. *Control patients clinical data.*

Neuropathological examination

A wide spectrum of neuropathological alterations were detected in both COVID-19 and control subjects. The brains of 20 COVID-19 subjects displayed gross macroscopic abnormalities including mild-to-moderate generalized cerebral atrophy (N=9), diffuse cerebral edema (N=9) and chronic territorial ischaemic injury (N=6). Histopathological evaluation revealed diffuse hypoxic / ischaemic damage as a common finding in the COVID-19 cohort, with most subjects presenting mild-to-moderate diffuse hypoxic / ischaemic damage of the cerebral hemispheres and brainstem (Figure 1C), quantified according a four-tiered semi-quantitative scale (reported in Table 1). Furthermore, acute ischaemic injuries were evident in 5 patients. Small vessels were congested in most subjects with moderate perivascular extravasation at the level of the medulla, pons and deep cerebellar nuclei in 6 cases. Variable degrees of astrogliosis were evident in all subjects in all assessed regions, but were more pronounced at the level of the brainstem, as testified by GFAP staining (Supplementary Figure 3; semi-quantitative evaluation of astrogliosis across brain regions is available in Supplementary Table 2). Alzheimer Disease (AD) neuropathological changes, evaluated according to NIA-AA criteria, as well as Cerebral Amyloid Angiopathy (CAA) were detected in 5 subjects. In one case, Parkinson's Disease neuropathological alterations (i.e. deterioration of the ventrolateral substantia nigra and nigral lewy bodies) were found.

Control subjects presented similar macroscopic and histopathological alterations: mild-to-moderate generalized cerebral atrophy (N=7), mild-to-moderate diffuse cerebral edema (N=11) and chronic territorial ischemic injury (N=7); most subjects who died due to pneumonia or respiratory failure presented variable degrees of diffuse hypoxic / ischaemic damage, with mild to moderate damage of the brainstem being a common finding, similarly to COVID-19 subjects (Figure 1C); individual findings for hypoxic / ischaemic injury are reported in Table 2. Four subjects presented AD neuropathological changes and CAA, with one subject presenting both AD and Lewy Body Dementia mixed pathology. The macroscopic and histopathological findings of both COVID-19 subjects and controls are reported in Table 1 and Table 2.

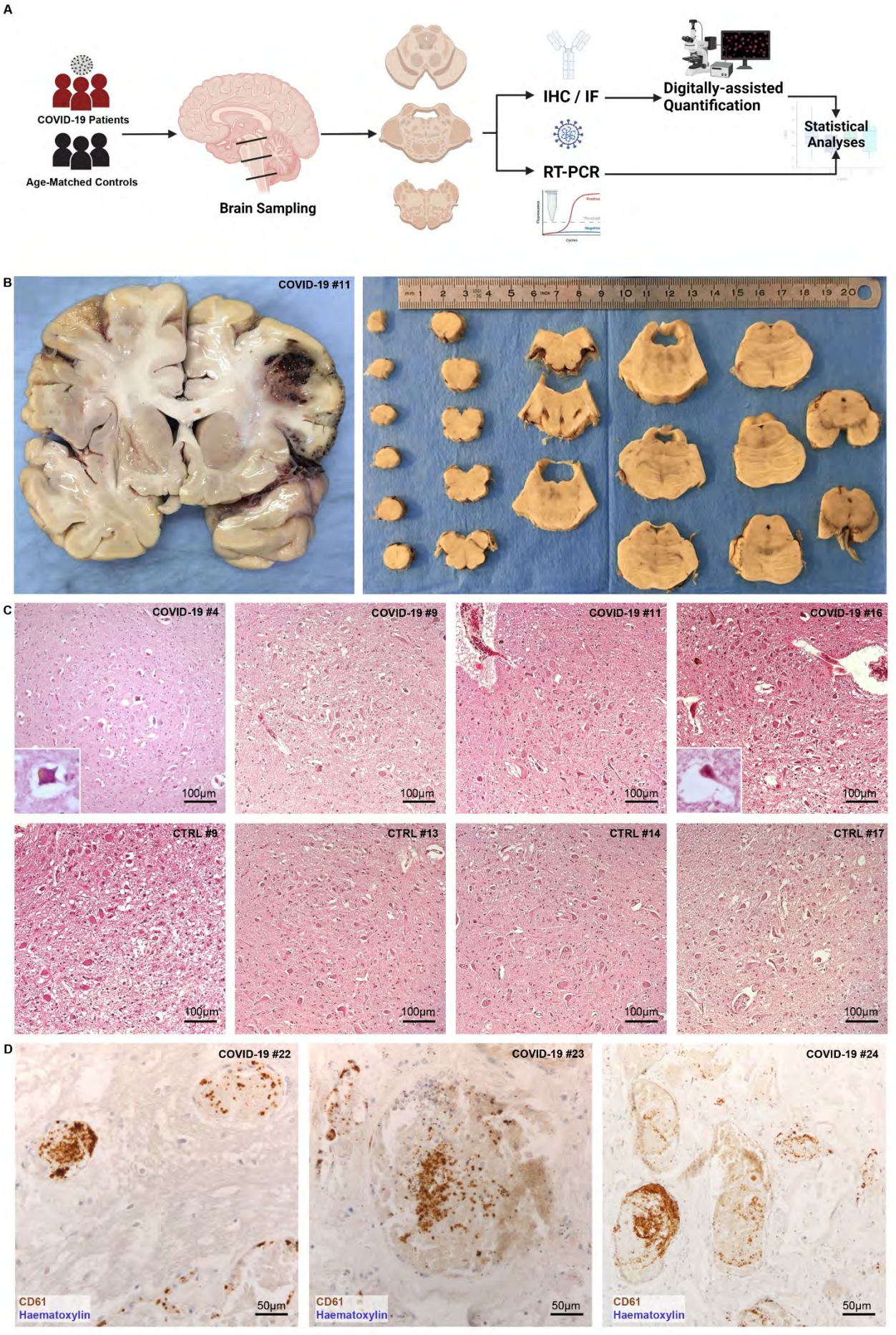
A
COVID-19 Patients
Age-Matched Controls
Brain Sampling
IHC / IF
RT-PCR
Digitally-assisted Quantification
Statistical Analyses
B
COVID-19 #11
C
COVID-19 #4
COVID-19 #9
COVID-19 #11
COVID-19 #16
CTRL #9
CTRL #13
CTRL #14
CTRL #17
100µm
D
COVID-19 #22
COVID-19 #23
COVID-19 #24
CD61
Haematoxylin
50µm

Figure 1. Study Workflow. Brain sections of multiple sites were sampled from 24 COVID-19 patients and 18 age- and sex-matched controls who died due to pneumonia and / or respiratory failure. B) *Left, coronal brain section of Subject #11 revealing extensive hemorrhagic injury in the territory of the middle cerebral artery. Right, sampling procedure of the brainstem through axial sections passing perpendicularly to the floor of the fourth ventricle.* ***C)*** *Haematoxylin and eosin photomicrographs of the Dorsal Motor Nucleus of the Vagus in the medulla oblongata displaying various degrees of hypoxic / ischaemic damage in COVID-19 subjects (upper row) and controls (lower row)* ***D)*** *Platelet microthrombi at the level of the pons and cerebral cortex, CD61 immunohistochemistry.*

CNS platelet-enriched microthrombi in small parenchymal vessels were detected in COVID-19 subjects, but not in controls. Small vessel thromboses were detected in 9 COVID-19 patients at the level of the pons, deep cerebellar nuclei and cerebral cortex, with one patient presenting small vessel thromboses in multiple sites. No CNS or systemic thromboses were detected in controls. In all COVID-19 cases, CD61 immunoperoxidase staining revealed platelet-rich microthrombi in small parenchymal vessels, with no evidence of arachnoid of meningeal vessels being involved, as seen in Figure 1D. Other organs were often affected, such as the lungs, liver, intestine, and hypopharynx and even the carotid body[10,27-28], as summarized in Table 1. In 3 out of 9 cases, microthromboses were identified only within the CNS, while in the remaining 6 subjects, pulmonary thromboses were also detected. Interestingly, 3 out of 9 subjects with CNS microthrombi were on antithrombotic medication, 4 were not actively treated prior to death, and in 2 cases clinical information regarding antithrombotic medication was incomplete. In line with previous findings in literature, CNS microthromboses appear to be peculiar to the COVID-19 cohort, with no control subject presenting either fibrin- or platelet-enriched microthrombi in the CNS or other organs regardless of the cause of death.

Microglial cells with an activated phenotype and frequent microglial nodules were found in COVID-19 subjects, but not in controls. In 23 COVID-19 subjects parenchymal microglia displayed an activated phenotype with characteristic thorny ramifications or amoeboid morphology (Figure 2A-B). Interestingly, homeostatic microglial marker TMEM119 was consistently expressed in our cohort (Figure 2A-D), even though it is known to be downregulated upon microglial activation in various neuropathological conditions[26]. A similar pattern of immunoreactivity is also seen in Matschke et al.[15] and Schwabenland et al.[17]. Considering the relatively short hospitalization time prior to death of our COVID-19 cohort

(14.5 days), and the similar immunoreactivity pattern compared to other available studies, it could be inferred that TMEM119 downregulation does not occur early in COVID-19.

While in both COVID-19 subjects and controls microglial marker TMEM119 and lysosomal-activity marker CD68 were found within the same cell (2A-D), COVID-19 subjects displayed a more widespread CD68+ immunoreactivity (2A-B), with statistically significant differences in CD68 immunoreactive area (A%) at the level of the medulla and midbrain, but not the pons, between the two groups (Figure 2E, Welch ANOVA W= 42.68; medulla $p<0.0001$; pons $p=0.733$; midbrain $p<0.0001$). Ki-67 immunoperoxidase staining, as well as Ki-67 / CD68 double label immunofluorescent staining did not reveal significant Ki-67 immunoreactivity ascribable to microglial cells, suggesting local microglial activation and migration without active proliferation in the considered cases. Microglial nodules associated with perineuronal HLA-DR+ / TMEM119+ / CD68+ cells were suggestive of neuronophagia in 18 COVID-19 subjects (Figure 3A-B, 4G, 6F) and were identified at the level of the substantia nigra (N=14), dorsal motor nucleus of the vagus (N=12), medullary reticular formation (N=9), area postrema (N=6) and basal ganglia (N=5); no microglial nodules were found in control cases, regardless of cause of death. Moreover, moderate to severe infiltration of CD68+/TMEM119- cells was found in 23 subjects (2A); given their prominent perivascular localization, these were likely monocyte-derived macrophages.

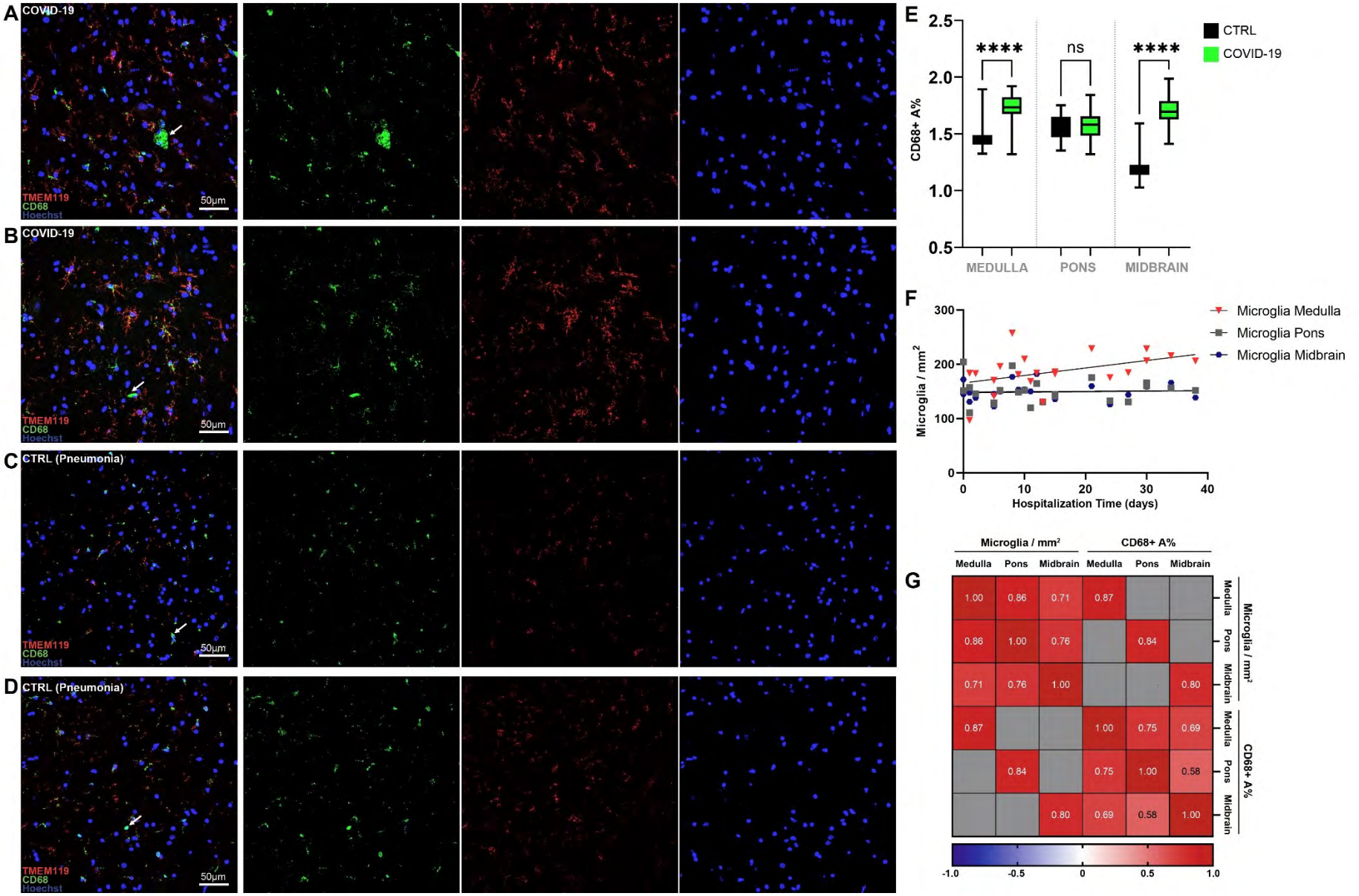
A
COVID-19
TMEM119
CD68
Hoechst
50µm
B
COVID-19
TMEM119
CD68
Hoechst
50µm
C
CTRL (Pneumonia)
TMEM119
CD68
Hoechst
50µm
D
CTRL (Pneumonia)
TMEM119
CD68
Hoechst
50µm
E
CD68+ A%
2.5
2.0
1.5
1.0
0.5
****
ns
****
CTRL
COVID-19
MEDULLA
PONS
MIDBRAIN
F
Microglia / mm²
300
200
100
0
0
10
20
30
40
Hospitalization Time (days)
Microglia Medulla
Microglia Pons
Microglia Midbrain
G
Microglia / mm²
CD68+ A%
Medulla
Pons
Midbrain
1.00 0.86 0.71 0.87
0.86 1.00 0.76 0.84
0.71 0.76 1.00 0.80
0.87 1.00 0.75 0.69
0.84 0.75 1.00 0.58
0.80 0.69 0.58 1.00
Microglia / mm²
CD68+ A%
-1.0
-0.5
0
0.5
1.0

Figure 2. Double label TMEM119 (microglia marker, red) / CD68 (lysosomal activity marker, green) fluorescent immunohistochemistry in COVID-19 and control subjects. *A-B) in COVID-19, microglial cells present a distinctly activated phenotype whilst maintaining homeostatic microglial marker TMEM119 (Red) and displaying increased lysosomal activity (CD68, green). Arrows indicate CD68+ / TMEM119- monocyte/macrophage in the parenchyma. C-D) In control subjects, TMEM119 marks both the soma and sparse ramifications of resident microglia, suggesting less prominent activation without significant marker downregulation. CD68 immunoreactivity (green) is also present, but not as distributed as in COVID-19. E) Welch one-way ANOVA of CD68+ A% in COVID-19 and controls reveals statistically significant differences between the two groups at the level of the medulla ($p<0.0001$) and midbrain ($p<0.0001$), but not the pons. F) Spearman correlation between microglial densities across brainstem levels and hospitalization time reveals a statistically significant positive correlation between medullary microgliosis and hospitalization time ($r= 0.44$; $p=0.044$). G) Correlation matrix between microglial densities and CD68+ A% across brainstem levels.*

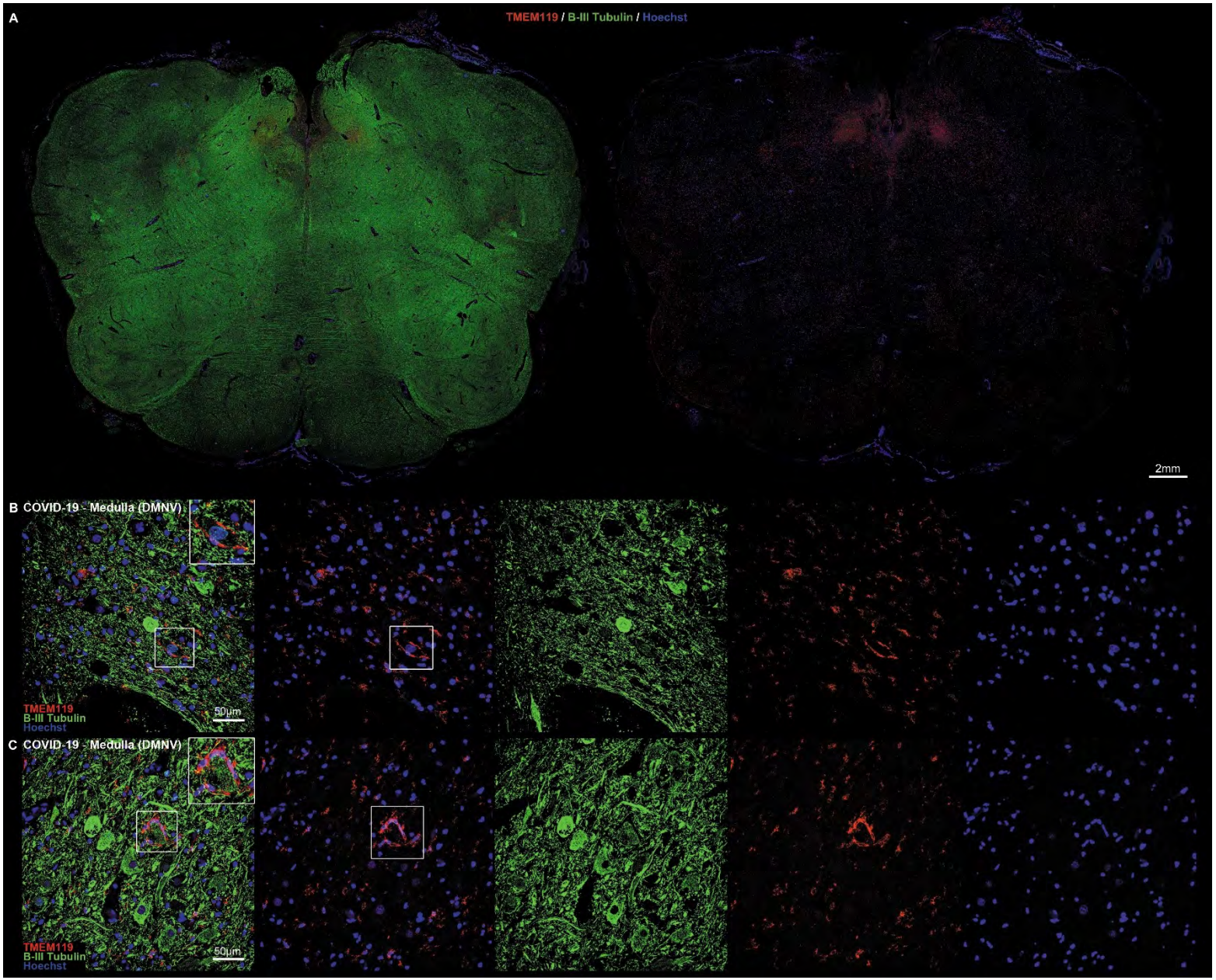
A
TMEM119 / B-III Tubulin / Hoechst
2mm
B COVID-19 - Medulla (DMNV)
TMEM119
B-III Tubulin
Hoechst
50µm
C COVID-19 - Medulla (DMNV)
TMEM119
B-III Tubulin
Hoechst
50µm

Figure 3. COVID-19 microgliosis and microglial nodules in the medulla oblongata A) *Low-magnification perspective of the medulla oblongata in COVID-19, displaying a ventral-to-dorsal increasing gradient of microglial densities (TMEM119, red; Beta-III Tubulin, green)* ***B-C)*** *Double label TMEM119 (microglial marker, red) and Beta-III Tubulin (neuronal marker, green) immunofluorescent staining at the level of the medulla oblongata. Insets display neuronophagia at the level of the dorsal motor nucleus of the vagus in two COVID-19 subjects.*

In COVID-19 subjects, a topographically defined pattern of microgliosis was found in the medulla oblongata and midbrain. At the level of the medulla oblongata, Welch one-way ANOVA of individual counting fields (FOVs) (Figure 4C, F) revealed statistically significant differences ($p<0.001$) in TMEM119+/CD68+ activated microglial cells between the medullary tegmentum (T, FOV-13; 216,84±52,26 microglia / mm^2) and the ventral medulla (pes, P, FOV4-6; 156,09±35,16 microglia / mm^2) (Figure 4E-F); no differences were found between individual counting fields of the same anatomical compartment. Furthermore, no significant differences were found when comparing microglial density between IOT and non-IOT COVID-19 patients, as well as AD and non-AD patients with SARS-CoV-2 infection (Figure 4A). When comparing microglial density between COVID-19 patients and the control cohort, statistically significant differences were found when considering overall medullary microgliosis, as well as single anatomical compartments (Figure 4C).

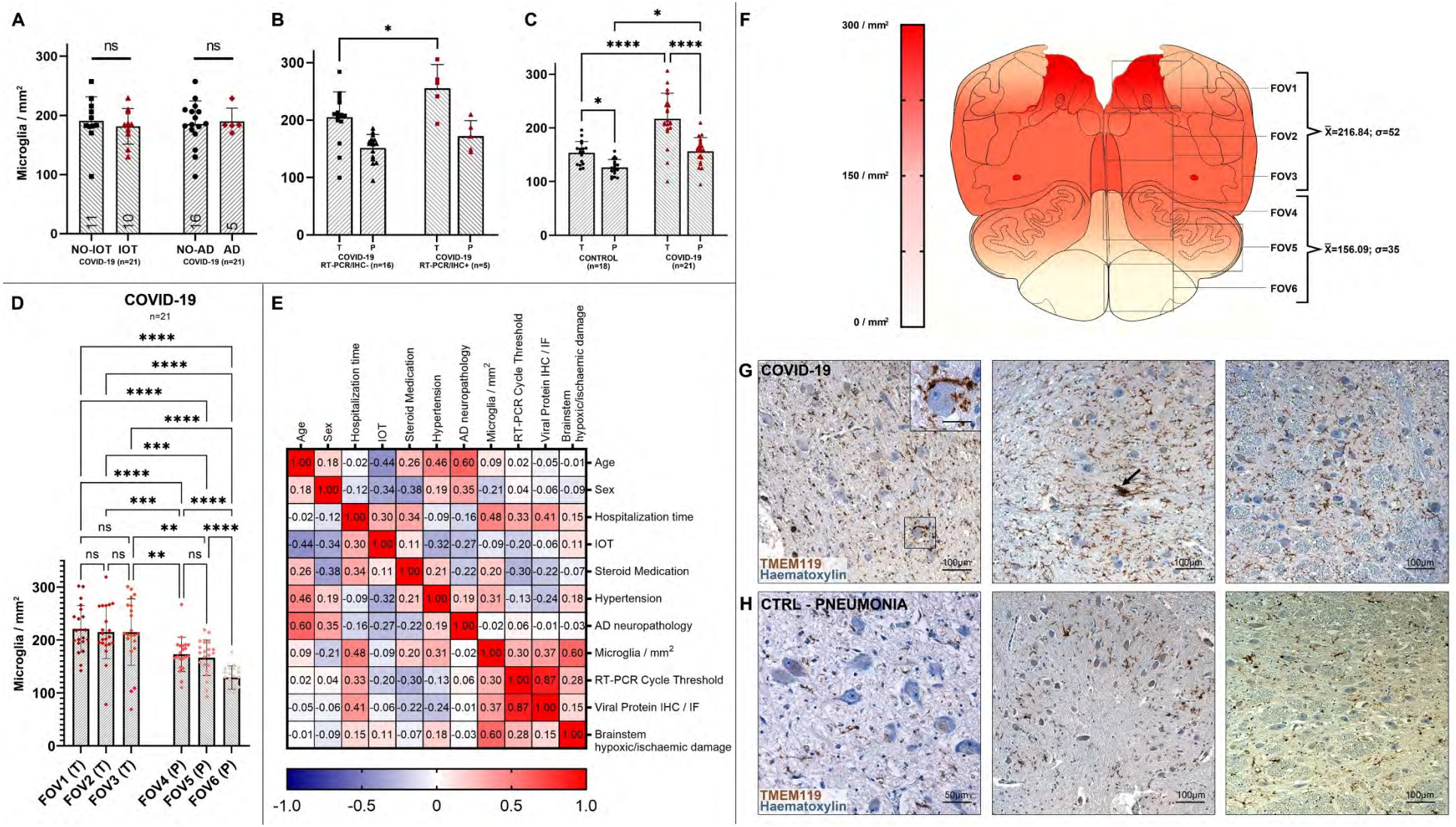
A
Microglia / mm²
NO-IOT
IOT
NO-AD
AD
COVID-19 (n=21)
B
COVID-19 RT-PCR/IHC- (n=16)
COVID-19 RT-PCR/IHC+ (n=5)
C
CONTROL (n=18)
COVID-19 (n=21)
D
COVID-19
n=21
FOV1 (T)
FOV2 (T)
FOV3 (T)
FOV4 (P)
FOV5 (P)
FOV6 (P)
E
Age
Sex
Hospitalization time
IOT
Steroid Medication
Hypertension
AD neuropathology
Microglia / mm²
RT-PCR Cycle Threshold
Viral Protein IHC / IF
Brainstem hypoxic/ischaemic damage
F
300 / mm²
150 / mm²
0 / mm²
FOV1
FOV2
FOV3
FOV4
FOV5
FOV6
X̄=216.84; σ=52
X̄=156.09; σ=35
G
COVID-19
TMEM119
Haematoxylin
H
CTRL - PNEUMONIA
TMEM119
Haematoxylin

Figure 4. Quantification of reactive microglia at the level of the medulla oblongata reveals an anatomically segregated pattern of inflammation. A) *Welch corrected T-test plot of microglial densities (microglia / mm^2) in the medulla oblongata of COVID-19 subjects treated (n=10, red) and not treated (n=11, black) with intensive oxygen therapy (p>0.05), and of COVID-19 subjects with (n=5, red) and without (n=16, black) Alzheimer's Disease neuropathological changes (p>0.05).* ***B)*** *Welch one-way ANOVA between anatomical compartments (T, tegmentum; P, pes) between COVID-19 subjects with (n=5, red) and without (n=16) viral tropism (RT-PCR/IHC+ versus RT-PCR/IHC-) reveals statistically significant differences at the level of the medullary tegmentum (p=0.017).* ***C)*** *Welch one-way ANOVA between anatomical compartments (T, tegmentum; P, pes) between COVID-19 subjects (n=21, red) and controls (n=18, black) reveals statistically significant differences both at the level of the medullary tegmentum (p<0.0001) and pes (p=0.017).* ***D)*** *Welch one-way ANOVA of microglial densities per counting fields (FOV) reveals statistically significant differences between FOVs of the Tegmentum (T; FOV1-3) when compared to FOVs of the Pes (P; FOV4-6).* ***E)*** *Correlation heatmap between COVID-19 subject clinical data and neuropathological findings.* ***F)*** *Anatomical heatmap of activated microglia within the medulla oblongata in COVID-19.* ***G-H)*** *TMEM119 immunoperoxidase staining of comparable regions of the medulla oblongata in COVID-19 subjects (above) and controls (below). Inset: neuronophagia in the dorsal motor nucleus of the vagus. Arrow: microglial nodule.*

At the level of the pons, Welch one-way ANOVA of individual counting fields revealed statistically significant differences only between the most dorsally located counting field comprising the locus coeruleus (FOV1), and other counting fields (FOV2-6) (Figure 5D, C). However, as for the medulla, no differences were found between IOT and non-IOT patients, as well as for AD versus non-AD patients (Figure 5A). Differences in overall microgliosis, as well as differences between anatomical compartments, were not significant between COVID-19 subjects and controls (Figure 5B). Hence, while there appears to be a higher degree of microgliosis in proximity to the locus coeruleus in COVID-19 when compared to other regions of the pons, no differences were found within COVID-19 subgroups and when compared to controls, indicating pontine microgliosis as a non-specific alteration in our cohort (Figure 5E-F).

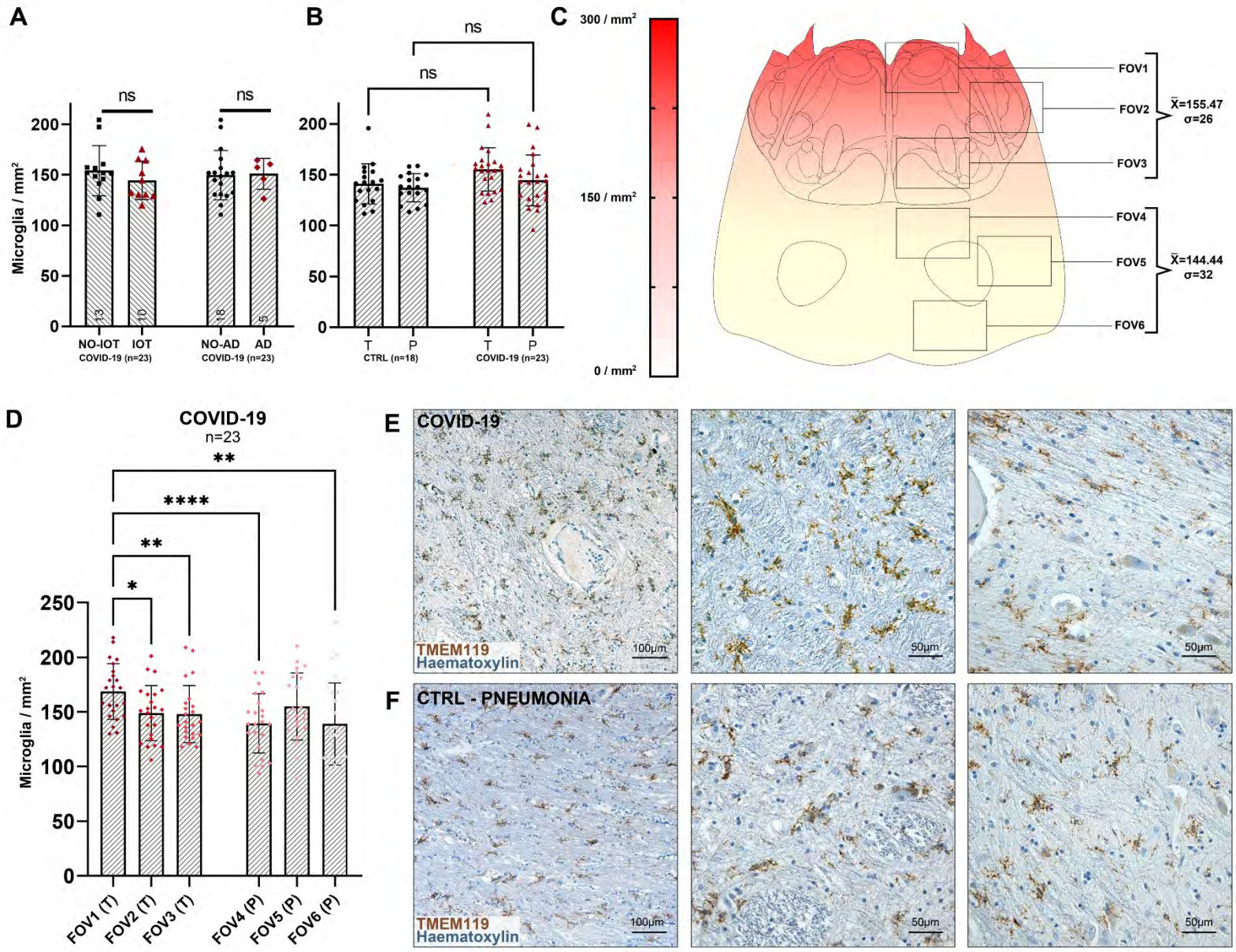
A
B
C
ns
ns
ns
ns
Microglia / mm²
200
150
100
50
0
13
10
18
5
NO-IOT
IOT
NO-AD
AD
COVID-19 (n=23)
COVID-19 (n=23)
T
P
T
P
CTRL (n=18)
COVID-19 (n=23)
300 / mm²
150 / mm²
0 / mm²
FOV1
FOV2
FOV3
FOV4
FOV5
FOV6
X̄=155.47
σ=26
X̄=144.44
σ=32
D
COVID-19
n=23
**
****
**
*
250
200
150
100
50
0
Microglia / mm²
FOV1 (T)
FOV2 (T)
FOV3 (T)
FOV4 (P)
FOV5 (P)
FOV6 (P)
E
COVID-19
TMEM119
Haematoxylin
100µm
50µm
50µm
F
CTRL - PNEUMONIA
TMEM119
Haematoxylin
100µm
50µm
50µm

Figure 5. No statistically-significant differences in microglial densities were found at the level of the pons. A) *Welch corrected T-test plot of microglial densities (microglia / mm^2) in the pons of COVID-19 subjects with (n=5, red) and without (n=16, black) Alzheimer's Disease neuropathological changes (p>0.05), and of COVID-19 subjects treated (n=10, red) and not treated (n=13, black) with intensive oxygen therapy (p>0.05).* ***B)*** *Welch one-way ANOVA between anatomical compartments (T, tegmentum; P, pes) between COVID-19 subjects (n=23, red) and controls (n=18, black) reveals no statistically significant differences either at the level of the medullary tegmentum (p=0.55) and pes (p=0.98).* ***C)*** *Anatomical heatmap of activated microglia within the pons in COVID-19.* ***D)*** *Welch one-way ANOVA of microglial densities per counting fields (FOV) reveals statistically significant differences between FOV1 (dorsal pons, including locus coeruleus) with other pontine counting fields.* ***E-F)*** *TMEM119 immunoperoxidase staining of comparable regions of the pons in COVID-19 subjects (above) and controls (below).*

At the level of the midbrain, COVID-19 subjects presented marked topographical differences between counting fields comprising the substantia nigra (midbrain tegmentum, FOV1-2 and FOV3, Figure 6C) when compared to counting fields of the midbrain tectum and pes (FOV4-6), as seen in Figure 6C-D. This anatomically segregated pattern of inflammation targeting mainly the substantia nigra, but also part of the pre-acqueductal tegmentum, indicates an increasing dorsal-to-ventral gradient of microgliosis which affects the gray matter of the midbrain, sparing counting fields falling within the cerebral peduncle (FOV5-6). Similar to other brainstem levels, no statistically significant differences in overall microgliosis were found when comparing IOT and non-IOT subjects, as well as AD and non-AD subjects (Figure 6A). When compared to controls, COVID-19 subjects presented significantly higher microglial densities when considering both overall microgliosis, as well as microglial densities within anatomical compartments (Figure 6E), suggesting for a COVID-19-specific microglial response at the level of the midbrain (Figure 6F-G).

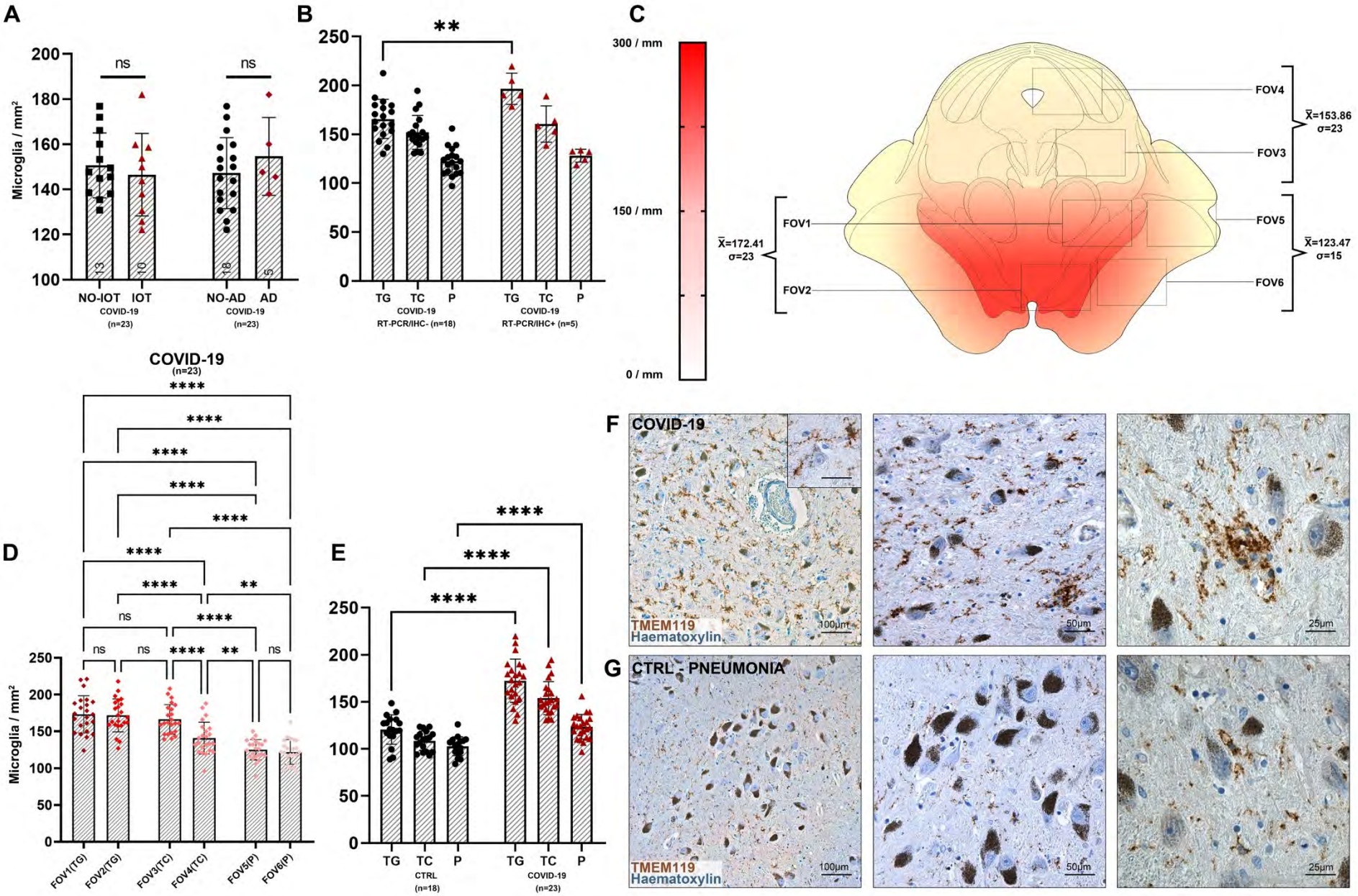
A
Microglia / mm²
ns
ns
NO-IOT
IOT
NO-AD
AD
COVID-19
(n=23)
B
**
TG
TC
P
COVID-19
RT-PCR/IHC- (n=18)
COVID-19
RT-PCR/IHC+ (n=5)
C
300 / mm
150 / mm
0 / mm
FOV1
FOV2
FOV3
FOV4
FOV5
FOV6
X̄=172.41
σ=23
X̄=153.86
σ=23
X̄=123.47
σ=15
D
COVID-19
(n=23)
FOV1(TG)
FOV2(TG)
FOV3(TC)
FOV4(TC)
FOV5(P)
FOV6(P)
E
CTRL
(n=18)
COVID-19
(n=23)
F
COVID-19
TMEM119
Haematoxylin
100µm
50µm
25µm
G
CTRL - PNEUMONIA
TMEM119
Haematoxylin
100µm
50µm
25µm

Figure 6. Anatomically segregated microgliosis of the ventral midbrain was significantly higher in COVID-19 when compared to pneumonia patients. A) *Welch corrected T-test plot of microglial densities (microglia / mm^2) in the midbrain of COVID-19 subjects with (n=5, red) and without (n=16, black) Alzheimer's Disease neuropathological changes (p>0.05), and of COVID-19 subjects treated (n=10, red) and not treated (n=11, black) with intensive oxygen therapy (p>0.05).* ***B)*** *Welch one-way ANOVA between anatomical compartments (TG, tegmentum; TC, tectum; P, pes) between COVID-19 subjects with (n=5, red) and without (n=18) viral tropism (RT-PCR/IHC+ versus RT-PCR/IHC-) reveals statistically significant differences at the level of the midbrain tegmentum (p=0.0074), but not other anatomical districts.* ***C)*** *Anatomical heatmap of activated microglia within the medulla oblongata in COVID-19.* ***D)*** *Welch one-way ANOVA of microglial densities per counting fields (FOV) reveals statistically significant differences between FOVs of the Tegmentum (T; FOV1-2) when compared to FOVs of the Pes (P; FOV5-6), suggesting for a localized pattern of microgliosis comprising the preacqueductal tegmentum and the substantia nigra.* ***E)*** *Welch one-way ANOVA between anatomical compartments (TG, tegmentum; TC, tectum; P, pes) between COVID-19 subjects (n=23, red) and controls (n=18, black) reveals statistically significant differences between all anatomical districts of the midbrain (p<0.0001).* ***F-G)*** *TMEM119 immunoperoxidase staining of comparable regions of the midbrain in COVID-19 subjects (above) and controls (below). Inset: perineuronal microglia in the substantia nigra. COVID-19 subjects often present distinct microglial nodules.*

We also found a strong correlation between microglial densities across the different levels of the brainstem, as well as CD68+ A% of the corresponding level, as summarized in Figure 2G. The strong positive correlation between microglial density and CD68 immunoreactive area further underlines the activated phenotype displayed by microglial cells in COVID-19. Interestingly, in the COVID-19 cohort, hospitalization time was positively correlated to microglial density in the medulla (r= 0.44; p=0.044), but not with microglial density in the pons and midbrain (Figure 2F). This appears to indicate an increase of microglial densities in the medulla as infection progresses, while the levels of microgliosis within the rest of the brainstem appear to remain relatively stable throughout time. Considering the numerous instances of microglial nodules and neuronophagia encountered in the medulla of the COVID-19 cohort, this is suggestive of prominent medullary impairment ongoing during COVID-19, regardless of oxygenation status or prior neurodegenerative pathology. Conversely, microglial density in the medulla also correlates with hypoxic / ischaemic damage of the brainstem, evaluated along a four-tiered semi-quantitative scale (r= 0.59; p=0.004), as also seen in Thakur et al.[18]. Hence, while microgliosis is strongly characteristic of COVID-19 subjects and differs from controls, brainstem hypoxia / ischaemia plays a major role in mediating medullary microgliosis, as seen in our cohort and in accordance to previous literature.

SARS-CoV-2 Viral proteins were detected in neurons of the medulla and midbrain in a subset of COVID-19 subjects, but not in controls. Immunoperoxidase and immunofluorescent staining for SARS-CoV-2 spike protein and nucleocapsid protein was performed on all samples of included subjects, showing only positive results in cases with SARS-CoV-2 infection, but not in controls, indicating specificity. In particular, viral proteins were detected in seven subjects (#3, #7, #9, #10, #11, #17, #18) within CNS parenchyma and in five subjects (#3, #7, #9, #10, #17) with immunoreactive neurons within the anatomically defined boundaries of the solitary tract nucleus, dorsal motor nucleus of the vagus, nucleus ambiguous and substantia nigra (Figure 7A-D). As seen in double immunofluorescence labeling, SARS-CoV-2 Nucleocapsid protein antibody can be detected in β-III Tubulin (a pan-neuronal marker) immunoreactive structures, such as neuronal somata and neurites in the medulla and midbrain (Figure 7E-H), with no labeling in controls (Figure 7I). At the level of the midbrain, Nucleocapsid protein immunofluorescence was also found within tyrosine hydroxylase immunoreactive neurons and neurites of the substantia nigra, indicating the presence of viral antigens within dopaminergic neurons (Figure 8A-E). Some of these subjects (#7, #9, #11, #17, #18) also displayed endothelial cell immunoreactivity in small vessels of the cerebral cortex (subject #11), deep cerebellar nuclei (#17-18) hippocampus (#7) (Supplementary Figure 2) and midbrain (#9) (Figure 7H); small vessel thromboses, perivascular extravasation and hemorrhagic injury were found within affected regions of these cases.

In case #7, ischaemic injury of the right rostral hippocampal formation due to posterior cerebral artery (PCA) occlusion was associated with perivascular extravasation, edema, fibrinogen leakage and viral protein immunoreactivity within small vessel endothelium, further confirmed by RT-PCR. Acute hemorrhagic injury in the territory of the right middle cerebral artery (MCA) in #11 (Figure 1B) was associated with endothelitis within perilesional tissue, displaying both viral protein immunoreactive endothelium and positive RT-PCR. Similarly, the deep cerebellar white matter and dentate nuclei in cases #17-18 presented small vessel thromboses and extensive hemorrhagic injury (case #17). Conversely, in some cases with small vessel thromboses within the pons and frontal cortex (e.g. #19-20), viral proteins and RNA was not detectable. There was no correlation between viral protein immunoreactivity / RT-PCR Cycle threshold and hospitalization time (Figure 4E), suggesting no apparent link between the detection of viral antigens and genomic sequences and post-infection interval. However, the actual length of infection, particularly prior to hospitalization, could not always be safely determined, as pre-symptomatic infection could not be excluded,

nor evaluated, from the available clinical data. ACE2 receptor protein and TMPRSS2 protein immunoreactivity was compatible with the anatomical distribution of SARS-CoV-2 antigens (Supplementary Figure 1, E-F), as detected with immunoperoxidase staining, but was not consistently replicated in immunofluorescent staining (data not shown). Both proteins were moderately expressed in vascular endothelial cells and brainstem neurons.

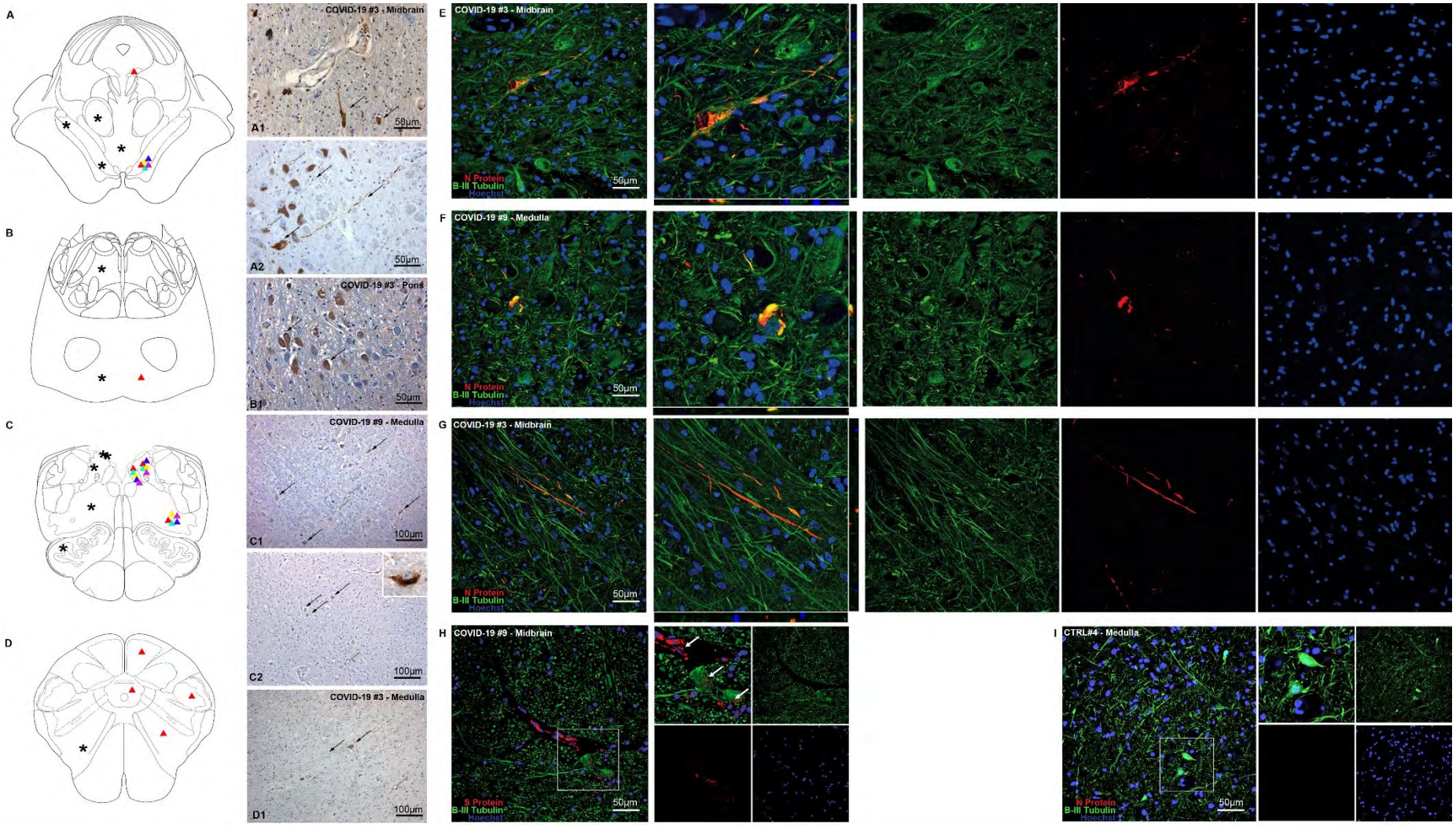

L) COVID-19 MEDULLA

	1	2	3	4	5	6	7	8	9	10	11	12	13	14	15	16	17	18	19	20	21	22	23	24
IHC - N	-	-		-	-	-	-	-			-	-	-	-	NA	-		-	-	-	-	-	-	-
IHC - S	-	-		-	-	-		-		-	-	-	-	-	NA	-		-	-	-	-	-	-	-
RT-PCR N Gene	-	-	32.30	-	-	-	35.49	-	37.40	-	-	-	-	-	NA	-	38.40	-	NA	NA	-	-	-	-
RNAseP	33.71	32.16	27.85	34.36	27.95	29.33	31.87	30.34	29.27	34.71	32.77	31.31	31.79	32.78	NA	30.73	26.95	27.39	NA	NA	30.71	32.78	31.12	29.34

M) COVID-19 MIDBRAIN

	1	2	3	4	5	6	7	8	9	10	11	12	13	14	15	16	17	18	19	20	21	22	23	24
IHC - N	-	-		-	-	-		-			-	-	-	-	NA	-		-	-	-	-	-	-	-
IHC - S	-	-		-	-	-		-		-	-	-	-	-	NA	-	-	-	-	-	-	-	-	-
RT-PCR N Gene	-	-	34.61	-	-	-	39.96	-	38.14	-	-	-	-	-	NA	-	-	-	NA	NA	-	-	-	-
RNAseP	33.41	29.26	29.43	31.33	26.81	29.42	31.42	31.36	28.81	36.07	31.44	34.27	29.74	32.62	NA	NA	27.75	27.21	NA	NA	32.53	31.67	30.69	29.15

Figure 7. SARS-CoV-2 viral antigens, S and N protein, were detected in the dorsal medulla and in the substantia nigra in 5 COVID-19 subjects. *Topographical localization of SARS-CoV-2 Viral Protein Immunoreactivities (Triangles, Right Half) and Microglial Nodules (Asterisks, Left Half) throughout the brainstem.* ***A)*** *At the level of the Mesencephalon, Immunoreactivities are found mainly within the boundaries of the substantia nigra, with the exception of Subject #3, which also presented immunoreactive neurons within the Interstitial Nucleus of Cajal; Microglial nodules were confined mainly within the boundaries of the tegmentum, and were not detected neither within the pes nor the tectum.* ***A1)*** *SARS-CoV-2 Spike Protein IHC at the level of the Substantia Nigra reveals immunoreactive neurons (mean of 2 immunoreactivities per mm^2) with well-marked processes (black arrows); negative neurons can also be found nearby (white arrows).* ***A2)*** *SARS-CoV-2 Nucleocapsid Protein IHC reveals a similar pattern of immunoreactive neurons and axons throughout the substantia nigra.* ***B)*** *At the level of the pons, Subject #3 presented immunoreactive neurons (mean of 5 immunoreactivities per mm^2) within the basilary nuclei, while microglial nodules were found both within the basis, as well as the dorsal pons in proximity to the facial nucleus.* ***B1)*** *SARS-CoV-2 Spike Protein IHC at the level of the pons in Subject #3, displaying immunoreactive neurons (black arrows) within the basilary nuclei of the pons; non-reactive cells can also be appreciated (white arrows)* ***C)*** *At the level of the upper medulla oblongata, immunoreactivities were found at the level of the dorsal motor nucleus of the vagus, solitary tract nucleus and nucleus ambiguus; microglial nodules were prominent within the Vagal Trigone and Area Postrema, but were also found within the reticular formation and the inferior olivary complex.* ***C1-2)*** *SARS-CoV-2 Spike Protein IHC at the level of the solitary tract nucleus and nucleus ambiguus; immunoreactive neurons can be seen within the anatomical boundaries of these nuclei (black arrows), along with non-reactive cells (white arrows). Inset of a single reactive neuron within the solitary tract nucleus, Spike Protein immunohistochemistry.* ***D)*** *At the level of the Lower Medulla Oblongata, Immunoreactivities were found at the level of the spinal trigeminal nucleus and medullary reticular formation. Microglial nodules were found within the medullary reticular formation.* ***D1)*** *SARS-CoV-2 Spike Protein IHC at the level of the medullary reticular formation in the lower medulla (black arrows); non-reactive cells are indicated with a white arrow.* ***E-I)*** *Double label N and S Protein (red) and Beta-III Tubulin (green) fluorescent immunohistochemistry in COVID-19 subjects (E-H) and controls (I). Distinct immunoreactive neurons and neurites can be appreciated in both the medulla (dorsal motor nucleus of the vagus) and midbrain (substantia nigra) (E-G). Juxtavascular immunoreactive neurons in proximity to an immunoreactive vessel in the midbrain of COVID-19 subject #9 (H, inset). Control subjects present no viral protein immunoreactivity (I).* ***L-M)*** *N and S protein IHC, real time RT-PCR Cycle Thresholds for SARS-CoV-2 N Gene and RNAseP quality control in our COVID-19 cohort at the level of the medulla (L) and midbrain (M).*

RT-PCR analyses of FFPE tissue sections detected viral RNA in COVID-19 cases with viral protein immunoreactivity. Molecular testing by real-time RT-PCR detected SARS-CoV-2 RNA in 10 out of 24 COVID-19 subjects, 9 of whom had also SARS-CoV-2 S and/or N protein-positive IHC / IF (Figure 7L-M, Supplementary Table 2). In positive tissue samples, threshold cycles (Ct) of real-time RT-PCR for SARS-CoV-2 RNA ranged between 33 and 38, while in all samples the Ct values of the internal control RNAseP ranged between 27 and 34. The cycle threshold values for each analyzed section are reported in Supplementary table 2 and in Figure 7L-M for the medulla and midbrain. SARS-CoV-2 subgenomic RNA was investigated but not detected in our specimens, likely due to RNA degradation within FFPE sections, as indicated by the low Ct values of RNAse P.

Viral antigens are associated to higher microglial densities within affected anatomical loci, but no differences are found in overall microgliosis, suggesting a specific topographical response. While overall levels of microgliosis within the medulla, pons and midbrain did not differ significantly between COVID-19 subjects with and without detectable viral antigens, Welch one-way ANOVA between anatomical compartments (i.e. tegmentum, tectum and pes) revealed statistically significant differences within the COVID-19 cohort. Indeed, subjects with detectable viral genomic sequences and antigens (RT-PCR+/IHC+) were characterized by higher microglial densities in the medullary ($p=0.017$) and midbrain tegmentum ($p=0.0074$) when compared to negative (RT-PCR-/IHC-) COVID-19 subjects, as seen in Figure 4B and 6B. In association with frequent instances of microglial nodules and perineuronal TMEM119+/CD68+ microglial cells suggestive of neuronophagia (Figure 3A-B), this finding suggests a peculiar microglial response towards anatomical loci of the brainstem in which SARS-CoV-2 antigens were detected, even though overall levels of microgliosis within brainstem regions did not appear to differ significantly. Taken together with little-to-no Ki-67 immunoreactivity and no detectable Ki-67+ / CD68+ immunofluorescent signal, migration of microglial cells towards the site of injury appears to be the more likely mechanism occurring in COVID-19 inflammation, rather than microglial proliferation within affected regions.

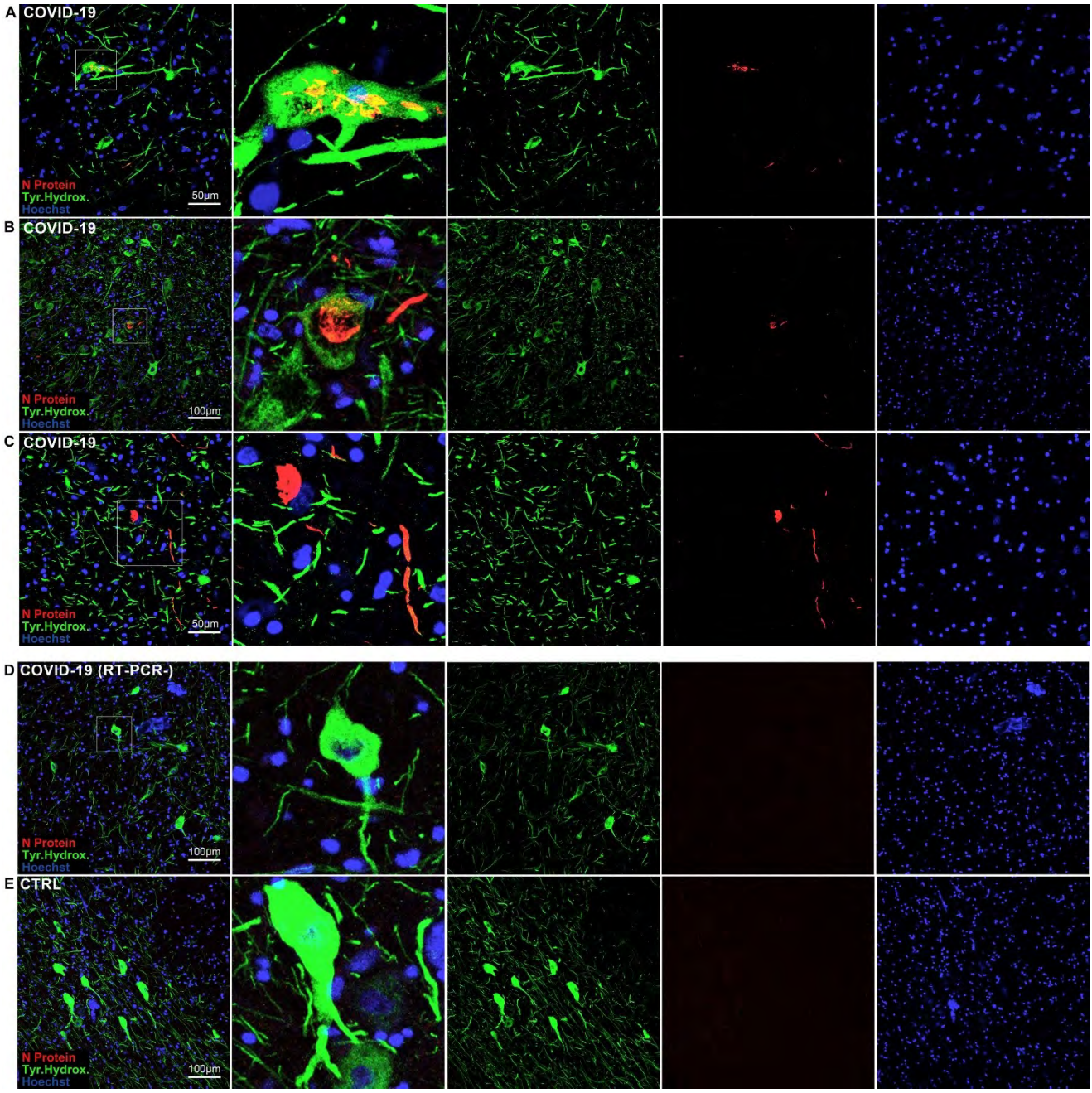

Figure 8. SARS-CoV-2 antigens were detected in both dopaminergic and non-dopaminergic neurons of the substantia nigra. *Double label N Protein (red) and Tyrosine Hydroxylase (green) fluorescent immunohistochemistry at the level of the substantia nigra in the midbrain.* ***A-C)*** *in COVID-19, Both TH+ and TH- neurons display N protein immunoreactivity.* ***D-E)*** *in COVID-19 subjects with negative RT-PCR/IHC (D) as well as non-COVID controls (E) no N protein staining was detected.*

DISCUSSION

In the present study, the neuropathological findings of 24 COVID-19 patients were examined and compared with age- and sex-matched controls who died due to pneumonia and / or respiratory insufficiency. Our findings indicate specific neuropathological alterations in the brains of COVID-19 patients, with particular regard to topographically-defined microgliosis within anatomical loci of the brainstem and viral immunoreactivity in specific CNS compartments, either within the boundaries of brainstem nuclei or in the context of ischaemic and hemorrhagic injuries. Platelet and fibrin microthrombi, in particular, were characteristic findings of the COVID-19 cohort, and often affected multiple organs, such as the lungs, liver, intestine, hypopharynx and even the carotid body[27-29], as summarized in Table 1. Microthromboses were more frequent within the pons, deep cerebellar nuclei and cerebral cortex. In some cases, hemorrhagic injury and microthromboses were found in regions with viral protein immunoreactivity in vascular endothelial cells.

SARS-CoV-2 viral antigens, on the other hand, were confined to specific loci of the CNS. As seen in Figure 7A-H, SARS-CoV-2 viral antigens appear to be localized preferentially within neurons of the vagal nuclei of the medulla and the substantia nigra, with the exception of one subject who also presented immunoreactive cells throughout the whole brainstem (#3). While Matschke et al.[15] reported SARS-CoV-2 invasion of cranial nerves IX-X, we were unable to replicate these findings within our cohort; furthermore, unlike Meinhardt et al.'s findings[16], viral proteins and RNA were not detectable in any of the sampled olfactory bulbs, tracts and bifurcations, even though moderate edema, moderate-to-severe astrogliosis and moderate microglial activation was encountered in most cases in our study. ACE2 Receptor and TMPRSS-2 protein immunohistochemistry support this topographical localization, with neurons within the dorsal motor nucleus of the vagus, solitary tract nucleus, nucleus Ambiguus and Substantia Nigra being moderately immunoreactive (Supplementary Figure 1, E-F).

While previous studies identified viral protein immunoreactivity in sparse cells throughout the brainstem[15,17] without specific topography, our findings appear to be in line with available animal studies on other coronaviruses, i.e. SARS-CoV and MERS-CoV, which are known to be able to infect the brainstem, and particularly the dorsal motor nucleus of the vagus, solitary tract nucleus and nucleus ambiguus, so that an analog pattern of neuroinvasion for SARS-CoV-2 has been suggested[14,30-32]. The peculiar and unexpected finding in our cohort was the detection of viral antigens and genomic sequences within the substantia nigra, not

matching any known models of coronavirus neurotropism. Interestingly, SARS-CoV-2 S and N protein were detected in both tyrosine hydroxylase positive and negative neurons (Figure 8). Immunoreactive neurons of the substantia nigra were frequently found in proximity to blood vessels, which were at times immunoreactive to viral proteins as well (Figure 7H, Supplementary Figure 2). Hence, aside from the reported olfactory-transmucosal transmission [16], and vagus/glossopharyngeal-mediated invasion [15], SARS-CoV-2 may gain access to other districts of the CNS either through a yet-unknown neuronal route or, as suggested by our findings in the midbrain by crossing the blood-brain-barrier and infecting structures of the peri- and juxtavascular compartment [17]. These data would support the hypothesis that SARS-CoV-2 infection may predispose, or quickly precipitate, the development of neurodegenerative diseases, especially Parkinson's Disease[33-35].This hypothesis arises both from the 1917 Spanish flu and von Economo's encephalitis lethargica pandemics, which have seen a surge of post-encephalitic parkinsonism following the waves of the pandemic, and the known association between viral infection and the development of transient or permanent movement disorders[36]. In fact, pathogens, and in particular respiratory viruses, have been suggested as a potential etiopathogenic factors for PD, leading to parkinsonism in subjects over the age of 50, regardless of genetic substrate[33,37]. Both the olfactory bulb and tract, as well as the medulla oblongata where the vagal nuclei are located, represent the very first sites of early PD neuropathology, and interestingly also represent the main sites of inflammation / infection encountered in COVID-19[38,39], as seen in our study. Furthermore, viral-related inflammation might render the CNS susceptible to preceding or subsequent stressors[40], even in the absence of direct viral invasion; indeed, past history of infection was associated with a 20% higher risk of presenting PD in the future[41]. We believe these findings encourage further research on the possibility that COVID-19 neuroinflammation may be the trigger of a neurodegenerative process, such as Parkinson disease, in susceptible individuals. Future studies on COVID-19 survivors and Long COVID patients are therefore warranted[40].

However, despite the detection of viral proteins and genomic sequences in restricted regions of the brainstem, we found no evident neuropathological alterations in SARS-CoV-2 infected cells, such as necrotic changes and other cytological alterations, that could hint towards possible direct consequences of viral invasion in human neurons. COVID-19 is characterized by different evolutionary phases and heterogeneous individual responses, and the short interval between infection and death in our cohort (mean hospitalization time = 14 days), as well as the fact that included patients died during the acute phase of the

disease, may not be sufficient to determine detectable neuropathological alterations in affected cells as a direct consequence of viral invasion, which may require more time to develop[3,32]. Lastly, the detection of viral proteins in a subset of patients (5 out of 24), as seen in this and previous studies may be related to the particularly severe disease, and concurring comorbidities, of the patients subject to neuropathological examination.

Hence, while the consequences of SARS-CoV-2 neurotropism in the medulla have been widely discussed in literature and are supported by the detection of viral proteins and genomic sequences in our study, the absence of direct neuronal damage and the impossibility of performing functional assays on post-mortem samples should be taken into consideration when discussing the clinical implications of COVID-19 neuropathology. Future studies on "long COVID" patients[3] may be able to shed a light on the long-term consequences of COVID-19, particularly concerning the detection of SARS-CoV-2 within the CNS after the acute phase of the disease, and whether or not this leads to specific neuropathological alterations as a consequence of viral invasion.

Concerning microglial activation and density, our findings appear to be in line with Schwabenland et al.[17], who identified microglial nodules and parenchymal reactive microglia as hallmark for COVID-19, in contrast to both controls and Extra Corporeal Membrane Oxygenation (ECMO) patients. In our cohort, patients with pneumonia and / or respiratory failure served as control group and, although also characterized by microglial activation, displayed lower microglial counts in the medulla and midbrain, but not in the pons, when compared to COVID-19 subjects. We also found no significant effect of oxygen therapy on microglial density within the COVID-19 group. Conversely, Deigendesh et al.[42] found significant differences in HLA-DR+ activated microglia when comparing COVID-19 subjects to non-septic controls, but no differences were found with patients who had died under septic conditions; according to the authors[42] this may represent a histopathological correlate of critical illness-related encephalopathy, rather than a COVID-19-specific finding. Aside from the distinct populations serving as control subjects, significant methodological differences between these studies must be taken into consideration. Our approach to microglial quantification was more similar to Schwabenland et al.[17], as digitally-assisted manual counting of TMEM119+ cells, a homeostatic microglia-specific marker, was performed to estimate microgliosis. Conversely Deigendesh et al.[42] quantified HLA-DR immunoreactive area, a marker expressed on both microglia and on infiltrating lympho-monocytic cells, as a

fraction of the counting field (A%), and not as individual particles, explaining differences between our studies.

Interestingly, while no evidence of direct neuronal damage was found in SARS-CoV-2 infected cells, microglial densities within affected anatomical loci differed between subjects with and without detectable viral antigens and genomic sequences (RT-PCR/IHC+ versus RT-PCR/IHC- in Figure 4B and 6B), suggesting a link between the detection of SARS-CoV-2 antigens and microglial response. Conversely, overall microglial density (i.e. without topographical delineation) did not differ between the two groups, and a strong correlation between microgliosis and hypoxic / ischaemic damage at the level of the brainstem was found. Hence, while we found a suggestive link between microgliosis and the detection of SARS-CoV-2 antigens in our cohort, other factors such as hypoxia / ischaemia and systemic inflammation / cytokine storm ongoing during COVID-19, as previously reported by Thakur et al[18], are likely to play a more prominent role in determining brainstem microgliosis, in accordance to previous studies[42].

CONCLUSIONS

The present study contributes to define the spectrum of neuropathological alterations in COVID-19, as well as the neuroinvasive potential of SARS-CoV-2 within the CNS, with particular regard to its implications for neurodegenerative diseases. Unlike previous findings, we have documented a subset of COVID-19 cases in which viral proteins and genomic sequences were detectable within anatomically defined regions of the CNS. Similarly, microglial activation in the brainstem appears to differ between COVID-19 and pneumonia / respiratory failure controls, with the former also presenting a pattern of increased microglial density in specific compartments of the medulla and midbrain. However, despite this evidence supporting the neuroinvasive potential of SARS-CoV-2, neuropathological alterations encountered in our cohort cannot be ascribed to viral antigens detected in the brainstem. In line with other studies in literature, hypoxic / ischaemic damage and systemic inflammation likely represent major contributors in determining neuropathological alterations in COVID-19, with little-to-no evidence indicating direct viral damage of the central nervous system in humans. Moreover, further investigation is required to determine whether or not SARS-CoV-2 neurotropism represents a major component of COVID-19 in the general population, as subjects included in neuropathological studies often present a much more severe course of the disease and major medical comorbidities.

Nevertheless, the findings of our study suggest the possibility that, although not frequently, SARS-CoV-2 may gain access to specific regions of the central nervous system, especially the vagal nuclei of the medulla and the substantia nigra in the midbrain. As direct neuropathological alterations determined by SARS-CoV-2 neurotropism may not be detectable in subjects deceased during the acute phase of the disease, future studies are required to determine whether or not SARS-CoV-2 neurotropism is present in chronic COVID-19 patients, or in COVID-19 survivors suffering from the long-term effects of infection, and if eventual neuropathological alterations in these subjects can be ascribed to viral tropism, rather than immune-mediated mechanisms. The possibility that COVID-19 neuroinflammation may trigger or exacerbate pre-existing neurodegenerative conditions especially Parkinson's disease must therefore be taken into serious consideration.

LIMITATIONS OF THE STUDY

This study is based on post-mortem tissue samples obtained during the first wave of the COVID-19 pandemic in Italy. While the neuropathological alterations encountered in our work contribute to define the pathological mechanisms of COVID-19 and SARS-CoV-2 infection in the CNS, the lack of exhaustive post-infection neurological evaluation of included patients does not allow for unequivocal clinico-pathological correlations. It must also be considered that most patients included in the study died during the peak of the sanitary emergency in Italy, one of the first countries to face the COVID-19 pandemic in Europe, and neurological evaluation was not always possible. Hence, it remains to be determined whether the neuropathological alterations observed in this study are also linked to neurological symptoms, and whether they are also present in COVID-19 survivors.

Unlike previous studies in literature, we have included 18 controls who died due to pneumonia, respiratory insufficiency or multiorgan failure, rather than healthy controls. Retrospective selection of control subjects, however, could lead to unwanted selection bias. Furthermore, from the available clinical data of our controls, we have found no instances of intensive oxygen therapy or mechanical ventilation, but incompleteness of available clinical records cannot entirely be excluded. For this purpose, we have also performed comparisons within the COVID-19 group, identifying no statistically significant differences between subjects with and without neurodegenerative conditions, and no influence of oxygen therapy on brainstem microgliosis. The involvement of other brain regions, such the cerebral and

cerebellar cortex and the basal ganglia, cannot be excluded but is beyond the scopes of this study. Moreover, as all patients died during the first wave of the COVID-19 pandemic, our findings may not reflect the possible neuropathological alterations encountered in patients affected by SARS-CoV-2 variants.

Limitations to viral antigen / RNA detection in our study must also be considered. Real-time RT-PCR cannot exclude detection of viral RNA in blood vessels within samples. While particular care was taken to avoid contamination by employing sterile instruments and disposable microtome blades when sampling FFPE sections for RT-PCR analyses, the main strength of our study was the complementary use of immunoperoxidase and immunofluorescent staining with different antibodies to detect viral antigen as an indicator of viral tropism. This is further strengthened by the strong concordance between these assays in our cohort, quantified by a statistically significant positive correlation between RT-PCR cycle threshold and IHC positivity ($r=0.87$, $p<0.0001$).

In conclusion, further investigation is required to determine the direct effects of viral invasion within the CNS, with particular regard to cases of long-lasting infection and in COVID-19 survivors.

DATA AVAILABILITY

All data and source measurements are available by the corresponding author upon reasonable request.

ACKNOWLEDGEMENTS

We are grateful to Prof. James E. Goldman for his feedback and suggestions concerning our study.

AUTHOR CONTRIBUTIONS

CB, SR, MDG, PC, AP, RDC performed the autopsies. AE, MS and MDB performed the immunohistochemical and histopathological stainings. AE and MS performed the immunofluorescent stainings and confocal imaging. AE, AP, RDC evaluated the histopathological findings and performed the morphometrical analyses. LB, EC, AS, SR performed the RT-PCR analyses. AE and RBB performed the statistical analyses. AE

designed the figures and tables and drafted the manuscript. All authors reviewed and approved the final version of the manuscript.

FUNDING

European Union's Horizon 2020 research and innovation programme [VEO, grant number 874735]
CARIPARO Foundation- NeuroCOVID project
CB is supported by the Registry for cardio-cerebro-vascular pathology, Veneto Region, Italy.

COMPETING INTERESTS

The authors declare no competing interests.

SUPPLEMENTARY MATERIAL

SUPPLEMENTARY TABLE 1. Anatomical boundaries and main structures contained in each examined Field of View, divided per level of sectioning.

LEVEL OF SECTIONING	**FOV1**	**FOV2**	**FOV3**	**FOV4**	**FOV5**	**FOV6**
MEDULLA	Tegmentum: Dorsal Motor Nucleus of the Vagus, Solitary Tract Nucleus, Area Postrema	Tegmentum: Hypoglossal Nucleus, Intercalate Nucleus, Medial Longitudinal Lemniscus, Dorsal Medullary Reticular Formation	Tegmentum: Nucleus Ambiguus, Ventral Medullary Reticular Formation.	Basis: Medial Lemniscus, Medial Accessory Olivary Nucleus, Inferior Olivary Complex (Medial Part)	Basis: Inferior Olivary Complex (Lateral Part).	Basis: Pyramidal Tract.
PONS	Tegmentum: Dorsal Tegmentum, Locus Coeruleus, Medial Longitudinal Fasciculus.	Tegmentum: Ventrolateral Tegmentum, Spinal Trigeminal Tract.	Tegmentum: Ventromedial Tegmentum, Medial lemniscus, Central Tegmental Tract.	Basis: Dorsomedial basis pontis, basilary nuclei of the pons, cortico-spinal tract.	Basis: Lateral basis pontis, basilary nuclei of the pons, cortico-spinal tract.	Basis: Ventromedial basis pontis, basilary nuclei of the pons, cortico-spinal tract.
MIDBRAIN	Tegmentum: Lateral part of the Substantia Nigra, Red Nucleus	Tegmentum: Medial part of the Substantia Nigra.	Tectum: Quadrigeminal Plate, Periacqueductal Gray.	Tegmentum / Tectum interface, Mesencephalic reticular formation.	Basis: lateral part of the cerebral peduncle.	Basis: medial part of the cerebral peduncle.

SUPPLEMENTARY TABLE 2. Histopathological and Immunohistochemical findings in the COVID-19 Subjects. N and S indicate the viral antigen detected in the tissue. N, Nucleocapsid Protein; S, Spike Protein; RT-CT, Real Time Cycle.

	Mild
	Moderate
	Severe
	Absent / Negative
	Present / Positive

CASE	SAMPLE / LEVEL	ASTROGLIOSIS (GFAP)	MICROGLIOSIS (TMEM119-CD68-HLA-DR)	THROMBOSES / SMALL VESSEL THROMBOSES (H&E – CD61)	VIRAL PROTEINS (IHC)	VIRAL RNA (RT-PCR)
#1	Medulla Oblongata					
	Pons					
	Midbrain					
	Cerebellar Cortex					
	Basal Ganglia					
	Frontal Cortex					
	Olfactory bulbs and tracts					
	Cranial Nerves (III-XI)					
	Leptomeninges					
	Choroid Plexuses					
#2	Medulla Oblongata					
	Pons					
	Midbrain					

	Cerebellar Cortex					
	Basal Ganglia					
	Frontal Cortex					
	Olfactory bulbs and tracts					
	Cranial Nerves (III-XI)					
	Leptomeninges				S	
	Choroid Plexuses					
#3	Medulla Oblongata				S, N	
	Pons				S, N	
	Midbrain				S, N	
	Cerebellar cortex					
	Basal Ganglia				S	
	Frontal Cortex					
	Olfactory bulbs and tracts					
	Cranial Nerves (III-XI)					
	Leptomeninges				S	
	Choroid Plexuses					
#4	Medulla Oblongata					
	Pons					
	Midbrain					

	Cerebellar Cortex					
	Basal Ganglia					
	Frontal Cortex					
	Olfactory bulbs and tracts					
	Leptomeninges					
	Choroid Plexuses					
#5	Medulla Oblongata					
	Pons					
	Midbrain					
	Cerebellar Cortex					
	Deep cerebellar nuclei					
	Basal Ganglia					
	Hippocampus					
	Frontal Cortex					
	Olfactory bulbs and tracts					
	Leptomeninges					
	Choroid Plexuses					
#6	Medulla Oblongata					
	Pons					
	Midbrain					

	Cerebellar Cortex					
	Deep cerebellar nuclei					
	Basal Ganglia					
	Hippocampus					
	Frontal Cortex					
	Leptomeninges					
	Choroid Plexuses					
#7	Medulla Oblongata				**S**	RT-CT=35,46
	Pons					
	Midbrain				**S**	RT-CT=39,96
	Cerebellar Cortex					
	Deep cerebellar nuclei					
	Basal Ganglia					
	Hippocampus				**S, N**	RT-CT=38,04
	Frontal Cortex					
	Leptomeninges					
	Choroid Plexuses					
#8	Medulla Oblongata					
	Pons					
	Midbrain					

	Cerebellar Cortex					
	Deep cerebellar nuclei					
	Basal Ganglia					
	Hippocampus					
	Frontal Cortex					
	Leptomeninges					
	Choroid Plexuses					
#9	Medulla Oblongata				**S, N**	RT-CT=37,4
	Pons					
	Midbrain				**N**	RT-CT=38,14
	Cerebellar Cortex					
	Deep cerebellar nuclei					
	Basal Ganglia					
	Hippocampus					
	Frontal Cortex					
	Leptomeninges				**S**	RT-CT=37,4
	Choroid Plexuses					
#10	Medulla Oblongata				**N**	ND
	Pons					
					N	ND

	Midbrain					
	Cerebellar Cortex					
	Deep cerebellar nuclei					
	Basal Ganglia					
	Frontal Cortex and subcortex				**S, N**	RT-CT=37,61
	Leptomeninges					
	Choroid Plexuses					
#11	Medulla Oblongata					
	Pons					
	Midbrain					
	Cerebellar Cortex					
	Deep cerebellar nuclei					
	Basal Ganglia					
	Frontal Cortex					
	Parietal Cortex				**S**	RT-CT=38,00
	Leptomeninges					
	Choroid Plexuses					
#12	Medulla Oblongata					
	Pons					

	Midbrain					
	Cerebellar Cortex					
	Deep cerebellar nuclei					
	Basal Ganglia					
	Frontal Cortex					
	Leptomeninges					
	Choroid Plexuses					
#13	Medulla Oblongata					
	Pons					
	Midbrain					
	Cerebellar Cortex					
	Deep cerebellar nuclei					
	Basal Ganglia					
	Frontal Cortex					
	Leptomeninges					
	Choroid Plexuses					
#14	Medulla Oblongata					
	Pons					
	Midbrain					
	Cerebellar Cortex					

	Deep cerebellar nuclei					
	Basal Ganglia					
	Frontal Cortex					
	Leptomeninges					
	Choroid Plexuses					
#15* Poor tissue quality	Medulla Oblongata					
	Pons					
	Midbrain					
	Deep cerebellar nuclei					
	Basal Ganglia					
	Frontal Cortex					
	Leptomeninges					
	Choroid Plexuses					
#16	Medulla Oblongata					
	Pons					
	Midbrain					
	Cerebellar Cortex					
	Deep cerebellar nuclei					
	Basal Ganglia					RT-CT=37,47
	Frontal Cortex					

	Leptomeninges					
	Choroid Plexuses					
#17	Medulla Oblongata				**S**	RT-CT=38,34
	Pons					
	Midbrain				**N**	ND
	Cerebellar Cortex					
	Deep cerebellar nuclei				**S, N**	ND
	Basal Ganglia					
	Frontal Cortex					
	Leptomeninges					
	Choroid Plexuses					
#18	Medulla Oblongata					
	Pons					
	Midbrain					
	Cerebellar Cortex					
	Deep cerebellar nuclei				**S**	RT-CT=37,33
	Basal Ganglia					
	Frontal Cortex					
	Leptomeninges					
	Choroid Plexuses					

#19	Pons					
	Midbrain					
	Cerebellar Cortex					
	Deep cerebellar nuclei					
	Basal Ganglia					
	Occipital Cortex					
	Frontal Cortex					
	Parietal Cortex					
	Temporal Cortex					
#20	Pons					
	Midbrain					
	Cerebellar Cortex					
	Deep cerebellar nuclei					
	Basal Ganglia					
	Occipital Cortex					
	Frontal Cortex					
	Parietal Cortex					
	Temporal Cortex					
#21	Medulla Oblongata					
	Pons					

	Midbrain					
	Cerebellar Cortex					
	Deep cerebellar nuclei					
	Basal Ganglia					
	Hippocampus					
	Frontal Cortex					
	Parietal Cortex					
	Temporal Cortex					
	Leptomeninges					
	Choroid Plexuses					
#22	Medulla Oblongata					
	Pons					
	Midbrain					
	Cerebellar Cortex					
	Deep cerebellar nuclei					
	Basal Ganglia					
	Hippocampus					
	Frontal Cortex					
	Parietal Cortex					
	Temporal Cortex					

	Leptomeninges					
	Choroid Plexuses					
#23	Medulla Oblongata					
	Pons					
	Midbrain					
	Cerebellar Cortex					
	Deep cerebellar nuclei					
	Basal Ganglia					
	Hippocampus					
	Frontal Cortex					
	Parietal Cortex					
	Temporal Cortex					
	Leptomeninges					
	Choroid Plexuses					
#24	Medulla Oblongata					
	Pons					
	Midbrain					
	Cerebellar Cortex					
	Deep cerebellar nuclei					
	Basal Ganglia					

	Hippocampus					
	Frontal Cortex					
	Parietal Cortex					
	Temporal Cortex					
	Leptomeninges					
	Choroid Plexuses					

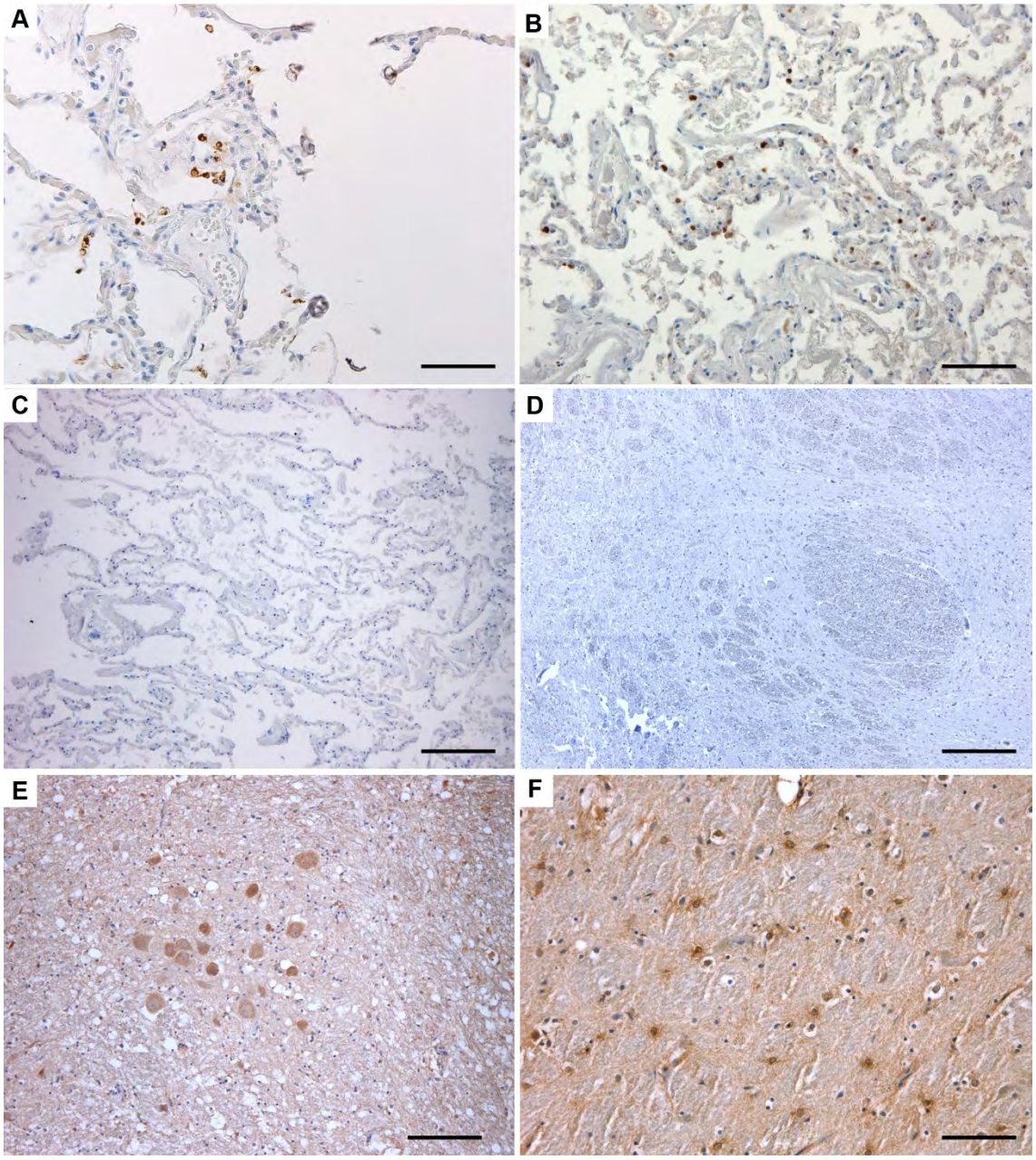

Supplementary Figure 1. A) *SARS-CoV-2 Spike Protein immunohistochemistry on RT-PCR+ lung tissue.* ***B)*** *S SARS-CoV-2 Nucleocapsid Protein immunohistochemistry on RT-PCR+ lung tissue.* ***C)*** *SARS-CoV-2 Spike Protein immunohistochemistry on lung tissue from control subjects, showing no immunoreactive elements.* ***D)*** *SARS-CoV-2 Spike Protein immunohistochemistry on brainstem tissue (solitary tract nucleus) from control subjects, showing no immunoreactive cells.* ***E)*** *ACE-2 Receptor immunohistochemistry at the level of the nucleus ambiguus in the medulla oblongata of a COVID-19 subject, showing diffuse immunoreactivity in the soma and surrounding neuropilum.* ***F)*** *TMPRSS-2 protein immunoreactivity in the mesencephalic tegmentum showing moderate reactivity of non-neuronal cells. Scale Bars: 200μm (C,D); 100μm (A,B,E,F).*

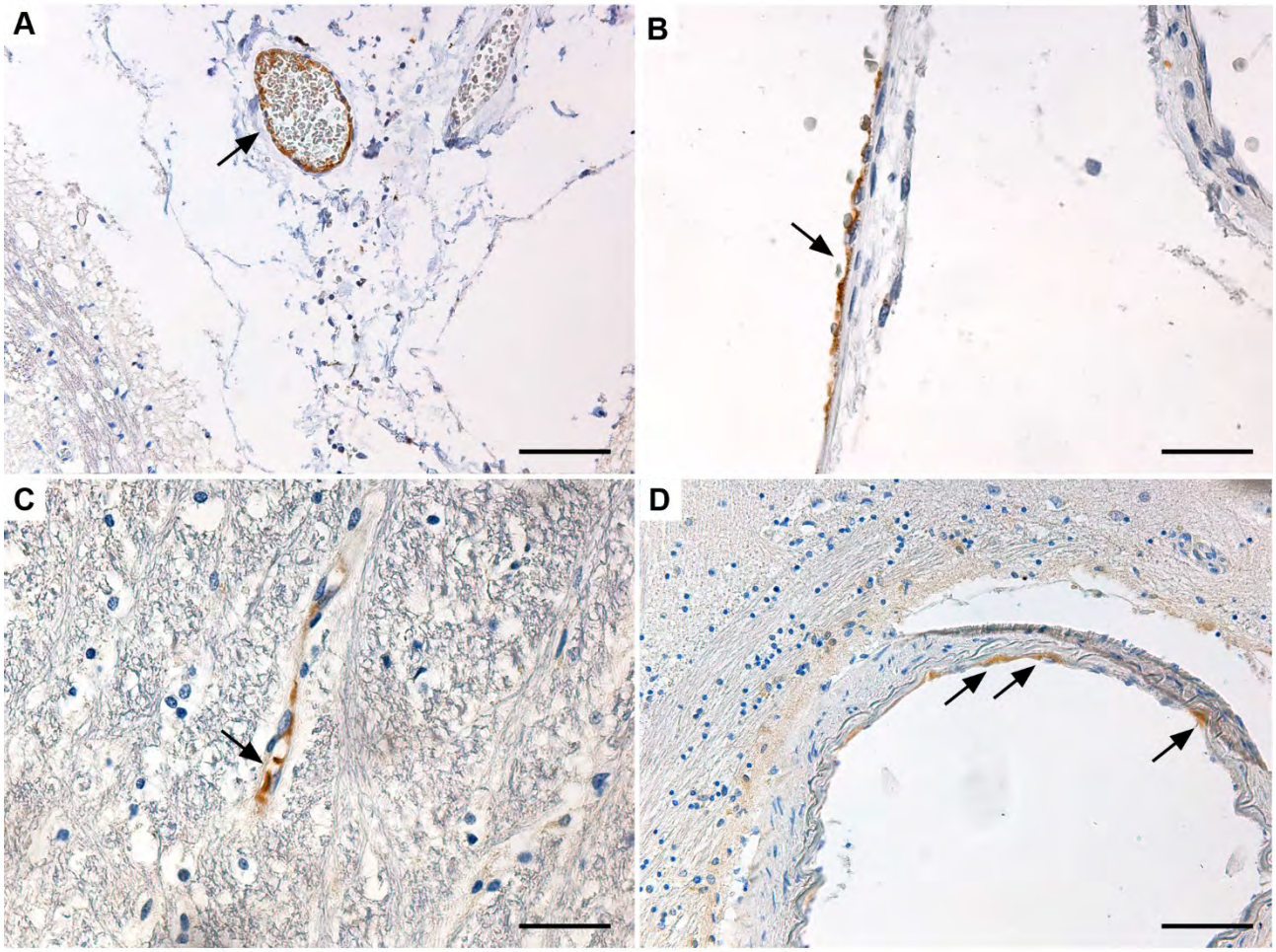

Supplementary Figure 2. A) *SARS-CoV-2 Spike Protein immunohistochemistry revealing endothelial cell reactivity in a leptomeningeal vessel of the medulla oblongata.* ***B)*** *SARS-CoV-2 Nucleocapsid Protein immunohistochemistry in a leptomeningeal vessel in the cerebellum.* ***C-D)*** *SARS-CoV-2 Spike Protein immunohistochemistry revealing endothelial cell immunoreactivity in the CNS parenchyma. Scale Bars: 50µm (A,D); 25µm (B,C).*

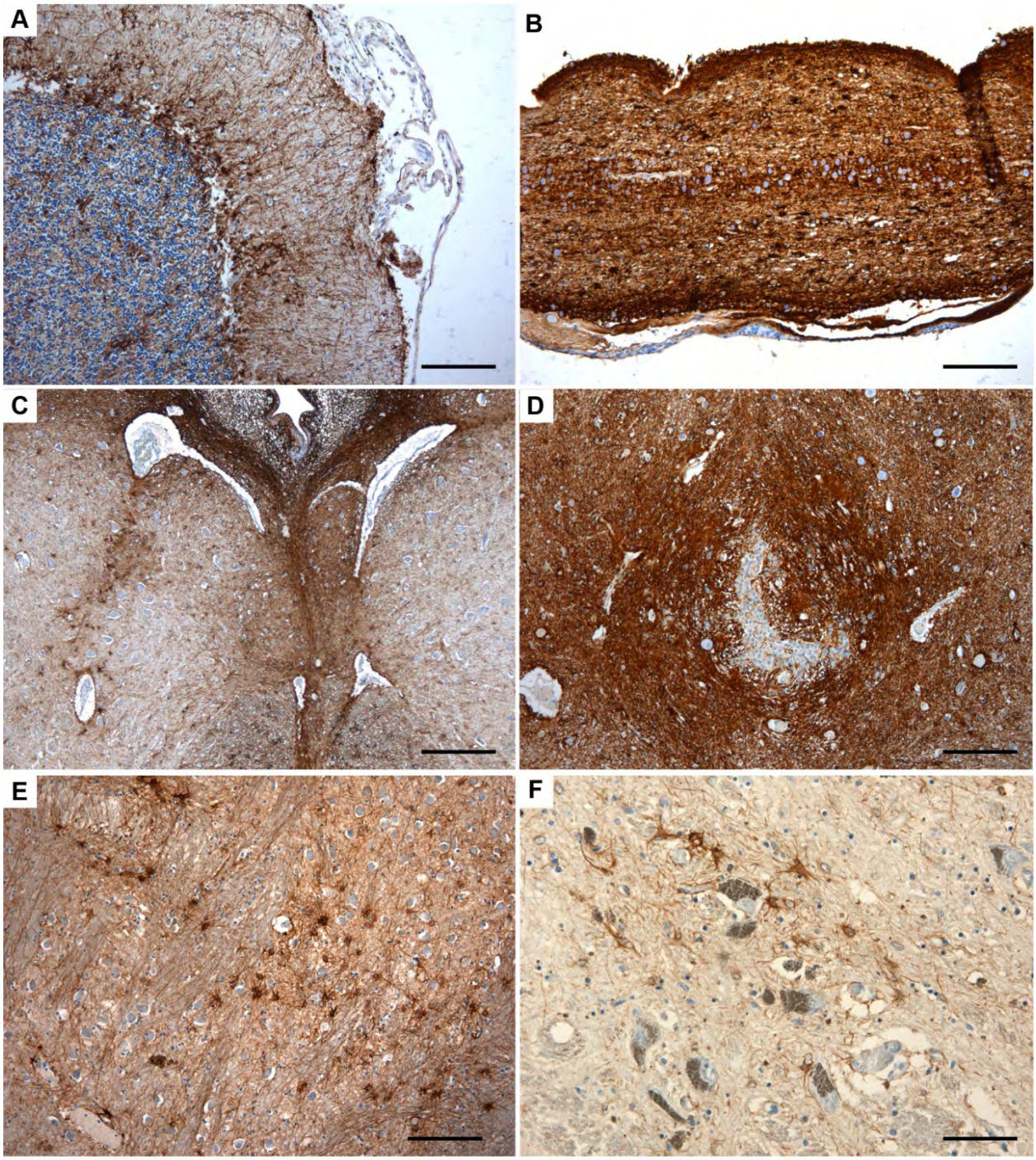

Supplementary Figure 3. *GFAP Immunohistochemistry.* ***A)*** *Reactive Bergmann Glia at the level of the cerebellar cortex in Subject #2.* ***B)*** *Marked astrogliosis with numerous corpora amylacea could be appreciated in this sagittal section of the olfactory tract.* ***C)*** *Reactive astrocytosis was marked within the subependymal regions of the medullary tegmentum, also displaying numerous reactive astrocytes within the hypoglossal nucleus.* ***D)*** *Reactive Astrocytosis surrounding the central canal of the lower medulla.* ***E)*** *Reactive astrocytes within the basilary pons in Subject #3.* ***F)*** *Reactive astrocytes at the level of the substantia nigra in the midbrain. Scale Bars: 200µm (C); 100µm (A,B,D,E); 50µm (F).*

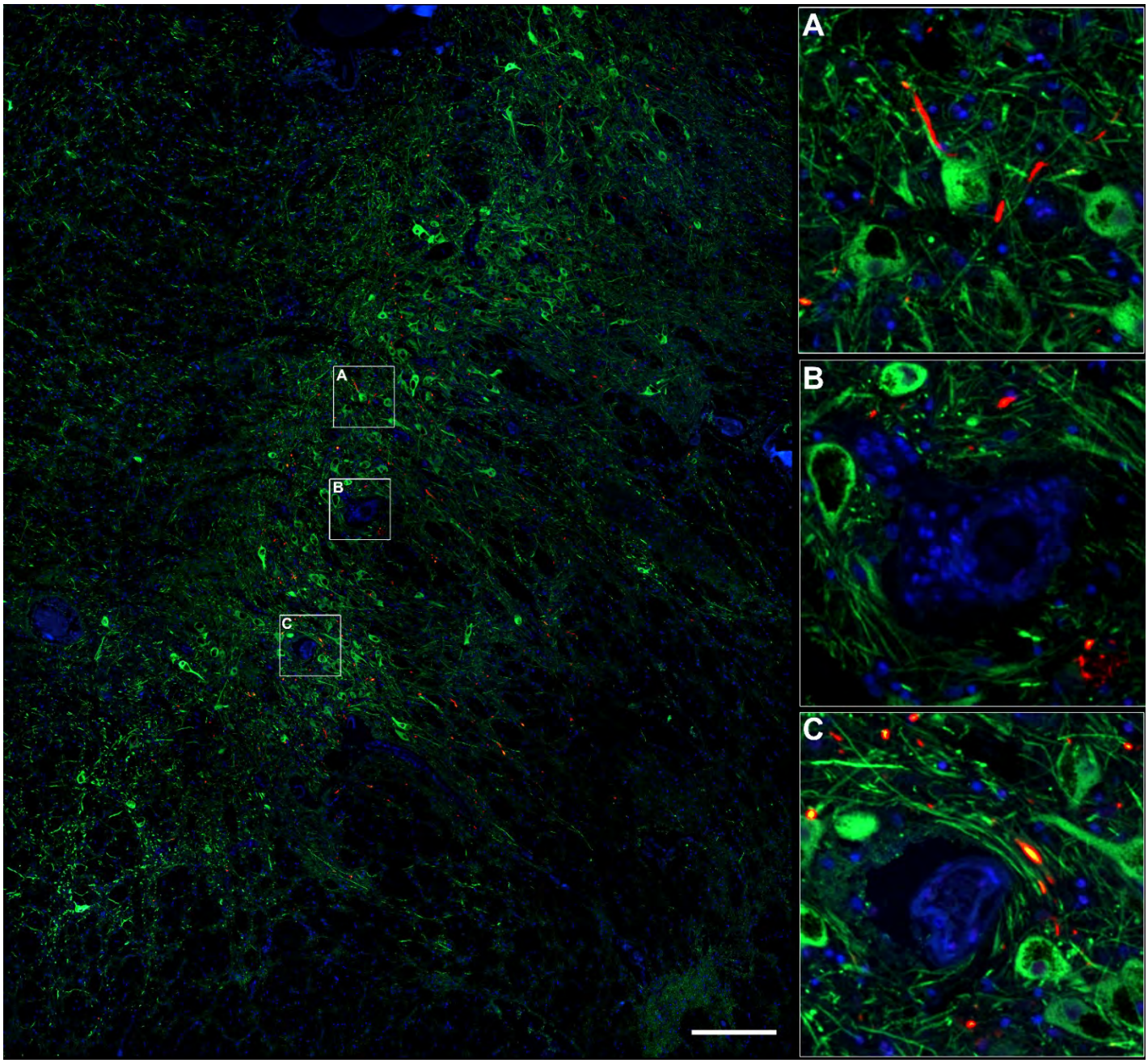

Supplementary Figure 4. *Tyrosine Hydroxylase (green), Nucleocapsid Protein (red) and Hoechst (blue) immunofluorescent staining. Nucleocapsid protein immunoreactivity can be detected within the boundaries of the substantia nigra in the midbrain and may be found within tyrosine hydroxylase positive neurites and neuronal somata.*

REFERENCES

1. Ellul, M. A. et al. Neurological associations of COVID-19. Lancet Neurol 19, 767-783, doi:10.1016/s1474-4422(20)30221-0 (2020).
2. Helms, J. et al. Neurologic Features in Severe SARS-CoV-2 Infection. N Engl J Med 382, 2268-2270, doi:10.1056/NEJMc2008597 (2020).
3. Huang, C. et al. 6-month consequences of COVID-19 in patients discharged from hospital: a cohort study. Lancet 397, 220-232, doi:10.1016/s0140-6736(20)32656-8 (2021).
4. Iadecola, C., Anrather, J. & Kamel, H. Effects of COVID-19 on the Nervous System. Cell 183, 16-27.e11, doi:10.1016/j.cell.2020.08.028 (2020).
5. Mao, L. et al. Neurologic Manifestations of Hospitalized Patients With Coronavirus Disease 2019 in Wuhan, China. JAMA neurology 77, 683-690, doi:10.1001/jamaneurol.2020.1127 (2020).
6. Puelles, V. G. et al. Multiorgan and Renal Tropism of SARS-CoV-2. The New England journal of medicine 383, 590-592, doi:10.1056/NEJMc2011400 (2020).
7. Solomon, I. H. et al. Neuropathological Features of COVID-19. N Engl J Med 383, 989-992, doi:10.1056/NEJMc2019373 (2020).
8. Trevisan, M., Riccetti, S., Sinigaglia, A. & Barzon, L. SARS-CoV-2 Infection and Disease Modelling Using Stem Cell Technology and Organoids. International journal of molecular sciences 22, 2356, doi:10.3390/ijms22052356 (2021).
9. Jacob, F. et al. Human Pluripotent Stem Cell-Derived Neural Cells and Brain Organoids Reveal SARS-CoV-2 Neurotropism Predominates in Choroid Plexus Epithelium. Cell Stem Cell 27, 937-950.e939, doi:10.1016/j.stem.2020.09.016 (2020).
10. 1Bauer, L. et al. Replication Kinetics, Cell Tropism, and Associated Immune Responses in SARS-CoV-2- and H5N1 Virus-Infected Human Induced Pluripotent Stem Cell-Derived Neural Models. mSphere 6, e0027021-e0027021, doi:10.1128/mSphere.00270-21 (2021).
11. Pellegrini, L. et al. SARS-CoV-2 Infects the Brain Choroid Plexus and Disrupts the Blood-CSF Barrier in Human Brain Organoids. Cell Stem Cell 27, 951-961.e955, doi:10.1016/j.stem.2020.10.001 (2020).
12. Song, E. et al. Neuroinvasion of SARS-CoV-2 in human and mouse brain. bioRxiv : the preprint server for biology, 2020.2006.2025.169946, doi:10.1101/2020.06.25.169946 (2020).
13. Zheng, J. et al. COVID-19 treatments and pathogenesis including anosmia in K18-hACE2 mice. Nature 589, 603-607, doi:10.1038/s41586-020-2943-z (2021).
14. Desforges, M., Le Coupanec, A., Stodola, J. K., Meessen-Pinard, M. & Talbot, P. J. Human coronaviruses: viral and cellular factors involved in neuroinvasiveness and neuropathogenesis. Virus Res 194, 145-158, doi:10.1016/j.virusres.2014.09.011 (2014).
15. Matschke, J. et al. Neuropathology of patients with COVID-19 in Germany: a post-mortem case series. The Lancet Neurology 19, 919-929, doi:10.1016/S1474-4422(20)30308-2 (2020).
16. Meinhardt, J. et al. (Cold Spring Harbor Laboratory, 2020).
17. Schwabenland, M. et al. Deep spatial profiling of human COVID-19 brains reveals neuroinflammation with distinct microanatomical microglia-T-cell interactions. Immunity 54, 1594-1610.e1511, doi:https://doi.org/10.1016/j.immuni.2021.06.002 (2021).
18. Thakur, K. T. et al. COVID-19 neuropathology at Columbia University Irving Medical Center/New York Presbyterian Hospital. Brain : a journal of neurology 144, 2696-2708, doi:10.1093/brain/awab148 (2021).

19. Fullard, J. F. et al. Single-nucleus transcriptome analysis of human brain immune response in patients with severe COVID-19. Genome Medicine 13, 118, doi:10.1186/s13073-021-00933-8 (2021).
20. Schurink, B. et al. Viral presence and immunopathology in patients with lethal COVID-19: a prospective autopsy cohort study. Lancet Microbe 1, e290-e299, doi:10.1016/S2666-5247(20)30144-0 (2020).
21. Yang, A. C. et al. Dysregulation of brain and choroid plexus cell types in severe COVID-19. Nature 595, 565-571, doi:10.1038/s41586-021-03710-0 (2021).
22. Barton, L. M., Duval, E. J., Stroberg, E., Ghosh, S. & Mukhopadhyay, S. COVID-19 Autopsies, Oklahoma, USA. Am J Clin Pathol 153, 725-733, doi:10.1093/ajcp/aqaa062 (2020).
23. Reichard, R. R. et al. Neuropathology of COVID-19: a spectrum of vascular and acute disseminated encephalomyelitis (ADEM)-like pathology. Acta neuropathologica 140, 1-6, doi:10.1007/s00401-020-02166-2 (2020).
24. Schaller, T. et al. Postmortem Examination of Patients With COVID-19. JAMA 323, 2518-2520, doi:10.1001/jama.2020.8907 (2020).
25. Mai, J. K. & Paxinos, G. in The Human Nervous System xi (Elsevier, 2012).
26. Schwabenland, M. et al. Analyzing microglial phenotypes across neuropathologies: a practical guide. Acta neuropathologica 142, 923-936, doi:10.1007/s00401-021-02370-8 (2021).
27. Porzionato, A. et al. Case Report: The Carotid Body in COVID-19: Histopathological and Virological Analyses of an Autopsy Case Series. Front Immunol 12, 736529, doi:10.3389/fimmu.2021.736529 (2021).
28. Basso, C. et al. Pathological features of COVID-19-associated myocardial injury: a multicentre cardiovascular pathology study. Eur Heart J 41, 3827-3835, doi:10.1093/eurheartj/ehaa664 (2020).
29. Porzionato, A. et al. Hypopharyngeal Ulcers in COVID-19: Histopathological and Virological Analyses - A Case Report. Frontiers in immunology 12, 676828-676828, doi:10.3389/fimmu.2021.676828 (2021).
30. Li, Y.-C., Bai, W.-Z. & Hashikawa, T. The neuroinvasive potential of SARS-CoV2 may play a role in the respiratory failure of COVID-19 patients. J Med Virol 92, 552-555, doi:10.1002/jmv.25728 (2020).
31. Porzionato, A. et al. Sympathetic activation: a potential link between comorbidities and COVID-19. FEBS J 287, 3681-3688, doi:10.1111/febs.15481 (2020).
32. Porzionato, A. et al. The potential role of the carotid body in COVID-19. Am J Physiol Lung Cell Mol Physiol 319, L620-L626, doi:10.1152/ajplung.00309.2020 (2020).
33. Beauchamp, L. C., Finkelstein, D. I., Bush, A. I., Evans, A. H. & Barnham, K. J. Parkinsonism as a Third Wave of the COVID-19 Pandemic? J Parkinsons Dis 10, 1343-1353, doi:10.3233/jpd-202211 (2020).
34. Bouali-Benazzouz, R. & Benazzouz, A. COVID-19 Infection and Parkinsonism: Is There a Link? Movement Disorders 36, 1737-1743, doi:https://doi.org/10.1002/mds.28680 (2021).
35. Brundin, P., Nath, A. & Beckham, J. D. Is COVID-19 a Perfect Storm for Parkinson's Disease? Trends Neurosci 43, 931-933, doi:10.1016/j.tins.2020.10.009 (2020).
36. Jang, H., Boltz, D. A., Webster, R. G. & Smeyne, R. J. Viral parkinsonism. Biochim Biophys Acta 1792, 714-721, doi:10.1016/j.bbadis.2008.08.001 (2009).
37. Tanner, C. M. et al. Parkinson disease in twins: an etiologic study. JAMA 281, 341-346, doi:10.1001/jama.281.4.341 (1999).

38. Hawkes, C. H., Del Tredici, K. & Braak, H. Parkinson's disease: a dual-hit hypothesis. Neuropathol Appl Neurobiol 33, 599-614, doi:10.1111/j.1365-2990.2007.00874.x (2007).
39. Klingelhoefer, L. & Reichmann, H. Pathogenesis of Parkinson disease—the gut–brain axis and environmental factors. Nature Reviews Neurology 11, 625-636, doi:10.1038/nrneurol.2015.197 (2015).
40. ulzer, D. et al. COVID-19 and possible links with Parkinson's disease and parkinsonism: from bench to bedside. NPJ Parkinson's disease 6, 18-18, doi:10.1038/s41531-020-00123-0 (2020).
41. Meng, L., Shen, L. & Ji, H. F. Impact of infection on risk of Parkinson's disease: a quantitative assessment of case-control and cohort studies. J Neurovirol 25, 221-228, doi:10.1007/s13365-018-0707-4 (2019).
42. Deigendesch, N. et al. Correlates of critical illness-related encephalopathy predominate postmortem COVID-19 neuropathology. Acta neuropathologica 140, 583-586, doi:10.1007/s00401-020-02213-y (2020).

Chapter 6

The potential role of the carotid body in COVID-19

*The present chapter has been previously published in: Porzionato A., **Emmi A**., Stocco E., Barbon S., et al. (2020) The role of the carotid body in COVID-19. Am J Phys. doi:10.1152/ajplung.00309.2020*

ABSTRACT

The carotid body (CB) plays a contributory role in the pathogenesis of various respiratory, cardiovascular, renal, and metabolic diseases through reflex changes in ventilation and sympathetic output. On the basis of available data about peripheral arterial chemoreception and severe acute respiratory syndrome-coronavirus 2 (SARS-CoV-2), a potential involvement in the coronavirus disease 2019 (COVID-19) may be hypothesized through different mechanisms. The CB could be a site of SARS-CoV-2 invasion, due to local expression of its receptor [angiotensin-converting enzyme (ACE) 2] and an alternative route of nervous system invasion, through retrograde transport along the carotid sinus nerve. The CB function could be affected by COVID-19-induced inflammatory/immune reactions and/or ACE1/ACE2 imbalance, both at local or systemic level. Increased peripheral arterial chemosensitivity and reflex sympatho-activation may contribute to the increased morbidity and mortality in COVID-19 patients with respiratory, cardiovascular, renal, or metabolic comorbidities

INTRODUCTION

The coronavirus disease 2019 (COVID-19) outbreak, with its devastating impact on health and economic systems, focused research attention on pathogenetic and clinical aspects, such as effects on the respiratory function, possible invasion of the nervous system, and mechanisms involved in the comorbidity-induced increase in morbidity and mortality. A large number of articles have appeared in recent months on the above topics; conversely, the potential role of peripheral arterial chemoreceptors has not yet been considered, despite cardio respiratory regulation is obviously mediated by a functional integration between central and peripheral nervous structures. Peripheral arterial chemoreception is mainly mediated by the carotid body (CB), which is stimulated by hypoxia, hypercapnia, and pH reduction, although a large body of literature supports its additional roles in immune and metabolic sensing. From a structural point of view, the CB is composed of lobules of type I and II cells. Type I cells are considered the true chemoreceptor elements, producing and releasing many neurotransmitters/neuromodulators. Type II cells are considered supportive cells enveloping type I cells, although they may also be stem cell precursors for type I cells and probably play a role in coordination of chemosensory transduction. Neurotransmitters/neuromodulators released by type I cells act on the afferent nerve terminals of the carotid sinus nerve(CSN), a sensitive branch of the glossopharyngeal nerve with neurons in the petrosal ganglion. Centrally, the CSN projects to the solitary tract nucleus, which increases ventilation and sympathetic output through other brainstem nuclei. In the present paper, the potential role of CB in COVID-19will be addressed.

The CB could be a potential site of SARS-CoV-2 infection and an alternative route of Central Nervous System invasion

Central nervous system manifestations in COVID-19 have been reported in percentages up to 25% (e.g., 9, 28, 41, 80). They include headache, dizziness, confusion, impaired consciousness, and acute cerebrovascular events. In addition, neurological manifestations are more frequent in severe patients [88% in the series by Mao et al. (41)].

Some autoptic and experimental data are present in the literature about neurotropism of other animal and human (H) coronaviruses (CoV). In particular, neuroinvasive capability has been demonstrated for most βCoV, such as SARS-CoV (22), Middle East respiratory syndrome-CoV (MERS-CoV) (34), HCoV-229E (66), HCoV-OC43 (17), mouse hepatitis virus (83), and porcine hemagglutinating encephalomyelitis coronavirus (HEV) (36, 37).

SARS-CoV particles have been demonstrated in the brain, with specific reference to neurons (16, 77). As a consequence, in the last months, some articles specifically considered and discussed the neuroinvasive potential of the severe acute respiratory syndrome-CoV-2 (SARS-CoV-2), considering the possibility that neuroinvasion and damage to the central respiratory nuclei may be involved in SARS-CoV-2-induced respiratory failure (e.g., 4, 35).

In addition, the potential role of the peripheral nervous system as entry route has been considered. Peripheral neurological symptoms have been reported by Mao et al. (41) in 8.9% of cases, hypogeusia (5.6%), and hyposmia (5.1%) being the more frequent ones. Thus, the olfactory epithelium and nerves have been proposed as a way of brain entrance (e.g., 7). SARS-CoV (46) and MERS-CoV (34) also enter the brain when given intranasally, probably through the olfactory nerves.

It has also been proposed that SARS-CoV-2 may enter the brainstem via peripheral vagal afferents and trans-synaptic transfer (35). This hypothesis is consistent with previous findings from SARS-CoV and other CoV. There is evidence that the brainstem, and particularly the solitary tract nucleus, is invaded by various CoV, such as the avian bronchitis virus (43), MERS-CoV (34) and SARS-CoV (44, 46), so that an analog pattern of neuroinvasion for SARS-CoV-2 is probable (35).

There is evidence that other CoVs (e.g., HEV67, avian bronchitis virus) may enter peripheral nerve terminals and then invade the brain through retrograde transport and trans-synaptic transfer (e.g., 2, 8, 36, 37, 43, 45). HEV has been identified in the neurons of sensory (trigeminal, inferior vagal, dorsal root) and autonomic (superior cervical) ganglia (2, 36). Virus entrance into satellite cells of dorsal root ganglia has also been reported, through releasing from the sensory neurons and phagocytosis by adjacent satellite cells, although without signs of viral replication (36).

The cellular receptor for SARS-CoV and SARS-CoV-2 is the angiotensin-converting enzyme 2 (ACE2), usually a membrane-bound homolog of angiotensin-converting enzyme. SARS-CoV-2 has been reported to show about fourfold (72) or 10- to 20-fold (75) higher receptor affinity than SARS-CoV. ACE2 is widely expressed not only in lungs but also in other organs, such as heart, brain, kidney, and intestine, where it may permit virus invasion.

SARS-CoV-2 RNA has been identified in blood, plasma, serum, and cellular fraction of blood (67, 73, 74, 82). In an autopsy study, viremia correlated with viral load in the heart, liver, and kidney, strongly suggesting organ invasion through the bloodstream (74). Transplacental transmission has also been demonstrated with ascertainment of both maternal and neonatal

viremia (71). Thus, the potential SARS-CoV-2 invasion of the CB may also be hypothesized, as the CB is one of the structures with highest blood flow (2,000 mL·100 g−1·min−1), and it expresses ACE2 (48). In fact, the CB has a locally expressed renin-angiotensin system, which plays a role in the modulation of chemoreceptive function. Retrograde transport in the afferent fibers of the CSN may also be possible (Fig. 1). Virus invasion of the CB and CSN could intrinsically affect peripheral chemoreception, as also proposed by Soliz et al. (65). Moreover, this route could represent an alternative entry way for the solitary tract nucleus, which also expresses ACE2 and is known to be invaded by other CoV.

ACE2 is also expressed by endothelial cells (19) and evidence was found of direct viral infection of endothelial cells, together with diffuse endothelial inflammation. In fact, viral inclusion structures were observed by electron microscopy in endothelial cells of the renal vasculature. Inflammatory cells associated with endothelium (endothelitis) were also found in vessels of lung, heart, kidney, liver, and small intestine submucosa (69). Local modifications in blood flow are involved in chemoreceptor discharge. Thus, viral infection also of the glomic microvasculature may be hypothesized, with possible contributory effects on chemoreception modifications. Analogously, it has been proposed that invasion of the cerebral vascular endothelium by the virus may reduce its functionality, contributing to the elevation of blood pressure and consequent blood vessel rupture (10, 63). The blood vessels of the CB are innervated by sympathetic and parasympathetic nerve terminals and retrograde transport through these nerves cannot be excluded.

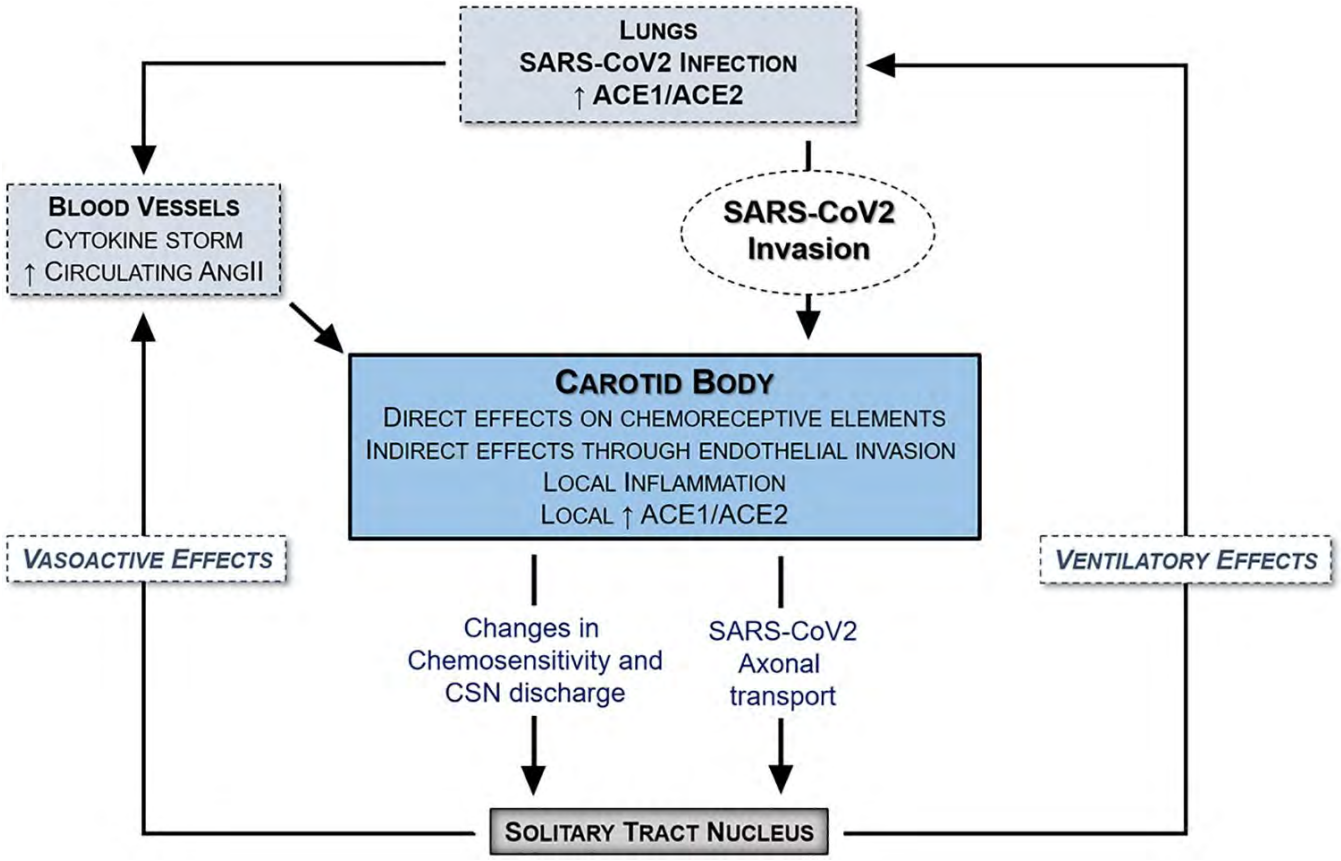

Figure 1. *Potential mechanisms of carotid body involvement in coronavirus disease 2019 (COVID-19). Severe acute respiratory syndrome-coronavirus 2 (SARS-CoV-2) infection could affect the carotid body through systemic and/or local effects with consequent decreased or increased hypoxic chemosensitivity on the basis of the specific mechanism involved. ACE, angiotensin-converting enzyme; ANG II, angiotensin 2; CSN, carotid sinus nerve.*

SARS-CoV-2 could affect peripheral arterial chemoreception through local or systemic inflammatory/immune stimuli

CB invasion by SARS-CoV-2 (at the level of chemoreceptive and/or endothelial structures) may induce local inflammatory reactions which could further contribute to derangement of chemoreception (Fig. 1). For instance, chronic carotid glomitis has been reported in aging and opiate-related deaths (55), and experimental studies have shown that the CB may show local inflammatory reactions also in response to systemic stimuli, with possible detrimental effects on ventilatory control.

Prenatal and postnatal lipopolysaccharide (LPS) administration affects peripheral chemoreception in different experimental animals (18, 42, 61). Maternal intraperitoneal LPS administration lowers baseline ventilation, increases apnea frequency, and produces hypersensitivity to hypoxia/hypercapnia in mouse newborns (61). In the rat, intraperitoneal postnatal LPS administration increases the frequency of desaturation episodes and reduces

hypoxic chemosensitivity. Increases in glomic inflammatory cytokines (IL-1β and IL-6) and in the volume fraction occupied by type II cells have also been found, together with reduced dopamine content and ultrastructural changes in type I cells (42).

In patients with severe COVID-19, the occurrence of a “cytokine storm” (IL-6, IL-10, and TNF-α) has been reported (e.g., 52). The CB also recognizes blood immunogens and cytokines (53), showing immunosensing properties, so that potential effects of SARS-CoV-2 cytokine storm on carotid chemoreception cannot be excluded, even in the absence of local invasion of the CB.

SARS-CoV-2 could affect peripheral arterial chemoreception through local or systemic ACE1/ACE2 imbalance

ACE1 and ACE2 show different enzymatic actions: ACE1 converts ANG I in ANG II, whereas ACE2 converts ANG I in ANG(1–9), then further converted in ANG(1–7), and may also convert ANG II in ANG(1–7). ACE2 decreases the production of ANG II in favor of ANG(1–7). ANG II mediates vasoconstriction, fibrosis, inflammation, hypertrophy, and sympatho-excitation through AT1R binding; ANG(1–7) mediates vasodilation, antifibrosis, anti-inflammation, antigrowth and sympatho-inhibition through MasR binding (e.g., 48). As a consequence, a balance is present in the different tissues between the two pathways (ACE1/ANG II/AT1R and ACE2/ANG(1–7)/MasR), and this balance can be affected in various clinical conditions.

As it regards COVID-19, internalization of SARS-CoV-2 causes inhibition of ACE2 activity and progressive depletion of membrane-bound ACE2 (23, 26, 27, 31, 81), with potential increase in ANG II, which has been proposed to contribute to lung damage through stimulation of fibrosis and inflammatory reaction (26).

The local renin-angiotensin system of the CB plays a pivotal role in the modulation of chemoreceptive function and in plastic changes of CB structure and function in response to hypoxia, heart failure, and inflammatory conditions (reviewed in Refs. 20, 26, 30, 33, 48, and 56). In fact, ANG II enhances the hypoxic sensitivity of type I cells, through interaction with oxygen-sensitive potassium channels and decreased voltage-gated currents (IKV) (38), whereas ANG(1–7) enhances IKV, through activation of neuronal nitric oxide synthase and nitric oxide production (62).

With it regards local effects of SARS-CoV-2 in the CB, it is possible that virus-induced depletion of membrane-bound ACE2 could contribute to imbalance of the two signaling pathways, in favor of the ACE/ANG II/AT1R one, with increased hypoxic sensitivity, afferent

discharge, and sympatho-activation (Fig. 1). ANG II may also activate macrophages and other immune cells to produce inflammatory cytokines, such as IL-6, TNF-α, and others (32, 58, 79).

Apart from locally produced ANG II, the CB is also stimulated from circulating ANG II (e.g., 20) and in COVID-19, circulating levels of ANG II are increased, even proportionally with viral loads (40). Thus, we may hypothesize that in COVID-19 the systemic production of ANG II may additionally invest the CB.

In conclusion, we hypothesize that CB and its innervation could represent another way through which SARS-CoV-2-induced ACE1/ACE2 imbalance (local and/or systemic) may exert noxious actions on respiratory regulation and cardiovascular function, through increased peripheral hypoxic chemosensitivity and sympathetic output.

Increased peripheral arterial chemosensitivity and sympathetic outflow may contribute to increased morbidity and mortality in COVID-19 with comorbidities

In COVID-19, higher morbidity and mortality are associated with comorbidities, such as chronic lung disease, cardiovascular pathologies, hypertension, diabetes mellitus, and obesity (e.g., 76 and 83). The US Centers for Disease Control and Prevention reported that 89.3% of COVID-19 patients who were hospitalized in March “had one or more underlying conditions; the most common were hypertension (49.7%), obesity (48.3%), chronic lung disease (34.6%), diabetes mellitus (28.3%), and cardiovascular disease (27.8%)” (21). In COVID-19 patients, diabetes mellitus is associated with mortality, severe COVID-19, acute respiratory distress syndrome (ARDS), and disease progression (29). All of the above pathologies are also known to affect peripheral arterial chemoreception, with modifications which may be in turn detrimental for pulmonary, cardiac, circulatory, renal, and metabolic functions. On the other hand, COVID-19 deaths are frequently caused by a final homeostasis dysregulation caused not only by pulmonary damage but also by cardiac, circulatory, renal, and/or metabolic effects. Thus, a potential role of CB should be considered and discussed (Fig. 2).

Consistent and reliable evidence is available about the fact that the CB is a metabolic sensor contributing to the regulation of whole body insulin sensitivity and that its dysfunction may be involved in metabolic and cardiovascular disturbances (e.g., 11, 12). Insulin can stimulate the CB by binding to its receptors on type I cells, inducing a rise in intracellular Ca2+ and eliciting the release of neurotransmitters, which act on the CSN terminals. The functional

effect of insulin-induced stimulation of the CB and CSN produces an increase in ventilation and an augmented sympathetic outflow. In metabolic conditions characterized by insulin resistance and hyperinsulinemia, the CB is overstimulated. In fact, in rats, hypercaloric diets produce CB overactivation and stimulation of the sympathetic nervous system (60). The insulin-mediated increase in sympathetic output is prevented by surgical section of the CSN (60) or hyperoxic silencing of peripheral chemoreception (39). It is important to stress that sympathetic overactivation in turn increases insulin resistance (detected by insulin tolerance test), producing a vicious circle, which can be experimentally prevented by CB denervation (60). Various respiratory diseases, such as obstructive sleep apnea syndrome, are characterized by chronic intermittent hypoxia, which is another condition increasing the peripheral chemosensory response to hypoxia and consequently inducing a sympathetic overactivation that can be prevented by CB denervation (e.g., 57, 59). It is widely shared that sympathetic overactivity is associated with obstructive sleep apnea syndrome, cardiovascular diseases, renal pathologies, and metabolic disturbances (diabetes, obesity, metabolic syndrome). Thus, increased chemosensitivity is strongly suggested to play a role in sympatho-activation of hypertension, heart failure, diabetes, obesity, obstructive sleep apnea syndrome, and chronic kidney disorders (e.g., 11–13, 51, 54). In the above conditions, the increased sympathetic outflow (at least partially induced by increased CSN discharge) may contribute to increased morbidity/mortality in COVID-19 through homeostasis derangement. Moreover, the increased sympathetic activity through stimulation of the chemoreceptive discharge may have specific detrimental respiratory effects by increasing pulmonary capillary leakage and favoring ARDS (1, 5, 14, 15).

Moreover, COVID-19-induced ACE1/ACE2 imbalance may acquire higher relevance in the presence of the above comorbidities, which share a relative prevalence of the ACE1/ANG II/AT1R pathway (70), with additional stimulatory effects on the CB. ACE2 deficiency may play a role in hypertension (49, 50) and seems to enhance susceptibility to heart failure (49). Diabetes mellitus is associated with reduced ACE2 expression, maybe due to glycosylation (47, 68, 78). Expression of ACE2 is reduced in the adipose tissue of obese animals (24). Fatty diet decreases ACE2 activity and increases ANG II and blood pressure in male rats (but not in female ones) (25). In these conditions, the ACE2 downregulation induced by SARS-CoV-2 could further imbalance the already critical ACE1/ACE2 equilibrium with homeostasis derangement. Conversely, because of the intrinsic high affinity of SARS-CoV-2 to ACE2 receptors (72, 75), in these pathologies the ACE2 deficiencies would not have a protective role from viral invasion (70).

In chronic heart failure, a reduced expression of ACE2 (62) and increased ACE1/ANG II/AT1R signaling have been reported in the CB. This imbalance enhances the hypoxic sensitivity and afferent discharge of the CB, with consequent increased sympathetic outflow (48).

On the basis of the above considerations about ANG II effects on the CB, it may be hypothesized that the systemic ACE1/ACE2 imbalance may exert its detrimental effect also through the CB, being widely shared that circulating ANG II increases hypoxic sensitivity and chemoreceptor discharge of the CB (e.g., 20). In COVID-19, the chemoreceptor-induced increase in sympathetic activity could obviously have negative effects also on pulmonary, cardiovascular, renal, and metabolic homeostasis.

On the contrary, it is also intriguing that high-altitude inhabitants seem to be less susceptible to severe COVID-19 (3), as they also show adaptative changes in peripheral arterial chemoreception and lower sympathetic reactivity (e.g., 6, 64).

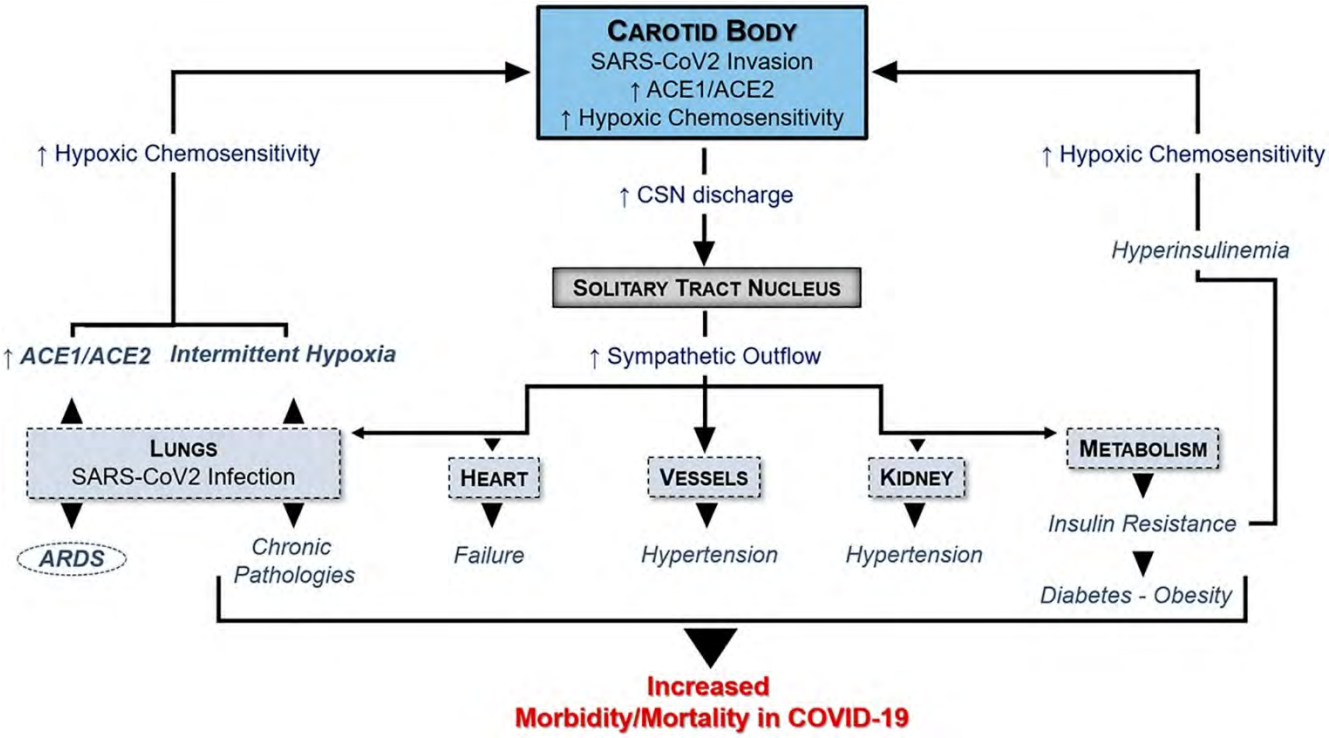

Figure 2. *Coronavirus disease 2019 (COVID-19) and comorbidities: potential mechanisms of carotid body involvement. In the presence of respiratory, cardiovascular, renal, or metabolic comorbidities, increased carotid body chemosensitivity and reflex sympathetic outflow would contribute to the detrimental effects in COVID-19, which in turn would further increase hypoxic chemosensitivity and sympatho-activation in a vicious circle. ACE, angiotensin-converting enzyme; ARDS, acute respiratory distress syndrome; CSN, carotid sinus nerve; SARS-CoV-2, severe acute respiratory syndrome-coronavirus 2.*

CONCLUSIONS

In the present article, we highlighted some potential mechanisms of CB involvement in COVID-19. In our opinion, these aspects deserve specific analysis, also to better address the pathophysiologic bases of the different therapeutic approaches.

DISCLOSURES

No conflicts of interest, financial or otherwise, are declared by the authors.

AUTHOR CONTRIBUTIONS

A.P., A.E., E.S., and S.B. prepared figures; A.P., A.E., and R.D.C. drafted manuscript; A.P., A.E., E.S., S.B., R.B.-B., V.M., and R.D.C. edited and revised manuscript; A.P., A.E., E.S., S.B., R.B.-B., V.M., and R.D.C. approved final version of manuscript.

Chapter 7

The Carotid Body in COVID-19: Histopathological and Virological Analyses of an Autopsy Case Series

*The present chapter has been previously published in: Porzionato A., **Emmi A.**, Contran M., Stocco E., Riccetti S., Sinigaglia A., Macchi V., Barzon L., De Caro R. The Carotid Body in COVID-19: histopathological and virological analyses of an autopsy case series. Frontiers in Immunology. doi: https://doi.org/10.3389/fimmu.2021.736529. This article is licensed under a CC BY license.*

ABSTRACT

Various authors have hypothesized carotid body (CB) involvement in Coronavirus Disease 2019 (COVID-19), through direct invasion or indirect effects by systemic stimuli ('cytokine storm', angiotensin-converting enzyme [ACE]1/ACE2 imbalance). However, empirical evidence is limited or partial. Here, we present an integrated histopathological and virological analysis of CBs sampled at autopsy from four subjects (2 males and 2 females; age: >70 years old) who died of COVID-19. Histopathological, immunohistochemical and molecular investigation techniques were employed to characterize Severe Acute Respiratory Syndrome – Coronavirus 2 (SARS-CoV2) viral invasion and inflammatory reaction. SARS-CoV2 RNA was detected in the CBs of three cases through Real-Time Reverse Transcription Polymerase Chain Reaction (RT-PCR). In these cases, positive immunostaining for Nucleocapsid and Spike protein were also demonstrated, mainly at the level of large roundish cells consistent with type I cells, confirming direct CB invasion. In these cases, T lymphocytes showed focal aggregations in the CBs, suggestive of local inflammatory reaction. Blood congestion and microthrombosis were also found in one of the positive cases. Intriguingly, microthrombosis, blood congestion and microhaemorrages were also bilaterally detected in the CBs of the negative case, supporting the possibility of COVID-19 effects on the CB even in the absence of its direct invasion. SARS-CoV-2 direct invasion of the CB is confirmed through both immunohistochemistry and RT-PCR, with likely involvement of different cell types. We also reported histopathological findings which could

be ascribed to local and/or systemic actions of SARS-CoV-2 and which could potentially affect chemoreception.

INTRODUCTION

The possibility of Severe Acute Respiratory Syndrome – Coronavirus 2 (SARS-CoV2) invasion of the carotid body (CB), with consequent chemosensitive impairment, has been hypothesized by various authors in the past months (1-5), as the CB expresses ACE2 (4, 6). The CB and carotid sinus nerve have also been considered as a potential alternative entry way for the solitary tract nucleus. Invasion of CB (3-5) and/or solitary tract nucleus (6) have also been proposed to explain the development of 'silent hypoxia' (or 'happy hypoxia') in some COVID-19 patients, i.e., severe hypoxemia without signs of respiratory distress (dyspnea) or breathing acceleration. Conversely, increased peripheral arterial chemosensitivity and reflex sympatho-activation have also been hypothesized to play a role in COVID-19 patients with comorbidities (8).

Apart from these perspective articles, few empirical data are available about CB in COVID-19 patients. Lambermont et al. (2021) detected SARS-CoV-2 in the CB of a 42-year-old COVID-19 patient, through Real-Time Reverse Transcription Polymerase Chain Reaction (RT-PCR) performed on paraffin-embedded sections after glomus tissue microdissection (9). However, histopathological and SARS-CoV-2 immunohistochemical findings were not reported. Conversely, Kantonen et al. (2021) analysed CBs from three subjects died of COVID-19, reporting negativity for SARS-CoV-2 Spike-protein immunohistochemistry and absence of pathological findings (6). RT-PCR was not performed (10).

In the present study, we performed an integrated histopathological and virological analysis of CBs of four patients who died for COVID-19.

Cases description

The CBs were obtained at autopsy from 4 subjects (2 males and 2 females) who died of COVID-19. All patients were tested positive for Sars-CoV-2 infection by means of RT-PCR performed on naso/oropharyngeal swabs along the clinical course. Clinical and pathological data are summarized in the timeline table (**Supplemental 1)**. Except for one patient who was comorbidities-free, all others presented pre-existing chronic medical conditions

including hypertension (N=3), diabetes (N=1), vascular dementia (N=2), Parkinson's disease (N=1). One patient died the same day of hospitalization; the other patients were hospitalized for a range of 4-35 days before death occurrence. SARS-CoV-2 infection was furtherly confirmed in all cases by positive post-mortem naso/oropharyngeal swabs and RT-PCR on paraffin-embedded sections from lung samples (threshold cycle values: Case 1, 21.3; Case 2, 35.5; Case 3, 35.3; Case 4, 32.6).

Bilateral CBs were sampled, except for Case 2 (only right CB sampled). In each case, multiple samples from the major organs were also performed for histological examination. CBs sampled from five subjects older than 70 years (age range 71-80; 3 males and 2 females) were also analysed as controls; death occurred at least one year before the COVID-19 pandemic.

Histological and immunohistochemical analyses were performed according to previously published protocols (11, 12). Specimens were fixed in 10% neutral buffered formalin and paraffin-embedded. For each case, histological examination was carried out on five longitudinal sections, 5 μm thick, at 50 μm distance from each other and stained with haematoxylin-eosin and Azan-Mallory.

Immunoperoxidase staining was performed on a Dako EnVision Autostainer according to manufacturer recommendations. Antibodies for CD3 (Polyclonal Rabbit Anti-Human, Dako Omnis, Code Number: GA503), CD20 (Monoclonal Mouse Anti-Human, Clone KP1, Dako Omnis, Code Number: M0814) and CD68 (Monoclonal Mouse Anti-Human, Clone L26, Dako Omnis, Code Number: M0756) were employed to characterize lympho-monocytic infiltrations. Anti-CD61 immunohistochemistry (Monoclonal Mouse Anti-Human, Clone Y2/51, Dako Omnis, Code Number: M0753) was also employed to evaluate the presence of platelet microthrombi. Anti-SARS-CoV-2 nucleocapsid (Rabbit Anti-Human, Sino Biologicals, 40143-R001) and -Spike Subunit 1 Antibody (Monoclonal Rabbit Anti-Human, Clone 007, Sino Biological, Code Number: 40150-R007) immunostainings were employed to evaluate viral tropism within the tissue. Nucleocapsid and Spike antibodies were validated through SARS-CoV-2 infected Vero E6 cells and autopsy-derived lung tissue from SARS-CoV-2 positive patients as positive controls; non-infected cells and lung and CB sections deriving from autopsy cases predating COVID-19 pandemic (2017) were used as negative controls. Peroxidase reactions were repeated at least three times to ensure reaction consistency. Slides were evaluated by experienced morphologists and disagreements were resolved by consensus.

RT-PCR analyses were performed to detect SARS-CoV-2. In order to specifically analyse SARS-CoV-2 RNA in the CB parenchyma, microdissections were performed on 20 µm thick paraffin-embedded sections along the margins of CB lobules. Total RNA was purified from this selected material using a RecoverAll™ Total Nucleic Acid Isolation kit (Thermo Fisher Scientific, Waltham, MA, USA) following the manufacturer's instructions. Real-time PCR analyses were performed by using primers and TaqMan probes as previously reported (13) and run on ABI 7900HT Sequence Detection Systems (Thermo Fisher Scientific).
In CBs of negative controls, preliminary immunohistochemical analyses for nucleocapsid and Spike proteins of SARS-CoV-2 did not show any reaction **(Supplemental 2)**.

Case 1

Molecular analyses did not detect SARS-CoV-2 RNA.
The right **(Figure 1)** and left **(Supplemental 3)** CBs showed severe blood congestion of microvasculature, with some small CD61-positive platelet thrombi. In the left CB, focal erythrocyte extravasations were also visible in the fibroadipose tissue immediately external to the CB. Immunohistochemical stainings for SARS-CoV-2 nucleocapsid and Spike proteins were negative. Bilaterally, CD68-positive macrophages and CD3-positive lymphocytes were sparsely present in the glomic parenchyma, without aggregations. CD20-positive B lymphocytes were very rare.

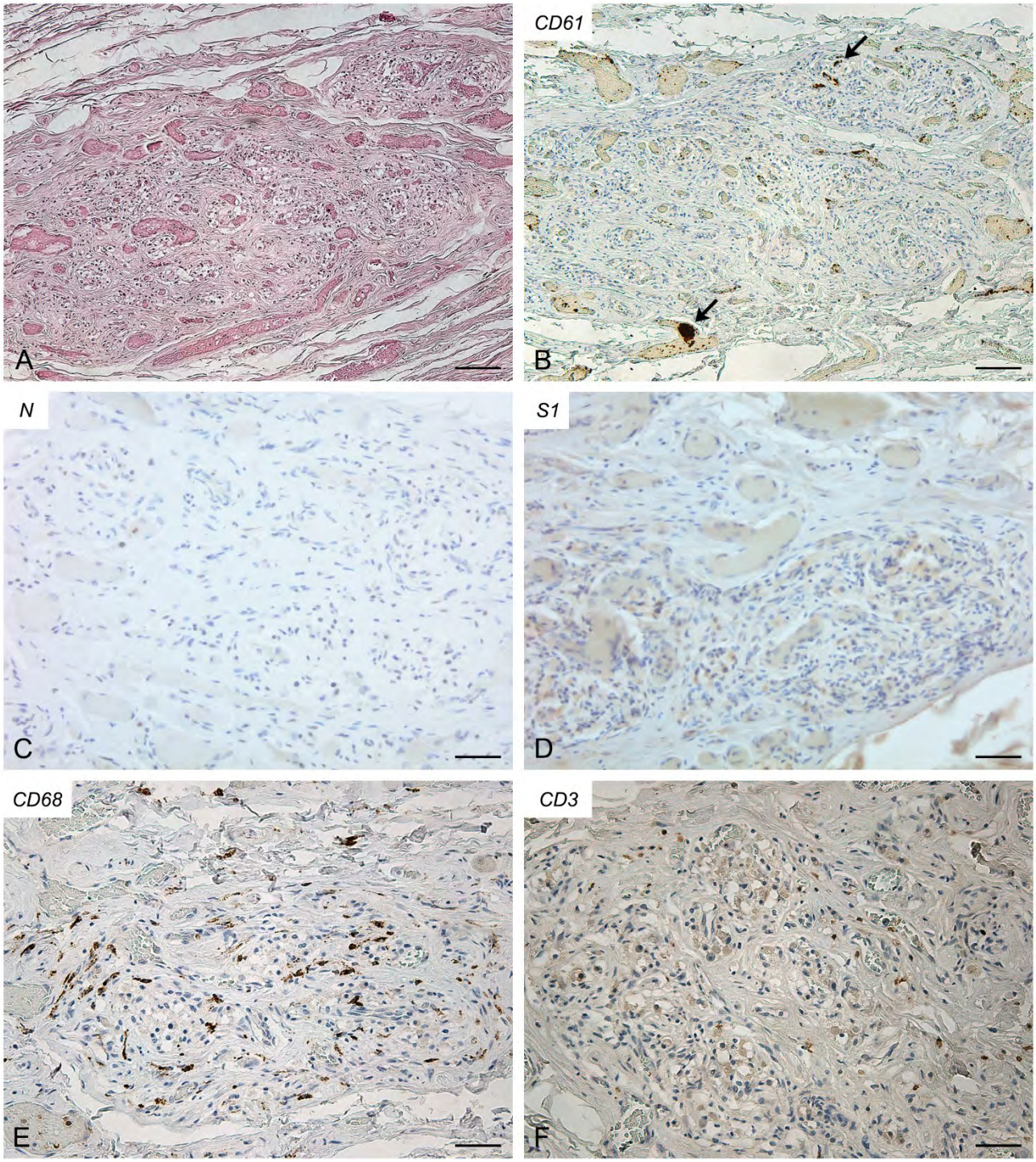

Figure 1. *Right carotid body of Case 1 – Haematoxylin-eosin (A) and immunohistochemitries for CD61 (B; arrows: fibrin/platelet microthrombosis), nucleocapsid (C), Spike (D), CD68 (E) and CD3 (F). Scale bars: 100 µm (A, B); 50 µm (C-F).*

Case 2

Molecular analyses detected SARS-CoV-2 RNA in the CB (threshold cycle value: 35.42). In this case **(Figure 2)**, some small CD61-positive platelet thrombi were also found in the vessels of the CB, in the presence of moderate congestion. Anti-SARS-CoV-2 nucleocapsid immunohistochemistry showed some cells clearly positive in the context of glomic parenchyma. These cells were quite large and displayed roundish nuclei, consistently with type I cells. Anti-Spike immunostaining also showed positive cells in the CB, although with overall weaker immunoreactivity. CD68-positive macrophages and CD3-positive lymphocytes were diffusely present in the glomic parenchyma. CD20-positive B lymphocytes were quite rare.

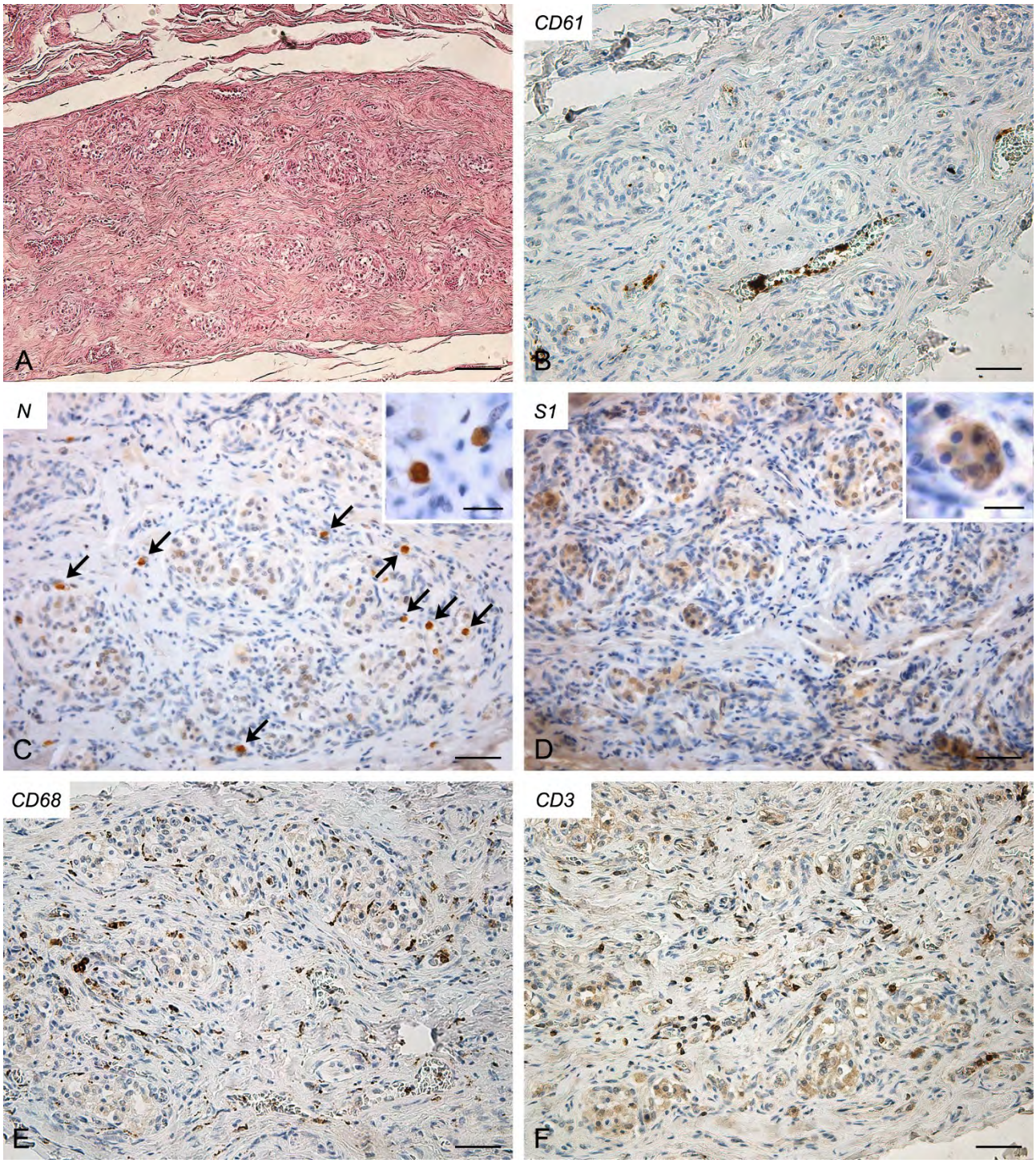

***Figure 2**. Right carotid body of Case 2 – Haematoxylin-eosin (A) and immunohistochemitries for CD61 (B), nucleocapsid (C; arrows: positive cells), Spike (D), CD68 (E) and CD3 (F). Scale bars: 100 µm (A); 50 µm (B-F). Inserts: high magnification of positive type I cells; Scale Bar: 15 µm.*

Case 3

Molecular analyses detected SARS-CoV-2 RNA in both CBs (threshold cycle value: right, 34.41; left, 35.12).

Both right **(Figure 3)** and left **(Supplemental 4**) CBs showed similar features, characterized by increased connective tissue in the absence of blood congestion or microthrombosis. Anti-SARS-CoV-2 nucleocapsid immunohistochemistry evidenced some clearly positive cells in the context of glomic parenchyma. These cells were quite large and endowed with roundish nuclei, consistently with type I cells. Anti-Spike immunostaining also showed positive cells in the CB, although with weaker reaction. Immunostaining mainly involved cells with type I appearance, although positive reactions in type II cells and/or macrophages cannot be ruled out due to aspects of diffuse positivity in some slides or fields. CD68-positive macrophages were diffusely present in the glomic parenchyma. Aggregates of CD3-positive T lymphocytes were found in the CB tissue, whereas only few CD20-positive B lymphocytes were found.

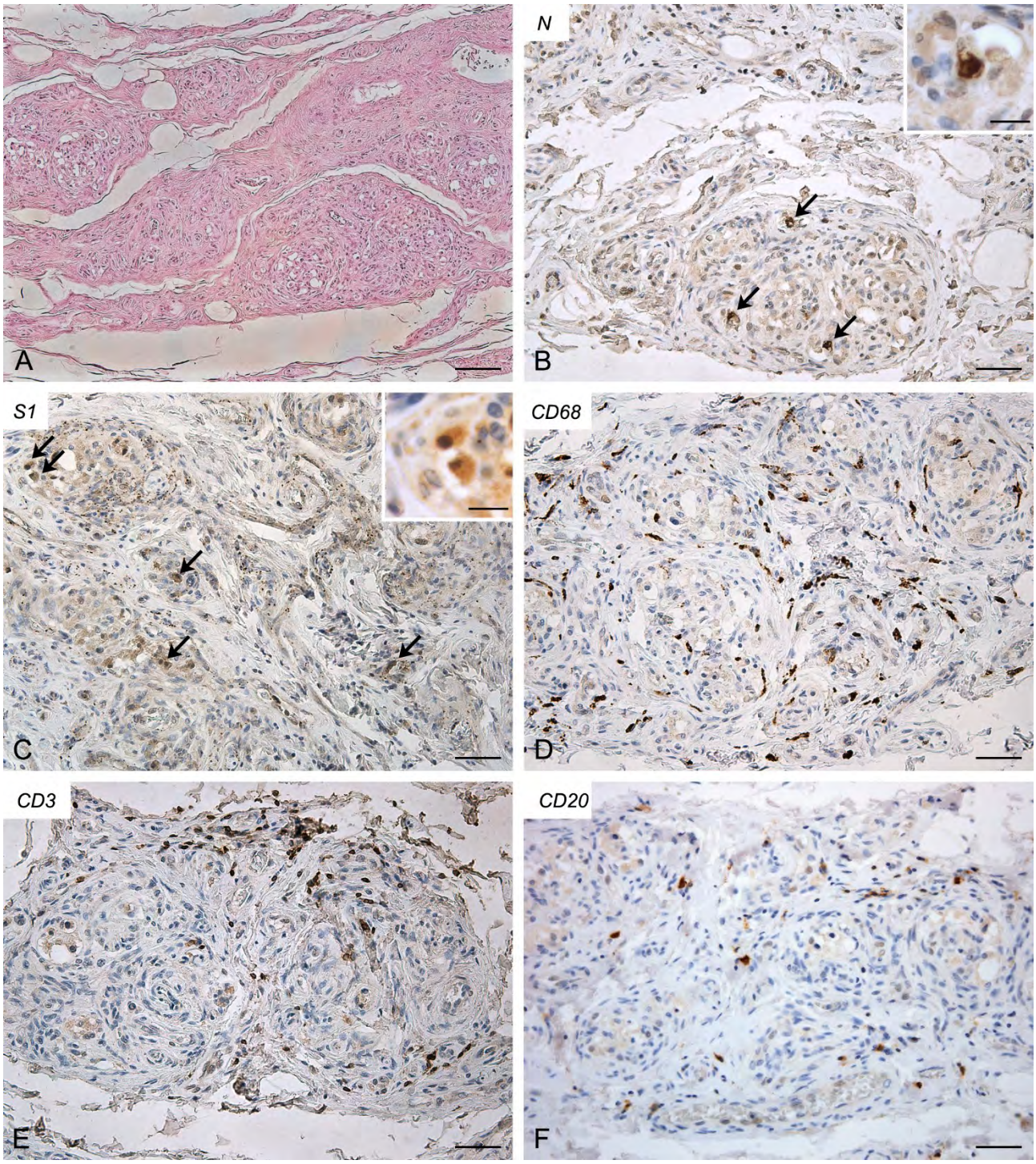

***Figure 3**. Right carotid body of Case 3 – Haematoxylin-eosin (A) and immunohistochemitries for nucleocapsid (B,C; arrows: positive cells), Spike (D), CD68 (E) and CD3 (F). Scale bars: 100 µm (A); 50 µm (B-F). Inserts: high magnification of positive type I cells. Scale Bar: 15 µm.*

Case 4

Molecular analyses detected SARS-CoV-2 RNA in both CBs (threshold cycle value: right, 30.56; left, 33.31).

Also in this case both CBs (right, **Figure 4**; left, **Supplemental 5**) exhibited similar features. They showed a slight increase in connective tissue. Blood congestion or microthrombosis were not found. Anti-SARS-CoV-2 nucleocapsid immunohistochemistry showed strongly positive cells in glomic parenchyma, bilaterally. Most of these cells were large and roundish, consistently with type I cell characteristics; however, some elongated positive cells were also found in the lobule periphery, potentially ascribable to type II cells or macrophages. Immunoreaction against SARS-CoV-2 Spike was weaker but positive cells, elongated or roundish, were visible in the glomic lobules. A high number of CD68-positive macrophages infiltrated the glomic parenchyma. Aggregates of CD3-positive T lymphocytes were also found, although less evident than in Case 2. Few CD20-positive B lymphocytes were detected.

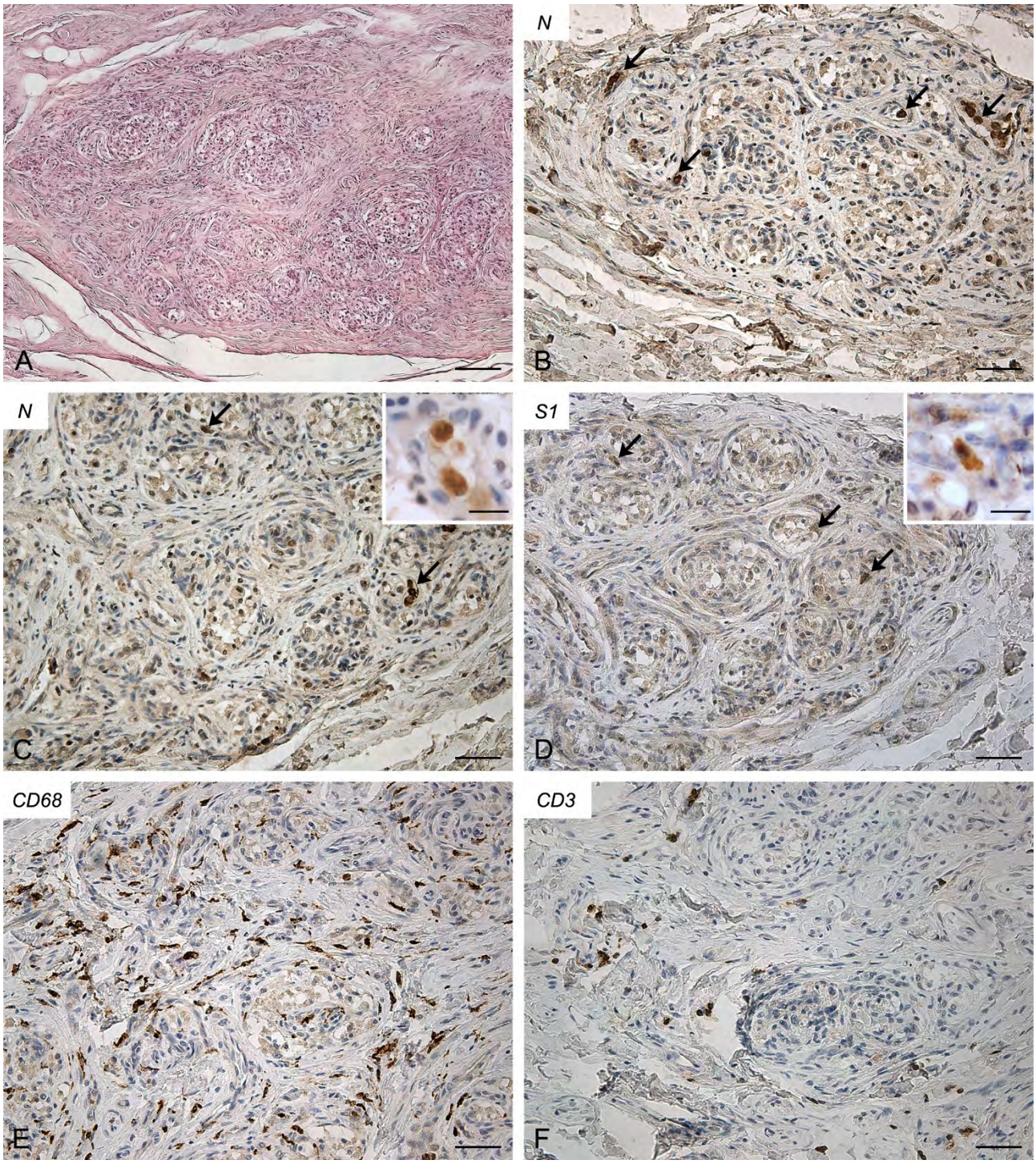

***Figure 4**. Right carotid body of Case 4 – Haematoxylin-eosin (A) and immunohistochemitries for nucleocapsid (B-C; arrows: positive cells), Spike (D; arrows: positive cells), CD68 (E) and CD3 (F). Scale bars: 100 µm (A); 50 µm (B-F). Inserts: high magnification of positive type I cells. Scale Bar: 15 µm.*

The CBs of the five control subjects did not show microthromboses or inflammatory infiltrations (**Supplemental 6**).

DISCUSSION

In the present study, virological and histopathological findings are shown giving evidence of the potential involvement of the CB in the complex pathological entity of COVID-19, although further analyses will be needed in larger studies.

In Case 1, RT-PCR and immunohistochemical analyses for SARS-CoV-2 nucleocapsid and Spike proteins did not allow for the identification of the virus in the CB. However, glomic vessels showed microthrombosis, blood congestion and microhaemorrhages. Apart from lungs, these findings have been reported in various organs and tissues of COVID-19 victims. Conversely, in this study, microthrombosis, blood congestion and microhaemorrhages were not found in control old subjects and, to the best of our knowledge, they have not been described before in human CB. Thus, these glomic findings may be included among the systemic effects of COVID-19, due to general mechanisms, such as the 'cytokine storm', coagulation dysfunction or ACE1/ACE2 imbalance, even in the absence of direct viral invasion. If confirmed, this could be particularly suggestive, as the CB is one of the structures characterized by the highest blood flow (14, 15); moreover, changes in local blood flow may play a role in chemoreception modulation.

Conversely, in Cases 2, 3 and 4, virological and immunohistochemical analyses confirmed the direct invasion of SARS-CoV-2 in the CB. Lambermont et al. (2021) also detected SARS-CoV-2 RNA in the CB of a COVID-19 case through RT-PCR (9) but these are the first demonstrations of CB invasion through an integrated approach, including molecular (RT-PCR) and immunohistochemical (nucleocapsid and Spike) methods. In these cases, bilateral CB involvement was found.

Concerning involved cell types, most positive cells showed clear cytological characteristics of type I cells, being roundish, large and mainly located in the center of the lobules (see inserts in Figures 2-5); however, some type II cells and macrophages were probably present among positive cells, as elongated positive-elements were also found at the lobular margins. We cannot exclude also an endothelial involvement, due to the intrinsic difficulty in identifying positive immunoreaction in the very small vessels of glomic microvasculature. Thus, while infection of type I cells is clearly evident in our immunohistochemical results, further analyses in larger casistics through double immunofluorescence will be needed to detail possible SARS-CoV-2 infection of other cell types (type II cells? endothelial cells? macrophages?) in the CB.

Immune/inflammatory cells infiltrating the CBs were also specifically evaluated. Positive CBs showed inflammatory infiltration by CD68 and CD3-positive macrophages and T lymphocytes, respectively. In particular, T lymphocytes displayed focal aggregations in the CBs with evidence of SARS-CoV-2 invasion. In our study, these findings were not found in the CB of control old subjects and they could be suggestive of specific local inflammatory reaction to SARS-CoV-2. However, we must also consider that they will need to be morphometrically confirmed in larger case series, as sparse and diffuse lympho-monocytic infiltrations have been already described in the CB, mainly in aging subjects (11, 16-20). Chronic carotid glomitis, defined by the presence of lymphocyte aggregates throughout its structure, has also been reported in subjects over the age of 50 (12, 16-20) or in opiate-related deaths (12). We cannot also theoretically exclude that comorbidities, mainly hypertension and diabetes, may have also contributed to produce or increase the inflammatory reaction. Animal experimental data are available about involvement of CB in hypertension and diabetes (21,22), although histopathological findings in human CB have not yet been described.

In conclusion, SARS-CoV-2 direct invasion of the CB is confirmed through both immunohistochemistry and RT-PCR, with likely involvement of different cell types. We also reported histopathological findings (inflammatory aggregates, microthrombosis, blood congestion and microhaemorrhages) which could be ascribed to local and/or systemic actions of SARS-CoV-2 and which could potentially affect chemoreception.

CONFLICT OF INTEREST

The authors declare that the research was conducted in the absence of any commercial or financial relationships that could be construed as a potential conflict of interest.

AUTHOR CONTRIBUTIONS

AP, RDC, VM, LB, ES designed the study; RDC and AP performed the autopsies; AE and MC performed the histological and immunohistochemical analyses; AP, RDC, AE and MC were responsible of histological and immunohistochemical findings interpretation; LB, SR, AS, performed molecular analyses and interpreted the data; AP drafted the manuscript; MC prepared the figures; AP, LB, VM, and ES revised the manuscript. All authors approved the submitted version.

SUPPLEMENTARY MATERIAL

Supplemental 1. Timeline table. Clinical and pathological characteristics of autopsy cases.

Case	Age	Gender	Interval between positive test and death (days)	Comorbidities	Clinical course	Autopsy and histopathological findings
1	72	Male	1	-	Recovery for dyspnoea Initially negative for SARS-CoV-2 Death for respiratory failure after SARS-CoV-2 positivization	Lung: - Diffuse alveolar damage - Lung vascular congestion - Platelet/fibrin microthrombosis - Alveolar and subpleural haemorrhagic infiltrations - Lymphomonocytic infiltrations Other organs: - Spleen white pulp depletion - Renal congestion and lymphomonocytic infiltrations - Congestion, platelet/fibrin microthrombosis and microhaemorrhages in brain
2	89	Female	16	Hypertension Diabetes Vascular dementia	Death for respiratory failure Non-invasive O_2 supply only few hours before death	Lung: - Chronic emphysema - Diffuse alveolar damage - Lung vascular congestion - Platelet/fibrin microthrombosis - Alveolar and subpleural haemorrhagic infiltrations - Lymphomonocytic infiltrations Other organs: - Pericardial lymphomonocytic infiltrations - Spleen subcapsular haemorrhages - Renal congestion and lymphomonocytic infiltrations
3	77	Female	2	Hypertension Chronic renal insufficiency	Recovery for dyspnoea and asthenia due to heart failure	Lung: - Chronic emphysema - Diffuse granulocytic infiltration (bacterial pneumonia)

					Klebsiella pneumoniae pneumonia Hospital-acquired SARS-CoV-2 infection Death for respiratory failure	- Diffuse alveolar damage - Lung vascular congestion - Platelet/fibrin microthrombosis - Alveolar haemorrhagic infiltrations - Focal lymphomonocytic infiltrations <u>Other organs:</u> - Spleen subcapsular haemorrhages and white pulp depletion - Renal congestion, lymphomonocytic infiltrations and corpuscles degeneration - Adrenal lymphomonocytic infiltrations
4	84	Male	20	Hypertension Parkinson's disease Vascular dementia	Recovery and death for respiratory failure	<u>Lung</u>: - Chronic emphysema - Diffuse alveolar damage - Lung vascular congestion - Platelet/fibrin microthrombosis - Alveolar and subpleural haemorrhagic infiltrations - Lymphomonocytic infiltrations

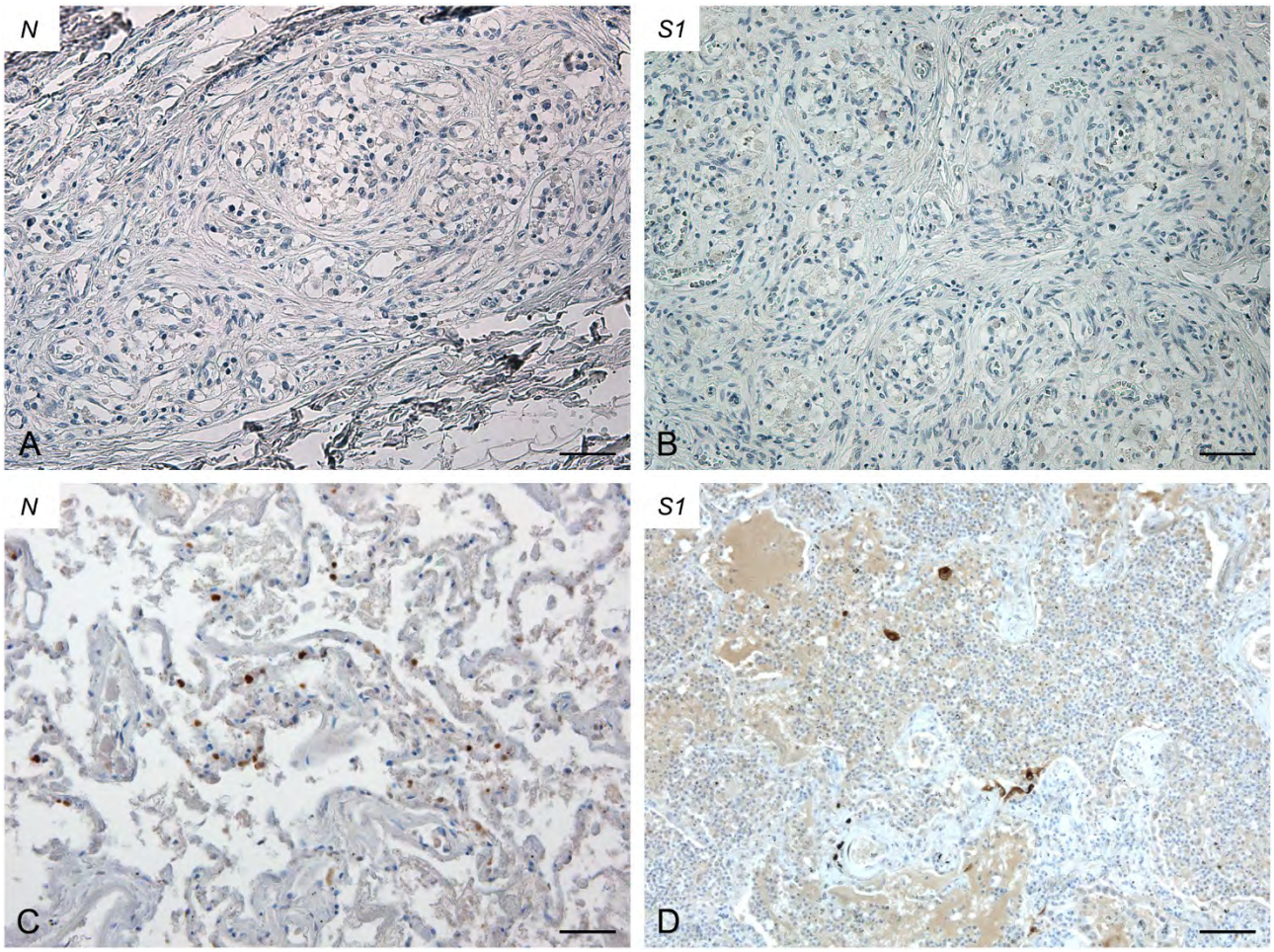

***Supplemental 2**. Negative controls for anti-nucleocapsid (A) and -Spike (B) immunohistochemistries in human carotid bodies from autopsy cases predating COVID-19 pandemic. Positive controls for anti-nucleocapsid (C) and -Spike (D) immunohistochemistries in human lung samples from ascertained COVID-19 victims. Scale bars: 50 µm (A, B); 100 µm (C, D).*

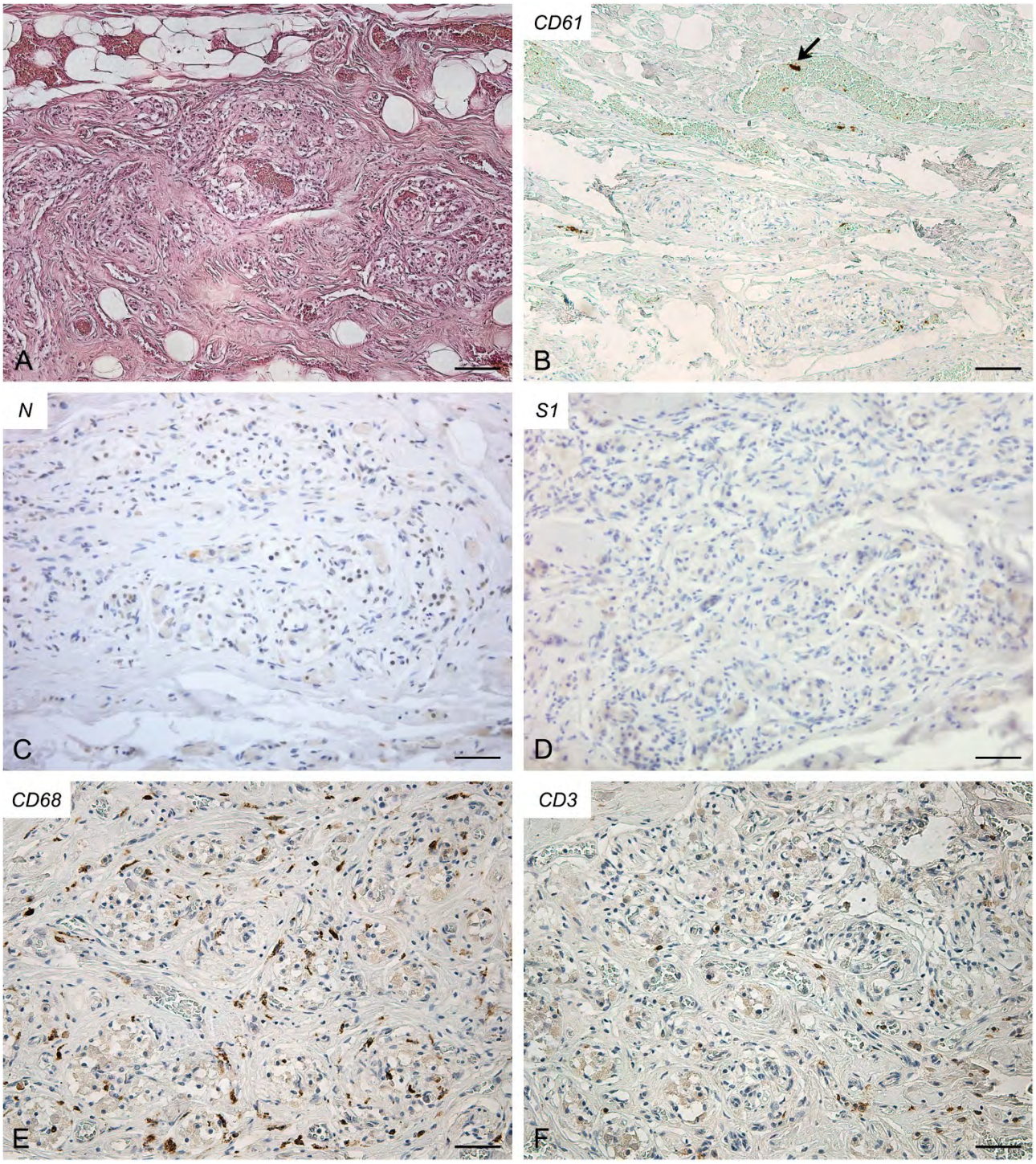

***Supplemental 3**. Left carotid body of Case 1 – Haematoxylin-eosin (A) and immunohistochemitries for CD61 (B; arrow: fibrin/platelet microthrombosis), nucleocapsid (C), Spike (D), CD68 (E) and CD3 (F). Scale bars: 100 µm (A, B); 50 µm (C-F).*

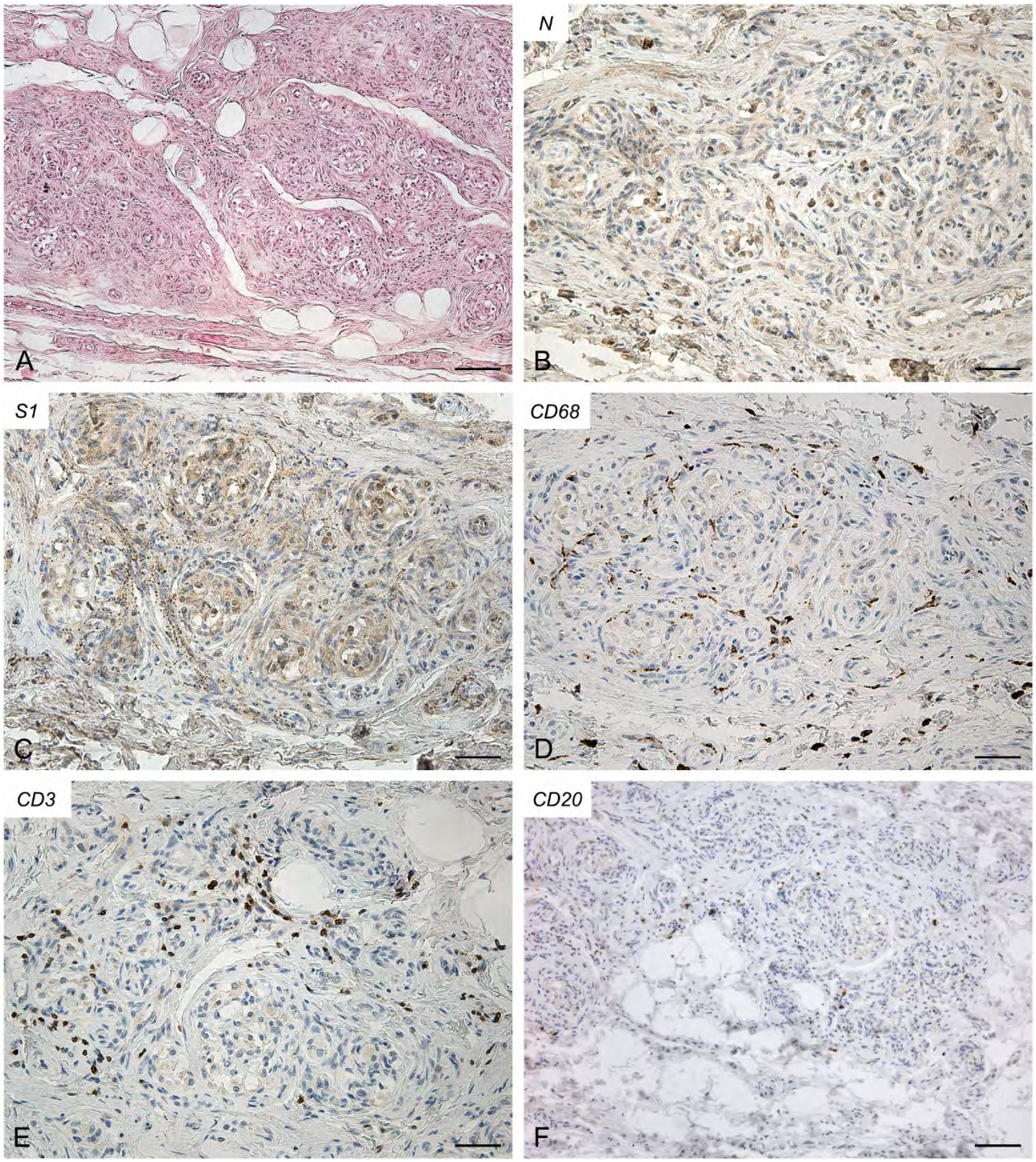

***Supplemental 4**. Left carotid body of Case 3 – Haematoxylin-eosin (A) and immunohistochemitries for nucleocapsid (B), Spike (C), CD68 (D), CD3 (E) and CD20 (F). Scale bars: 100 µm (A, F); 50 µm (B-E).*

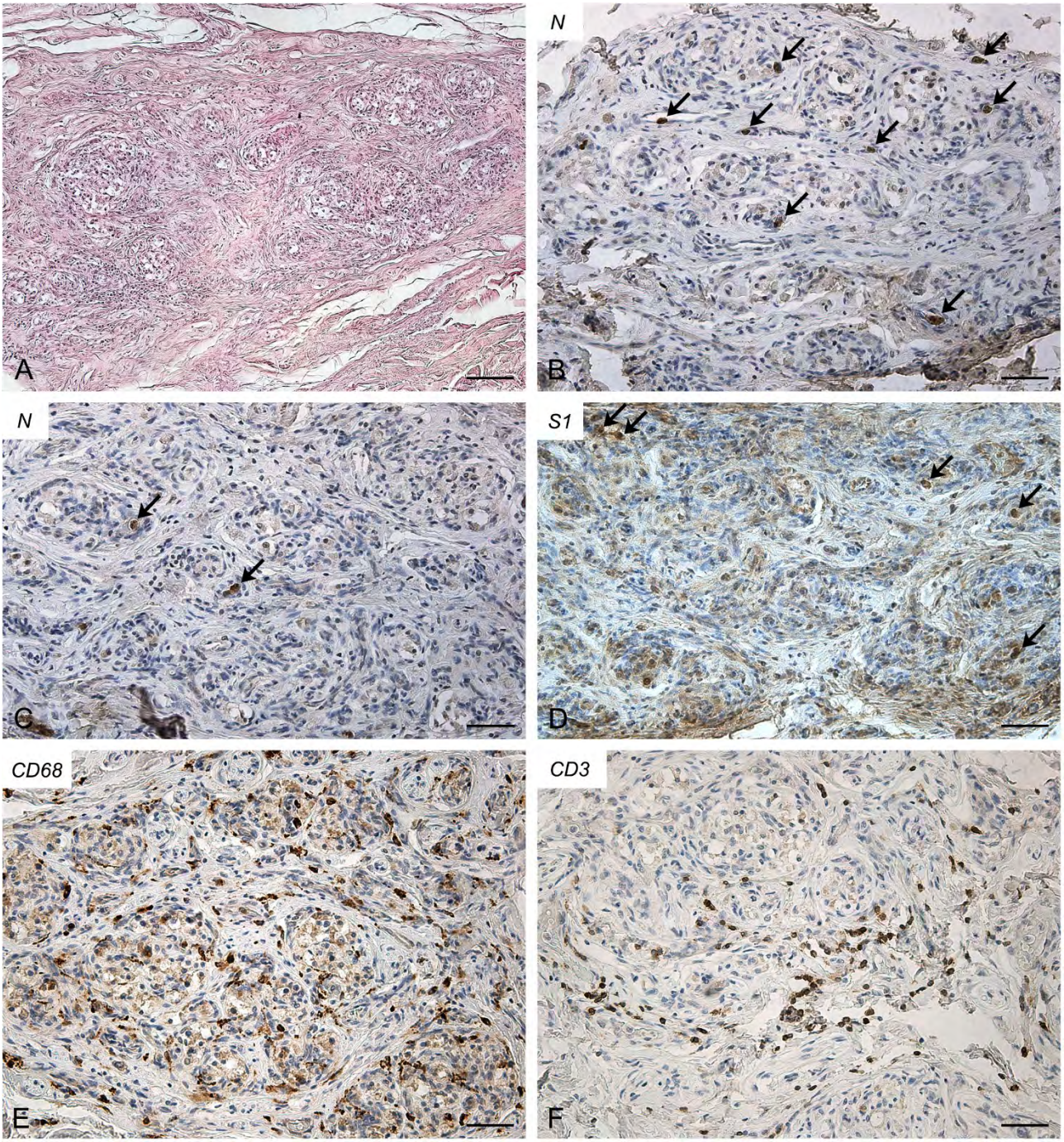

***Supplemental 5**. Left carotid body of Case 4 – Haematoxylin-eosin (A) and immunohistochemitries for nucleocapsid (B-C; arrows: positive cells), Spike (D; arrows: positive cells), CD68 (E) and CD3 (F). Scale bars: 100 µm (A); 50 µm (B-F).*

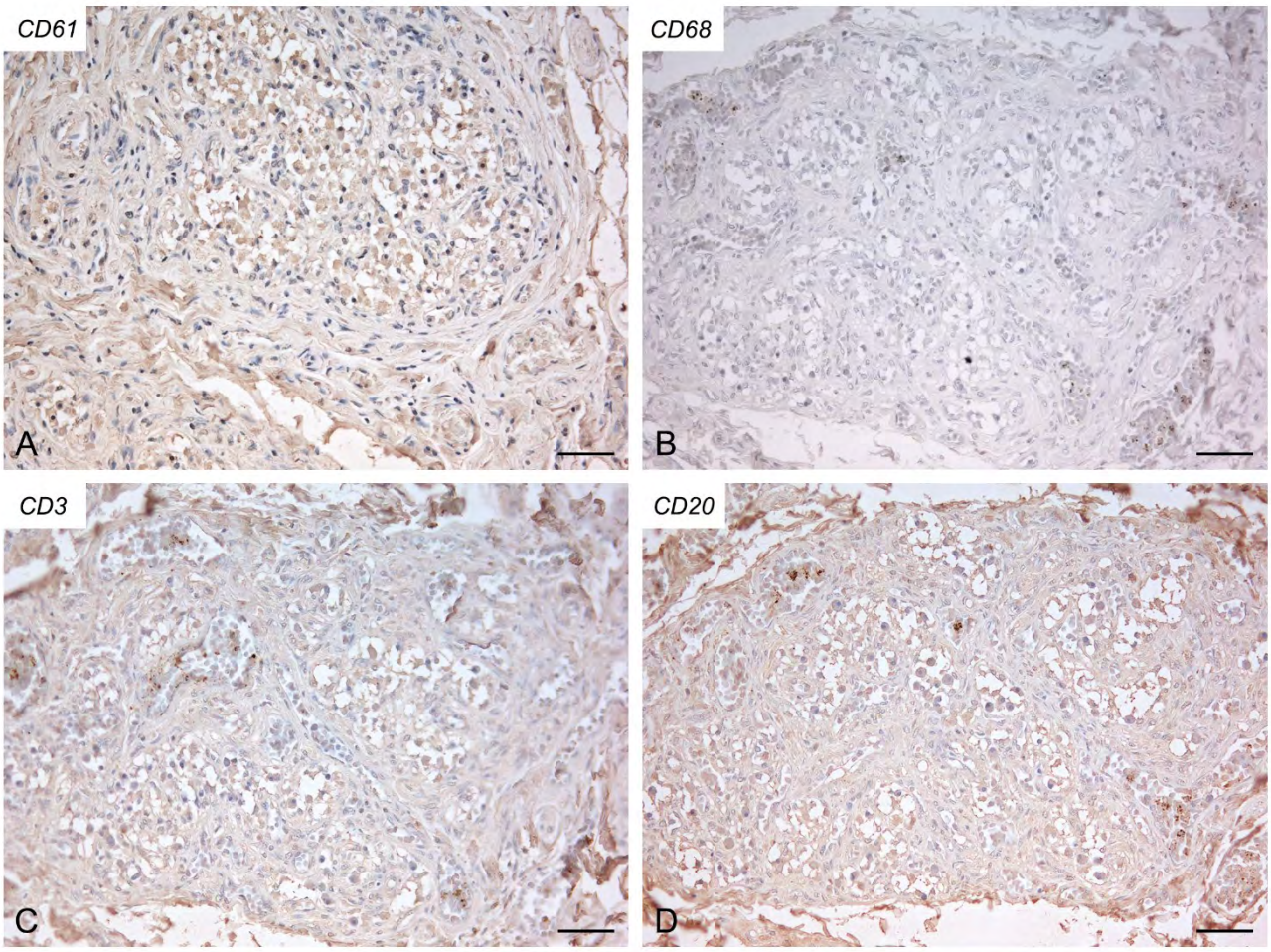

Supplemental 6. *Carotid body of control old subjects – Immunohistochemitries for CD61 (A), CD68 (B), CD3 (C) and CD20 (D). Scale bars: 50 µm (B-E).*

REFERENCES

1. Soliz J, Schneider-Gasser EM, Arias-Reyes C, Aliaga-Raduan F, Poma-Machicao L, Zubieta-Calleja G, et al. Coping with hypoxemia: Could erythropoietin (EPO) be an adjuvant treatment of COVID-19? *Respir Physiol Neurobiol* (2020) 279:103476. doi: 10.1016/j.resp.2020.103476.
2. Porzionato A, Emmi A, Stocco E, Barbon S, Boscolo-Berto R, Macchi V, et al. The potential role of the carotid body in COVID-19. *Am J Physiol Lung Cell Mol Physiol* (2020) 319:620-626. doi: 10.1152/ajplung.00309.2020
3. Simonson TS, Baker TL, Banzett RB, Bishop T, Dempsey JA, Feldman JL, et al. Silent hypoxaemia in COVID-19 patients. *J Physiol* (2021) 599:1057-1065. doi: 10.1113/JP280769.
4. Villadiego J, Ramírez-Lorca R, Cala F, Labandeira-García JL, Esteban M, Toledo-Aral JJ, et al. Is Carotid Body Infection Responsible for Silent Hypoxemia in COVID-19 Patients? *Function* (2020) zqaa032. doi: 10.1093/function/zqaa032.
5. Machado BH, Paton JFR. Relevance of carotid bodies in COVID-19: A hypothetical viewpoint. *Auton Neurosci* (2021) 233:102810. doi: 10.1016/j.autneu.2021.102810.
6. Patel KP, Schultz HD. Angiotensin peptides and nitric oxide in cardiovascular disease. *Antioxid Redox Signal* (2013) 19:1121-1132. doi: 10.1089/ars.2012.4614.
7. Anoop UR, Verma K. Happy Hypoxemia in COVID-19-A Neural Hypothesis. *ACS Chem Neurosci (*2020) 11:1865-1867. doi: 10.1021/acschemneuro.0c00318.
8. Porzionato A, Emmi A, Barbon S, Boscolo-Berto R, Stecco C, Stocco E, et al. Sympathetic activation: a potential link between comorbidities and COVID-19. *FEBS J* (2020) 287:3681-3688. doi: 10.1111/febs.15481.
9. Lambermont B, Davenne E, Maclot F, Delvenne P. SARS-CoV-2 in carotid body. *Intensive Care Med* (2021) 47:342-343. doi: 10.1007/s00134-021-06351-z.
10. Kantonen J, Mahzabin S, Mäyränpää MI, Tynninen O, Paetau A, Andersson N, et al. Neuropathologic features of four autopsied COVID-19 patients. *Brain Pathol* (2020) 30:1012-1016. doi: 10.1111/bpa.12889.
11. Porzionato A, Macchi V, Guidolin D, Parenti A, Ferrara SD, De Caro R. Histopathology of carotid body in heroin addiction. Possible chemosensitive impairment. *Histopathology* (2009) 46:296-306. doi: 10.1111/j.1365-2559.2005.02060.x.
12. Porzionato A, Macchi V, Parenti A, De Caro R Chronic carotid glomitis in heroin addiction. *Histol Histopathol* (2009) 24:707-715. doi: 10.14670/HH-24.707.
13. Lavezzo E, Franchin E, Ciavarella C, Cuomo-Dannenburg G, Barzon L, Del Vecchio C, et al. Suppression of a SARS-CoV-2 outbreak in the Italian municipality of Vo'. *Nature* (2020) 584:425-429. doi: 10.1038/s41586-020-2488-1.
14. Daly MB, Lambertsen CJ, Schweitzer A. Observations on the volume of blood flow and oxygen utilization of the carotid body in the cat. *J Physiol* (1954) 125:67-89. doi: 10.1113/jphysiol.1954.sp005143.
15. Barnett S, Mulligan E, Wagerle LC, Lahiri S. Measurement of carotid body blood flow in cats by use of radioactive microspheres. *J Appl Physiol* (1988) 65:2484-2489. doi: 10.1152/jappl.1988.65.6.2484.
16. Hurst G, Heath D, Smith P. Histological changes associated with ageing of the human carotid body. *J Pathol* (1985) 147:181-187. doi: 10.1002/path.1711470306.
17. Heath D, Khan Q. Focal chronic thyroiditis and chronic carotid glomitis. *J Pathol* (1989) 159:29-34. doi: 10.1002/path.1711590109.

18. Khan Q, Heath D, Nash J, Smith P. Chronic carotid glomitis. *Histopathology* (1989) 14:471-481. doi: 10.1111/j.1365-2559.1989.tb02183.x.
19. Khan Q, Heath D. Chronic carotid glomitis and the glomus pulmonale. J Clin Pathol (1990) 43:39-42. doi: 10.1136/jcp.43.1.39.
20. Khan Q, Smith P, Heath D. The distribution of enkephalins in human carotid bodies showing cellular proliferation and chronic glomitis. *Arch Pathol Lab Med* (1990) 114:1232-1235.
21. Sacramento JF, Andrzejewski K, Melo BF, Ribeiro MJ, Obeso A, Conde SV. Exploring the Mediators that Promote Carotid Body Dysfunction in Type 2 Diabetes and Obesity Related Syndromes. Int J Mol Sci (2020) 21:5545. doi: 10.3390/ijms21155545.
22. Iturriaga R, Alcayaga J, Chapleau MW, Somers VK. Carotid body chemoreceptors: physiology, pathology, and implications for health and disease. Physiol Rev (2021) 101:1177-1235. doi: 10.1152/physrev.00039.2019.

DISCUSSION

In the studies comprised in this PhD Thesis we have investigated the role of SARS-CoV-2 infection in determining neuropathological alterations underlying neurological manifestations in COVID-19, with particular regard to neurodegenerative diseases.

Our results indicate that while SARS-CoV-2 may directly enter the nervous system, either by crossing the blood-brain barrier or through retrograde spread throughout the vagus nerve, this occurs only in a fraction of subjects affected by COVID-19. Viral antigens and genomic sequences were detected in anatomically defined regions of the brainstem, specifically at the level of the vagal nuclei of the medulla and the substantia nigra of the midbrain, with evident similarities compared to both animal models of the disease and other known coronaviruses, such as SARS-CoV and MERS-CoV. However, despite the detection of markers suggestive of neuroinvasion, no direct damage to infected neurons was observed, with no evidence of neuronal necrosis, nuclear pyknosis, chromatolisis, somatic or nuclear inclusions or other morphological anomalies. It must be considered, however, that most patients died from 1 to 38 days following hospitalization, and thus died during the acute phases of COVID-19. Hence, it appears that in the acute phases of severe COVID-19, SARS-CoV-2 may enter the nervous system without directly causing damage to the brain. It is however unkown wheter damage may occur in later stages, or in patients who suffered a more chronic and prolonged course of the illness, as in our cohort the severity of the disease quickly led to patient exitus. Conversely, most neuropathological alterations detected in our cohort were to be attributed to hypoxic / ischaemic damage, small-vessel and microthromboses, microglial activation and overall neuroinflammation. While we detected statistically significant differences in local microgliosis between COVID-19 patients with and without viral antigens / genomic sequences in investigated anatomical loci, overall brainstem microgliosis did not differ within the COVID-19 group, and was more strongly associated to the degree of hypoxic / ischaemic damage of the brainstem. Nevertheless, we found statistically significant differences in brainstem microgliosis when comparing COVID-19 subjects to controls suffering from other respiratory infections / pneumonia, suggesting that neuroinflammation in COVID-19 is significantly more prominent and represents an important hallmark of the disease. Within the COVID-19 cohort, we also identified topographical differences in brainstem microgliosis, with the dorsal medulla and the ventral midbrain being significantly more affected. Microglia also displayed a peculiar phenotype,

characterized by throny morphology and expressing both homeostatic as well as activated markers. These findings indicate a peculiarity of neuroinflammation occurring in COVID-19, which appears to more likely explain brain damage and neurological manifestations compared to direct viral invasion occurring in our cohort, while also setting the disease apart from other respiratory infections. Hence, neuropathological alterations and neuroinflammation in COIVD-19 are likely caused by systemic infection and the ongoing cytokine storm, as well as occurring hypoxic / ischaemic damage, rather than direct viral invasion of the CNS, at least in the acute phases of the disease that can be evaluated in the neuropathological setting. Nevertheless, the documented viral antigens and genomic sequences in specific regions of the brainstem appear to support the neuroinvasive potential of SARS-CoV-2, and even though no direct damage was observed, these phenomena could represent the physiopathological bases for neurological manifestations occurring in cases of chronic infection, as well as post-COVID syndromes, such as “Long COVID”. In this context, the detection of SARS-CoV-2 antigens in the vagal nuclei of the medulla, which are responsible for the parasympathetic modulation of cardio-respiratory patterns as well as cardiochronotropic rhythms, could lead to progressive disruption of neuronal activity, as known to occur for other coronaviruses, and negatively influence patient respiratory conditions, further worsening the consequences of alveolar damage occurring at the level of the lungs. Furthermore, as the substantia nigra (both dopaminergic and non-dopaminergic part) appears to be affected in a similar manner, the presence of viral antigens and the co-occurring neuroinflammation (microgliosis, microglial nodules and instances of neuronophagia) is particularly concerning due to the well-known intrinsic neuropathological vulnerability of the structure. Prolonged infection and ongoing inflammation at the level of the substantia nigra can represent precipitating factors for neurodegeneration, and subsequent development of motor symptoms and parkinsonism.
Data deriving from our Genomic Surveillance Study also suggests that neurological manifestations and the severity of COVID-19 symptomatology are not likely related to variants of the viral genome, but rather to individual differences in the immune response. This further reinforces our findings concerning COVID-19 neuroinflammation in ex-vivo.

Moreover, our studies indicate that aside from the central nervous system, SARS-CoV-2 may affect the autonomic nervous system and peripheral chemoreceptorial structures as well, including the Carotid Body. These findings suggest that SARS-CoV-2 infection of the Carotid Body could potentially affect chemoreception. As a consequence, increased

peripheral arterial chemosensitivity and reflex sympatho-activation may contribute to the increased morbidity and mortality in COVID-19 patients with respiratory, cardiovascular, renal, or metabolic comorbidities.

CONCLUSION

Despite being originally considered as respiratory virus, SARS-CoV-2 leads to the development of a disease, known as COVID-19, that presents clinically-relevant multiorgan implications, including neuropathological alterations and neurological manifestations.

The findings of our studies indicate that SARS-CoV-2 may access the central nervous system in a small set of severe COVID-19 cases with fatal outcome. However, neuropathological alterations are to be ascribed to occurring neuroinflammation, hypoxic / ischaemic damage and microthromboses, with little evidence supporting direct damage to neuronal or glial cells by SARS-CoV-2. Our genomic surveillance study further supports our findings, suggesting no apparent relationship between viral genome mutations and neurological manifestations, but rather differences in individual immunitary responses in mediating clinical outcome. Furthermore, the involvement of the autonomous nervous system and the documented infection of peripheral chemoreceptors, such as the Carotid Body, help to characterize the mechanisms underlying COVID-19 severity and mortality in vulnerable populations, allowing to draw a distinct boundary between SARS-CoV-2 and other respiratory infections, as already demonstrated by our investigation on COVID-19 neuroinflammation.

Nevertheless, these findings, and the peculiar anatomical localization of viral antigens pave the road for further investigation, with particular regard to the role of viral infections in determining or precipitating neurodegeneration. Additional studies are required to clarify the long term effects of SARS-CoV-2 infection and the chronic outcome of occurring neuroinflammation. Fugure investigation on Long-COVID patients and on chronic COVID-19 survivors are therefore crucial to determine whether our findings represent a correlate of the acute phases of severe forms of the disease, or mediate disruptive long-term effects on the central nervous system with potential implications in neurodegenerative diseases.

AKNOWLEDGEMENTS

My gratitude and respect goes to the numerous people who contributed to our studies. First and foremost, to the patients who tragically died due to the effects of the pandemic, and to the body donors of the Institute of Human Anatomy, who willingly donated their body to Science, allowing us to perpetuate our research.

To Prof. Angelo Antonini and Prof. Raffaele De Caro, mentors and friends. To Prof. Andrea Porzionato and Prof. Veronica Macchi, for their guidance, continuous unconditioned support and patience. To Prof. Cristina Basso and Prof. Luisa Barzon, for their expertise and availability, without whom most of this research would not have been possible, and their respective teams, with whom it was a pleasure to collaborate. And to all colleagues, friends and family who supported the realization of this work.

OTHER RESEARCH CARRIED OUT DURING THE PhD

frontiers in Neuroanatomy

ORIGINAL RESEARCH
published: 16 April 2021
doi: 10.3389/fnana.2021.663399

3D Reconstruction of the Morpho-Functional Topography of the Human Vagal Trigone

Aron Emmi†, Andrea Porzionato†, Martina Contran, Enrico De Rose, Veronica Macchi and Raffaele De Caro*

Department of Neuroscience, Institute of Human Anatomy, University of Padua, Padua, Italy

The Vagal Trigone, often referred to as Ala Cinerea, is a triangular-shaped area of the floor of the fourth ventricle that is strictly involved in the network of chardiochronotropic, baroceptive, respiratory, and gastrointestinal control systems of the medulla oblongata. While it is frequently identified as the superficial landmark for the underlying Dorsal Motor Nucleus of the Vagus, this correspondence is not univocal in anatomical literature and is often oversimplified in neuroanatomy textbooks and neurosurgical atlases. As the structure represents an important landmark for neurosurgical procedures involving the floor of the fourth ventricle, accurate morphological characterization is required to avoid unwanted side effects (e.g., bradychardia, hypertension) during neuorphysiological monitoring and cranial nerve nuclei stimulation in intraoperative settings. The aim of this study was to address the anatomo-topographical relationships of the Vagal Trigone with the underlying nuclei. For this purpose, we have conducted an anatomo-microscopical examination of serial sections deriving from 54 Human Brainstems followed by 3D reconstruction and rendering of the specimens. Our findings indicate that the Vagal Trigone corresponds only partially with the Dorsal Motor Nucleus of the Vagus, while most of its axial profile is occupied by the dorsal regions of the Solitary Tract Nucleus. Furthermore, basing on literature and our findings we speculate that the neuroblasts of the Dorsal Motor Nucleus of the Vagus undergo neurobiotaxic migration induced by the neuroblasts of the dorsolaterally located solitary tract nucleus, giving rise to the Ala Cinerea, a topographically defined area for parasympathetic visceral control.

Keywords: neuroanatomy, vagal trigone, dorsal motor nucleus of the vagus, solitary tract nucleus, 3D reconstruction, 3D printing

OPEN ACCESS

Edited by:
R. Alberto Travagli, Pennsylvania State University, United States

Reviewed by:
Terry L. Powley, Purdue University, United States
Kirsteen Browning, Pennsylvania State University (PSU), United States

****Correspondence:***
Veronica Macchi
veronica.macchi@unipd.it

†These authors have contributed equally to this work and share first authorship

Received: *02 February 2021*
Accepted: *23 March 2021*
Published: *16 April 2021*

Citation:
Emmi A, Porzionato A, Contran M, De Rose E, Macchi V and De Caro R (2021) 3D Reconstruction of the Morpho-Functional Topography of the Human Vagal Trigone. Front. Neuroanat. 15:663399. doi: 10.3389/fnana.2021.663399

INTRODUCTION

The Vagal Trigone, also known as Ala Cinerea, is a topographical region of the Human Rhomboid Fossa located laterally to the Hypoglossal Trigone and medially to the Vestibular Trigone.

These medullary trigones represent important surface landmarks at the level of the rhomboid fossa during the dorsal approach to intraaxial pontomedullary lesions or during the ultimate exposure of the fourth ventricular floor as an intraventricular tumor is excised (Skinner, 2011). However, as visualized anatomy alone cannot be entirely relied upon before brainstem incision (Skinner, 2011) due to possible distortions given by intraventricular lesions or intraaxial tumors (Morota and Deletis, 2006), intraoperative electrophysiological stimulation, and monitoring is

employed to map the caudal rhomboid fossa and to assess nuclear integrity, particularly at the level of the Hypoglossal and Vagal Trigone. During stimulation, particular care must be taken to avoid injury to brainstem structures or excessive stimulation of vagal nuclei, which can lead to severe bradycardia or abrupt blood pressure changes: the vagal trigone is, in fact, topographically and functionally involved in the network of cardiochronotropic, baroceptive, respiratory, and gastrointestinal control systems of the medulla oblongata (De Caro et al., 2000; Travagli and Anselmi, 2016; Porzionato et al., 2019).

Although both neuroanatomy textbooks and neurosurgical atlases (e.g. Linn et al., 2009; Naidich et al., 2009; Skinner, 2011; Vanderah and Gould, 2015; Standring, 2018; Mirza and Das, 2020) identify a direct correspondence between the Vagal Trigone and the Dorsal Motor Nucleus of the Vagus, the topographical description of the district varies noticeably in literature. Furthermore, the anatomical terminology of these structures, with particular regard to the Dorsal Motor Nucleus of the Vagus (DMNV) and the Solitary Tract Nucleus (STN), does not appear to be univocal.

While the detailed delineation of the boundaries and subnuclear divisions of brainstem nuclei has already been characterized in literature, the relationship between superficial landmarks (such as the Vagal Trigone) and underlying structures has been investigated only in few studies, mostly based on observations deriving from a single specimen (Streeter, 1903; Weed, 1914). For this purpose, we have reviewed the scientific literature regarding the anatomical organization of the rhomboid fossa and conducted an anatomo-topographical study of serial sections of the human brainstem deriving from 54 Body Donors of the Body Donation Program of the University of Padua.

Background and Brief Review of Literature

The relationship between the morphology of the rhomboid fossa and the underlying nuclei of the brainstem tegmentum has been a subject of investigation since the early studies of Friederich Arnold and Benedikt Stilling (Stilling, 1842). With particular regard to the Vagal Trigone, Stilling described three triangular areas on each side of the dorsal median sulcus at the level of the caudal part of the rhomboid fossa: the Hypoglossal Trigone, the Vagal Trigone (Ala Cinerea), and the Vestibular Trigone. The Author first identifies the Vagal Trigone (Ala Cinerea) as a dark colored triangular area, hence the latin term "*cinerea*" (ashen, gray), extending from the Calamus Scriptorius, medially, to the acoustic striae, laterally.

According to Stilling, the Vagal Trigone is divided by a small ridge at the level of the base of the triangle, identifying anteriorly the area corresponding to the nucleus of the Vagus Nerve (X), and posteriorly the area of the nucleus of the Accessory Nerve (XI).

In 1896, Magnus Gustaf Retzius provides the most detailed description of the human rhomboid fossa, which is still largely used in modern anatomy textbooks (Retzius, 1896; Streeter, 1903). According to the Author, the Ala Cinerea is located laterally to the hypoglossal trigone and medially to the area acustica (comprising the vestibular trigone). The Vagal Trigone is separated from the caudally located Area Postrema by a well-marked ridge of ependyma, known as "Funiculus Separans," and extends forward between the area acustica and the trigonum hypoglossi, taking on the shape of a triangle with inferior base. According to Retzius (1896), Streeter (1903), and Weed (1914), the Ala Cinerea corresponds to the underlying Nucleus of the Ala Cinerea.

According to Dejerine (1902) there is a topographical correspondence between the Fasciculus Separans and the Solitary Tract. This, however, has not been found in Streeter's study (1903), who evidenced no apparent relation between the two structures.

In the work of Chiarugi and Bucciante (1965), the Authors identify two main nuclei at the level of the Ala Cinerea: the dorsal parasympathetic motor nucleus (dorsal motor nucleus of the vagus), visceromotor, and the nucleus of the Ala Cinerea, viscerosensory. The latter is described as lateral to the dorsal parasympathetic motor nucleus, and appears to be distinct from the solitary tract and the STN, which is described more ventrally; the STN described by the Authors corresponds exclusively to the mantle of gray matter strictly surrounding the solitary tract, with the Nucleus of the Ala Cinerea being considered as a separate structure. More recently McRitchie and Törk (1993) performed a detailed delineation of the outer boundaries and subnuclear divisions of the human STN, correlating the subdivisions to their homologs described in animals. Furthermore, the boundaries of the DMNV and of the other nuclei of the brainstem tegmentum were clearly delineated in humans by Paxinos and Huang (1995).

Within this context, it is necessary to define the relationship between the surface morphology of the rhomboid fossa and the underlying nuclei of the brainstem tegmentum in light of the more recent definition of the boundaries of these structures, not only for their proper description in neuroanatomy textbooks (Standring, 2018), but also for their relevance in neurosurgery and neurophysiological monitoring (e.g. Skinner, 2011).

MATERIALS AND METHODS

Fifty-four Human Brains with no history of neurological or psychiatric disorders deriving from the Body Donation Program of the University of Padua (Italy) (Porzionato et al., 2012; Boscolo-Berto et al., 2020) (mean age 63.4 years) were employed for the topographic examination of the rhomboid fossa. The brains were fixed in-toto in 4% phosphate-buffered paraformaldehyde for at least 3 weeks and subsequently sectioned in order to anatomically isolate the brainstem from the cerebrum at the level of the mesencephalon. The brainstem was then isolated from the cerebellum by sectioning the cerebellar pedicles in proximity to the cerebellar hylum. The choroid plexus of the fourth ventricle was then removed in order to clearly evaluate the morphology of the rhomboid fossa (**Figure 1**). Axial sections of the brainstem were then conducted perpendicular to the floor of the fourth ventricle, according to the schema in **Figure 2**.

Scaled photographs were taken of the cut surface prior and following tissue processing, in order to evaluate the amount of shrinkage induced by further processing according to previously published protocol (Porzionato et al., 2020a). Tissue sections were dehydrated, cleared in xylene, and embedded in paraffin.

FIGURE 1 | Morphology of the human rhomboid fossa. **(A)** Structures and landmarks of the rhomboid fossa. The Vagal Trigone (Ala Cinerea) appears as a triangular structure emerging from the Calamus Scriptorius and ending with its apex at the level of the Striae Medullares; caudally it is separated from the Area Postrema by the Funiculus Separans. AP, Area Postrema; FS, Funiculus Separans; VT, Vagal Trigone (Ala Cinerea); HT, Hypoglossal Trigone (Ala Bianca Interna); SL, Sulcus Limitans; SM, Striae Medullares (Acustic Striae of Piccolomini); SF, Superior Fovea; FC, Facial Colliculus. **(B–E)** Posterior view of four brainstems employed in the study, anatomically sectioned at the level of the mesencephalon, cranially to the superior colliculi, and at the level of the cerebellar pedicles.

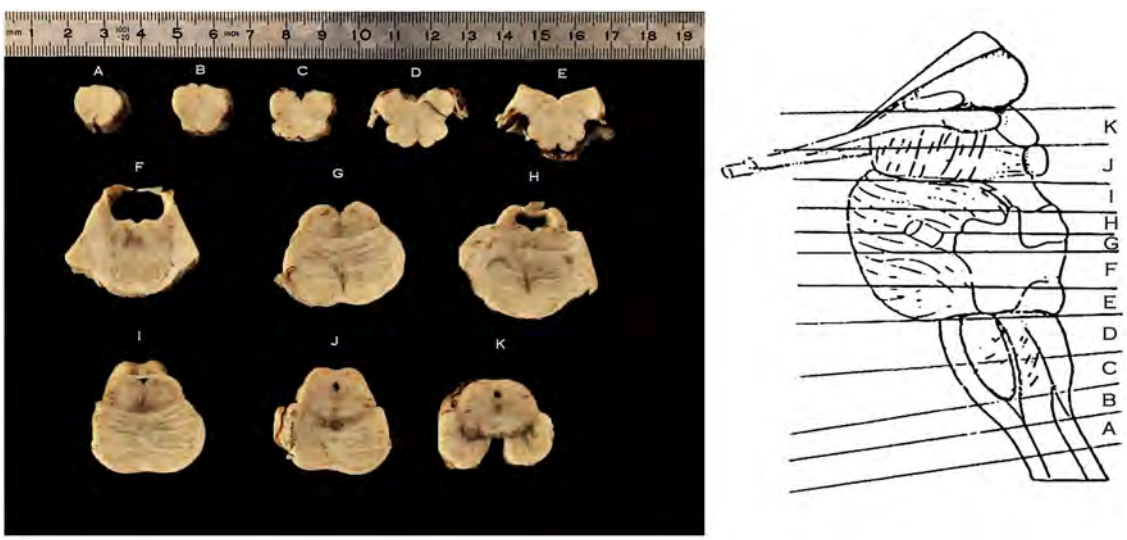

FIGURE 2 | Right, schematic representation of the levels of sectioning of the Human Brainstem, lateral perspective following isolation of the cerebellum; Left, axial sections of the brainstem according to the schema on the right; caudal surface facing upwards. From caudal to cranial: **(A)** section at the level of the decussation of the pyramids; **(B)** section at the level of the sensory decussation; **(C)** section at the level of the inferior half of the medullary olivary complex; **(D)** section at the level of the superior half of the medullary olivary complex; **(E)** section at the level of the caudal pons and the colliculus facialis; **(F,G)** section at the level of the intermediate pons; **(H,I)** section at the level of the cranial pons; **(J)** section at the level of the mesencephalo-pontine sulcus; **(K)** section at the level of the mesencephalon.

Since the Ala Cinerea was contained in most specimen in sections B–D, these were serially sectioned in 10-μm-thick axial sections using a calibrated rotatory microtome (RM 2235, Leica Microsystems, Wetzlar, Germany). Disposable metal microtome blades (Bio-Optica, Milan, Italy) were used with a cutting angle of about 5°. Systematic and uniform random sampling of the sections containing the Ala Cinerea was performed. In each specimen, three consecutive series of adjacent sections were taken at 1/10 interval, and stained (1) for Haematoxylin-Eosin (2) Cresyl Violet (Nissl), and (3) Luxol-Van Gieson stain.

Color images of the consecutive sections were acquired using a digital camera (Optikam HDMI, Optika srl, Italy), attached to a stereo microscope (SZM-2, Optika srl, Italy) operating with transmitted light at a primary magnification of x0.67. This allowed to acquire the whole profile of the sections for 3D reconstruction purposes.

Microscopic examination of the sections was performed under a Leica DM4500B microscope (Leica Microsystems) equipped with a motorized object table and a microcator with digital readout for measuring movements in the Z-direction with 0.5 μm precision. The microscope was connected to a Leica DFC320 high-resolution digital camera (Leica Microsystems) and a computer equipped with softwares for image acquisition (QWin, Leica Microsystems) and analysis (ImageJ).

The profile of the reliefs of the rhomboid fossa, along with the boundaries of the hypoglossal nucleus, dorsal motor nucleus of the vagus, solitary tract, and solitary tract nucleus were defined on 1.25x magnification according to Mai and Paxinos (2012) and drawn by three independent anatomists (RDC, AP, AE) employing ImageJ software, as seen in **Figure 3**. Briefly, Atlas boundaries and histochemical images were confronted with on-screen digital images of the specimen. Criteria for discerning neurons belonging to the different nuclei were identified as (1) topographical location along the medio-lateral axis; (2) average cell size; and (3) peculiar characteristics of specific nuclei defined in past anatomical literature (i.e., hyaline cytoplasmatic inclusions in hypoglossal neurons, pigmented neurons intercalated in STN, etc). Emphasis was set on the relationship between surface landmarks and underlying nuclear masses.

3D reconstruction procedures were employed on every specimen at the level of sections B–D, while one brasinstem was completely sectioned in its whole cranio-caudal extent and reconstructed in-toto for representation purposes.

Images of the consecutive sections were registered and aligned employing the Marquardt-Levenberg algorithm for non-linear least-squares optimization (Porzionato et al., 2020b). Cresyl violet stained sections were segmented through manual thresholding in order to isolate the neuronal somata (violet) from the background (unstained); thresholded images were then confronted with the original photomicrographs to ensure that no relevant elements were lost and to define the previously drawn boundaries. Hypoglossal nucleus, DMNV, Area Postrema, STN, and ST were defined as Regions of Interest (ROI) and coded with different colors (**Figures 4**, **5**).

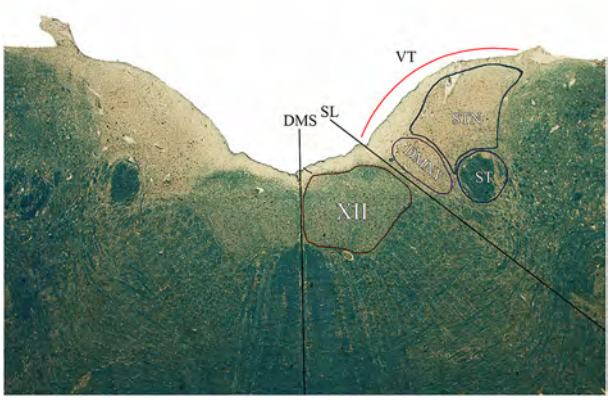

FIGURE 3 | Axial section of the brainstem tegmentum at the level of section C according to the Schema in **Figure 2**. DMS, dorsal median sulcus; SL, Sulcus Limitans; VT, Vagal Trigone; XII, Hypoglossal Nucleus; DMNV, Dorsal Motor Nucleus of the Vagus; ST, Solitary Tract; STN, Solitary Tract Nucleus.

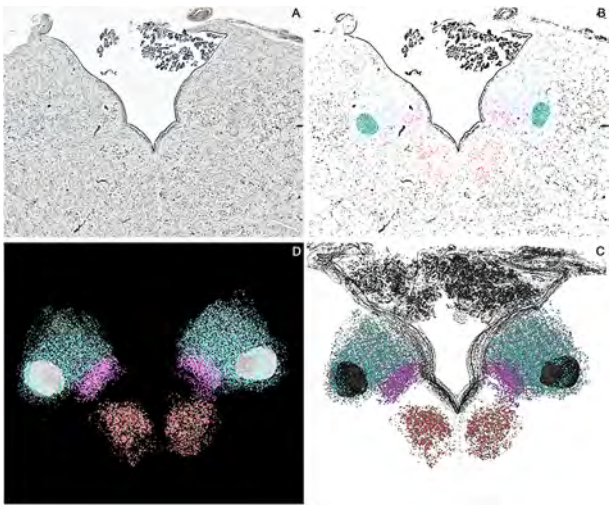

FIGURE 4 | Axial sections of one brainstem specimen at the level of the Ala Cinerea (Tissue sections **(B,C)** according to **Figure 1**). **(A)** Nissl Stained section, 1.25x Magnification. **(B)** Thresholded photomicrograph with color-labeled Regions of Interest (ROIs) for the Hypoglossal Nucleus (Red), Dorsal Motor Nucleus of the Vagus (Violet), Solitary Tract and Solitary Tract Nucleus (Blue). **(C)** 3D reconstruction of the neuronal profiles of the Hypoglossal Nucleus (Red), Dorsal Motor Nucleus of the Vagus (Violet), Solitary Tract, and Solitary Tract Nucleus (Blue) at the level of the Ala Cinerea [Tissue sections **(B,C)**]. **(D)** 3D Reconstruction of the Rhomboid Fossa along with the neuronal populations of the nuclei of the brainstem tegmentum (Hypoglossal Nucleus in Red; Dorsal Motor Nucleus of the Vagus in Violet; Solitary tract and nucleus in Blue).

Three-dimensional surface rendering was performed using the Visualization Toolkit (VTK, version 7.0), an open source library developed by Kitware Inc. (New York, USA) freely available at http://www.vtk.org. The 3D surfaces of the brainstem and of the defined ROIs were smoothed with a Gaussian Filter with 0.3 intensity and saved as.vtk files, which were then rendered

as a single scene in the Paraview software (version 5.0.1, Kitware Inc.). Labeling of surface structures was performed according to Paxinos and Huang (1995) and the review of literature.

In order to compare the virtual reconstruction to the real specimen prior to sectioning, 3D printing was performed on the in-toto reconstructed specimen in order to re-create the physical structure of the examined brainstem and to evaluate the quality of the reconstruction. For this purpose, Digital Light Processing 3D Printer (Elegoo Mars 3D Printer) was employed. Digital Light Processing based machines are used to create small models that require high resolution (10 μ on Z axis and 47 μ on X/Y axis) with a UV-sensitive (405 nm) liquid resin. The resulting model can be appreciated in **Figure 6**.

RESULTS

Upon macroscopic examination of the floor of the fourth ventricle, 47 (87.1%) specimen presented a slightly dark colored Ala Cinerea, with a typical triangular profile with the base emerging from the calamus scriptorius and the apex pointing toward the acoustic striae (**Figure 1**). In the remaining specimen (12.9%) the Ala Cinerea was also morphologically identifiable but presented a less prominent dark coloration.

The Vagal Trigone was found laterally to the Hypoglossal Trigone and medially to the Vestibular Trigone, as described by previous authors.

By comparing the boundaries identified by McRitchie and Törk (1993) and Paxinos and Huang (1995) with the nuclei described by the authors of the late nineteenth and early twentieth century (e.g., Stilling; Retzius; Streeter; Weed; Dejerine), it appears that: (a) the nucleus of the ala cinerea described by Stilling (1842), Streeter (1903), and Weed (1914) corresponds to Paxinos and Huang (1995) DMNV; (b) the nucleus of the ala cinerea described by Chiarugi and Bucciante (1965) corresponds to the medial subnucleus of the STN, while the STN defined by Chiarugi and Bucciante (1965) corresponds to the interstital, ventral, and ventrolateral subnuclei of the STN described by Paxinos and Huang (1995).

Microscopic examination of brainstem serial sections (sectioned according to the schema in **Figure 2**) revealed a topographical correspondence between the axial profile of the Vagal Trigone and the parasympathetic viscerosensory nuclei of the medullary tegmentum. In particular, both the DMNV and the STN were found within the axial surface of the Vagal Trigone. The DMNV was located medially, at the boundary between the Vagal Trigone and the Hypoglossal Trigone, while the STN was found laterally to the DMNV, representing most of the underlying gray matter of the Vagal Trigone (approximately two-thirds of the structure). The STN extended, in every specimen, from the DMNV to the medial border of the vestibular complex, as seen in **Figure 3**, and is represented caudally by the dorsolateral subnucleus, and rostrally by the dorsal subnucleus. Neurons of both DMNV and STN nuclei were found in close proximity to the ependymal surface of the fourth ventricle.

The sulcus limitans was clearly defined and identifiable in 47 specimen (87.1%), with a minor percentage showing a more flat profile of the floor of the fourth ventricle in microscopic examination; these findings match the macroscopic examination prior to sectioning, as stated above. In every specimen with a clearly marked sulcus limitans, the DMNV was located laterally, and in close proximity, to the sulcus itself. In a smaller percentage of specimen (eight specimen, i.e., 14.8% of the total sample) a superficial depression could be identified laterally to the DMNV. This depression, which did not match to the funiculus separans or any other previously described sulci, appeared to partially mark the superficial territory of the DMNV from the STN in these specimen. Laterally, the Ala Cinerea was bounded by a vertically descending sulcus, separating it from the vestibular trigone. This less prominent sulcus was evident 24 specimen (44%), while in the remaining percentage appeared as a less prominent depression at the level of the boundary between the lateral fringe of the Solitary Tract Nucleus and the nuclei of the vestibular trigone. When present, the sulcus originated cranially as a branching of the sulcus limitans, marking the boundary between Ala Cinerea and Vestibular Trigone.

3D reconstruction confirmed the aforementioned microscopic findings (**Figures 4–6**). In **Figure 4**, the axial perspective of the reconstruction identifies a correspondence between the Ala Cinerea and the DMNV (occupying the medial third of the Ala cinerea) and the STN (occupying the lateral two-thirds of the structure). **Figure 5A** shows the 3D rendering of the reconstructed brainstem, rendered in order to highlight surface morphology, while **Figure 5B** shows the segmented ROIs corresponding to the nuclei of the brainstem tegmentum. In **Figure 5C**, the surface projection of the aforementioned nuclei clearly shows the correspondence between the Ala Cinerea and the DMNV and STN, with the sulcus limitans and the funiculus separans separating the vestibular trigone from the hypoglossal trigone and the area postrema, respectively. 3D reconstruction of specimen presenting the accessory depression laterally to the DMNV did not reveal an appreciable landmark in surface morphology, being only visible in transverse sections during microscopic examination. 3D printing revealed good correspondence between the actual specimen and the reconstructed and 3D printed model, according to **Figure 6**.

DISCUSSION

The relationship between surface morphology and underlying brainstem nuclei arises from an historical interest that finds modern applications in neurosurgical procedures and neuroanatomical education.

The Vagal Trigone is an important landmark of the human rhomboid fossa, as it contains the main parasympathetic visceromotor and viscerosensory nuclei of the brainstem. The trigone is morpho-functionally embedded into the network of cardiochronotropic, baroceptive, and respiratory control systems of the medullary tegmentum, as well as gastrointestinal regulatory circuits (Browning and Travagli, 2019). With particular regard to cardiovascular control systems, the STN receives baroreceptor afferences from the carotid sinus nerve (Porzionato et al., 2019), while the nucleus ambiguus outputs

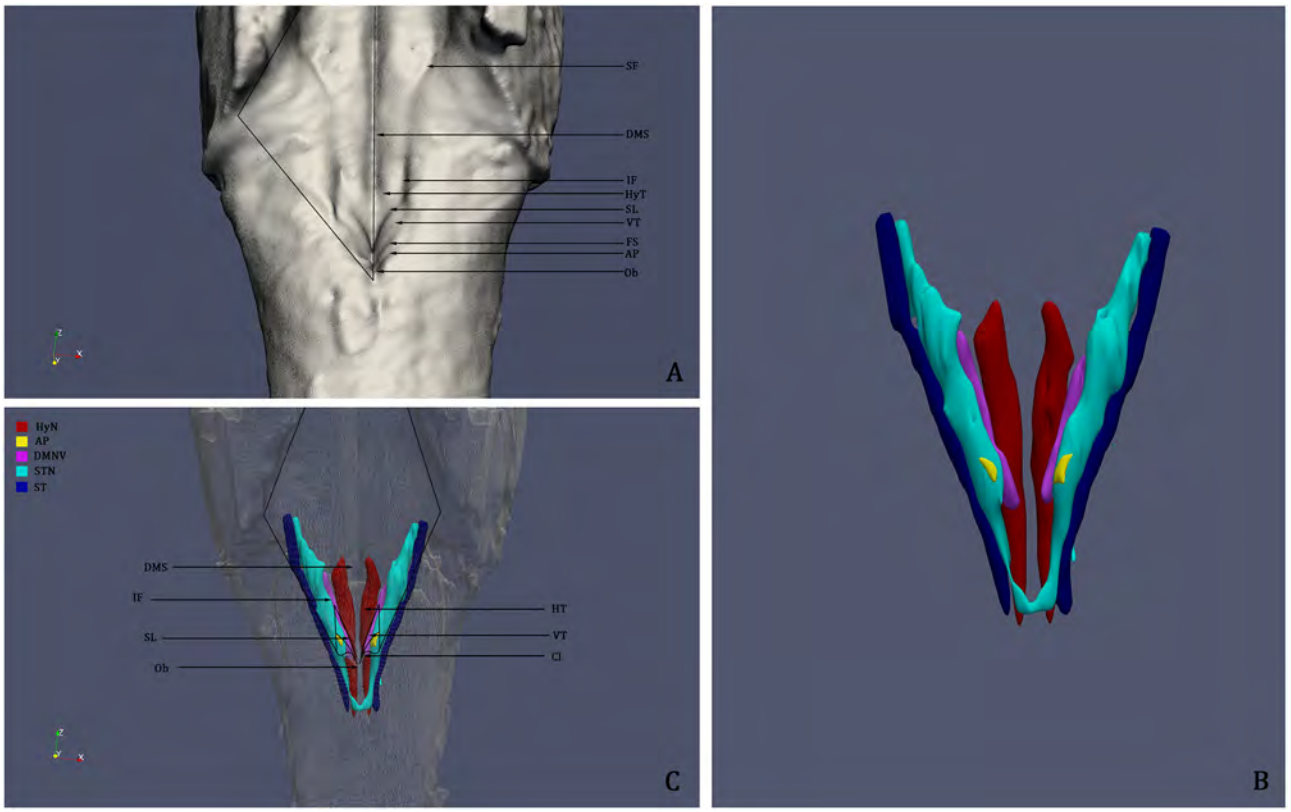

FIGURE 5 | (A) 3D reconstruction and rendering of the Human Brainstem, perspective on the Rhomboid Fossa. **(B)** 3D reconstruction of the nuclei of the brainstem tegmentum; **(C)** Surface projection of the nuclei of the tegmentum on the floor of the fourth ventricle; the rendering clearly shows that the Vagal Trigone (VT) contains both the Dorsal Motor Nucleus of the Vagus and the Solitary Tract Nucleus. DMS, Dorsal Median Sulcus; SF, Superior Fovea; IF, Inferior Fovea; SL; Sulcus Limitans; FS, Fasciculus Separans; HT, Hypoglossal Trigone; VT, Vagal Trigone; Ob, Obex; HyN, Hypoglossal Nucleus; AP, Area Postrema; DMNV, Dorsal Motor Nucleus of the Vagus; STN, Solitary Tract Nucleus; ST, Solitary Tract.

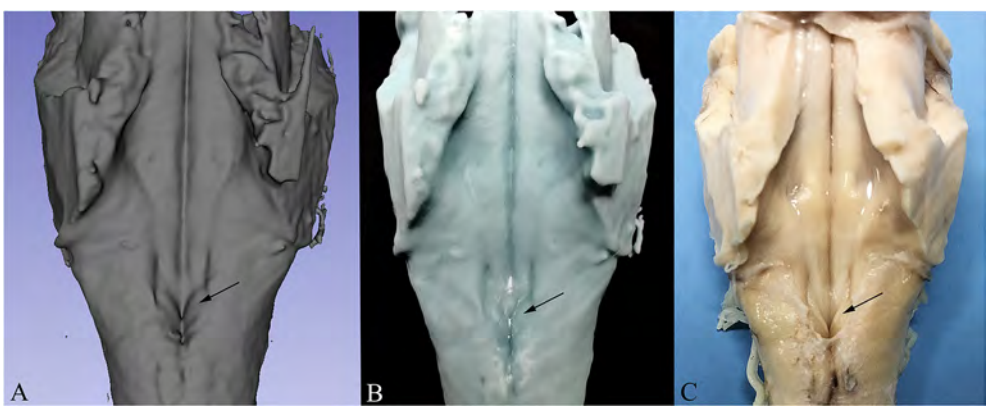

FIGURE 6 | Comparison between 3D Reconstruction **(A)**, 3D Print based on the reconstructed model **(B)** and the real specimen prior to sectioning **(C)**. The arrow indicates the Vagal Trigone in all three images.

cardioregulatory efferents, with a minor contribution from the DMNV. Electrical stimulation or mechanical injury during neurosurgical procedures at the level of the Vagal Trigone may lead to bradycardia, hypotension, or severe hypertension, particularly when the STN is involved (Colombari et al., 2001; Dampney et al., 2003; Skinner, 2011). Gastrointestinal dysfunction determined by vagal trigone injury must also be considered, as it may represent a relevant post-operatory concern

given the crucial role of the DMNV and STN in viscerosensory and visceromotor control of the alimentary tract (Mann et al., 1998; Travagli and Anselmi, 2016). Hence, accurate knowledge of the topography of the region is crucial in avoiding severe unwanted side effects during neurosurgery.

Embryologically, the sulcus limitans represents the primordial boundary between the motor Basal Plate and the sensory Alar Plate (Mai and Paxinos, 2012). In the adult spinal cord, the orthosympathetic visceromotor and general viscerosensory centers are found at the level of the boundary between the basis of the ventral and dorsal horn (Rexed Lamina 7 and 10) (Mai and Paxinos, 2012), with the viscerosensory centers being located more medially (intermediomedial nucleus) and the visceromotor centers (intermediolateral nucleus) being located laterally and matching the profile of the lateral horn. Similarly, at the level of the rhomboencephalon, the visceromotor and viscerosensory centers are located at the boundary between the derivates of the Basal Plate and the Alar Plate, in close proximity to the sulcus limitans, with the visceromotor DMNV being more ventro-medial and the viscerosensory STN being more dorso-lateral.

The peculiar disposition of these structures at the level of the rhomboencephalon, compared to their spinal cord homologs, can be inferred by the embryonal development of the rhombonecephalon. Starting from the 6th week of development, the basal plate differentiates into three distinct columns, with the most lateral one becoming the general visceral efferent column and giving rise to the DMNV at the level of rhombomers 7–8. In particular, ventrally migrating neuroblasts of the basal lamina give rise to the nucleus ambiguus (or Somatic Branchial Column), dorsally migrating neuroblasts give rise to the DMNV (General Visceromotor Column), while the Somatic Somitic Column (Hypoglossal Nucleus) remains in proximity of the midline. Conversely, the Alar Plate gives rise to the general visceral afferent column, being separated from the ventro-medially located general visceral efferent column by the sulcus limitans.

This disposition, which reflects the organization of the rhomboid fossa during early development, and in particular before the 9th gestational week (Paxinos and Huang, 1995; Cheng et al., 2004; Mai and Paxinos, 2012), does not appear to entirely match the topographical disposition of the visceromotor and viscerosensory centers of the brainstem tegmentum in adults, as testified by our current findings: the DMNV appears to be located laterally to the sulcus limitans, forming the Vagal Trigone along with the STN.

Interestingly, Cheng et al. (2004) used carbocyanine tracing to label DMNV neurons in the developing fetus (9th to 28th gestational week), identifying numerous labeled cells in proximity to the sulcus limitans. By closely examining the figures and the data reported in Cheng et al.'s work, it appears that: (a) the DMNV is located medially to the sulcus limitans in the 9 g.w. specimen and that (b) the same nucleus is found laterally to the sulcus limitans in older specimen (from g.w. 13th to 28th).

The dorsolateral migration of DMNV neuroblasts is also supported by morphological and pathological findings in cases of Sudden Infant Death Syndrome (Macchi et al., 2002). In these conditions, incomplete migration of the DMNV neuroblasts gives rise to morphological alterations in the brainstem tegmentum, such as hypocellular, more-medially located DMNV and hypercellular homolateral hypoglossal nucleus, possibly leading to abnormal autonomic cardio-respiratory control.

Together with our findings it could be speculated that neurons of the DMNV migrate dorsolaterally toward the STN starting from the 9th g.w. onwards, positioning laterally to the sulcus limitans. This phenomenon, which may be ascribed to neurobiotaxis, a chemotactic effect of visceral sensory neuroblasts on visceromotor neuroblasts, can explain the topography of the DMNV in adult humans, as evidenced by our anatomo-topographical investigation.

These events eventually lead to the morphological delineation of the Ala Cinerea, a specialized and topographically defined area for parasympathetic visceral control that, unlike its oversimplified representation in neuroanatomy textbooks and atlases, does not correspond entirely with the DMNV, but actually comprises the dorsal parts of the STN for two-thirds of its axial profile.

CONCLUSIONS

In the present paper, we present the anatomo-topographical organization of the nuclei underlying the human vagal trigone, or Ala Cinerea, following microscopical examination and 3D reconstruction of 54 brainstems. Our findings indicate that in every examined specimen, the Dorsal Motor Nucleus of the Vagus is located laterally and in close proximity to the sulcus limitans and forms the Vagal Trigone together with the STN, which occupies the lateral two-thirds of the axial profile of this structure.

The relevance of this study is not merely morphological, but resides in the anatomo-functional and clinical significance of the parasympathetic control centers in the brainstem, which are often oversimplified in neuroanatomy textbooks and represent an important landmark for neurophysiological monitoring during surgical procedures. While electrophysiological stimulation and recording are crucial for mapping the caudal rhomboid fossa during brainstem neurosurgery, particular care must be taken when evaluating the vagal trigone. Unlike its typical depiction in literature, only the medial third of the trigone corresponds to the DMNV, while the remaining lateral two-thirds corresponds to the dorsal and dorsolateral regions of the STN. According to our findings, the most constant superficial landmark for the identification of the underlying DMNV is represented by the sulcus limitans, which is located medially and in close proximity to the nucleus. As excessive electrical stimulation or injury to the STN is known to cause severe, at times irreversible, hypertension, bradychardia, and gastrointestinal dysfunction (Colombari et al., 2001; Dampney et al., 2003; Skinner, 2011), anatomical knowledge of the district appears crucial to avoid unwanted intra and postoperatory side effects given by injury to the areas of vagal trigone occupied by the STN.

Furthermore, previous studies have examined the role of the STN in acute heart failure (De Caro et al., 2000), which is anatomically located in a watershed zone that represents the last meadow (i.e., the periphery of a vascular territory vulnerable to low blood perfusion) in the case of sudden fall of the systemic blood flow due to acute heart failure. The STN and the DMNV have also received significant interest in COVID-19 research (Porzionato et al., 2020c), with particular regard to viral neurotropism. Considering the anatomical, clinical, and surgical relevance of these structures, and their peculiar organization in the human brainstem, detailed anatomo-topographical definition may represent a reference basis for further applied and clinical research, as demonstrated for other neuroanatomical structures (Emmi et al., 2020).

DATA AVAILABILITY STATEMENT

The raw data supporting the conclusions of this article will be made available by the authors, without undue reservation.

ETHICS STATEMENT

Ethical review and approval was not required for the study on human participants in accordance with the local legislation and institutional requirements. The patients/participants provided their written informed consent to participate in this study.

AUTHOR CONTRIBUTIONS

AE, RD, and AP conceived the study and examined the specimen. AE drafted the manuscript and the figures, and performed the 3D reconstructions. MC, ED, and VM critically reviewed the manuscript. All authors contributed to the final version of the manuscript.

ACKNOWLEDGMENTS

We are thankful to Dr. Anna Rambaldo for their technical support.

REFERENCES

Boscolo-Berto, R., Porzionato, A., Stecco, C., Macchi, V., and De Caro, R. (2020). Body donation in Italy: lights and shadows of law No. 10/2020. *Clin. Anat*. 33, 950–959. doi: 10.1002/ca.23623

Browning, K. N., and Travagli, R. A. (2019). Central control of gastrointestinal motility. *Curr. Opin. Endocrinol. Diabetes Obes*. 26, 11–16. doi: 10.1097/MED.0000000000000449

Cheng, G., Zhou, X., Qu, J., Ashwell, K. W., and Paxinos, G. (2004). Central vagal sensory and motor connections: human embryonic and fetal development. *Auton. Neurosci*. 114, 83–96. doi: 10.1016/j.autneu.2004.06.008

Chiarugi, G., and Bucciante, L. (1965). Istituzioni di Anatomia dell'Uomo. Milan: Vallardi Editore.

Colombari, E., Sato, M. A., Cravo, S. L., Bergamaschi, C. T., Campos, R. R. Jr., and Lopes, O. U. (2001). Role of the medulla oblongata in hypertension. *Hypertension* 38, 549–554. doi: 10.1161/01.HYP.38.3.549

Dampney, R. A., Horiuchi, J., Tagawa, T., Fontes, M. A., Potts, P. D., and Polson, J. W. (2003). Medullary and supramedullary mechanisms regulating sympathetic vasomotor tone. *Acta Physiol. Scand*. 177, 209–218. doi: 10.1046/j.1365-201X.2003.01070.x

De Caro, R., Parenti, A., Montisci, M., Guidolin, D., and Macchi, V. (2000). Solitary tract nuclei in acute heart failure. *Stroke* 31, 1187–1193. doi: 10.1161/01.STR.31.5.1187

Dejerine, J. (1902). *Anatomie des Centres Nerveux*. Paris: Rueff Editeurs.

Emmi, A., Antonini, A., Macchi, V., Porzionato, A., and De Caro, R. (2020). Anatomy and connectivity of the subthalamic nucleus in humans and non-human primates. *Front. Neuroanat*. 14:13. doi: 10.3389/fnana.2020.00013

Linn, J., Moriggl, B., Schwarz, F., Naidich, T. P., Schmid, U. D., Wiesmann, M., et al. (2009). Cisternal segments of the glossopharyngeal, vagus, and accessory nerves: detailed magnetic resonance imaging-demonstrated anatomy and neurovascular relationships. *J. Neurosurg*. 110, 1026–1041. doi: 10.3171/2008.3.17472

Macchi, V., Snenghi, R., De Caro, R., and Parenti, A. (2002). Monolateral hypoplasia of the motor vagal nuclei in a case of sudden infant death syndrome. *J. Anat*. 200, 195–198. doi: 10.1046/j.0021-8782.2001.00013.x

Mai, J. K., and Paxinos, G. (2012). *The Human Nervous System, 3rd Edn*. Amsterdam: Elsevier.

Mann, S. D., Danesh, B. J., and Kamm, M. A. (1998). Intractable vomiting due to a brainstem lesion in the absence of neurological signs or raised intracranial pressure *Gut* 42, 875–877. doi: 10.1136/gut.42.6.875

McRitchie, D. A., and Törk, I. (1993). The internal organization of the human solitary nucleus. *Brain Res Bull*. 31, 171–193. doi: 10.1016/0361-9230(93)90024-6

Mirza, M., and Das, J. (2020). "Neuroanatomy, area postrema [Updated 2020 Aug 10]," in *StatPearls [Internet]* (Treasure Island, FL: StatPearls Publishing).

Morota, N., and Deletis, V. (2006). The importance of brainstem mapping in brainstem surgical anatomy before the fourth ventricle and implication for intraoperative neurophysiological mapping. *Acta Neurochir*. 148, 499–509. doi: 10.1007/s00701-005-0672-6

Naidich, T. P., Duvernoy, H. M., Delman, B. N., Sorensen, A. G., Kollias, S. S., and Haacke, E. M. (2009). *Duvernoy's Atlas of the Human Brain Stem and Cerebellum*. Wien: Springer-Verlag. doi: 10.1007/978-3-211-73971-6

Paxinos, G., and Huang, X. F. (1995). *Atlas of the Human Brainstem*. San Diego, CA: Academic Press.

Porzionato, A., Emmi, A., Barbon, S., Boscolo-Berto, R., Stecco, C., Stocco, E., et al. (2020a). Sympathetic activation: a potential link between comorbidities and COVID-19. *FEBS J*. 287, 3681–3688. doi: 10.1111/febs.15481

Porzionato, A., Emmi, A., Stocco, E., Barbon, S., Boscolo-Berto, R., Macchi, V., et al. (2020b). The potential role of the carotid body in COVID-19. *Am. J. Physiol. Lung Cell Mol. Physiol*. 319, L620–L626. doi: 10.1152/ajplung.00309.2020

Porzionato, A., Guidolin, D., Emmi, A., Boscolo-Berto, R., Sarasin, G., Rambaldo, A., et al. (2020c). High-quality digital 3D reconstruction of microscopic findings in forensic pathology: the terminal pathway of a heart stab wound. *J. Forensic Sci*. 65, 2155–2159. doi: 10.1111/1556-4029.14497

Porzionato, A., Macchi, V., Stecco, C., and De Caro, R. (2019). The carotid sinus nerve-structure, function, and clinical implications. *Anat. Rec. (Hoboken)*. 302, 575–587. doi: 10.1002/ar.23829

Porzionato, A., Macchi, V., Stecco, C., Mazzi, A., Rambaldo, A., Sarasin, G., et al. (2012). Quality management of Body Donation Program at the University of Padova. *Anat. Sci. Educ*. 5, 264–272. doi: 10.1002/ase.1285

Retzius, G. (1896). Das Menschenhirn. *Studien in der makroskopischen Morphologie. I–II (Text und Tafeln)*. Stockholm: Norstedt.

Skinner, S. A. (2011). Neurophysiologic monitoring of the spinal accessory nerve, hypoglossal nerve, and the spinomedullary region. *J. Clin. Neurophysiol*. 28, 587–598. doi: 10.1097/WNP.0b013e31824079b3

Standring, S. (2018). *Gray's Anatomy: The Anatomical Basis of Clinical Practice*. Elsevier.

Stilling, B. (1842). Uber die Medulla *Oblongata*. Enke.

Streeter, G. L. (1903). Anatomy of the floor of the fourth ventricle. (The relations between the surface markings and the underlying structures.). *Am. Anat.* 2, 299–313. doi: 10.1002/aja.1000020303

Travagli, R. A., and Anselmi, L. (2016). Vagal neurocircuitry and its influence on gastric motility. *Nat. Rev. Gastroenterol. Hepatol.* 13, 389–401. doi: 10.1038/nrgastro.2016.76

Vanderah, T. W., and Gould, D. J. (2015). *Nolte's The Human Brain: An Introduction to Its Functional Anatomy*, *7th Edn*. Elsevier.

Weed, L. H. (1914). *Reconstruction of the Nuclear Masses in the Lower Portion of the Human Brain-Stem*. Washington DC: Carniege Institution Publisher.

Conflict of Interest: The authors declare that the research was conducted in the absence of any commercial or financial relationships that could be construed as a potential conflict of interest.

frontiers in Neuroanatomy

REVIEW
published: 22 April 2020
doi: 10.3389/fnana.2020.00013

Anatomy and Connectivity of the Subthalamic Nucleus in Humans and Non-human Primates

Aron Emmi[1], Angelo Antonini[2], Veronica Macchi[1], Andrea Porzionato[1] and Raffaele De Caro[1]*

[1] Institute of Human Anatomy, Department of Neuroscience, University of Padua, Padua, Italy, [2] Parkinson and Movement Disorders Unit, Neurology Clinic, Department of Neuroscience, University of Padua, Padua, Italy

The Subthalamic Nucleus (STh) is an oval-shaped diencephalic structure located ventrally to the thalamus, playing a fundamental role in the circuitry of the basal ganglia. In addition to being involved in the pathophysiology of several neurodegenerative disorders, such as Huntington's and Parkinson's disease, the STh is one of the target nuclei for deep brain stimulation. However, most of the anatomical evidence available derives from non-human primate studies. In this review, we will present the topographical and morphological organization of the nucleus and its connections to structurally and functionally related regions of the basal ganglia circuitry. We will also highlight the importance of additional research in humans focused on validating STh connectivity, cytoarchitectural organization, and its functional subdivision.

Keywords: subthalamic nucleus, Parkinson, anatomy, connectivity, topography

OPEN ACCESS

Edited by:
Yoland Smith,
Emory University, United States

Reviewed by:
Adriana Galvan,
Emory University, United States
Martin Parent,
Laval University, Canada

***Correspondence:**
Andrea Porzionato
andrea.porzionato@unipd.it

Received: *07 December 2019*
Accepted: *13 March 2020*
Published: *22 April 2020*

Citation:
Emmi A, Antonini A, Macchi V, Porzionato A and De Caro R (2020) Anatomy and Connectivity of the Subthalamic Nucleus in Humans and Non-human Primates. Front. Neuroanat. 14:13. doi: 10.3389/fnana.2020.00013

INTRODUCTION

The Subthalamic Nucleus (STh)[1], also known as Corpus Luysii, is an oval-shaped diencephalic structure located ventrally to the thalamus (Allheid et al., 1990; Parent and Hazrati, 1995; Joel and Weiner, 1997), playing a fundamental role in the circuitry of the basal ganglia. Described for the first time by Jules Bernard Luys (1865) (1828–1897), its functions remained largely unknown until 1927, when J. P. Martin reported the first case of hemichorea following lesion of the STh (Martin, 1927). As a key structure involved in the pathophysiology of several neurological disorders (e.g., Fedio et al., 1979; Martin and Gusella, 1986; Reiner et al., 1988; Albin et al., 1989b, 1990a,b; Alexander et al., 1990; Bahatia and Marsden, 1994; Ferrante et al., 1994; Lozano et al., 2002; Temel et al., 2006a; Temel and Visser-Vandewalle, 2006; Hardman et al., 1997), the STh has also become a target for deep brain stimulation (DBS) in Parkinson's Disease (PD) to modulate its firing patterns and improve clinical manifestations (Ranck, 1975; Lozano et al., 2002). In PD, the progressive loss of dopaminergic neurons in the substantia nigra pars compacta causes an alteration of the striatopallidal and pallidosubthalamical pathways in the basal ganglia, resulting in an abnormal burst-firing pattern in STh neurons (Magill et al., 2000; Urbain et al., 2002; Temel et al., 2005). DBS modulates STh firing,

[1]The abbreviation "STh," as seen in G. Paxinos's texts, is preferred over the more widely used "STN," as it may be confused for an abbreviation of Solitary Tract Nucleus.

resulting in improvement in motor and non-motor disability as well as quality of life (Grill and Mcintyre, 2001; Dostrovsky and Lozano, 2002; Grill et al., 2004; Mcintyre et al., 2004). However, adverse side effects of the treatment are not to be underestimated (Saint-Cyr et al., 2000; Berney et al., 2002; Kulisevsky et al., 2002; Temel et al., 2006a,b): in a recent review Temel et al. (2006a,b) reported that out of 1389 patients who underwent bilateral STh DBS, 41% presented cognitive dysfunctions and decline in executive functions, 8% exhibited major depression symptoms and further 4% showed signs of hypomania. Even though the authors evidenced no association between the surgical approach to STh DBS and the side effects of the treatment, a possible explanation for cognitive and affective dysfunctions following DBS may reside in the functional subdivision of the STh, which is known to project to different circuits of the basal ganglia in primates (Carpenter et al., 1981b; Smith et al., 1990; Shink et al., 1996; Joel and Weiner, 1997). Thus, the stimulation of specific areas of the nucleus may modulate connectivity within associative and limbic circuits of the basal ganglia (Vergani et al., 2007; Dafsari et al., 2016, 2018a,b; Fabbri et al., 2017; Hamel et al., 2017; Antonini and Obeso, 2018; Petry-Schmelzer et al., 2019). In the following review we critically assess the available literature on STh morphology, morphometry and structural connectivity. With respect to other reviews in literature, we present a detailed description of the topographical organization of STh connectivity by comparing non-human primate tracing studies and human fiber tracking studies, evidencing similarities and differences between humans and non-human primates and methodological approaches used. The evolution of STh functional subdivision models is also briefly assessed and compared to progress achieved in human and non-human primate connectivity studies. Hence, our aim is to summarize the available anatomical evidence regarding connections and functional subdivisions of the STh, while suggesting aspects that require further investigation.

ANATOMY OF THE SUBTHALAMIC NUCLEUS

As a diencephalic structure, the STh has a close topographical relationship with the nuclei of the basal ganglia and with the structures of the mesencephalon (**Figures 1**, **2A**). Dorsally, the STh confines with the zona incerta (ZI); the Field H2 of Forel, in particular the lenticular fasciculus, defines the dorsolateral margin of the nucleus, while the Field H1 of Forel, constituted mainly by the thalamic fasciculus, delineates part of its dorsomedial margin. The latter originates from the conjunction of the ansa lenticularis and part of the adjoining fibers of the lenticular fasciculus (Williams and Warwick, 1980), which separates the STh from the nucleus of the zona incerta. The ventromedial margin of the STh is delimitated by the ansa lenticularis, a white matter bundle originating from the ventral aspect of the lenticular nucleus which then joins the lenticular fasciculus to form the thalamic fasciculus, circumnavigating the medial aspect of the STh, as seen in **Figures 2B,C**.

Ventrally, the rostral regions of the STh confine with the dorsomedial aspect of the internal capsule as it continues into the base of the cerebral peduncle in the mesencephalon, while the most caudal part of the STh is situated atop the rostral extent of the substantia nigra (Allheid et al., 1990), in particular the dorsolateral aspect of the pars reticulata (**Figures 2B,C**). Dopaminergic nigrostriatal fibers pass dorsomedially to the STh through the medial forebrain bundle, where they enter the Fields of Forel and ascend to the striatum (Parent et al., 2000).

The STh is characterized by rich iron deposits (Rutledge et al., 1987) which can be evidenced through Perl's stain in histological sections (Massey and Yousry, 2010; Massey et al., 2012); furthermore, these deposits are known to accentuate in pathological conditions, such as PD (Kosta et al., 2006). The vascular supply of the STh derives mainly from the perforating branches of the anterior choroidal artery and the posterior communicating artery, originating from the internal carotid artery, and posteromedial choroidal arteries, which derive from the superior cerebellar artery, hence from the vertebrobasilar circulation (Hamani et al., 2004).

From a cytoarchitectonical perspective, the STh of rodents, non-human primates and humans is largely characterized by the presence of excitatory glutamatergic neurons (Type I Grey Neurons), even though a small population of γ-aminobutyric acid interneurons (Type II Grey Neurons) has been identified (Iwahori, 1987; Albin et al., 1989a; Parent and Hazrati, 1995; Shink et al., 1996; Clarke et al., 1997; Kearney and Albin, 2000; Wang et al., 2000; Tai et al., 2001; Levesque and Parent, 2005; Marani et al., 2008). In rodents Kita et al. (1983) evidenced two morphologically diverse subpopulations of projection neurons in the STh through horseradish peroxidase labeling:

1. Type I STh Neurons, characterized by (a) axon collaterals contacting STh neurons at a local level, and by (b) dense dendritic arborizations, especially in proximity of the perykarion.
2. Type II STh Neurons, which possess no axon collaterals at a local level and present fewer dendrites at a proximal level.

Both neuron types found in the rodent STh possess, however, a fundamental common feature which consists in a main axon dividing into two opposite-facing branches; the first branch ascends toward the lenticular nucleus, contacting mainly, but not exclusively, the globus pallidus; the second branch descends toward the mesencephalon and contacts the neurons of the substantia nigra pars compacta and pars reticulata (Gerfen et al., 1982; Kita et al., 1983; Kita and Kitai, 1987; Groenewegen and Berendse, 1990), as seen in **Figure 3**.

In primates, glutamatergic neurons in the STh are characterized by a large oval-shaped perykarion with a transverse diameter variable between 25 and 40 μm, whilst possessing wide dendritic arborizations which extend up to 400 μm from the soma; interneurons are more sparse, with fewer dendritic arborizations and generally smaller somata (Rafols and Fox, 1976; Yelnik and Percheron, 1979). Sato et al. (2000b) evidenced a branching pattern which varies in relationship to the target of the neurons: neurons contacting both the substantia nigra and the pallidal complex bifurcate in rostral and caudal branches

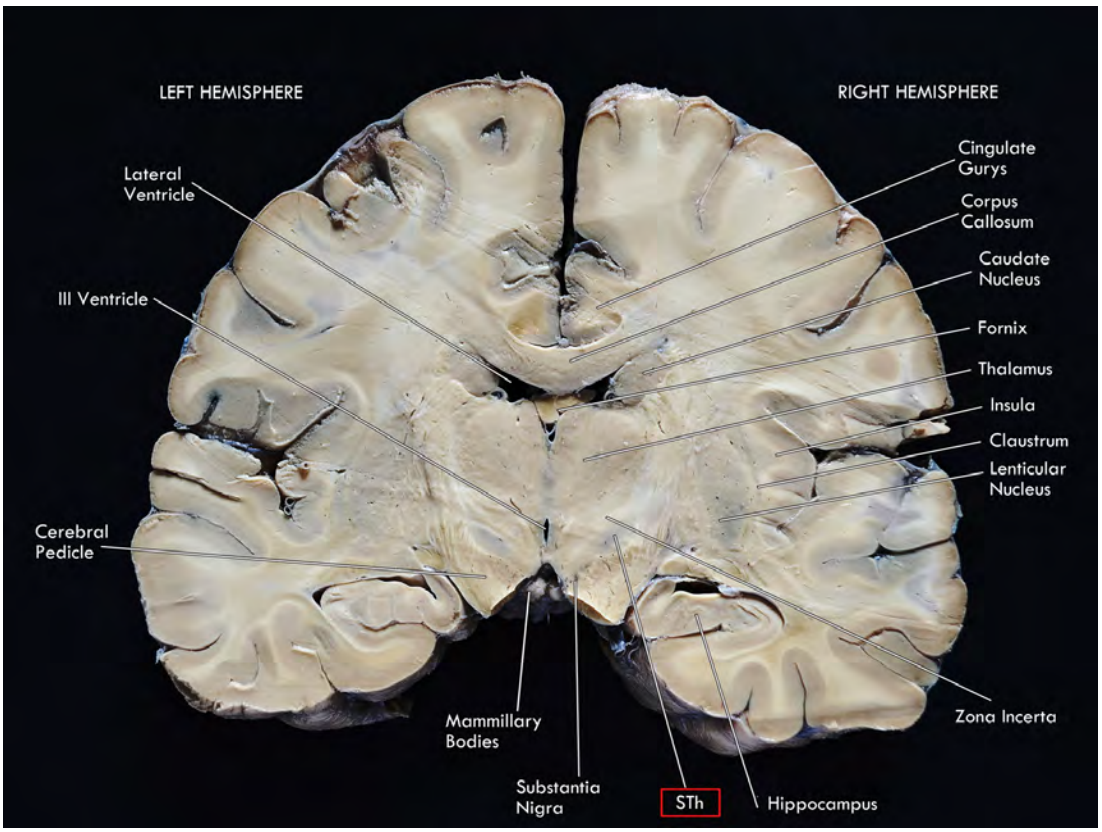

FIGURE 1 | Coronal macrosection of the human brain at the level of the mammillary bodies. Human specimen from the body donation program of the Institute of Human Anatomy of the University of Padua. The STh (Subthalamic Nucleus) appears as the slightly dark area dorsal to the Substantia Nigra and ventral to the Zona Incerta.

similarly to the neurons identified in rodents by Kita et al. (1983), while neurons projecting only to the striatum or the pallidal complex present a single branch which bifurcates in proximity of its target; in particular, the authors identified five subtypes of subthalamic neurons in non-human primates based on their axon branching patterns: (1) neurons projecting to the SNr, GPi, and GPe (21.3%); (2) neurons projecting to the SNr and GPe (2.7%); (3) neurons projecting to the GPi and GPe (48%); (4) neurons projecting to the GPe (10.7%); (5) neurons projecting to the striatum (17.3%). It appears evident that, compared to rodents, non-human primates present a more diverse population of subthalamic neurons with different axon branching patterns. The typical axonal bifurcation encountered in rodents by Kita et al. (1983; Kita and Kitai, 1987) is present only in a small portion of primate STh neurons (type I and II STh neurons according to Sato et al. (2000b) accounting only for the 24% of the total population identified by Sato et al. (2000b). The remaining neurons present a branching pattern that has no direct correspondence in rodents.

Even though the morphology of subthalamic neurons has been adequately studied in rodents, primates, and even in minipigs (Larsen et al., 2004), only few studies have examined human specimen (Levesque and Parent, 2005), thus representing a potential field for further investigations.

Levesque and Parent (2005) studied the morphological characteristics of GABAergic interneurons within the STh compared to the main population projection neurons. The interneurons were identified by a distinct glutamic acid decarboxylase (GAD) immunoreactivity and presented smaller somata than projection neurons (12 versus 24 μm) with thinner and less numerous dendrites. According to the authors, these neurons appear similar to the interneurons identified in non-human primates by Rafols and Fox (1976) through Golgi silver impregnation. Another interesting aspect identified by Levesque and Parent (2005) is the lack of parvalbumin (PV) and calretinin (CR) immunoreactivity of human GABAergic interneurons within the STh; in fact, only projection neurons appear to be immunoreactive for these calcium binding proteins. Furthermore PV + neurons appear more abundant dorsolaterally within the STh, while CR + neurons were predominant in the ventromedial STh.

Through stereology, Hardman et al. (2002) compared the neuronal population of the STh in rodents, non-human primates and humans. While the number of neurons was proportional to the cross-sectional area of the STh across species, the proportional amount of neurons expressing parvalbumin (a calcium binding protein) was significantly lower in rodents compared to non-human primates and humans. Considering

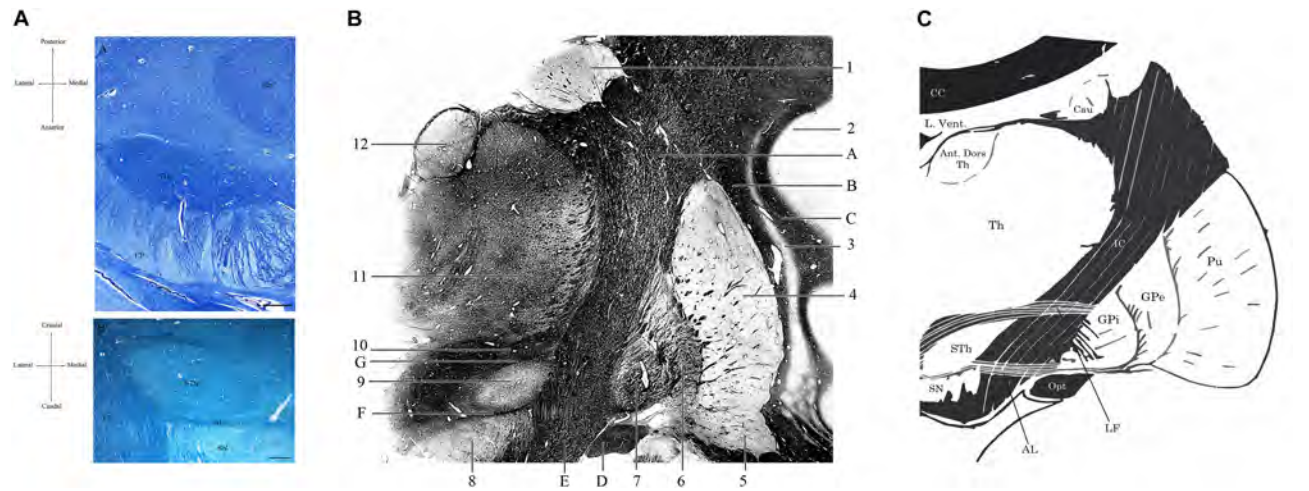

FIGURE 2 | (A) Horizontal section of the human brain at the level of the mesencephalon (A). Klüver-Barrera Stain. 1.25× Magnification, scale bar = 500 μm. STh, subthalamic nucleus; CP, cerebral peduncle; RN, Red Nucleus. (B) Coronal section of the brain passing through the Subthalamic Nucleus, posteriorly to the anterior commissure. Luxol Fast Blue Stain. 1.25× Magnification, scale bar = 500 μm. STh, subthalamic nucleus; CP, cerebral peduncle; AL, ansa lenticularis; LF, lenticular fasciculus; SN, substantia nigra; ZI, zona incerta. Human specimen from the body donation program of the Institute of Human Anatomy of the University of Padua. **(B)** Coronal section passing through the postcommissural basal ganglia and the subthalamic nucleus, Weigert-Pal Stain. Human specimen from the body donation program of the Institute of Human Anatomy of the University of Padua. 1, Caudate nucleus; 2, Insular cortex; 3, Putamen; 4, Claustrum; 5, Ventral regions of the putamen, in relationship with the substantia innominata; 6, External Globus Pallidus; 7, Internal Globus Pallidus; 8, Substantia Nigra; 9, Subthalamic Nucleus; 10, Zona Incerta; 11, Lateral and medial thalamic nuclei; 12, Anterior dorsal nucleus of the thalamus. A, Internal capsule; B, External capsule; C, Extreme Capsule; D, Optic tract; E, Cerebral peduncle; F, Ansa lenticularis; G, Lenticular Fasciculus. **(C)** Digital schematization of a coronal section passing through the postcommissural basal ganglia, similar to the section seen in panel **(B)**. STh, Subthalamic Nucleus; SN, Substantia Nigra; GPi, Internal Globus Pallidus. GPe, External Globus Pallidus; Pu, Putamen; Th, thalamus; Ant. Dors Th, Anterior Dorsal nuclei of the Thalamus; Cau, Caudate nucleus; L. Vent., Lateral Ventricle; CC, Corpus Callosum; IC, Internal Capsule; Opt, Optic Tract; LF, Lenticular Fasciculus; AL, Ansa Lenticularis.

FIGURE 3 | Neuron types in the STh according to rodent studies by Kita et al. (1983). **(A)** Type I STh neuron, characterized by local axon collaterals and dense proximal dendritic arborizations. **(B)** Type II STh neuron, with only two axon ramifications and less dense dendrites at a proximal level. GP, Globus Pallidus; SN, Substantia Nigra.

that the amount of PV + neurons increases in primates compared to rodents (Hardman et al., 2002) and that primate STh neurons present different axonal branching patterns compared to rodents (Sato et al., 2000b), one point of further investigation could be related to the expression of calcium binding proteins, such as parvalbumin, in the morphologically

different populations of neurons within the STh. Given that the expression of calcium binding proteins is related to different firing properties of neurons (Hardman et al., 2002), a combined morphological and molecular characterization of neuronal populations within the STh could improve our understanding of the physiology of STh's efferences and how external afferences are processed.

Unlike non-human primates, the morphology of human STh neurons has not yet been investigated through silver impregnation techniques. Morphologically different classes of STh neurons could represent functional subpopulations within the structure, possibly connected to different basal ganglia and cortical circuits.

Cytoarchitectonics: Further Investigation

The morphological characterization of Human STh represents one of the main areas which requires further investigation. In humans, technical limitations determined by silver impregnation techniques, such as the incomplete impregnation of fine structures like axons and smaller dendrites in formalin fixed tissue, do not allow for a complete visualization of axonal branching patterns. However, features such as somata size and shape, number of dendrites and dendritic branching pattern could help in the identification of morphologically distinct neuronal subpopulations in humans. Another point of interest is the topographical distribution of the morphologically defined neuronal subpopulations within the structure: for example, what is the dendritic branching pattern of neurons found in the ventromedial STh compared to neurons in the dorsolateral STh? Does the neuronal morphology reflect the type of afferences received? Is there a relationship between morphological characteristics of STh neurons and functional territories within the structure?

Morphometry of the STh

Few authors have approached the human STh from a morphometrical perspective and through the aid of unbiased stereology (Lange et al., 1976; Hardman et al., 2002; Levesque and Parent, 2005; Salvesen et al., 2015; Zwirner et al., 2017). We have reported stereology based studies on subjects with no clinical or pathological evidence in **Table 1**. Studies focused exclusively on subjects with clinical or pathological features were excluded, while only the values of healthy controls were included in the case of comparative studies between clinical and non-clinical populations (Salvesen et al., 2015).

From a methodological aspect, it must be noted that the stereological design varied notably across studies. Some authors (Hardman et al., 2002; Levesque and Parent, 2005) performed counting on 50–55 μm thick sections sampled at low ratio (1/20) with approximately 6–9 total sections evaluated, while other authors performed counting on 20 μm-thick paraffin-embedded sections sampled at higher ratio (1/10) (Zwirner et al., 2017). The age of the subjects included in the studies was also variable within and across studies (range is reported when standard deviation is missing): Lange et al. (1976): 50 years (24–99 range); Hardman et al. (2002): 74 ± 10 years; Levesque and Parent (2005): 50 ± 22.5 years; Salvesen et al. (2015): 69 years (60–75 range); Zwirner et al. (2017) 82 ± 10 years.

Tissue processing was also variable: in the case of Hardman et al. (2002) and Levesque and Parent (2005) the specimen were fixed in paraformaldehyde (PFA), cryoprotected in sucrose enriched phosphate-buffered saline (PBS) and cut with a cryostat. Lange et al. (1976), Salvesen et al. (2015) and Zwirner et al. (2017) employed paraffin embedding following formalin fixation. Due to the extensive dehydration of specimen during paraffin-embedding, significant shrinkage occurs and must be accounted for when estimating the volume of structures (Porzionato et al., 2015). While Zwirner et al. (2017) explicitly described shrinkage correction for volume estimation, the other two authors did not explicitly mention it in the manuscript.

The number of estimated neurons and the neuronal density in the STh varied significantly among studies. In the case of Salvesen et al. (2015), the values reported (900×10^3) refer to the bilateral number of neurons obtained by multiplying by two the estimated number of neurons; hence, the mean unilateral value corresponds to 450×10^3, and was reported as such in **Table 1** (no standard deviation or variance was reported). The studies by Zwirner et al. (2017) and Salvesen et al. (2015) were conducted on more subjects compared to previous studies (14 versus 10, respectively) and reported more concordant values for the estimated amount of neurons ($431 \pm 72 \times 10^3$ versus 450×10^3, respectively); also, as stated by Zwirner et al. (2017) their reported morphometrical parameters also appeared to be concordant with Hardman et al. (2002) (561 ± 30), but not with Levesque and Parent (2005) (239.5 ± 31.9). This could be related to tissue processing, subject variability and age.

According to Levesque and Parent (2005), the neuronal density of the STh displays a decreasing gradient from the posterior to the anterior aspect of the nucleus, whilst displaying an increasing gradient from the dorsal to the ventral part of the structure; this is also confirmed by Zwirner et al. (2017). Furthermore, the authors evidenced how the ventral aspect, and in particular the medial and posterior thirds of the nucleus, displayed the highest neuronal density of the entire structure. This appears to be coherent with the tripartite subdivision of the STh, as a higher density of projection neurons and interneurons is a typical feature of associative/limbic areas and is thought to reflect the complex integrative activity of these regions (Wu and Parent, 2000; Levesque and Parent, 2005), thus supporting the role of ventral (medial and lateral) aspects of the nucleus in associative/limbic circuitry.

As for the volume, three out of five studies found in literature displayed similar values (ranging from 114 to 144 mm^3), while the remaining two displayed higher values, ranging from 174 to 240 mm^3 (Hardman et al., 2002; Levesque and Parent, 2005). As previously stated, the difference may be attributable to the employment of formalin fixation and paraffin embedding by the three studies reporting lower values, even though shrinkage correction was applied in most cases. Zwirner et al. (2017) combined post-mortem 3 Tesla MRI volume estimation with unbiased stereology, with highly consistent results. To date, this is the only study which has compared STh volumes through both methods.

TABLE 1 | Morphometric studies on the human STh employing unbiased stereology.

Author	Embedding/ tissue processing	Number of subjects	Section thickness	Section interval	Number of sections	Stereological method	Number of neurons (10^3)	Volume (mm^3)	Neuronal density ($10^3/mm^3$)
Lange et al. (1976)	Paraffin	NS	NS	NS	NS	NS	286–306	134–144	–
Hardman et al. (2002)	Immersion in PFA, cryoprotected, cut with freezing microtome	5	50 μm	1/20	6	Optical fractionator	561 ± 30	240 ± 23	–
Levesque and Parent (2005)	Immersion in PFA, cryoprotected, cut with freezing microtome	5	55 μm	1/20	6–9	Optical disector	239.5 ± 31.9	174.5 ± 20.4	Anteroposterior axis: 1.14 (anterior); 1.39 (middle); 1.52 (posterior). Dorsoventral axis: 1.30 (dorsal); 1.36 (central); 1.44 (ventral). Mediolateral axis: 1.56 (medial); 1.25 (central); 1.39 (lateral).
Salvesen et al. (2015)	Paraffin	10	40 μm	1/4	NS	Optical disector	450 (SD not available)	114.4 (SD not available)	8.0 (SD not available)
Zwirner et al. (2017)	Paraffin	14	20 μm	1/10	NS	Optical fractionator	431 ± 72	131.58 ± 19.83	4.8 ± 1.32 (Dorsal) 8.0 ± 2.1 (Ventral) 6.3 ± 0.91 (Medial)

Morphometry: Further Investigation

Ultra-high field MRI should be employed in conjunction with unbiased stereology to accurately estimate STh volume. Gender and age related variations in volume, neuronal population and neuron density should also be taken into consideration.

SUBTHALAMIC NUCLEUS CONNECTIVITY: FUNCTIONAL SUBDIVISIONS OF BASAL GANGLIA CIRCUITRY AND METHODS OF INVESTIGATION

According to literature, the STh is characterized by several functional and regional subdivisions, with each region of the STh being structurally connected to either the sensomotor, cognitive or limbic circuit of the basal ganglia (Kita and Kitai, 1987; Smith et al., 1990; Parent and Hazrati, 1995; Joel and Weiner, 1997, 2000; Temel et al., 2006a). While several subdivisions of the basal ganglia have been proposed (Albin et al., 1989b), the most influential model of the organization of these structures views them as components of circuits connecting distinct thalamic, cortical and subcortical areas in a parallel manner, giving rise to relatively segregated connections, both anatomically and functionally (Alexander et al., 1986, 1990; Parent and Hazrati, 1995; Joel and Weiner, 1997, 2000). More recently, however, the structural segregation of the circuits of the basal ganglia has been questioned by several authors (Percheron et al., 1987, 1994; Reiner et al., 1988; Percheron and Fillon, 1991), providing evidence on the convergence of different afferent projections on dendritic fields in neurons of these subcortical structures (Smith et al., 1990, 1995; Shink et al., 1996). According to the classical tripartite organization proposed by Alexander et al. (1986), the basal ganglia can be subdivided into a motor and oculomotor circuit (forming together the general sensory-motor circuit of the basal ganglia); a dorsolateral prefrontal and lateral orbitofrontal circuit (forming the associative circuit); and an anterior cingulate circuit (also known as the limbic circuit).

- The motor circuit comprises mainly the primary, supplementary and pre-motor cortex; the dorsolateral part of the caudal putamen (postcommissural) and of the head of the caudate nucleus; the ventrolateral two thirds of the pallidal complex and part of the lateral substantia nigra; the ventrolateral, ventral anterior and centromedian nucleus of the thalamus.
- The associative circuit comprises mainly the dorsolateral and ventrolateral prefrontal cortex; the rostral regions of the striatum (precommissural); the dorsomedial regions of the pallidal complex and most of the substantia nigra; the parvocellular part of the dorsomedial nucleus of the thalamus.
- The limbic circuit comprises the orbitofrontal cortical regions and the anterior cingulate; the nucleus accumbens and the ventral pallidum; the rostral External Globus Pallidus (GPe) and the rostral ventromedial Internal Globus Pallidus (GPi); the medial regions of the substantia nigra and the ventral tegmental area of the mesencephalon; the parvocellular part of the ventral anterior nucleus and the magnocellular part of the dorsomedial nucleus of the thalamus.

Connectivity and Functional Subdivision of Subcortical Structures: Methods of Investigation

The connectivity and functional subdivision of nervous structures can be effectively studied through different means of investigation.

In non-human primates, the elective method to study the connectivity of subcortical structures such as the basal ganglia and the STh is represented by retrograde, anterograde or bidirectional tracing (Carpenter et al., 1981b; Smith et al., 1990; Joel and Weiner, 1997, 2000; Haynes and Haber, 2013; Coudé et al., 2018) and autoradiography (Nauta and Cole, 1978). Axonal tracing is currently considered the gold standard for studying anatomical connectivity in non-human primates. Through iontophoretic injection, bidirectional or anterograde tracers such as PHA-L (phaseolus vulgaris leucoagglutinin) and biotinylated dextran amine (Coudé et al., 2018) or retrograde tracers such as Fluoro-Gold (FG) and cholera toxin B (CTb) are injected in targeting sites through stereotaxic surgery, whilst animals are allowed to survive between 48 h and 14 days post-injection. The brains are then removed from the subjects and either postfixed in order to be processed for immunohistochemistry, or processed for autoradiography or confocal imaging; other tracing methods, such as the Marchi method (Whittier and Mettler, 1949) and silver techniques (Knook, 1965) were particularly popular in earlier studies, but are rarely found in recent literature.

In humans, structural and diffusion imaging techniques represent an important non-invasive tool for investigating STh connectivity both *in vivo* and *ex vivo*, even though important limitations must be considered. As far as DWI is concerned, the anatomical accuracy of brain connections derived from diffusion MRI tractography appears to be inherently limited (Jones et al., 2013; Thomas et al., 2014). According to Thomas et al. (2014) the anatomical accuracy of fiber reconstructions deriving from diffusion MRI appears to be highly dependent upon parameters of the tractography algorithm, with different optimal values for mapping different pathways. Tractography presents an inherent limitation in determining long-range anatomical projections based on voxel-averaged estimates of local fiber orientation obtained from DWI data. Furthermore, directionality of fibers can not be inferred, while the values regarding the connection strength between structures must be interpreted with care.

According to numerous authors (e.g., Jones et al., 2013; Thomas et al., 2014; Petersen et al., 2019) it appears necessary to complement tractography with histological and electrophysiological data in order to accurately map structural connectivity. In the case of STh research, MRI derived tractography should be based on the anatomical evidence derived by non-human primate tracing studies, as the electrophysiological properties of the STh can be studied

effectively and accurately only through recordings in DBS patients, given the subcortical localization of the structure.

However, while electrophysiological recordings in DBS patients have greatly improved our understanding of the STh's electrophysiological properties, measurements derive from an invasive approach requiring neurosurgery that allows recording only from patients with medical need for DBS (Alkemade et al., 2015). Hence, translation to normal STh physiology appears to be difficult, as it can be investigated in humans only in pathological states. Furthermore, the anatomical accuracy of these methods can not be compared to non-human primate fiber tracing and human MRI derived fiber tracking; while compelling results were provided by some authors (Fogelson et al., 2006) suggesting functional sub-loops between the STh and the motor areas of the cortex, the spatial resolution was too low to establish whether or not the recordings actually derived from the subthalamic area.

Considering the advantages and limitations of the aforementioned methods of investigation, anatomical evidence deriving from different sources should be integrated in order to generate an accurate representation of axonal pathways arising from and directed to the human STh.

Recently, Petersen et al. (2019) developed an holographic interface that allows the reconstruction of axonal pathways within the human brain by integrating different anatomical data deriving both from humans and non-human primates. In particular, the authors focused on the subthalamic region, with particular regard to STh connectivity. Data deriving from the vast array of non-human primate axon tracing studies was implemented within the interface and integrated with human histological and structural MRI studies. The holographic nature of the developed interface allowed for shared group sessions in which expert neuroanatomists reconstructed axonal pathways within the human subthalamic region basing on multifaceted anatomical evidence. According to the authors, the generated pathway atlas integrates anatomical detail regarding the STh in a manner that exceeds by far the capabilities of currently available tractography algorithms.

While the construction of the pathway atlas by Petersen et al. (2019) represents an important advance in modeling STh connectivity in humans, with important educational, clinical and research applications, limitations must also be considered. In fact, most connections reconstructed in the human pathway atlas derived from non-human primate studies. According to the authors, this requires inter-species assumptions on (a) the exact origin and termination points of fibers and (b) the maintenance of the somatotopic organization of the projections. Hence, non-human primate data should be integrated with other sources of anatomical evidence in humans, such as ultra-high field MRI (7 Tesla), to further enhance the accuracy of reconstructions.

STh Functional Subdivision: Tripartite Hypothesis

As a fundamental part of the basal ganglia circuitry, the STh is also connected to the circuits of the basal ganglia and presents, according to classical literature, a relatively distinct functional subdivision. The subdivision of the STh is founded on the connections which arise from the different brain regions conjoining with the aforementioned functional circuits. Thus, a peculiar region of the STh is defined mainly by the connections it forms with other cortical and subcortical structures and their relationship with the functional circuitry of the basal ganglia, while its intrinsic cytoarchitecture remains a current topic of investigation.

Among the very first to extensively review STh connectivity in non-human primates, although without considering its functional subdivision, Whittier and Mettler (1949) evidenced that out of 44 authors, 22 reported connections between the STh and the globus pallidus, while fewer reported projections to other areas, such as the mesencephalic tegmentum, putamen, substantia nigra, caudate nucleus, red nucleus, thalamus and commissural connections with the controlateral STh. As for afferent projections, extensive input appeared to originate mainly from the GPe (Ranson and Berry, 1941; Ranson et al., 1941; Nauta and Mehler, 1966). Successive studies further confirmed the importance of pallido-subthalamic projections, whilst expanding the STh circuitry by evidencing cortico-subthalamic, reticulo-subthalamic and thalamo-subthalamic afferences (Nauta and Cole, 1978; Smith et al., 1990; Parent and Hazrati, 1995; Shink et al., 1996). Basing on non-human primate tracing studies, a functional subdivision of the nucleus has been proposed by Parent and Hazrati (1995) and expanded by Joel and Weiner (1997): according to the authors, the medial third of the rostral two-thirds of the STh is connected mainly, but not exclusively, to the limbic circuit; the dorsolateral aspect of the rostral two thirds and most of the caudal third of the STh is connected mainly with the motor circuit; the ventrolateral aspect of the rostral two thirds and a small ventromedial region of the caudal third of the STh is connected with the associative circuit, as seen in **Figure 4**. This gives rise to a functional tripartition of the structure, which represents the main trend in classical literature on STh regionalization and connectivity, and has layed the ground for investigations on STh functional subdivision and connectivity in humans.

As for STh connectivity in humans, Aravamuthan et al. (2007) were among the first authors to employ diffusion MRI (1.5 Tesla) to study STh connectivity in living subjects through probabilistic tractography. The authors identified several regions with high probability of connection to the STh; these included the dorsal premotor cortex, the supplementary motor area, and the primary motor area for the lower limbs, trunk, arm and forearm, while the probable subcortical connections of the STh included the thalamus, pallidal complex, substantia nigra, and pedunculopontine nucleus. A topographical organization of the STh was also reported, with the motor cortical regions being connected to the dorsal STh and the associative cortical regions being connected to the inferior and medial STh. It must be noted, however, that the authors defined a single voxel based on surrounding landmarks that they were confident fell within the STh (Lambert et al., 2012); hence, results must be considered with caution, as the STh was not actually anatomically identified.

On the other hand, Lambert et al. (2012) were the first to employ a data driven method with DWI (in living human subjects) that evidenced three distinct clusters within the STh

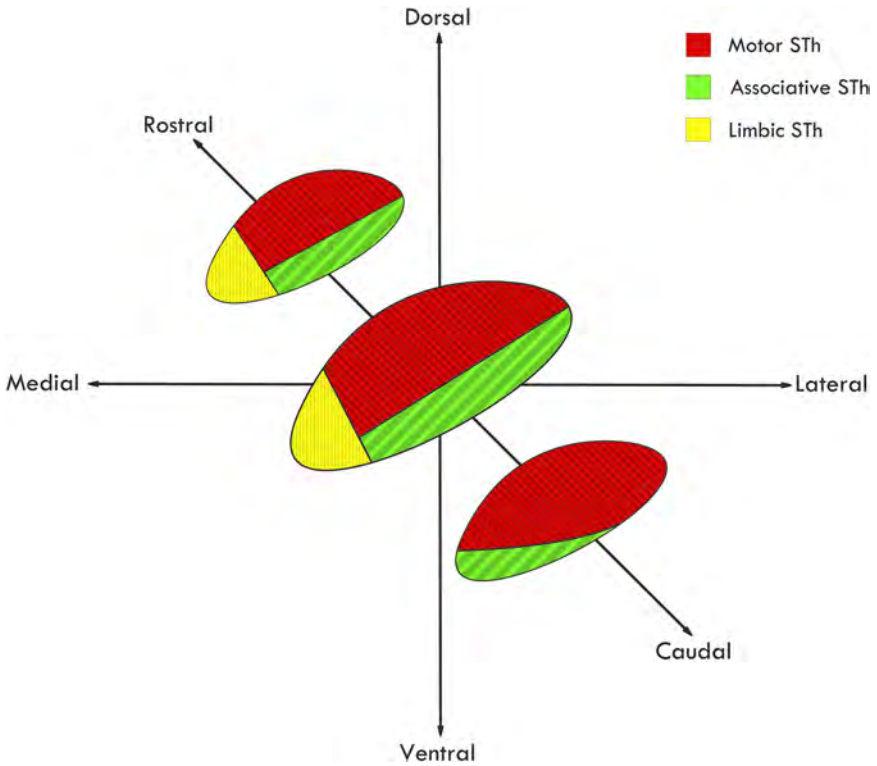

FIGURE 4 | Functional subdivision of the STh according to the classical tripartite hypothesis. Redrawn from various sources (Parent and Hazrati, 1995; Hamani et al., 2004).

based on brain connectivity profiles, largely corresponding to the functional tripartition hypothesized in non-human primates. The authors sub-parcellated the STh into the aforementioned functional territories and evidenced connections between the STh and subcortical structures that were coherent with the tripartite hypothesis; most cortical regions, on the other side, possessed some connections to all of the defined STh territories.

- The posterior aspect of the STh was identified as the motor region and showed connections with the posterior insula, posterior putamen and GPe, mid-caudate and ventro-lateral thalamic nuclei.
- The anterior STh was defined as the limbic region and was connected to the baso-lateral amygdala, mid-inferior putamen, mid-GPe and ventral-anterior thalamus.
- The associative STh was defined as a region with connections to both limbic and motor circuits which represented more of a functional gradient between motor and limbic territories rather than a distinct subregion.

It must be noted that, even though Lambert et al.'s (2012) study seems to support the tripartite hypothesis basing on the STh subparcellization, the authors clearly state that the STh territory commonly defined as associative actually represents an overlapping and topographically arranged transition between the limbic and motor territories, thus supporting the idea of functionally overlapping regions within the STh (Lambert et al., 2015).

Probabilistic tractography, employed by both groups albeit with significantly different methodologies, presents inherent limitations, as it estimates the probability of connection between seed and target regions. As stated by Lambert et al. (2012), seed and target region size, distance of tracking, regions with dense crossing fibers, MRI artifact and noise are all factors which can greatly influence fiber tracking. Again, results deriving from tractography must be interpreted with care and require complementary validation by histology and non-human primate studies.

Challenges to the Tripartite Hypothesis

A recent review by Keuken et al. (2012) has evidenced how variability across non-human primate tracing studies is not to be underestimated, with many authors disagreeing on both the number of STh subdivisions and on the localization of such subregions. Keuken et al. (2012) also advance the hypothesis of more than three functional subdivisions within the STh, with regard to Alexander et al. (1990) aforementioned hypothesis of five parallel loop circuits within the basal ganglia (sensorimotor, oculomotor, dorsolateral prefrontal, orbitofrontal, and anterior cingulate circuits).

Another critical point in the classical tripartite hypothesis of the STh is the segregation of anatomo-functional circuits; while

earlier studies suggested relatively segregated and defined STh subdivisions, more recent evidence points toward overlapping subregions and converging axonal afferents on large dendritic fields of neuronal populations of the structure (Percheron et al., 1987, 1994; Reiner et al., 1988; Smith et al., 1990, 1995; Percheron and Fillon, 1991,; Shink et al., 1996; Haynes and Haber, 2013; Alkemade et al., 2015).

As summarized by Alkemade and Forstmann (2014), evidence points toward a topographical organization of the STh without defined anatomical borders, with at least partial overlap between functional subregions within the structure; furthermore, according to the authors, the extent of functional overlap within STh subregions is still unclear and represents a point of further investigation.

On the other hand, numerous tracing studies aimed to identify the connections between the STh and other brain structures without considering their intrinsic functional subdivision. In fact, distribution of tracers is related to (a) injection site and (b) diffusion of the tracer within the injected structure; numerous studies, especially early tracing studies prior to the 1980s, did not consider the functional subdivision of the injection sites (Kim et al., 1976; Nauta and Cole, 1978; Smith and Parent, 1986; Parent and Smith, 1987). This is also related to the difficulty of selectively injecting small brain structures and to the intrinsic diffusion of the tracer within the site, along with the issue related to tracer diffusion to unrelated fibers passing within or close by large injection site. Furthermore, other studies only considered the connection between specific structures (such as the brainstem nuclei) and the STh (Lavoie and Parent, 1994c; Rico et al., 2010), which may or may not be related to the functional subdivision of the basal ganglia. Confirmation for the classical tripartite hypothesis has been recently provided by the very large tracing study carried out by Haynes and Haber (2013), indicating topographically organized projections arising from cortical areas directed to specific regions within the STh compatible with the subdivision proposed by previous authors (Parent and Hazrati, 1995; Joel and Weiner, 1997).

In conclusion, controversy on STh subdivision location, boundaries and circuit segregation remains a topic of current debate between research groups, and further confirmation is needed by combining ultra-high field MRI, histology and cytoarchitectonics (Alkemade et al., 2015).

In the following paragraphs, the connectivity of the STh will be studied considering mainly non-human primate tracing studies, whilst also integrating information coming from the few available human fiber tracking studies through DTI and DWI both *in vivo* and *ex vivo*, in order to highlight aspects which require further investigation in humans. For an extensive revision of non-human primate *in vivo* tracing studies involving the STh, refer to **Table 2**.

STh CONNECTIONS IN NON-HUMAN PRIMATES AND HUMANS

Cortical Connections With the STh

The existence of cortico-subthalamic projections is well documented in non-human primates (Kunzle and Akert, 1977; Von Monakow et al., 1978; Parent and Hazrati, 1995; Haynes and Haber, 2013; Ishida et al., 2016; Coudé et al., 2018), with few studies investigating the pathway also in humans through DTI and DWI. This pathway is also referred to as the "hyperdirect pathway" of the basal ganglia, in regards to the direct and indirect pathway subdivision.

Non-human Primate Studies

The very first authors to report cortico-subthalamic projections were Kunzle and Akert (1977), evidencing diffuse projections to the STh originating from Brodmann area 8. Further investigation by Von Monakow et al. (1978) evidenced a peculiar topography of the connections arising from the frontal cortex: Brodmann area 4 appears to be connected with the dorsolateral regions of the STh; Brodmann area 6 appears to be connected to the central third of the STh, while Brodmann area 8 appears to be connected to the ventral regions of the STh. The authors were unable to identify any projections arising from Brodmann areas 9 and 3,1,2.

Recently, Haynes and Haber (2013) conducted an extensive study on the cortical projections to the STh in non-human primates, evidencing the following connections: the dorsal anterior cingulate cortex appears to be connected to the medial tip of the STh (limbic circuit); the dorsal prefrontal cortex (Brodmann area 9 and 46) projects to the medial half of the STh; the rostral dorsal prefrontal cortex (rostral Brodmann area 6) projects to the medial half of the caudal STh; the caudal dorsal prefrontal motor cortex (caudal Brodmann area 6) projects to the ventrolateral STh, while the primary motor cortex shows connections to the dorsolateral regions of the STh (thus part of the motor circuit). No clear connections between the ventromedial prefrontal cortex and the STh were evidenced. These results were further confirmed by Ishida et al. (2016) and Coudé et al. (2018) which revealed that the ventral premotor cortex is connected mainly to the caudal dorsolateral STh and rostral ventrolateral STh, and that the projections arising from the motor cortex originate from the V layer (deep pyramidal cell layer). Interestingly, Coudé et al. (2018) evidenced how the cortico-subthalamic fibers are actually axon collaterals of corticofugal fibers that in most cases also project to the zona incerta and the red nucleus. Hence, in accordance to these results, the hyperdirect pathway from the cortex is not exclusively devoted to the STh, but projects also to other subcortical nuclei.

With particular regard to the projections arising from the primary motor cortex (M1), a somatotopic organization is reported (Parent and Hazrati, 1995; Hamani et al., 2004): the leg, arm and orofacial structures appear to be represented in the medial, lateral and dorsolateral portions of the STh, respectively. According to Nambu et al. (1996, 1997, 2000) the lateral portion of the STh receives projections from the primary motor cortex and presents a medial to lateral representation of the leg, arm and face, while the medial portion of the nucleus receives fibers from the supplementary motor area, dorsal and ventral premotor cortex and presents an inverse somatotopic distribution. The somatotopic organization of M1 projections to STh has been confirmed in Miyachi et al.'s study (2006), in accordance to Nambu et al. (1996, 2000).

To date, no studies reported subthalamo-cortical projections.

TABLE 2 | Non-human primate axon tracing studies.

Author(s)	Species	Technique	Tracing agent	PI.T.*	Injection site(s)	Connection(s) evidenced
Carpenter et al. (1976)	*Rhesus monkeys*	Anterograde tracing (Autoradiography)	[^{3}H]- aminoacids (L-leucine, L-proline, L-lysine)	68 h–22 days	Rostrolateral SN	Whole extent of the STh
					Caudolateral SN	No connections to STh evidenced
					Rostromedial SN	Medial STh
					Central SN	No connections to STh evidenced
Kim et al. (1976)	*Rhesus monkeys*	Anterograde tracing (Autoradiography)	[^{3}H]- aminoacids (L-leucine, L-proline, L-lysine)	5–28 days	GPi	No connections to STh evidenced
					GPe	Whole STh except caudal and medial regions
					Putamen	No connections to STh evidenced
Kunzle and Akert (1977)	*Macaca fascicularis*	Anterograde tracing (Autoradiography)	^{3}H-proline	2–3 days	Brodmann area 8	Subthalamic nucleus (no topography specified)
Nauta and Cole (1978)	*Macaca mulatta*	Anterograde tracing (Autoradiography)	Tritiated aminoacids (NS)	7–13 days	STh	1. Pallidal complex 2. SN 3. Ventral lateral and ventral anterior thalamic nuclei 4. PPT (pars compacta) 5. Putamen
Von Monakow et al. (1978)	*Macaca fascicularis*	Anterograde tracing (Autoradiography)	Radioactive labels: arginine, leucine and proline.	2–8 days	Brodmann area 4	Dorsal and lateral STh
					Brodmann area 6	Central STh
					Brodmann area 8	Ventral STh
					Brodmann area 9	No connections to STh
					Brodmann area 3,1,2	No connections to STh
DeVito et al. (1980)	*Macaca mulatta*	Retrograde tracing	Horseradish peroxidase	48–65 h	GPi	Central and ventromedial STh
Carpenter et al. (1981a)	Squirrel monkey (*Samiri sciureus*)	Retrograde tracing	Horseradish peroxidase	24–72 h	Outer portion of the GPi (rostral and dorsal regions)	Ventral and medial thirds of the caudal third of the STh
					Central GPi	Medial third of the caudal third of the STh
					Apical GPi	Medial third of the caudal two thirds of the STh
					Rostral division of the GPe	Medial third of the middle third of the nulceus
					Central division of the GPe	Whole rostral third of the STh; central and dorsal regions of the caudal two-thirds of the STh

(Continued)

TABLE 2 | Continued

Author(s)	Species	Technique	Tracing agent	PI.T.*	Injection site(s)	Connection(s) evidenced
		Anterograde tracing (Autoradiography)	^{3}H-aminoacids (NS)	NS	GPi	No connections evidenced to STh
					Rostral division of the GPe	Medial two-thirds of the rostral third of the STh; Central part of the middle third of the STh
					Central division of the GPe	Lateral third of the STh
Carpenter et al. (1981b)	Squirrel monkey (*Samiri sciureus*)	Retrograde tracing	Horseradish peroxidase	48 h	Subthalamic nucleus	1. GPe, regions adjacent to the lateral medullary lamina 2. SN (pars compacta and pars reticulata) 3. PPT 4. Dorsal nucleus of raphe
		Anterograde tracing (Autoradiography)	L-leucine + L-proline	5–8 days	Subthalamic nucleus	1. Pallidal complex (with inverse dorsoventral topography) 2. Substantia nigra 3. Ventral anterior, ventral lateral and dorsomedial nuclei of the thalamus
					Substantia Nigra	Subthalamic nucleus (no topography specified)
DeVito and Anderson (1982)	*Macaca Mulatta*	Anterograde tracing (Autoradiography)	L-proline + L-leucine + L-lysine	48–65 h	Internal Globus Pallidus	Uncertain connection to STh
					External Globus Pallidus	Whole STh
Smith and Parent (1986)	Squirrel monkey (*Samiri sciureus*)	Bidirectional tracing	Wheat germ agglutinin – horseradish peroxidase conjugate (WGA-HRP)	48 h	Putamen	Dorsolateral STh
					Caudate nucleus	Ventromedial STh
					Motor and premotor cortex	No connections evidenced to STh
Parent and Smith (1987)	Squirrel monkey (*Samiri sciureus*)	Anterograde tracing	• Wheat germ agglutinin – horseradish peroxidase conjugate (WGA-HRP) • Nuclear yellow • Fast blue	18–48 h	Putamen	Rostral dorsolateral two-thirds of the STh
					Caudate nucleus	Rostral ventromedial STh
					Substantia nigra	Ventromedial STh
					Globus pallidus	Whole STh, more evident in dorsolateral STh
					Pedunculopontine nucleus	Central regions of the STh

(Continued)

TABLE 2 | Continued

Author(s)	Species	Technique	Tracing agent	PI.T.*	Injection site(s)	Connection(s) evidenced
Smith et al. (1990)	Squirrel monkey (*Samiri sciureus*)	Anterograde tracing	Phaseolus vulgaris-leucoagglutinin	10–12 days	STh	1. Pallidal complex 2. Striatum (middle third of the putamen and caudate nucleus) 3. SN pars compacta 4. SN pars reticulata 5. Mesencephalic and pontine tegmentum (PPT and periacqueductal gray)
Sadikot et al. (1992)	Squirrel monkey (*Samiri sciureus*)	Anterograde tracing	Phaseolus vulgaris-leucoagglutinin	12–14 days	Centromedian nucleus	Dorsolateral STh
					Parafascicular nucleus	Medial and rostral STh
Hazrati and Parent (1992)	Squirrel monkey (*Samiri sciureus*)	Anterograde tracing	Phaseolus vulgaris-leucoagglutinin; Biocytin	2–12 days	Putamen	No connections investigated to the STh
					STh	Globus pallidus (no topography specified)
Lavoie and Parent (1994)	Squirrel monkey (*Samiri sciureus*)	Anterograde tracing	Phaseolus vulgaris-leucoagglutinin; [H]leucine	6–12 days	PPT	Whole extent of the STh
Shink et al. (1996)	Squirrel monkey (*Samiri sciureus*)	Anterograde tracing	Biotin dextran amine	7–10 days	Pallidal complex (both segments) – different injection sites	Inverse dorsoventral topography of STh connections (i.e., dorsal pallidal regions are connected with ventral STh regions, and vice-versa)
					GPi – different injection sites	
			Phaseolus vulgaris-leucoagglutinin	7–10 days	GPe – different injection sites	
François et al. (2000)	*Cercopithecus aethiops*	Anterograde tracing	Biotin dextran amine	10 days	Peri- and retrorubral area (cathecolaminergic cell group A8)	Whole extent of the STh
					SN pars compacta (cathecolaminergic cell group A9)	Anteromedial STh
		Retrograde tracing	Fluoro-gold	10 days	STh	Whole mesencephalon
Sato et al. (2000a)	*Macaca fascicularis*	Anterograde tracing	Biotin dextran amine	48–72 h	GPe	Medial GPe is connected to Medial STh Dorsal GPe is connected to Ventral STh Ventral GPe is connected to Dorsal STh
Sato et al. (2000b)	*Macaca fascicularis*	Anterograde tracing	Biotin dextran amine	48–72 h	STh	1. SN pars reticulata 2. GPe 3. GPi 4. Striatum

(Continued)

TABLE 2 | Continued

Author(s)	Species	Technique	Tracing agent	PI.T.*	Injection site(s)	Connection(s) evidenced
Giolli et al. (2001)	*Macaca mulatta* and *Macaca fascicularis*	Anterograde tracing (Autoradiography)	[H]-leucine	5–7 days	Different cortical areas	No connections investigated to the STh
		Retrograde tracing	Wheat germ agglutinin – horseradish peroxidase conjugate (WGA-HRP)	48 h	Nucleus reticularis tegmenti pontis	STh (topography not specified)
Kelly and Strick (2004)	*Cebus Apella*	Retrograde tracing	Rabies virus	4 days	Primary motor area (M1)	3rd Order neurons within the dorsolateral STh
					Brodmann area 46	3rd Order neurons within the rostral ventromedial STh
Karachi et al., 2005	*Cercopithecus aethiops* and *Macaca mulatta* and *Macaca fascicularis*	Retrograde tracing	Wheat germ agglutinin – horseradish peroxidase conjugate (WGA-HRP)	3 days	Motor GPe Associative GPe Limbic GPe	Motor GPe is connected to posterior and dorsal regions of the STh Assocative GPe is connected to anterior central and posterior ventrolateral STh Limbic GPe is connected to the anterior medioventral STh
		Anterograde tracing	Biotin dextran amine	10 days	Motor GPe Associative GPe Limbic GPe	
Tandé et al. (2006)	*Cercopithecus aethiops* and *Macaca mulatta*	Retrograde tracing	Fluoro-gold	10 days	Subthalamic Nulceus	Parafascicular nulceus
Miyachi et al. (2006)	Macaque monkeys	Retrograde tracing	Rabies virus	4 days	Somatotopically defined regions of the primary motor cortex (M1)	Orofacial M1 is connected to ventrolateral STh; Hindlimb M1 is connected to dorsomedial STh; Forelimb M1 is connected to the two aforementioned STh regions.
Rico et al. (2010)	*Macaca fascicularis*	Retrograde tracing	Cholera toxin B	14 days	Ventral anterior and ventral lateral nuclei of the thalamus	Mainly medial STh
Bostan et al., 2010	*Cebus apella*	Retrograde Tracing	Rabies virus	42 h	Crus IIp and lobule VIIb of the cerebellum	Controlateral STh; Crus IIp presents more connections to the rostral STh and more ventromedially, while lobule VIIb presents more connections to the caudal STh
Haynes and Haber (2013)	Macaque Monkeys (*Macaca fascicularis* + *Macaca nemestrina*)	Anterograde + Bidirectional tracing	Lucifer Yellow, Fluororuby or Fluorescin coniugated with dextran amine or tritiated amino acids.	12–14 days	Orbitofrontal cortex/ventromedial prefrontal cortex	Uncertain (mostly outside the medial border of STh)

(Continued)

TABLE 2 | Continued

Author(s)	Species	Technique	Tracing agent	PI.T.*	Injection site(s)	Connection(s) evidenced
					Dorsal Anterior Cingulate Cortex	Medial tip of the STh
					Dorsal prefrontal cortex (B.A. 9–46)	Medial half of the STh
					Rostral dorsal prefrontal cortex (rostral B.A. 6)	Medial half of the STh, mainly caudal.
					Caudal dorsal prefrontal cortex (caudal B.A. 6)	Ventrolateral STh
					Primary motor cortex	Dorsolateral STh
Ishida et al. (2016)	*Macaca fuscata*	Retrograde tracing	Rabies virus	3–4 days	Ventral premotor cortex	Caudal dorsolateral STh and rostral ventrolateral STh
Coudé et al. (2018)	*Macaca fascicularis*	Anterograde tracing	Biotin dextran amine	8–10 days	Layer V of primary motor cortex	Dorsolateral STh

**PI.T.: Post injection time, i.e., period between tracer injection and sacrifice. STh, Subthalamic Nucleus; GPe, External Globus Pallidus; GPi, Internal Globus Pallidus; SN, Substantia Nigra; PPT, pedunculopontine tegmental nucleus; B.A., Brodmann area.*

From a cytoarchitectural and chemoarchitectural perspective, the cortico-subthalamic pathway utilizes glutamate as main neurotransmitter, and the terminals of the projections contact mainly small dendrites; in particular, projections arising from the motor cortex appear to contact mainly, but not exclusively, distal dendrites and other afferent axons directed toward the STh (Coudé et al., 2018).

Human Tractography Studies

Connectivity between the cortex and the STh has been investigated in humans using DTI and DWI in both controls and PD patients (Aravamuthan et al., 2007; Lambert et al., 2012; Petersen et al., 2017; Isaacs et al., 2018; Plantinga et al., 2018). The studies by Aravamuthan et al. (2007) and Lambert et al. (2012) were discussed previously and will be briefly summarized with regard to cortical connections to the STh. Through probabilistic tractography Aravamuthan et al. (2007) evidenced connections between the motor cortical areas and the dorsal STh, while associative regions of the cortex were connected to the inferior and medial STh. Lambert et al. (2012), on the other hand, evidenced how most cortical regions possessed at least some connections to all of the functional territories identified within the STh, without a precise topographical organization. Petersen et al. (2017) investigated cortico-subthalamic projections in PD patients and controls, using both probabilistic and deterministic tractography; projections to the STh derived mainly from the motor cortex, with particular regard to BA6 and BA4. The probabilistic method further identified a larger portion of projections connecting BA6 to the STh, compared to the projections from the BA4 to the STh. As for the target STh regions, the authors identified the dorsolateral aspect of the nucleus as the main site of projection of cortical fibers; this appears to be coherent with the tripartite hypothesis of the STh, where the dorsolateral aspect represents the motor subregion of the structure. Isaacs et al. (2018) studied the projections arising from the cortex and directed to the STh and the striatum by employing DWI and resting-state functional MRI. The cortical areas of interest were identified basing on primate tracing studies. Comparatively, the striatum appeared to receive more projections from the cortex when compared to the STh, with the exception of the orbitofrontal cortex and the ventromedial prefrontal cortex, whose tract strength were stronger for the STh. Both structures received strong projections from the cingulate motor area and from the supplementary motor area. The study did not assess the topographical organization of the projections, but rather focused on tract strengths between cortical areas and subcortical targets. However, several limitations to the estimation of connection strengths must be noted. As stated by the authors, the exact identification of white matter "entrance points" within the cortex appears particularly challenging, giving rise to what is generally referred as "gyral biases" (Isaacs et al., 2018). Furthermore, the term "tract strength" is referred to the amount of streamlines originating from the seed region (i.e., the cortex) and terminating on the target area (i.e., subcortical structures, including the STh), but does not quantify the actual number of white matter fibers, and its values are related to the size of the target structure. Hence,

results related to tract strengths should not be over interpreted (Jones et al., 2013).

Plantinga et al. (2018) studied the connectivity between cortical areas and the STh with regards to the parcellation of the structure in PD patients using 7 Tesla MRI. The authors evidenced connections between the motor areas of the cortex (Primary motor, supplementary motor and premotor cortex) and the posterior dorsolateral aspect of the STh, the associative areas of the cortex and the central region of the STh, partially overlapping with the motor area, and the limbic areas of the cortex (hippocampus, amygdala, cingulate gyrus, orbitofrontal cortex) with the anterior ventromedial aspect of the STh; the authors also identified volumetric differences between the areas, with the 55.3 ± 14%, 55.6 ± 15.9% and 20.3 ± 16.3% of the total volume of the nucleus being occupied by the posterior dorsolateral motor region, central associative region and anterior ventromedial limbic region, respectively. This subdivision seems to confirm, along with the other human tracing studies, the classical tripartite hypothesis.

Future Perspectives

To date, the presence of cortico-subthalamic fibers has been evidenced in humans only through tractography. Histological studies present inherent technical limitations in reconstructing fiber pathways from the cortex to the STh due to the conspicuous length of the fibers. Within this context, post-mortem MRI-derived tractography could be employed to further characterize the connections between the cortex and the STh, similarly to Plantinga et al.'s (2016) study on STh connections to the GPe and SN. The higher resolution achievable through longer scan times could provide useful information on the characterization of connections between the cortex and the STh.

Another point of further investigation is related to the overlap between functional territories within the STh. As recent literature suggests (Alkemade and Forstmann, 2014; Lambert et al., 2015), the associative territories of the STh could represent a transition gradient between motor and limbic regions, rather than an anatomically distinct area with defined boundaries. The high resolution achieved through Ultra-High field MRI on *ex vivo* human specimen could shed more light on the precise topography of cortical connections with the STh.

Pallidal (GPe and GPi) Connections With the STh

Subthalamo-Pallidal Projections

Non-human Primate Studies

Through autoradiography, Nauta and Cole (1978) confirmed the existence of a highly organized subthalamo-pallidal projection which, originating from the STh, traverses the internal capsule and ends on the pallidal complex (both segments) describing a route identical, but with opposite directionality, to the second division of the ansa lenticularis. In particular, the medial part of the rostral third of the STh projects to the rostral GPe and ventromedial GPi, including the ventral pallidum, while the dorsal regions of the caudal STh project toward the ventrolateral two thirds of the caudal pallidal complex. Furthermore, the authors were unable to confirm any commissural connection between the STh of each hemisphere. According to Carpenter et al. (1981a,b); Carpenter and Jayaraman (1990) projections from the STh possess a topographical organization. Subthalamo-pallidal (efferent) projections directed toward the GPe are organized as follows: the rostral third of the STh projects to the central part of the GPe; the central third of the STh projects to the rostral part of the GPe; the caudal third, especially the lateral surface, projects toward the caudal GPe. Subthalamo-pallidal (efferent) projections directed toward the GPi originate mainly from the medial third of the caudal STh. According to the authors, the rostral regions of the STh do not project to the GPi. A common characteristic of subthalamo-pallidal projections evidenced by both Nauta and Cole (1978) and Carpenter et al. Carpenter et al. (1981a,b); Carpenter and Jayaraman (1990) is the inverse dorsoventral topography of the fibers, i.e., the dorsal regions of the STh project to the ventral regions, while the ventral regions of the STh project to the dorsal regions of the pallidal complex. These findings were further confirmed and extended by Shink et al. (1996) and Smith et al. (1990, 1995), who also evidenced a convergence at a synaptic level: many STh neurons projecting to the GPi received synaptic input from GPe collaterals, whose neurons were originally directed to the same area of the GPi. Similarly, GPe neurons projecting to the GPi received input from axon collaterals of STh neurons mainly projecting to the same areas of the GPi.

A more detailed description of the subthalamo-pallidal topography has been proposed by Joel and Weiner (1997) by integrating the findings of Nauta and Cole (1978); Carpenter and Jayaraman (1990), Shink et al. (1996) and Smith et al. (1990, 1995): the medial third of the rostral two-thirds of the STh projects mainly to the rostral GPe (associative circuit), to the ventral pallidum (limbic circuit) and to the rostral-ventromedial GPi (associative and limbic circuits); the lateral two thirds of the rostral two thirds of the STh project mainly to the central and caudal GPe and GPi; in particular, the dorsolateral two-thirds of this region project to the ventrolateral GPe and GPi (motor circuit), while the ventrolateral third projects to the dorsomedial third of the GPe and GPi (associative circuit). The caudal STh projects mainly to the ventrolateral GPe and GPi (thus converging on the motor circuit) apart of a small ventromedial portion projecting toward the associative circuit (dorsomedial GPe and GPi). This organization appears to be coherent with the hypothesis of the functional tripartition of the STh. **Figure 5** shows a schematic representation of the aforementioned topography.

On both segments, the subthalamo-pallidal efferents terminate in the form of dense elongated bands that lie parallel to the medullary laminae (Parent and Hazrati, 1995). The target pallidal cells present an elongated dendritic domain parallel to the medullary laminae and are organized in rostrocaudally oriented cell layers, with each subthalamo-pallidal band contacting several pallidal cells. These bands are formed by thick non-varicose axons coursing in a caudorostral direction and giving rise to multiple thin and varicose axon collaterals forming a dense network around the dendrites and soma of pallidal neurons (Parent and Hazrati, 1995). This organization appears to be

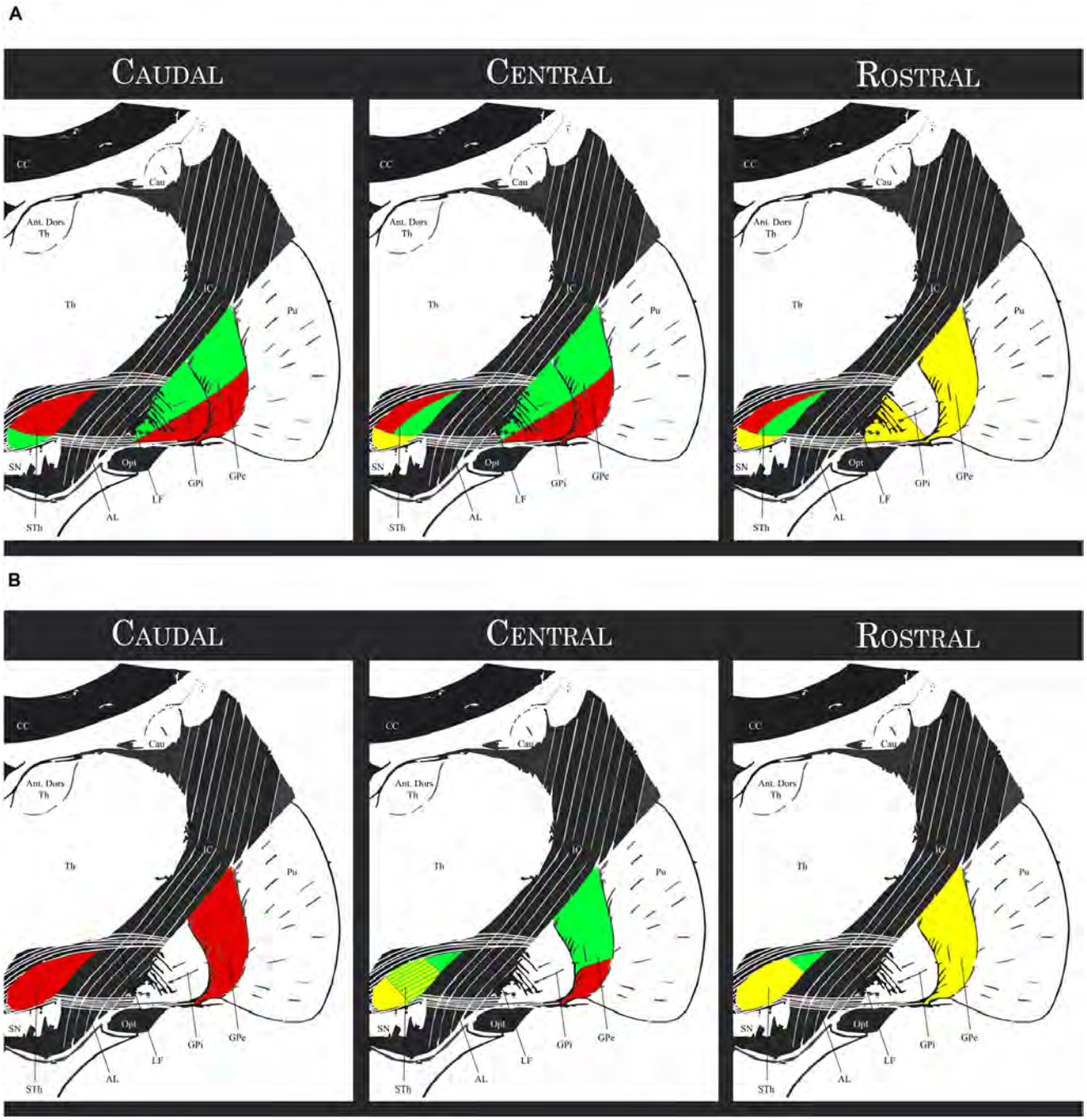

FIGURE 5 | (A) Schematic topography of the Subthalamo-pallidal efferents. Red regions: motor circuits; Green regions: associative circuit; Yellow regions: limbic circuit. **(B)** Schematic topography of the pallido-subthalamic afferents. Red regions: motor circuit; Green regions: exclusively associative circuit; Yellow regions: associative and limbic circuit. STh, Subthalamic Nucleus; SN, Substantia Nigra; GPi, Internal Globus Pallidus. GPe, External Globus Pallidus; Pu, Putamen; Th, thalamus; Ant. Dors Th, Anterior Dorsal nuclei of the Thalamus; Cau, Caudate nucleus; CC, Corpus Callosum; IC, Internal Capsule; Opt, Optic Tract; LF, Lenticular Fasciculus; AL, Ansa Lenticularis (for representation purposes, the topographical relationship between structures within the anteroposterior levels were simplified and depicted with the same schematic).

very similar to the vertically oriented terminal bands formed by striato-pallidal fibers, with the main difference being the distribution of the efferent arborizations: while the subthalamo-pallidal efferents present a quite uniform arborization throughout the whole extent of the pallidal complex, the striato-pallidal projections present a more heterogeneous arborization pattern and an opposite directionality. Furthermore, the proximal part of the striatal axons contacts the soma of the pallidal neurons

while the terminal portion of the axon branches in order to entwine the dendrites of a more caudally located pallidal neuron; conversely, the subthalamic axons send numerous collaterals which entwine the dendrites and soma of several pallidal neurons, with the main axon continuing its caudorostral course (Parent and Hazrati, 1995). This indicates that the STh exerts a relatively widespread influence on the pallidal segments, contacting vast fields of pallidal neurons.

Pallido-Subthalamic Projections

Non-human Primate Tracing Studies

One of the main afferent pathways to the STh is represented by the pallido-subthalamic fibers, which originates exclusively from the GPe (Parent and Hazrati, 1995; Joel and Weiner, 1997, 2000; Sato et al., 2000a; Hamani et al., 2004). To date, no afferences from the GPi have been described; hence, the term pallido-subthalamic afferences refers to axons arising from the GPe. The majority of pallidal terminals within the STh exhibited numerous varicosities reminiscent of boutons en passant or boutons terminaux and displayed GAD and GABA immunoreactivity, forming synapses predominantly with proximal dendrites and less frequently with the soma and the distal dendrites (Parent and Hazrati, 1995; Sato et al., 2000a).

Rostral GPe (associative and supposedly limbic circuit) projects to the medial two-thirds of the rostral STh and to the central third of the middle STh, and to a lesser extent to the medial third of the central STh. Central GPe can be divided into two parts: (1) the dorsal two thirds, part of the associative circuit, project to the lateral two thirds of the central regions of the STh; (2) the ventral third of the GPe, part of the motor circuit, projects along with the whole caudal third of the GPe to the lateral and caudal regions of the STh. The ventral pallidum (part of the limbic circuit) appears to be reciprocally connected to the limbic STh. There also appears to be an inverse dorsoventral topography, with dorsal regions of the GPe projecting more ventrally, and ventral regions projecting more dorsally in the STh.

More recently, Karachi et al. (2005) studied the pallido-subthalamic pathway with particular regard to recent evidence on the functional subdivision of the GPe. According to the authors, the motor GPe is connected to the posterior and dorsal regions of the STh; the associative GPe is connected to the anterior central and posterior ventrolateral STh, while the Limbic GPe is connected with the anterior medioventral STh. These findings are coherent with the functional tripartite hypothesis of the STh and in accordance with previous literature.

Figure 5 evidences the aforementioned topography. Comparing the afferent projections to the efferent projections exposed in the previous paragraph, a correspondence between the GPe terminal field in the STh and the area of the nucleus projecting to the corresponding region of the GPi was evidenced, but appeared not to be absolute. Furthermore, the associative GPe appears to be reciprocally connected with the STh, but also projects to the dorsolateral regions of the central STh which are primarily connected to the motor pallidum. The pallido-subthalamic projection is thus considered as the essential component of the indirect pathway of the basal ganglia, conveying striatal information to the STh and GPi (Parent and Hazrati, 1995).

Human Histology and Tractography Studies

Lambert et al. (2012) evidenced a topographical organization of GPe connections with the STh: the posterior GPe is connected to the posterior STh (motor regions), while the middle GPe is connected to the anterior STh. This appears to be coherent with the functional subdivision of the GPe and with data deriving from non-human primate tracing studies. Pujol et al. (2017) explored the connectivity between the STh and the GP *in vivo* using fiber tracking. The fibers connecting the STh and the GPe crossed the anterior two-thirds of the posterior limb of the internal capsule and connected to the mediodorsal and medioventral aspects of the GPe. Connections between the STh and the GPi were found within the ventromedial aspect of the STh, while no topography of the projections on the GPi was reported. Plantinga et al. (2016) employed Ultra-high field MRI (7T) on a human *ex vivo* specimen to study the structural connectivity between the STh, the GP and the SN. The authors evidenced distinct connections with anteromedial aspect of the STh; these fibers circled around the internal capsule and connected to the anterior and inferior margins of the GPi, following a course compatible with the ansa lenticularis. The STh connections with the GPe, on the other hand, coursed either anteriorly around the internal capsule, in a bundle dorsal to the fibers connected to the GPi, or could be found running through the internal capsule and connected to the medial border of the GPe.

Recently, Alho et al. (2019) employed histological sections, ultra-high field MRI and connectome analysis to describe a bundle of fibers connecting the anterior and medial STh to the ventral GPi in humans. This bundle of fibers, known as ansa subthalamica, appears to be distinct from other bundles connecting the STh to the pallidal complex such as the ansa lenticularis, and constitutes a fundamental anatomical pathway for the limbic circuit of the basal ganglia. According to the authors this bundle could represent an interesting target for stereotactic surgery in psychiatric disorders, as it may play a crucial role within the fronto-striato-subthalamo-pallidal network engaged in goal-directed behaviors (Alho et al., 2019).

Further Perspective

While the connections between the GPe and STh have been extensively studied in non-human primates, data deriving from human subjects is still scarce. The connections between functional territories of the STh and functional territories of the GPe require more investigation in humans, and must be guided by the large amount of anatomical evidence deriving from non-human primate studies.

Striatal Connections to the STh

Subthalamo-Striatal Projections

Non-human Primate Tracing Studies

Subthalamic projections to the Striatum, both Caudate nucleus and Putamen, are scarce compared to other subthalamic targets (Nauta and Cole, 1978; Smith and Parent, 1986; Parent and Smith, 1987; Sato et al., 2000b). According to

Smith and Parent (1986; Parent and Smith, 1987), projections to the putamen arise mainly from the dorsolateral STh (part of the motor circuit), while projections to the caudate nucleus arise mainly from the ventromedial associative and limbic regions of the STh. According to Sato et al. (2000b), approximately 17% of the STh neurons labeled present a single axon projecting toward the striatum. However, the terminal arborizations of these labeled neurons could not be visualized in this study.

Subthalamo-striatal fibers are characterized by long, varicose axons with few collaterals, scattered throughout wide areas of both striatal components (Smith and Parent, 1986; Parent and Smith, 1987; Parent and Hazrati, 1995). According to Parent and Hazrati (1995), these projections likely exert an en passant type of excitatory influence on vast populations of striatal cells. No striato-subthalamical projections have been evidenced in non-human primates so far.

Human Fiber Tracking Studies

According to Lambert et al. (2012) the posterior putamen is connected to the motor STh, in particular the posterior parts of the nucleus, while the mid-inferior putamen is connected to the limbic STh, in particular the anterior regions of the nucleus.

Further Perspectives

Literature on STh connections with the Striatum in both non-human primates and humans appears scarce and requires further investigation. Considering the functional subdivision of the striatum and the morphofunctional difference between striosomes and matrix, it could be interesting to define if, and how, these territories are connected with the functional subdivisions of the STh.

Nigral Connections With the STh

Subthalamo-Nigral Projections

Non-human Primate Studies

The substantia nigra represents one of the main targets of the STh (Carpenter et al., 1981b; Parent and Smith, 1987; Smith et al., 1990; François et al., 2000). These fibers enter the substantia nigra pars reticulata (SNr) mainly by coursing through the cerebral peduncle, arborizing along the basis of the SNr and forming several distinct terminal plexuses (Carpenter et al., 1981b; Parent and Hazrati, 1995). Even though most fibers terminate at the level of the reticulate part, some fibers ascend along the dopaminergic cell columns of the substantia nigra pars compacta (SNc), thus influencing both dopaminergic and non-dopaminergic cells (Smith et al., 1990). The subthalamo-nigral pathway appears to arise from neurons mainly in the ventromedial regions of the STh, displaying an approximate mediolateral topography (Smith et al., 1990). At the level of the substantia nigra, these fibers form several terminal fields consisting of networks of axon collaterals showcasing both en passant and terminal boutons (Smith et al., 1990); prominent perisomatic arborization has been highlighted, but appears to be inconsistent throughout different studies. These terminals showcase certain similarities to the subthalamo-pallidal terminals, suggesting that both projections arise from the same neuronal population (Parent and Hazrati, 1995).

Nigro-Subthalamical Projections

The nigro-subthalamical pathway appears to be less prominent in primates than in rodents (Parent and Hazrati, 1995). While the nucleus appears to be surrounded by several dopaminergic fiber systems, only few appear to contact its neurons by entering the mediodorsal regions. According to tracing studies in rodents, the nigro-subthalamical projection arises mainly from the substantia nigra pars compacta, while the STh projects mainly to the pars reticulata (Brown et al., 1979).

In non-human primates, François et al. (2000) evidenced extensive projections arising from dopaminergic areas A8, A9, and A10 in the mesencephalon. Through anterograde tracing, the authors confirmed projections arising from the mesencephalon and targeting the STh. The dopaminergic nature of these afferences was confirmed through positivity for tyrosine hydroxylase. In particular, the labeled axons originating from the mediodorsal part of area A9 project to the anteriomedial STh, while the fibers originating from area A8 project to the whole extent of the STh.

The dopaminergic fibers arising from the substantia nigra appear to be characterized by numerous axon varicosities; some axons branch extensively within the STh in order to contact numerous target neurons, while other axons selectively target very few neurons within the structure (Lavoie et al., 1989; François et al., 2000; Hamani et al., 2004).

Human Tractography Studies

Connections between the STh and the SN were reported in a post-mortem human specimen by Plantinga et al. (2016) using DWI. The authors evidenced connections between the inferolateral border of the STh and the superior border of the SN. The connection with the SNc is located more anteriorly within the STh compared to the connections with the SNr. According to the authors, the connection with the SNc appears to be significantly larger than the connection with the SNr.

Further Perspectives

Few studies have addressed the structural connectivity between the STh and the substantia nigra in non-human primates and in humans. Aspects such as the precise termination of SN projections to the STh remain to be clearly determined. From a functional perspective, the dopaminergic innervation of the STh may play a fundamental role in the regulation of STh afferences, such as corticosubthalamic fibers (Mathai and Smith, 2011). From an anatomical perspective, the exact identification and subcellular localization of dopaminergic synapses within the human STh could significantly improve our understanding of the dopaminergic modulation of the STh. Considering the topographical vicinity between the STh and the SN, *ex vivo* tracing methods could be employed to study the connections between the SN and the STh without incurring in significant technical difficulties related to tracer transport over long distances (i.e., from the cortex to subcortical structures) within *ex vivo* human brain tissue. While this information does not resolve most of the questions posed by Mathai and Smith (2011) regarding the physiological and pathological implications of dopaminergic modulation of STh afferences, it could represent

a starting point for the morphofunctional characterization of extrastriatal dopaminergic innervations in humans.

Thalamic Connections With the STh

Non-human Primate Tracing Studies

The thalamo-subthalamic pathway arises mainly from the parafascicular nucleus of the thalamus and from the centromedian nuclei (Sadikot et al., 1992; Tandé et al., 2006). The centromedian nucleus appears to project mainly to the motor division of the STh, in particular to the dorsolateral regions of the nucleus. The parafascicular nucleus innervates mainly the medial and rostral regions of the STh, constituting the limbic/associative territories of the nucleus. The axon terminals of this pathway appear to contact mainly the dendrites of the STh cells, displaying glutamatergic immunoreactivity (Hamani et al., 2004).

More recently, bidirectional connections with the ventral anterior and ventral lateral thalamus have been described (Rico et al., 2010). These fibers connect mainly the medial STh to the aforementioned thalamic nuclei, playing a role in both motor and associative control.

Cerebellar Connections With the STh

Even though indirect connections arising from and terminating on the STh were not considered within this review, the recent discovery and the morphofunctional relevance of indirect connections between the STh and the Cerebellum could represent an important stimulus to functional and connectivity research, along with their clinical implications, within the network of basal ganglia circuits, and will therefore briefly discussed.

Non-human Primate Tracing Studies

Recently, indirect connections between the STh and the cerebellum have been identified by Bostan et al. (2010). Through the injection of rabies virus (retrograde tracer) in the cerebellum of non-human primates, the authors identified a disynaptic pathway connecting the STh to the pontine nuclei, which in turn projected toward the controlateral cerebellar cortex. In particular, injections within the Crus IIp of the cerebellum displayed numerous labeled neurons within the rostral and ventromedial STh, while injections within the lobule VIIb displayed numerous labeled neurons within the caudal STh. According to the authors, modulation of the subthalamo-cerebellar pathway could be provided by the nucleus reticularis tegmenti pontis and other pontine nuclei, which are also structurally connected to the STh (Giolli et al., 2001).

Human Fiber Tracking Studies

Based on Bostan et al.'s (2010) results, Pelzer et al. (2013) identified connections between the STh and the cerebellar cortex in living humans through DTI. According to the authors, the STh was connected to both regions identified by Bostan et al. (2010), but appeared to also be connected to lobule VIII and IX. These fibers crossed the midline at the level of the pons and entered the cerebellum passing through the middle cerebellar peduncle.

Milardi et al. (2016) extensively examined the connections between the basal ganglia and the cerebellum, confirming and expanding the findings of previous authors. However, unlike Pelzer et al. (2013), the authors identified an ipsilateral connection between the STh and the cerebellar cortex.

Wang et al. (2020) employed high definition fiber tractography to identify cortico-subthalamo-cerebellar connections. According to the authors, fibers connecting the STh and the cerebellum pass through the cerebral peduncle along the course of the cortico-cerebellar fibers. At the level of the pons they connect in two opposite directions to join the middle cerebellar pedicle on both sides. Most fibers connected bilaterally to Crus I in the cerebellum, while the remaining fibers crossed the midline and connected to Crus II. Interestingly, the authors evidenced a positive correlation between the numbers of fibers connecting mesial BA8 to the STh and the number of fibers connecting the STh with Crus I. Since the hyperdirect pathway between BA8 and the STh seems to be involved in decision making (Wang et al., 2020), the fibers connecting the STh to Crus I and II could represent a continuation of such pathway and also contribute to higher cognitive functions.

Further Perspectives

While human fiber tracking studies provide compelling information on the subthalamo-cerebellar circuitry, more data deriving from non-human primate tracing studies is required to further characterize these connections. In fact, it must be considered that Bostan et al. (2010) tracing study is based on the observation of only two subjects and two main injection sites.

The identification of second order neurons and mediating nuclei, along with the topographical organization of subthalamo-cerebellar projections represent aspects that require further clarification: is there a topographically organized projection arising from the motor areas of the STh that maintains the somatotopic representation of cortical afferences? What is the role of deep cerebellar nuclei, such as the dentate nucleus, in the subthalamo-cerebellar pathway? Hopefully, more non-human primate tracing studies will provide information on these aspects.

Brainstem Connections to the STh

Non-human Primate Tracing Studies

The STh appears to be connected to several brainstem nuclei, such as the pedunculopontine tegmental nucleus (PPT), the ventral tegmental area of the mesencephalon, the periacqueductal gray and the dorsal raphe nucleus (Nauta and Cole, 1978; Carpenter et al., 1981b; Parent and Smith, 1987; Smith et al., 1990; Lavoie and Parent, 1994a,b,c). The PPT projects conspicuously to the whole extent of the STh, representing the main cholinergic input to the nucleus (Lavoie and Parent, 1994c). These fibers appear to modulate the activity of neurons in the STh and other basal ganglia structures. A minor pathway arising from the STh and directed toward the PPT has also been identified, which is thought to relay basal ganglia information to the lower brainstem and spinal cord via the mesencephalic locomotor region (Parent and Hazrati, 1995), in particular through the activation of the nucleus reticular gigantocellularis, which regulates the activity of spinal interneurons through the reticulospinal tract (Pahapill and Lozano, 2000; Hamani et al., 2004). Thus, the circuit appears to be involved in the facilitation of locomotion and in the regulation of cardiorespiratory activity during motor exercise

(Eldridge et al., 1985). According to Lavoie and Parent (1994c), the terminals of the PPT-STh projection form contacts with the soma and proximal dendrites of STh neurons; however, these information seem to derive from rodent and feline studies (Morizumii et al., 1987). Information on these terminals in non-human primates seems to be lacking.

The dorsal raphe nucleus appears to consistently innervate the STh through widespread 5-HT immunoreactive fibers, even though their physiological activity remains controversial (Rinvik et al., 1979; Carpenter et al., 1981b; Mori et al., 1985).

Several other nuclei projecting to the STh have been identified, even though the organization and the functional role of these projections remains unclear; these include: the reticular nucleus of the thalamus, the hypothalamus, the amygdaloid nuclei, the locus coeruleus, the zona incerta and the parabrachial nuclei (Rinvik et al., 1979; Canteras et al., 1990).

Human Fiber Tracking Studies

Through DTI, Muthusamy et al. (2007) and Aravamuthan et al. (2007) were the first to identify the connection between the PPT and the STh in humans. In particular, the two structures appeared to be connected at the level of the medial, posterior and superior eight of the PPT and at the level of the medial and inferior STh (Aravamuthan et al., 2007). Again, results deriving from diffusion based approaches should be interpreted with care: even though the connections evidenced largely match those found in animal studies, all non-human primate axon tracing studies known to us identify projections arising from the PPT with diffuse terminations and extensive branching throughout the whole extent of the STh, and do not describe an inferomedial termination of afferences (Nauta and Cole, 1978; Carpenter et al., 1981b; Parent and Smith, 1987; Smith et al., 1990; Lavoie and Parent, 1994a,b,c). Interestingly, Lavoie and Parent (1994c) evidenced that PPT fibers enter the STh from its medial tip and dorsal surface and arborize profusely and uniformly throughout the nucleus; considering the technical limitations of DTI, it could be speculated that Aravamuthan et al.'s (2007) study reconstructed PPT projections to the STh entering the nucleus from its medial tip, in accordance to animal studies, without being able to reconstruct the arborization of these fibers within the structure. More evidence from human fiber tracking studies, possibly with higher spatial resolution, could help to clarify this aspect.

Synaptic Contacts of the Major Afferents to the Subthalamic Nucleus

Table 3 shows the distribution and cellular localization of synaptic contacts at the level of STh cells. Fibers originating from the motor cortex (in particular area M1 and PMC), centromedian and parafascicular nuclei of the thalamus, substantia nigra pars compacta, pedunculopontine tegmental nucleus and dorsal raphe nucleus contact STh neurons mainly at the level of distal dendrites (Rinvik et al., 1979; Carpenter et al., 1981b; Mori et al., 1985; Morizumii et al., 1987; Smith et al., 1990; François et al., 2000; Tandé et al., 2006; Rico et al., 2010; Coudé et al., 2018), whilst pallidal fibers contact mainly the soma and proximal dendrites of STh cells (Parent and Hazrati, 1995; Sato et al., 2000a).

FUNCIONAL SEGREGATION OR FUNCTIONAL CONVERGENCE? ANATOMICAL EVIDENCE OF STH OPEN AND CLOSED-LOOP CIRCUITS

The previous paragraphs highlighted the intricate network of connections directed to and originating from the STh. Given the tripartite division of the striatum, pallidum and STh, the parallel segregated principle predicts the existence of indirect pathways connecting functionally corresponding subregions of the striatum, GPe, GPi and STh. In particular, it has been evidenced that efferents originating from the GPe contact STh neurons projecting to GPi and SNr, thus providing an anatomical support for the existence of an indirect pathway (Joel and Weiner, 1997). Initially the original hypothesis was rejected by Parent and Hazrati (1995) due to lack of firm anatomical evidence for the existence of the indirect pathway, as previous studies were unable to confirm GPe connections to the STh territory containing neurons projecting toward the GPi/SNr. According to the authors, an indirect pathway connecting the GPe to the output structures of the basal ganglia (i.e., GPi and SNr) required either direct connections between the GPe and the aforementioned nuclei, or an indirect GPe-STh-GPi/SNr projection, which in turn relied on the existence of a link between the dorsolateral STh (receiving GPe input) and the ventromedial STh (giving rise to GPi/SNr projections) (Parent and Hazrati, 1995). Supporting data was subsequently provided by Shink et al. (1996), identifying the connection between GPe fibers and STh neurons projecting to the GPi through electron microscopy.

However, the functional segregation initially proposed appears to be only partially confirmed: segregation seems to be maintained with regard to the associative subregions of the striatum (associative regions being contacted exclusively by other associative regions), but not at the level of the motor circuits (motor regions being contacted by other functional division, in particular the associative ones).

Two possible hypotheses arise:

1. The associative and motor circuit project to the same neurons of the motor STh, which integrates the information originating from both circuits and redirects them to the motor GPi.
2. The associative circuit and the motor circuit project to different subpopulations of neurons within the STh. These subpopulation would differ only for the afferences received, whilst projecting on the same neurons at the level of the motor GPi.

However, regardless of whether the projections from the motor and associative GPe remain segregated in the motor STh or converge on the same neurons, information is still transferred from the associative striatum through associative GPe and motor

TABLE 3 | Localization of subcellular afferences to monkey STh.

Afferent structure	Principal neurotransmitter	Localization of main synaptic contacts	References
Motor cortex	Glutamate	Distal dendrites and spines	Coudé et al., 2018
GPe	GABA	Cell body and proximal dendrites	Parent and Hazrati, 1995; Sato et al., 2000a
Thalamus	Glutamate	Distal dendrites	Tandé et al., 2006; Rico et al., 2010
SNc	Dopamine	Dendrites	Smith et al., 1990; Parent and Hazrati, 1995; François et al., 2000
PPT (Tegmentum)	ACh	Distal dendrites and soma	Rodent and feline studies (Morizumii et al., 1987); confirmation required from non-human primate studies.
Dorsal Raphe	5-HT	Distal dendrites	Rinvik et al., 1979; Carpenter et al., 1981b; Mori et al., 1985

STh to the motor GPi (Joel and Weiner, 1997). The consequences of this anatomical organization will be discussed further.

According to Joel and Weiner's hypothesis (1997), two types of indirect pathways can be identified in regard to the topographical organization of STh afferent and efferent projections:

1. Closed indirect pathway: this pathway terminates in the same GPi/SNr subregion as the direct pathway arising from the corresponding striatal subregion. This leads to the connection of functionally related regions of the striatum, pallidal complex and STh according to the parallel segregation scheme. The closed indirect pathway contributes to the processing of information within the basal ganglia-thalamocortical circuits.
2. Open indirect pathway: this pathway terminates in a different subregion of the GPi/SNr than the direct pathway, thus connecting functionally non-corresponding subregions of the striatum, pallidal complex and STh. The open indirect pathway contributes to the connection between circuits of the basal ganglia.

Thus, three possible closed pathways can be hypothesized, each one connecting the corresponding functional regions of the striatum, pallidal complex, STh and SNr. On the other hand, among the open indirect pathways it is possible to identify the one linking the associative striatum to the motor GPi passing through the associative GPe and motor STh (one further open indirect pathway is the one connecting the associative regions to the ventral pallidum and the limbic circuit; for more information, consult Joel and Weiner, 1997).

Empirical evidence for the open versus closed loop circuits hypothesis in non-human primates and humans remains controversial. Kelly and Strick (2004) employed rabies virus retrograde tracing to define closed and open loop circuits within the primate cortico-basal ganglia-thalamo-cortical circuits. Even though the authors evidenced mostly closed-loop circuits between motor and limbic areas, an open-loop circuit connecting (indirectly) the ventral putamen to M1 has also been identified. The ventral putamen belongs to the limbic circuit of the basal ganglia (Parent and Hazrati, 1995), and seems to be connected to limbic structures such as the amygdala (Parent and Hazrati, 1995; Joel and Weiner, 1997; Kelly and Strick, 2004). According to the authors, this connection could represent the anatomical demonstration in primates for an open-loop circuit between the limbic circuit and the motor circuit of the basal ganglia.

More recently, a study on rodents (Aoki et al., 2019) has provided some interesting insight on the anatomo-functional organization of closed and open loop circuits within the rat basal ganglia. By combining genetic and viral approaches, the authors mapped the limbic and motor circuits between the cortex, the basal ganglia and the thalamus in rodents. Despite evidencing largely closed loops within each functional domain, the authors discovered an unidirectional influence of the limbic over the motor loop via ventral striatum-substantia nigra (SNr)-motor thalamus circuitry; furthermore, activity within the ventral striatum of the rat seems to modulate the activity of the primary motor cortex. These results appear to be in line with Kelly and Strick's (2004) findings in non-human primates. Interestingly, this pathway seems to form synapses with the SNr, rather than the GPi. Kelly and Strick (2004) did not report any retrogradely labeled neurons within the SNr, but only in the GPi. Therefore, it could be speculated that the non-human primate open loop circuit connecting the ventral putamen to the motor cortex passes through the GPi, rather than the SNr. According to Hardman et al. (2002), the SNr plays a much more important role as an output structure of the basal ganglia in rodents compared to non-human primates, while the opposite seems to be true for the GPi.

Considering the increasing importance of the STh in processing different types of information through phylogenesis (Hardman et al., 2002), the definition of the STh's role in open versus closed loop circuits could represent an important aspect regarding information processing within the human basal ganglia.

CONCLUSION AND FUTURE PERSPECTIVES

Even though the STh represents a topic of interest in current neuroscience research, most anatomical data available derives from histological and tracing studies in non-human primates. Data on humans is limited to very few studies employing mostly MRI in combination with unbiased stereology applied to

histological sections. According to our perspective, it is possible to identify three main points of interest within human STh research which require further and detailed investigation: connectivity, cytoarchitectural and chemoarchitectural organization, and functional subdivision.

Connectivity

Currently, the connectivity of the STh has been investigated in non-human primates through *in vivo* tracing studies, and in humans in both *in vivo* and *ex vivo* specimen through MRI, specifically through DTI and DWI. Conversely, the connectivity of the human STh has never been investigated through post-mortem tracing methods, such as Carbocyanine tracing or Neuro Vue Dyes. These tracers allow for the anterograde and retrograde tracing of axons even in formalin fixed human specimens (Heilingoetter and Jensen, 2017), and could be employed to study the connectivity between the STh and closely related structures, such as the substantia nigra, the globus pallidus, and the nucleus of the zona incerta. For long distance tracing, complications may arise due to the very long incubation times required (from several months to years) and due to technical difficulties with the cryostat-sectioning of macrosections. Even though these techniques may present inherent limitations, such as long incubation periods and possible tracer diffusion during sectioning, they also appear to be significantly more accurate than *in vivo* tracing studies (Heilingoetter and Jensen, 2017); furthermore, given the increasingly important role of the STh through phylogenesis (Hardman et al., 2002), these tracing techniques could identify a different organization of afferent and efferent projections in humans compared to monkeys, whilst also expanding on the topography of STh connections.

Post-mortem tracing techniques can be used in conjunction with ultra high field MRI, DTI and DWI of *ex vivo* specimens to confirm the anatomo-radiological findings and to expand on several aspects of connectivity which are still unclear, such as the topography of projections, eventual subpopulations of target cells and the type of synapse formed (e.g., axo-axonic, axo-somatic, or axo-dendritic synapses).

Cytoarchitectonics and Chemoarchitectonics

While the cellular morphology and different cellular populations have been identified in rodents, cats and primates, there are no conclusive studies in humans. The morphology of human subthalamic neurons can be studied through Golgi silver impregnation techniques, such as the Golgi-Cox and Golgi-De Bubenaite methods, even though formalin fixed human tissue generally leads to artifact formation and incomplete precipitation of metallic silver, if not appropriately pre-treated. On the other hand, fresh tissue can be impregnated using osmic acid as a fixative (Golgi-Cox variation), after isolating the STh in a freshly cut hemisphere. Otherwise, carbocyanines and Neuro Vue dyes can also be employed to evidence the morphology of single neurons and, unlike silver impregnation techniques, also allow for the visualization of synaptic contacts in traced neurons.

A general overview of the axonal and dendritic network within the STh can be further investigated through the aid of the Cajal-De Castro photographic silver techniques, allowing for the impregnation not only of formalin fixed bulks of tissue, but also of paraffin embedded sections.

Immunohistochemistry should be employed to characterize the distribution of different receptors or molecules of interest; it must be noted, however, that the quality of Immunohistochemistry depends on the method and time of fixation: specimen fixed for longer periods (>1 year) in formalin yield generally worse results than fresh and appropriately fixed specimen. The definition of neuronal populations expressing specific proteins or receptors, as well as their distribution within the structure, should be investigated through the aid of unbiased stereology in both health and disease, with particular regard to movement disorders and α-sinucleopathies. The chemoreceptorial characterization of STh neurons could help define fundamental functional aspects of the structure.

Hence, both cytoarchitectonics and chemoarchitectonics could provide evidence for different subpopulations of neurons within the STh, receiving and processing different types of informations, with particular regard to the functional subdivision hypothesis.

Functional Subdivision

This aspect remains one of the most crucial in STh research. The identification of functional subdivisions within the nucleus, and their clear definition in terms of topography, connectivity, cell population, and receptor and protein expression could provide novel insights on how different types of information are processed within the basal ganglia. Furthermore, considering the fundamental role played by the STh in DBS, the identification of functional divisions of the structure which are both safe to stimulate and easy to target could significantly improve treatment outcome.

AUTHOR CONTRIBUTIONS

AA conceived the review. AE drafted the manuscript and designed the figures. AE, RD, AP, and VM revised the manuscript. All authors contributed to the final manuscript.

REFERENCES

Albin, R. L., Aldridge, J. W., Young, A. B., and Gliman, S. (1989a). Feline subthalamic nucleus neurons contain glutamate-like but not GABA-like or glycine-like immunoreactivity. *Brain Res.* 491, 185–188. doi: 10.1016/0006-8993(89)90103-0

Albin, R. L., Young, A. B., and Penney, J. B. (1989b). The functional anatomy of basal ganglia disorders. *Trends Neurosci.* 12, 366–375.

Albin, R. L., Reiner, A., Anderson, K. D., Penney, J. B., and Young, A. B. (1990a). Striatal and nigral neuron subpopulations in rigid Huntington's disease: implications for the functional anatomy of chorea and rigidity-akinesia. *Ann. Neurol.* 27, 357–365. doi: 10.1002/ana.410270403

Albin, R. L., Young, A. B., Penney, J. B., Handelin, B., Balfour, K. D., Markel, D. S., et al. (1990b). Abnormalities of striatal projection neurons and N-methyl-d-aspartate receptors in perisymptomatic Huntington's disease. *N. Engl. J. Med.* 322, 1293–1298. doi: 10.1056/nejm199005033221807

Alexander, G. E., Crutcher, M. D., and Delong, M. R. (1990). Basal ganglia thalamocortical circuits: parallel substrates for motor, oculomotor, prefrontal and limbic functions. *Prof. Brain Res.* 85, 119–146. doi: 10.1016/s0079-6123(08)62678-3

Alexander, G. E., Delong, M. R., and Stick, P. L. (1986). Parallel organization of functionally segregated circuits linking basal ganglia and cortex. *Annu. Rev. Neurosci.* 9, 357–381. doi: 10.1146/annurev.ne.09.030186.002041

Alho, E. J. L., Alho, A. T. D. L., Horn, A., Martin, M., da, G. M., Edlow, B. L., et al. (2019). The ansa subthalamica: a neglected fiber tract. *Mov. Disord.* 35, 75–80. doi: 10.1002/mds.27901

Alkemade, A., and Forstmann, B. (2014). Do we need to revise the tripartite subdivision hypothesis of the human subthalamic nucleus (STN)? *Neuroimage* 95, 326–329. doi: 10.1016/j.neuroimage.2014.03.010

Alkemade, A., Schnitzler, A., and Forstmann, B. U. (2015). Topographic organization of the human and non-human primate subthalamic nucleus. *Brain Struct. Funct.* 220, 3075–3078. doi: 10.1007/s00429-015-1047-2

Allheid, G. F., Heimer, L., and Switzer, R. C. (1990). "Basal ganglia," in *The Human Nervous System*, ed. G. Paxinos (San Diego, CA: Academic Press).

Antonini, A., and Obeso, J. A. (2018). DBS for Parkinson's disease with behavioural disturbances. *Lancet Neurol.* 17, 195–197. doi: 10.1016/s1474-4422(18)30044-9

Aoki, S., Smith, J. B., Li, H., Yan, X., Igarashi, M., Coulon, P., et al. (2019). An open cortico-basal ganglia loop allows limbic control over motor output via the nigrothalamic pathway. *eLife* 8:e49995. doi: 10.7554/eLife.49995

Aravamuthan, B. R., Muthusamy, K. A., Stein, J. F., Aziz, T. Z., and Johansen-Berg, H. (2007). Topography of cortical and subcortical connections of the human pedunculopontine and subthalamic nuclei. *Neuroimage* 37, 694–705. doi: 10.1016/j.neuroimage.2007.05.050

Bahatia, K. P., and Marsden, C. D. (1994). The behavioral and motor consequences of focal lesions of the basal ganglia in man. *Brain* 117, 859–876. doi: 10.1093/brain/117.4.859

Berney, A., Vingerhoets, F., and Perrin, A. (2002). Effect on mood of subthalamic DBS for Parkinson's disease: a consecutive series of 24 patients. *Neurology* 59, 1427–1429. doi: 10.1212/01.wnl.0000032756.14298.18

Bostan, A. C., Dum, R. P., and Strick, P. L. (2010). The basal ganglia communicate with the cerebellum. *Proc. Natl. Acad. Sci. U.S.A.* 107, 8452–8456. doi: 10.1073/pnas.1000496107

Brown, L. L., Markman, M. H., Wolfson, L. I., Dvorkin, B., Warner, C., and Karzman, R. (1979). A direct role of dopamine in the rat subthalamic nucleus and an adjacent intrapeduncular area. *Science* 206, 1416–1418. doi: 10.1126/science.505015

Canteras, N. S., Shammah-Lagnado, S. J., Silva, B. A., and Ricardo, J. A. (1990). Afferent connections of the subthalamic nucleus; a combined retrograde and anterograde horse radish peroxidase study in the rat. *Brain Res.* 513, 43–59.

Carpenter, M. B., Batton, R. R., Carleton, S. C., and Keller, J. T. (1981a). Interconnections and organization of pallidal and subthalamic nucleus neurons in the monkey. *J. Comp. Neurol.* 197, 579–603. doi: 10.1002/cne.901970404

Carpenter, M. B., Carleton, S. C., Keller, J. T., and Conte, P. (1981b). Connections of the subthalamic nucleus in the monkey. *Brain Res.* 224, 1–29. doi: 10.1016/0006-8993(81)91113-6

Carpenter, M. B., and Jayaraman, A. (1990). "Subthalamic nucleus afferents: anatomical and immunocytochemical features," in *The Basal Ganglia III*, Vol. 1991, eds G. Bernardi, M. B. Carpenter, G. Di Chiara, M. Morelli, and P. Stanzione (New York, NY: Plenum Press), 109–117. doi: 10.1007/978-1-4684-5871-8_12

Carpenter, M. B., Nakano, K., and Kim, R. (1976). Nigrothalamic projections in the monkey demonstrated by autoradiographic technics. *J. Comp. Neurol.* 165, 401–415. doi: 10.1002/cne.901650402

Clarke, N. P., Bevan, M. D., Cozzari, C., Hartman, B. K., and Bolam, J. P. (1997). Glutamate-enriched cholinergic synaptic terminals in the entopeduncular nucleus and subthalamic nucleus of the rat. *Neuroscience* 81, 371–385. doi: 10.1016/s0306-4522(97)00247-9

Coudé, D., Parent, A., and Parent, M. (2018). Single-axon tracing of the corticosubthalamic hyperdirect pathway in primates. *Brain Struct. Funct.* 223, 3959–3973. doi: 10.1007/s00429-018-1726-x

Dafsari, H. S., Petry-Schmelzer, J. N., Ray-Chaudhuri, K., Ashkan, K., Weis, L., Dembek, T. A., et al. (2018a). Non-motor outcomes of subthalamic stimulation in Parkinson's disease depend on location of active contacts. *Brain Stimul.* 11, 904–912. doi: 10.1016/j.brs.2018.03.009

Dafsari, H. S., Weiß, L., Silverdale, M., Rizos, A., Reddy, P., Ashkan, K., et al. (2018b). Short-term quality of life after subthalamic stimulation depends on non-motor symptoms in Parkinson's disease. *Brain Stimul.* 11, 867–874. doi: 10.1016/j.brs.2018.02.015

Dafsari, H. S., Reddy, P., Herchenbach, C., Wawro, S., Petry-Schmelzer, J. N., Visser-Vandewalle, V., et al. (2016). Beneficial effects of bilateral subthalamic stimulation on non-motor symptoms in Parkinson's Disease. *Brain Stimul.* 9, 78–85. doi: 10.1016/j.brs.2015.08.005

DeVito, J. L., and Anderson, M. E. (1982). An autoradiographic study of efferent connections of the globus pallidus in *Macaca Mulatta*. *Exp. Brain Res.* 46, 107–117. doi: 10.1007/bf00238104

DeVito, J. L., Anderson, M. E., and Walsh, K. E. (1980). A horseradish peroxidase study of afferent connections of the globus pallidus in *Macaca mulatta*. *Exp. Brain Res.* 38, 65–73.

Dostrovsky, J. O., and Lozano, A. M. (2002). Mechanisms of deep brain stimulation. *Mov. Disord.* 17(Suppl. 3), S63–S68.

Eldridge, F. L., Millhorn, D. E., Kiley, J. P., and Waldrop, T. G. (1985). Stimulation by central command of locolmotion, respiration and circulation during exercise. *Respir. Physiol.* 59, 313–337. doi: 10.1016/0034-5687(85)90136-7

Fabbri, M., Coelho, M., Guedes, L. C., Rosa, M. M., Abreu, D., Gonçalves, N., et al. (2017). Acute response of non-motor symptoms to subthalamic deep brain stimulation in Parkinson's disease. *Parkinsonism Relat. Disord.* 41, 113–117. doi: 10.1016/j.parkreldis.2017.05.003

Fedio, P., Cox, C. S., Neophytides, A., Conal-Frederick, G., and Chase, T. N. (1979). Neuropsychological profile of Huntington's disease: patients and those at risk. *Adv. Neurol.* 23, 239–255.

Ferrante, R. J., Beal, M. F., and Kowall, N. W. (1994). "Mechanisms of neural degeneration in Huntington's disease," in *The Basal Ganglia IV: New Ideas and Data on Structure and Function*, eds G. Percheron, J. S. McKenzie, and J. Feger (New York, NY: Plenum Press), 149–161.

Fogelson, N., Williams, D., Tijssen, M., van Bruggen, G., Speelman, H., and Brown, P. (2006). Different functional loops between cerebra.l cortex and the subthalamic area in Parkinson's disease. *Cereb. Cortex* 16, 64–75 doi: 10.1093/cercor/bhi084

François, C., Savy, C., Jan, C., Tande, D., Hirsh, E. C., and Yelnik, J. (2000). Dopaminergic innervation of the subthalamic nucleus in the normal state, in MPTP-treated monkeys, and in Parkinson's disease patients. *J. Comp. Neurol.* 425, 121–129. doi: 10.1002/1096-9861(20000911)425:1<121::aid-cne10>3.0.co;2-g

Gerfen, C. R., Staines, W. A., Arbuthnott, G. W., and Fibiger, H. C. (1982). Crossed connections of the substantia nigra in the rat. *J. Comp. Neurol.* 207, 283–303. doi: 10.1002/cne.902070308

Giolli, R. A., Gregory, K. M., Suzuki, D. A., Blanks, R. H., Lui, F., and Betelak, K. F. (2001). Cortical and subcortical afferents to the nucleus reticularis tegmenti pontis and basal pontine nuclei in the macaque monkey. *Vis. Neurosci.* 18, 725–740. doi: 10.1017/s0952523801185068

Grill, W. M., and Mcintyre, C. (2001). Extracellular excitation of central neurons: implications for the mechanism of deep brain stimulation. *Thalamus Relat. Syst.* 1, 269–277. doi: 10.1016/s1472-9288(01)00025-5

Grill, W. M., Snyder, A. N., and Miocinovic, S. (2004). Deep brain stimulation creates an informational lesion of the stimulated nucleus. *Neuroreport* 15, 1137–1140. doi: 10.1097/00001756-200405190-00011

Groenewegen, H. J., and Berendse, H. W. (1990). Connections of the subthalamic nucleus with ventral striatopallidal parts of the basal ganglia in the rat. *J. Comp. Neurol.* 294, 607–622. doi: 10.1002/cne.902940408

Hamani, C., Saint-Cyr, J. A., Fraser, J., Kaplitt, M., and Lozano, A. M. (2004). The subthalamic nucleus in the context of movement disorders. *Brain* 127, 4–20. doi: 10.1093/brain/awh029

Hamel, W., Köppen, J. A., Alesch, F., Antonini, A., Barcia, J. A., Bergman, H., et al. (2017). Targeting of the subthalamic nucleus for deep brain stimulation: a survey among Parkinson Disease specialists. *World Neurosurg.* 99, 41–46. doi: 10.1016/j.wneu.2016.11.012

Hardman, C. D., Halliday, G. M., McRitchie, D. A., and Morris, J. G. (1997). The subthalamic nucleus in Parkinson's disease and progressive supranuclear palsy. *J. Neuropathol. Exp. Neurolol.* 56, 132–142.

Hardman, C. D., Henderson, J. M., Finkelsen, D. I., Horne, M. K., Paxinos, G., and Halliday, G. M. (2002). Comparison of the basal ganglia in rats, marmosets, macaques, baboons and humans: volume and neuronal number for the output, internal relay and striatal modulating nuclei. *J. Comp. Neurol.* 445, 238–255. doi: 10.1002/cne.10165

Haynes, W. I., and Haber, S. N. (2013). The organization of the prefrontal-subthalamic inputs in primates provides an anatomical substrate for both functional specificity and integration: implications for basal ganglia models and deep brain stimulation. *J. Neurosci.* 33, 4804–4814. doi: 10.1523/JNEUROSCI.4674-12.2013

Hazrati, L. N., and Parent, A. (1992). Convergence of subthalamic and striatal efferents at pallidal level in primates: an anterograde double-labeling study with biocytin and PHA-L. *Brain Res.* 569, 336–340. doi: 10.1016/0006-8993(92)90648-s

Heilingoetter, C. L., and Jensen, M. B. (2017). Histological methods for ex vivo axon tracing: a systematic review. *Neurol. Res.* 38, 561–569. doi: 10.1080/01616412.2016.1153820

Isaacs, B. R., Forstmann, B. U., Temel, Y., and Keuken, M. C. (2018). The connectivity fingerprint of the human frontal cortex, subthalamic nucleus and striatum. *Front. Neuroanat.* 12:60. doi: 10.3389/fnana.2018.00060

Ishida, H., Inoue, K., Takada, M., and Hoshi, E. (2016). Origins of multisynaptic projections from the basal ganglia to the forelimb region of the ventral premotor cortex in macaque monkeys. *Eur. J. Neurosci.* 43, 258–269. doi: 10.1111/ejn.13127

Iwahori, N. (1987). A Golgi study on the subthalamic nucleus of the cat. *J. Comp. Neurol.* 182, 383–397. doi: 10.1002/cne.901820303

Joel, D., and Weiner, I. (1997). The connections of the primate subthalamic nucleus: indirect pathways and the open-interconnected scheme of basal ganglia-thalamocortical circuitry. *Brain Res. Brain Res. Rev.* 23, 62–78. doi: 10.1016/s0165-0173(96)00018-5

Joel, D., and Weiner, L. (2000). The connections of the dopaminergic system with the striatum in rats and primates: an analysis with respect to the functional and compartmental organization of the striatum. *Neuroscience* 96, 451–474. doi: 10.1016/s0306-4522(99)00575-8

Jones, D. K., Knösche, T. R., and Turner, R. (2013). White matter integrity, fiber count, and other fallacies: the do's and don'ts of diffusion MRI. *Neuroimage* 73, 239–254. doi: 10.1016/j.neuroimage.2012.06.081

Karachi, C., Yelnik, J., Tandé, D., Tremblay, L., Hirsch, E. C., and François, C. (2005). The pallidosubthalamic projection: an anatomical substrate for nonmotor functions of the subthalamic nucleus in primates. *Mov. Disord.* 20, 172–180. doi: 10.1002/mds.20302

Kearney, J. A., and Albin, R. L. (2000). Intrasubthalamic nucleus metabotropic glutamate receptor activation: a behavioral, Fos immunohistochemical and [14C]2-deoxyglucose autoradiographic study. *Neuroscience* 95, 409–416. doi: 10.1016/s0306-4522(99)00439-x

Kelly, R. M., and Strick, P. L. (2004). Macro-architecture of basal ganglia loops with the cerebral cortex: use of rabies virus to reveal multisynaptic circuits. *Prog. Brain Res.* 143, 449–459.

Keuken, M. C., Uylings, H. B., Geyer, S., Schäfer, A., Turner, R., and Forstmann, B. U. (2012). Are there three subdivisions in the primate subthalamic nucleus? *Front. Neuroanat.* 6:14. doi: 10.3389/fnana.2012.00014

Kim, R., Nakano, K., Jayaraman, A., and Carpenter, M. B. (1976). Projections of the globus pallidus and adjacent structures: an autoradiographic study in the monkey. *J. Comp. Neurol.* 169, 263–290.

Kita, H., Chang, H. T., and Kitai, S. T. (1983). The morphology of intracellularly labeled rat subthalamic neurons: a light microscopic analysis. *J. Comp. Neurol.* 215, 245–257. doi: 10.1002/cne.902150302

Kita, H., and Kitai, S. T. (1987). Efferent projections of the subthalamic nucleus in the rat: light and electron microscopic analysis with the PHA-L method. *J. Comp. Neurol.* 260, 435–452. doi: 10.1002/cne.902600309

Knook, H. L. (1965). *The Fibre-Connections of the Forebrain*. thesis. Van Gorcum and Co. N. V. Leiden.

Kosta, P., Argyropoulou, M. I., and Markoula, S. (2006). MRI evaluation of the basal ganglia size and iron content in patients with Parkinson's disease. *J. Neurol.* 253, 26–32. doi: 10.1007/s00415-005-0914-9

Kulisevsky, J., Berthier, M. L., and Gironell, A. (2002). Mania following deep brain stimulation for Parkinson's disease. *Neurology* 59, 1421–1424. doi: 10.1212/wnl.59.9.1421

Kunzle, H., and Akert, K. (1977). Efferent connections of cortical area 8 (frontal eye field) in Macaca Fascicularis. a reinvestigation using the autoradiographic technique. *J. Comp. Neurol.* 173, 147–164.

Lambert, C., Zrinzo, L., Nagy, Z., Lutti, A., Hariz, M., Foltynie, T., et al. (2012). Confirmation of functional zones within the human subthalamic nucleus: patterns of connectivity and sub-parcellation using diffusion weighted imaging. *Neuroimage* 60, 83–94. doi: 10.1016/j.neuroimage.2011.11.082

Lambert, C., Zrinzo, L., Nagy, Z., Lutti, A., Hariz, M., Foltynie, T., et al. (2015). Do we need to revise the tripartite subdivision hypothesis of the human subthalamic nucleus (STN)? Response to Alkemade and Forstmann. *Neuroimage* 110, 1–2. doi: 10.1016/j.neuroimage.2015.01.038

Lange, H., Thorner, G., Hopf, A., and Schroder, K. F. (1976). Morphometric studies of the neuropathological changes in choreatic diseases. *J. Neurol. Sci.* 28, 401–425. doi: 10.1016/0022-510x(76)90114-3

Larsen, M., Bjarkam, C. R., Østergaard, K., West, M. J., and Sørensen, J. C. (2004). The anatomy of the porcine subthalamic nucleus evaluated with immunohistochemistry and design-based stereology. *Anat. Embryol.* 208, 239–247.

Lavoie, B., and Parent, A. (1994a). Pedunculopontine nucleus in the squirrel monkey: cholinergic and glutamatergic projections to the substantia nigra. *J. Comp. Neurol.* 344, 232–241. doi: 10.1002/cne.903440205

Lavoie, B., and Parent, A. (1994b). Pedunculopontine nucleus in the squirrel monkey: distribution of cholinergic and monoaminergic neurons in the mesopontine tegmentum with evidence for the presence of glutamate in cholinergic neurons. *J. Comp. Neurol.* 344, 190–209. doi: 10.1002/cne.903440203

Lavoie, B., and Parent, A. (1994c). Pedunculopontine nucleus in the squirrel monkey: projections to the basal ganglia as revealed by anterograde tract-tracing methods. *J. Comp. Neurol.* 344, 2010–2031.

Lavoie, B., Smith, Y., and Parent, A. (1989). Dopaminergic innervation of the basal ganglia in the squirrel monkey, as revealed by tyrosine hydroxylase immunohistochemistry. *J. Comp. Neurol.* 289, 36–52. doi: 10.1002/cne.902890104

Levesque, J. C., and Parent, A. (2005). GABAergic interneurons in human subthalamic nucleus. *Mov. Disord.* 20, 574–584. doi: 10.1002/mds.20374

Lozano, A. M., Dostrovsky, J., Chen, R., and Ashby, P. (2002). Deep brain stimulation for Parkinson's disease: disrupting the disruption. *Lancet Neurol.* 1, 225–231. doi: 10.1016/s1474-4422(02)00101-1

Luys, J. (1865). *Recherches sur le systeme nerveux cerebro-spinal: sa structure, ses fonctions et ses maladies*. Paris: Bailliere.

Magill, P., Bolam, J., and Bevan, M. (2000). Relationship of activity in the subthalamic nucleus-globus pallidus network to cortical electroencephalogram. *J. Neurosci.* 20, 820–833. doi: 10.1523/jneurosci.20-02-00820.2000

Marani, E., Heida, T., Lakke, E. A., and Usunoff, K. G. (2008). The subthalamic nucleus. Part I: development, cytology, topography and connections. *Adv. Anat. Embryol. Cell. Biol.* 198, 1–113.

Martin, J. D., and Gusella, J. F. (1986). Huntington's disease: pathogenesis and management. *N. Eng. J. Med.* 315, 1267–1276.

Martin, J. P. (1927). Hemichorea resulting from a local lesion of the brain (the syndrome of the body of Luys). *Brain* 50, 637–651.

Massey, L. A., Miranda, M. A., Zrinzo, L., Al-Helli, O., Parkes, H. G., Thornton, J. S., et al. (2012). High resolution MR anatomy of the subthalamic nucleus: imaging at 9.4 T with histological validation. *Neuroimage* 59, 2035–2044. doi: 10.1016/j.neuroimage.2011.10.016

Massey, L. A., and Yousry, T. A. (2010). Anatomy of the substantia nigra and subthalamic nucleus on MR imaging. *Neuroimaging Clin. N. Am.* 20, 7–27. doi: 10.1016/j.nic.2009.10.001

Mathai, A., and Smith, Y. (2011). The corticostriatal and corticosubthalamic pathways: two entries, one target. So what? *Front. Syst. Neurosci.* 1:64. doi: 10.3389/fnsys.2011.00064

Mcintyre, C. C., Grill, W. M., Sherman, D. L., and Thakor, N. V. (2004). Cellular effects of deep brain stimulation: model-based analysis of activation and inhibition. *J. Neurophysiol.* 91, 1457–1469.

Milardi, D., Arrigo, A., Anastasi, G., Cacciola, A., Marino, S., Mormina, E., et al. (2016). Extensive direct subcortical cerebellum-basal ganglia connections in human brain as revealed by constrained spherical deconvolution tractography. *Front. Neuroanat.* 10:29. doi: 10.3389/fnana.2016.00029

Miyachi, S., Lu, X., Imanishi, M., Sawada, K., Nambu, A., and Takada, M. (2006). Somatotopically arranged inputs from putamen and subthalamic nucleus to primary motor cortex. *Neurosci. Res.* 56, 300–308.

Mori, S., Takino, T., Yamada, H., and Sano, Y. (1985). Imunohistochemical demonstration of serotonin nerve fibers in the subthalamic nucleus of the rat, cat and monkey. *Neurosci. Lett.* 62, 305–309.

Morizumii, T., Nakamura, Y., Kitao, Y., and Kudo, M. (1987). Ultrastructural anlyses of afferent terminals in the subthalamic nucleus of the cat with a combined degeneration and horseradish peroxidase tracing method. *J. Comp. Neurol.* 265, 159–174.

Muthusamy, K. A., Aravamuthan, B. R., Kringelbach, M. L., Jenkinson, N., Voets, N. L., Johansen-Berg, H., et al. (2007). Connectivity of the human pedunculopontine nucleus region and diffusion tensor imaging in surgical targeting. *J. Neurosurg.* 107, 814–820.

Nambu, A., Takada, M., Hamada, I., Kita, H., Imanishi, M., Akazawa, T., et al. (2000). Excitatory cortical inputs to pallidal neurons via the subthalamic nucleus in the monkey. *J. Neurophysiol.* 84, 289–300.

Nambu, A., Takada, M., Inase, M., and Tokuno, H. (1996). Dual somatotopical representations in the primate subthalamic nucleus: evidence for ordered but reversed body-map transformations from the primary motor cortex and supplementary motor area. *J. Neurosci.* 16, 2671–2683.

Nambu, A., Tokuno, H., Inase, M., and Takada, M. (1997). Corticosubthalamic input zones from forelimb representations of the dorsal and ventral divisions of the premotor cortex in the macaque monkey: comparison with the input zones from the primary motor cortex and the supplementary motor area. *Neurosci. Lett.* 239, 13–16.

Nauta, H. J. W., and Cole, M. (1978). Efferent projections of the subthalamic nucleus: an autoradiographic study in monkey and cat. *J. Comp. Neurol.* 180, 1–16.

Nauta, W. J., and Mehler, W. R. (1966). Projections of the lentiform nucleus in the monkey. *Brain Res.* 1, 3–42.

Pahapill, P. A., and Lozano, A. M. (2000). The pedunculopontine nucleus and Parkinson's disease. *Brain* 123, 1767–1783.

Parent, A., and Hazrati, L. N. (1995). Functional anatomy of the basal ganglia. II. The place of subthalamic nucleus and external pallidum in basal ganglia circuitry. *Brain Res. Brain Res. Rev.* 20, 128–154.

Parent, A., Sato, F., Wu, Y., Gauthier, J., Levesque, M., and Parent, M. (2000). Organization of the basal ganglia: the importance of axonal collateralization. *Trends Neurosci.* 23 (10 suppl.), S20–S27.

Parent, A., and Smith, Y. (1987). Organization of efferent projections of the subthalamic nucleus in the squirrel monkey as revealed by retrograde labeling methods. *Brain Res.* 436, 296–310.

Pelzer, E. A., Hintzen, A., Goldau, M., von Cramon, D. Y., Timmermann, L., and Tittgemeyer, M. (2013). Cerebellar networks with basal ganglia. Feasibility for tracking cerebello-pallidal and subthalamo-cerebellar projections in the human brain. *Eur. J. Neurosci.* 38, 3106–3114. doi: 10.1111/ejn.12314

Percheron, G., Filion, M., and Yelnik, J. (1987). "Spatial organization and information processing in the core of the basal ganglia," in *The Basal Ganglia II: Structure and Function – Currecnt Concepts*, eds M. B. Carpenter and A. Jayraman (New York, NY: Plenum Press), 205–226.

Percheron, G., and Fillon, M. (1991). Parallel processing in the basal ganglia: up to a point. *Trends Neurosci.* 14, 55–56.

Percheron, G., Francois, C., Yelnik, J., Fenelon, G., and Talbi, B. (1994). "The basal ganglia related systems of primates: definition, description and informational analysis," in *The Basal Ganglia IV: New Ideas and Data on Structure and Function*, eds G. Percheron, J. S. McKenzie, and J. Feger (New York, NY: Plenum Press), 3–20.

Petersen, M. V., Lund, T. E., Sunde, N., Frandsen, J., Rosendal, F., Juul, N., et al. (2017). Probabilistic versus deterministic tractography for delineation of the cortico-subthalamic hyperdirect pathway in patients with Parkinson disease selected for deep brain stimulation. *J. Neurosurg.* 126, 1657–1668. doi: 10.3171/2016.4.JNS1624

Petersen, M. V., Mlakar, J., Haber, S. N., Parent, M., Smith, Y., Strick, P. L., et al. (2019). Holographic reconstruction of axonal pathways in the human brain. *Neuron* 104, 1056–1064. doi: 10.1016/j.neuron.2019.09.030

Petry-Schmelzer, J. N., Krause, M., Dembek, T. A., Horn, A., Evans, J., Ashkan, K., et al. (2019). Non-motor outcomes depend on location of neurostimulation in Parkinson's disease. *Brain* 142, 3592–3604. doi: 10.1093/brain/awz285

Plantinga, B. R., Roebroeck, A., Kemper, V. G., Uludağ, K., Melse, M., Mai, J., et al. (2016). Ultra-High field MRI post mortem structural connectivity of the Human Subthalamic Nucleus, Substantia Nigra, and Globus Pallidus. *Front. Neuroanat.* 10:66. doi: 10.3389/fnana.2016.00066

Plantinga, B. R., Temel, Y., Duchin, Y., Uludag, K., Patriat, R., Roebroeck, A., et al. (2018). Individualized parcellation of the subthalamic nucleus in patients with Parkinson's Disease with 7T MRI. *Neuroimage* 168, 403–411.

Porzionato, A., Macchi, V., Zaramella, P., Sarasin, G., Grisafi, D., Dedja, A., et al. (2015). Effects of postnatal hyperoxia exposure on the rat dentate gyrus and subventricular zone. *Brain Struct. Funct.* 220, 229–247. doi: 10.1007/s00429-013-0650-3

Pujol, S., Cabeen, R., Sébille, S. B., Yelnik, J., François, C., Fernandez Vidal, S., et al. (2017). In vivo Exploration of the connectivity between the subthalamic nucleus and the globus pallidus in the human brain using multi-fiber tractography. *Front. Neuroanat.* 10:119. doi: 10.3389/fnana.2016.00119

Rafols, J. A., and Fox, C. A. (1976). The neurons in the primate subthalamic nucleus: A Golgi and electron microscopic study. *J. Comp. Neurol.* 168, 75–112.

Ranck, J. B. (1975). Which elements are excited in electrical stimulation of mammalian central nervous system: a review. *Brain Res.* 98, 417–440.

Ranson, S. W., and Berry, C. (1941). Observations on monkeys with bilateral lesions of the globus pallidus. *Arch. Neurol. Psychat.* 46, 504–508.

Ranson, S. W., Ranson, S. W. Jr., and Ranson, M. (1941). Fiber connections of the corpus striatum as seen in Marchi preparations. *Arch. Neurol. Psychat.* 46, 230–249.

Reiner, A., Albin, R. L., Anderson, K. D., D'Amato, C. J., Penney, J. B., and Young, A. B. (1988). Differential loss of striatal projection neurons in Huntington's disease. *Proc. Nat. Acad. Sci. U.S.A.* 85, 5733–5737.

Rico, A. J., Barroso Chinea, P., Conte-Perales, L., Roda, E., Gomez-Bautista, V., Gendive, M., et al. (2010). A direct projection from the subthalamic nucleus to the ventral thalamus in monkeys. *Neurobiol. Dis.* 39, 381–392.

Rinvik, E., Grofova, I., Hammond, C., Féger, J., and Deniau, J. M. (1979). A study of the afferent connections of the subthalamic nucleus in the monkey and the cat using the HRP technique. *Adv. Neurol.* 24:53.

Rutledge, J. N., Hilal, S. K., and Silver, A. J. (1987). Study of movement disorders and brain iron by MR. *Am. J. Roentgenol.* 149, 365–379.

Sadikot, A. F., Parent, A., and François, C. (1992). Efferent connections of the centromedian and parafascicular talami nuclei in the squirrel monkey: a PHA-L study of subcortical projections. *J. Comp. Neurol.* 315, 137–159.

Saint-Cyr, J. A., Trepanier, L. L., Kumar, R., Lozano, A. M., and Lang, A. E. (2000). Neuropsychological consequences of chronic bilateral stimulation of the subthalamic nucleus in Parkinson's disease. *Brain* 123, 2091–2108.

Salvesen, L., Ullerup, B. H., Sunay, F. B., Brudek, T., Lokkegaard, A., Agander, T. K., et al. (2015). Changes in total cell numbers of the basal ganglia in patients with multiple system atrophy – A stereological study. *Neurobiol. Dis.* 74, 104–113. doi: 10.1016/j.nbd.2014.11.008

Sato, F., Lavallée, P., Lévesque, M., and Parent, A. (2000a). Single-axon tracing study of neurons of the external segment of the globus pallidus in primate. *J. Comp. Neurol.* 417, 17–31.

Sato, F., Parent, M., Levesque, M., and Parent, A. (2000b). Axonal branching pattern of neurons of the subthalamic nucleus in primates. *J. Comp. Neurol.* 424, 142–152.

Shink, E., Bevan, M. D., and Bolam, J. P. (1996). The subthalamic nucleus and the external pallidum: two tightly interconnected structures that control the output of the basal ganglia in the monkey. *Neuroscience* 73, 335–357.

Smith, Y., Hazrati, L. N., and Parent, A. (1990). Efferent projections of the subthalamic nucleus in the squirrel monkey as studied by the PHA-L anterograde tracing method. *J. Comp. Neurol.* 294, 306–323.

Smith, Y., and Parent, A. (1986). Differential connections of caudate nucleus and putamen in the squirrel monkey (*Saimiri sciureus*). *Neuroscience* 18, 347–371.

Smith, Y., Shink, E., Bevan, M. D., and Bolan, J. P. (1995). The subthalamic nucleus and the external pallidum: two tightly interconnected structures that

control the output of the basal ganglia in primates. *Brain Res. Ass. Abstr.* 12:89.

Tai, L. S., Ng, T. K., Mak, N. K., and Yung, K. K. (2001). Co-localization of AMPA-type glutamate receptor immunoreactivity in neurons of the rat subthalamic nucleus. *Brain Res.* 895, 95–103.

Tandé, D., Féger, J., Hirsch, E. C., and François, C. (2006). Parafascicular nucleus projection to the extrastriatal basal ganglia in monkeys. *Neuroreport* 17, 277–280.

Temel, Y., Blokland, A., Steinbusch, H. W., and Visser-Vandewalle, V. (2005). The functional role of the subthalamic nucleus in cognitive and limbic circuits. *Prog. Neurobiol.* 76, 393–413.

Temel, Y., Kessels, A., Tan, S., Topdag, A., Boon, P., Visser-Vandewalle, V., et al. (2006a). Behavioural changes after bilateral subthalamic stimulation in advanced Parkinson disease a systematic review. *Parkinsonism Relat. Disord.* 12, 265–272.

Temel, Y., Visser-Vandewalle, V., Kaplan, S., Kozan, R., Daemen, M. A., Blokland, A., et al. (2006b). Protection of nigral cell death by bilateral subthalamic nucleus stimulation. *Brain Res.* 1120, 100–105.

Temel, Y., and Visser-Vandewalle, V. (2006). Targets for deep brain stimulation in Parkinson's Disease. *Expert. Opin. Ther. Targets* 10, 355–362. doi: 10.5137/1019-5149.JTN.25028-18.3

Thomas, C., Ye, F. Q., Ifranoglu, M. O., Modi, P., Saleem, K. S., Leopold, D. A., et al. (2014). Anatomical accuracy of brain connections derived from diffusion MRI tractography is inherently limited. *Proc. Natl. Acad. Sci. U.S.A.* 111, 16574–16579. doi: 10.1073/pnas.1405672111

Urbain, N., Rentero, N., Gervasoni, D., Renaud, B., and Chouvet, G. (2002). The switch of subthalamic neurons from an irregular to a bursting pattern does not solely depend on their GABAergic inputs in the anesthetic-free rat. *J. Neurosci.* 22, 8665–8675.

Vergani, F., Landi, A., Antonini, A., Parolin, M., Cilia, R., Grimaldi, M., et al. (2007). Anatomical identification of active contacts in subthalamic deep brain stimulation. *Surg. Neurol.* 67, 140–146.

Von Monakow, K. H., Akert, K., and Kuzle, H. (1978). Projections of the precentral motor cortex and other cortical areas f the frontal lobe to the subthalamic nucleus in the monkey. *Exp. Brain. Res.* 33, 395–403.

Wang, X. S., Ong, W. Y., Lee, H. K., and Huganir, R. L. (2000). A light and electron microscopic study of glutamate receptors in the monkey subthalamic nucleus. *J. Neurocytol.* 29, 743–754.

Wang, Z. M., Wei, P. H., Shan, Y., Han, M., Zhang, M., Liu, H., et al. (2020). Identifying and characterizing projections from the subthalamic nucleus to the cerebellum in humans. *Neuroimage* 210:116573. doi: 10.1016/j.neuroimage.2020.116573

Whittier, J. R., and Mettler, F. A. (1949). Studies on the subthalamus of the rhesus monkey. I. Anatomy and fiber connections of the subthalamic nucleus of Luys. *J. Comp. Neur.* 90, 281–318.

Williams, P. L., and Warwick, R. (1980). "The ventral thalamus or subthalamus," in *Gray's Anatomy*, 36th Edn, eds P. L. Williams and R. Warkick (Edinburgh: Churchill Livingstone), 963–965.

Wu, Y., and Parent, A. (2000). Striatal interneurons expressing calretinin, parvalbumin or NADPH- diaphorase: a comparative study in the rat, monkey and human. *Brain Res.* 863, 182–191.

Yelnik, J., and Percheron, G. (1979). Subthalamic neurons in primates: a quantitative and comparative analysis. *Neuroscience* 4, 1717–1743.

Zwirner, J., Mobius, D., Bechmann, I., Arendt, T., Hoffmann, K. T., Jager, C., et al. (2017). Subthalamic nucleus volumes are highly consistent but decrese age-dependently – a combined magnetic resonance imaging and stereology approach in humans. *Hum. Brain Mapp.* 38, 909–922. doi: 10.1002/hbm.23427

Conflict of Interest: The authors declare that the research was conducted in the absence of any commercial or financial relationships that could be construed as a potential conflict of interest.

frontiers | Frontiers in Neuroscience

TYPE Brief Research Report
PUBLISHED 09 August 2022
DOI 10.3389/fnins.2022.945574

OPEN ACCESS

EDITED BY
Giuseppe Anastasi,
University of Messina, Italy

REVIEWED BY
Francesco Fornai,
University of Pisa, Italy
Manuel Narvaez Peláez,
University of Malaga, Spain

*CORRESPONDENCE
Andrea Porzionato
andrea.porzionato@unipd.it

†These authors have contributed equally to this work and share first authorship

SPECIALTY SECTION
This article was submitted to Neurodegeneration, a section of the journal Frontiers in Neuroscience

RECEIVED 16 May 2022
ACCEPTED 20 July 2022
PUBLISHED 09 August 2022

CITATION
Emmi A, Antonini A, Sandre M, Baldo A, Contran M, Macchi V, Guidolin D, Porzionato A and De Caro R (2022) Topography and distribution of adenosine A_{2A} and dopamine D_2 receptors in the human Subthalamic Nucleus.
Front. Neurosci. 16:945574.
doi: 10.3389/fnins.2022.945574

Topography and distribution of adenosine A_{2A} and dopamine D_2 receptors in the human Subthalamic Nucleus

Aron Emmi[1,2,3†], Angelo Antonini[2,3†], Michele Sandre[2,3], Andrea Baldo[1], Martina Contran[1], Veronica Macchi[1,2], Diego Guidolin[1], Andrea Porzionato[1,2*] and Raffaele De Caro[1,2]

[1]Department of Neurosciences, Institute of Human Anatomy, University of Padova, Padua, Italy, [2]Center for Neurodegenerative Disease Research (CESNE), University of Padova, Padua, Italy, [3]Movement Disorders Unit, Neurology Clinic, University Hospital of Padova, Padua, Italy

The human Subthalamic Nucleus (STh) is a diencephalic lens-shaped structure located ventrally to the thalamus and functionally implicated in the basal ganglia circuits. Despite recent efforts to characterize the neurochemical and functional anatomy of the STh, little to no information is available concerning the expression and distribution of receptors belonging to the dopaminergic and purinergic system in the human STh. Both systems are consistently implicated in basal ganglia physiology and pathology, especially in Parkinson's Disease, and represent important targets for the pharmacological treatment of movement disorders. Here, we investigate the topography and distribution of A_{2A} adenosine and D_2 dopamine receptors in the human basal ganglia and subthalamic nucleus. Our findings indicate a peculiar topographical distribution of the two receptors throughout the subthalamic nucleus, while colocalization between the receptors opens the possibility for the presence of A_{2A}R- D_2R heterodimers within the dorsal and medial aspects of the structure. However, further investigation is required to confirm these findings.

KEYWORDS

D_2R, A_{2A}R, subthalamic nucleus, receptor-receptor interactions, neuroanatomy, Parkinson's disease, deep brain stimulation, neurodegeneration

Introduction

The human Subthalamic Nucleus (STh) is a diencephalic lens-shaped structure located ventrally to the thalamus and functionally implicated in the basal ganglia circuits. While we have previously described the structure, topography and connectivity of the subthalamic nucleus in humans and non-human primates (Emmi et al., 2020), recent work by Alkemade et al. (2019) has focused on the characterization of the functional microscopic anatomy of the structure, with particular regard to the distribution of GABAergic, glutammatergic, dopaminergic and serotoninergic signaling markers.

However, despite recent efforts to characterize the neurochemical and functional anatomy of the STh, little to no information is available concerning the expression and distribution of receptors belonging to the dopaminergic and purinergic system in the human STh. Both systems are consistently implicated in basal ganglia physiology and pathology in several movement disorder incuding Parkinson's Disease (PD), and represent important targets for the pharmacological treatment of motor symptoms in PD. For this purpose, the characterization of dopaminergic and purinergic receptor expression and distribution within the human basal ganglia, and in particular the STh, appears to be highly relevant for their supposed role in the pathophysiology of PD, as previously demonstrated in rodent and non-human primate models.

Dopaminergic system and receptors

Despite the known connections between the STh and the substantia nigra pars compacta (SNpc) (Emmi et al., 2020) SNpc dopaminergic fibers have been reported to travel across the STh without forming synapses, projecting mainly the striatum (Hedreen, 1999; Alkemade et al., 2015). Only a low number of SN fibers actually appear to form dopaminergic synapses within the STh, mainly in its mediodorsal aspect (Emmi et al., 2020). In rodents, dopaminergic receptor D1 showed variable immunoreactivity that ranged from absent to moderate (Dawson et al., 1986; Dubois et al., 1986; Fremeau et al., 1991; Johnson et al., 1994). Only Savasta et al. (1986) reported a high expression of D_1R whithin rodent STh, while Mansour et al. (1992) evidenced dense D_1 receptor binding but no evidence of D_1 mRNA. D_2R expression in rodent STh was reported as low by Dubois et al. (1986) and moderate by Johnson et al. (1994). In non-human primates, D_1 and D_2 receptors were found presynaptically, on preterminal axons and putative glutamatergic and GABAergic terminals (Galvan et al., 2014). Studies of the human STh displayed no evidence for D_1R expression (Augood et al., 2000; Hurd et al., 2001) and reported conflicting results as far as D_2R is concerned, ranging from negative (Augood et al., 2000), to low (Hurd et al., 2001) or moderate (Wang et al., 2001). The expression of other dopaminergic receptors, such as D_3R and D_4R, was documented by Wang et al. (2001) and Matsumoto et al. (2002) respectively.

Purinergic system and receptors

Very little evidence is available on the expression and distribution of purinergic receptors in the human and non-human primate basal ganglia, despite the recent interest in the purinergic modulation of basal ganglia circuitry and the approval of the first purinergic drug for the treatment of Parkinson's Disease in the United States and Japan. The expression of adenosine receptor A_1 within the human STh was described by Misgeld et al. (2007), while we are not aware of any studies addressing the presence of A_2 receptor within the STh in humans.

In the present study, we investigate the distribution of $A_{2A}R$ purinergic and D_2 dopaminergic receptors within the rostro-caudal extent of the human STh and the surrounding basal ganglia district. Both receptors have been functionally implicated in the modulation of basal ganglia circuitry and represent potential targets for the pharmacological treatment of movement disorders, such as Parkinson's Disease, with little-to-no studies addressing their expression and distribution in the human basal ganglia.

Materials and methods

Tissue preparation

Ten (10) Human Brains with no history of neurological or psychiatric disorders obtained from the Body Donation Program of the Institute of Human Anatomy of University of Padova (Porzionato et al., 2012; Emmi et al., 2021a,b) were employed for the study. All procedures were carried out according to the ethical standards of the Body Donation Program and to the Declaration of Helsinki. The mean age of the body donors was 56,5 ± 20 years (**Table 1**). The post-mortem delay was within 24-72h. All specimens were sampled and fixed in-toto in 4% phosphate-buffered formalin solution. Whole-volume coronally sectioned tissue blocks containing the rostro-caudal extent of the STh and the surrounding basal ganglia district were manually processed for paraffin embedding. Paraffin-embedded samples were serially sectioned at 5-micron thickness using a calibrated sliding microtome. Specimen tissue quality and general histopathology was evaluated on

TABLE 1 Clinical data of the study cohort.

Id	Age	Sex	Cause of death
#1	75	M	Myocardial infarction
#2	48	F	Cervical carcinoma, Cardio-respiratory failure
#3	38	M	Carotid artery dissection
#4	36	F	Cardio-respiratory failure
#5	60	M	Cardio-respiratory failure
#6	20	F	Acute Myeloid Leukemia
#7	66	M	Prostatic Cancer
#8	75	F	Cardio-respiratory failure
#9	78	F	Myocardial Infarction
#10	69	M	Cardio-respiratory failure
MEAN	**56,5±20 Years**		

Haematoxylin & Eosin stained sections (Porzionato et al., 2020). A fraction of 1/30 serial slides, for an average of 20 ± 2 slides per subject, were employed for immunoperoxidase and immunofluorescent staining.

Immunoperoxidase staining and microscopy

Immunohistochemical staining for A_{2A} Adenosine receptor (7F6-G5-A2, Abcam, Cambridge, United Kingdom, dilution 1:200) and D_2 Dopamine receptor (Abcam, Cambridge, United Kingdom, dilution 1:100) were employed to characterize receptor distribution within the tissue. Antigen retrieval was performed using DAKO EnVision water bath station; A_{2A}R antigen retrieval was performed in a high pH EDTA-buffered bath at 95° Celsius for 15 min, while D_2R antigen retrieval was performed in a low pH Citrate buffered solution at 95° Celsius for 15 min. Sections were incubated in 0.3 % hydrogen peroxide for 5 min at room temperature to remove endogenous peroxidase activity, and then in blocking serum (3.6% bovine serum albumin A2153, Sigma-Aldrich, Milan, Italy and 0,05% Triton-X in PBS) for 90 min at room temperature. Primary antibodies were incubated for 1h at room temperature followed by correspective secondary antibodies for 30 min at room temperature. Lastly, sections were developed in Diamino-benzidine (DAB, Sigma-Aldrich, Milan, Italy) and counterstained with Haematoxylin. Photomicrographs were acquired with a Leica LMD6 (Leica Microsystems) connected to a Leica DFC320 high-resolution digital camera (Leica Microsystems) and a computer equipped with software for image acquisition (LasX, Leica Microsystems) and analysis (ImageJ). Images of the whole sections were acquired at 20x and 40x magnification and corrected for shading before being loaded into ImageJ software for semi-automatic immunoreactivity quantification, according to previosuly established methodology (Porzionato et al., 2021a,b; Emmi et al., 2022a,b).

Immunofluorescent staining and microscopy

Fluorescent immunohistochemistry was performed manually. Antigen retrieval was performed on de-paraffinized tissue sections using Dako EnVision PTLink station according to manufacturer recommendations. Following antigen retrieval, autofluorescence was quenched with a 50 mM NH_4Cl solution for 10 min. Sections were treated with permeabilization and blocking solution (15% vol/vol Goat Serum, 2% wt/vol BSA, 0.25% wt/vol gelatin, 0.2% wt/vol glycine in PBS) containing 0.5% Triton X-100 for 90 min before primary antibody incubation. Primary antibodies were diluted as above in blocking solution and incubated at 4°C overnight; additional immunofluorescent staining was performed for β-III Tubulin (#T8578; 1:300, anti-mouse; #T2200, 1:300, anti-rabbit) and Tyrosine Hydroxylase (#T2928; 1:6000) in combination with the aforementioned A_{2A}R and D_2R antibodies. Alexa-Fluor plus 488 Goat anti-Mouse secondary antibody (Code number: A32723) and Alexa-Fluor plus 568 anti-Rabbit secondary antibody (Code number: A-11011) were diluted 1:200 in blocking solution as above and incubated for 60 min at room temperature. To further avoid background signal and tissue autofluorescence, slides were incubated for 10 min in 0.5% Sudan Black B solution in 70% ethanol at room temperature and abundantly washed with PBS, followed by Hoechst 33258 nuclear staining (Invitrogen, dilution: 1:10000 in PBS) for 10 min. Slides were mounted and coverslipped with Mowiol solution (prepared with Mowiol 4-88 reagent, MerckMillipore, Code number: 475904-100GM). Epifluorescence z-stack images were acquired on a Leica LMD6 Microscope at 20x and 40x magnification. Images were acquired at a 16-bit intensity resolution over 2048 × 2048 pixels. Z-stacks images were converted into digital maximum intensity z-projections, processed, and analyzed using ImageJ software.

Semi-automatic immunoreactivity quantification

Serial sections of each STh were divided into rostral, central and caudal thirds (6 ± 2 slides per level). Digital photomicrographs of the lateral, dorsal, ventral and medial sectors were taken for each slide and morphometrical values were averaged within sections belonging to each assigned level, according to the schematization seen in Lévesque and Parent (2005), as seen in **Figure 4**. Digital photomicrographs taken with the aforementioned scheme were loaded as stack in ImageJ. The area of the sections was quantified by manually drawing the boundaries of the specimens. A Maximum Entropy Threshold was applied and manually adjusted for each section in order to discern immunoreactive elements from background and negative tissue. Quality control of the applied threshold was performed by an expert morphologist by overlying the thresholded images to the original photomicrographs. Particle analysis was employed with an experimentally defined pixel threshold in order to evidence immunoreactive elements quantity and total area, expressed as percentage (A%) within the digital image.

Statistical analyses

Statistical Analyses. Statistical analyses and visualizations were performed using GraphPad Prism 9. One-way non-parametric ANOVA (Friedman's test) was performed to evaluate receptor distribution throughout STh sectors, as seen in

Figures 4B,C. Further statistical details for each plot can be found in the corresponding figure legend. Throughout the text * indicates $p < 0.05$, ** $p < 0.01$, *** $p < 0.001$ and **** $p < 0.0001$.

Results

Distribution of A_{2A} and D_2 receptors

Immunoperoxidase staining for A_{2A} adenosine and D_2 dopamine receptors in the basal ganglia revealed a peculiar topographical organization, as shown in Figure 1. While D_2R appears to be uniformly distributed with mild-to-moderate expression within the basal ganglia (Figure 1A), $A_{2A}R$ immunoreactivity is particularly marked at the level of the Caudate Nucleus, Putamen and External Globus Pallidus (GPe) (Figures 1D,G), with very mild immunoreactivity detectable within the Claustrum (Figure 1F), Thalamus, Subthalamic Nucleus (Figures 1H,I) and Internal Globus Pallidus (Figure 1E). In the STh, D_2R immunoperoxidase staining revealed a predominantly neuritic immunoreactivity (Figure 1C), with dot-like reactivities representing the most common finding; sporadic cytoplasmic immunoreactivity of neuronal somata was also detected (range: 1–2 somatic reactivities per mm^2). Similarly, $A_{2A}R$ immunoperoxidase staining revealed mild reactivity detectable as oblongated neurite-like structures and sparse dot-like reactivities. Sporadic cytoplasmic immunoreactivity of neuronal somata was also detected (range: 1–2 somatic reactivities per mm^2).

Distribution of D_2 receptors in the human Subthalamic Nucleus

Double immunofluorescent staining for β-III-tubulin, a pan-neuronal marker, and receptor proteins ($A_{2A}R$ / D_2R) confirmed immunoperodidase staining findings (Figure 2). D_2R reactivity was found predominantly at the level of the dendritic spines of β-III-tubulin positive neurites (Figures 2A,B,B1,B2); while colocalization of D_2R signal (red channel) with β-III-tubulin (green channel) was predominant, sporadic non-colocalizing D2R signal was detected, compatible with reports in literature describing D_2R expression in non-neuronal (β-III-tubulin negative) cells, such as astrocytes (Pelassa et al., 2019). D_2R reactivity appears to follow a ventromedial-to-dorsal decreasing gradient (Figures 2A,B, 3A, 4A). As seen in Figures 3A, 4A, there appears to be a statistically significant difference in D_2R density between the Ventral and Dorsal STh in both the central (VC vs. DC) and posterior (VP vs. DP) third ($p = 0.0017$; $p = 0.0194$), as well as the Ventral and Medial STh ($p = 0.0017$; $p = 0.0109$); no difference was found between the ventral STh and the lateral pole, and throughout all sectors of the anterior third of the STh ($p > 0.05$).

Distribution of A_{2A} receptors in the human Subthalamic Nucleus

As seen in Figures 2C,D, A_{2A} receptor seems to be localized with a similar sub-cellular distribution as D2 receptors; indeed, most of the A_{2A} signal was detected as dot-like reactivities colocalizing predominantly with β-III-Tubulin positive neurites (Figure 2D), with the exception of sporadic somatic reactivites (Figure 2C) and non-β-III-tubulin positive structures [likely glial cells, as previously reported by Pelassa et al. (2019)]. Topographically, $A_{2A}R$ appear to follow a dorsal to ventral decreasing gradient, as seen in Figures 3A, 4C. Single-way Friedman test revealed statistically significant differences in $A_{2A}R$ density within these sectors of the STh, as seen in Figure 4D. While the distribution of $A_{2A}R$ appears to be more uniform within the anterior STh, marked differences between ventral and dorso-medial / dorso-lateral sectors become evident at the level of the central and posterior STh.

Colocalization of A_{2A} and D_2 receptors

Limited to the information obtained by double-immunofluorescence assays, colocalization between A_{2A} and D_2R signals was found throughout the STh, with a more prominent distribution of colocalizations found at the level of the medial and dorsal STh, as seen in Figures 3A–D. Interestingly, despite the lower distribution of D_2 receptors in the dorsal STh, the presence of $A_{2A}R$ colocalizations within the dorsal STh may indicate the presence of A_{2A}- D_2 receptor heterodimers, which are known to modulate dopaminergic afferences in the striatum. On the other hand, colocalization of D_2R and A_{2A} immunofluorescent signal does not prove the presence of A_{2A}-D2 heterodimers, which needs to be investigated with appropriate methodologies, such as proximity ligation assay (PLA).

Discussion

A_{2A} receptors are known to play an important role within the basal ganglia circuitry, in particular as postsynaptic facilitators in the GABAergic striato-pallidal neurons of the indirect pathway. Furthermore, $A_{2A}R$ are also expressed in the presynaptic terminals of glutamatergic neurons, in particular the context of cortico-striatal and thalamo-striatal pathways. In the STh, $A_{2A}R$ was detected at the level of β-III Tubulin immunoreactive dendritic spines and also in non-neuronal cells. Our findings also suggest a topography-specific distribution of

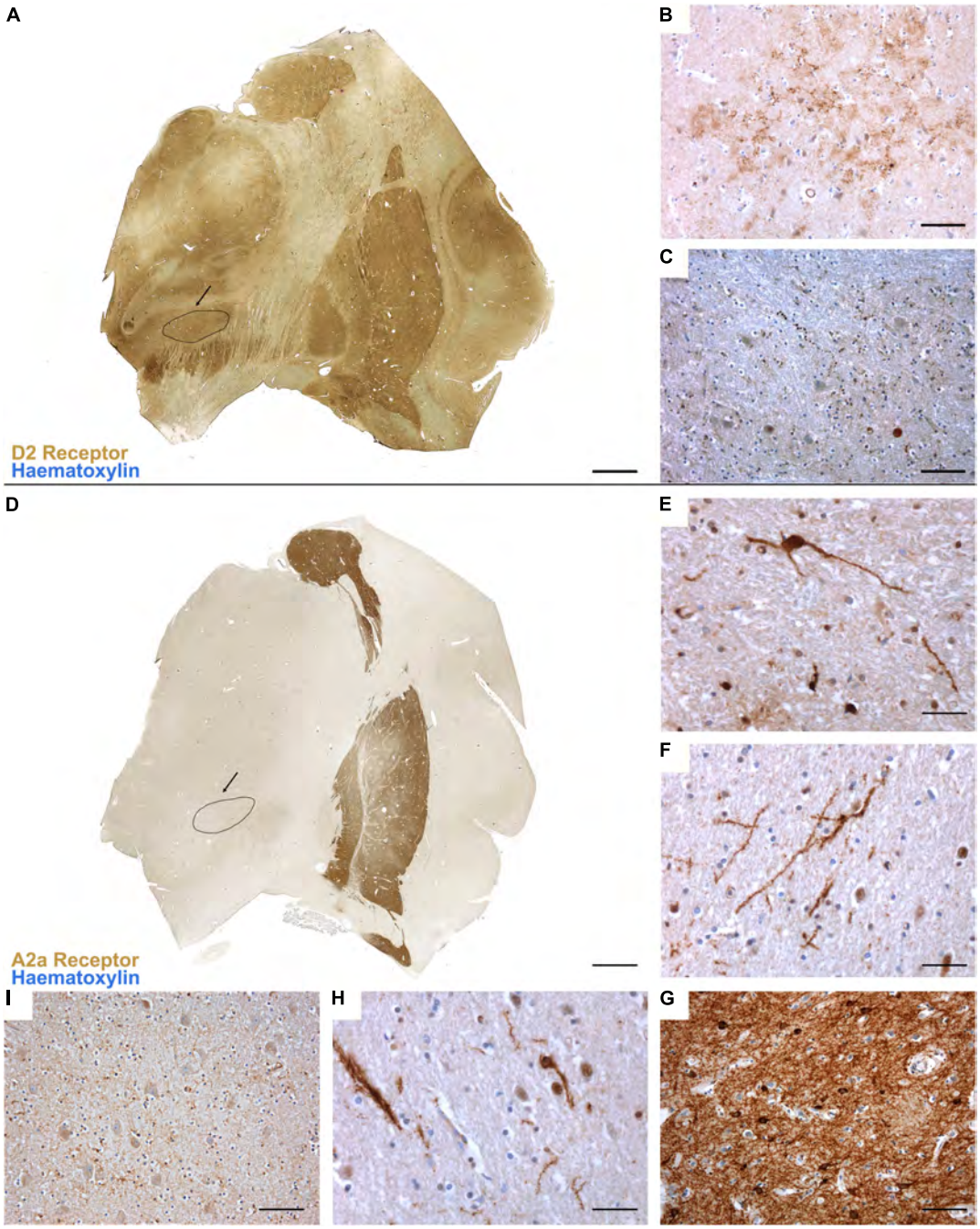

FIGURE 1
(A) Topographical distribution of D_2 dopamine receptor in the basal ganglia. Immunoperoxidase staining reveals a moderate, yet diffuse, distribution of the receptor, with no marked differences between the striatum, globus pallidus and subthalamic nucleus (evidenced in black). **(B)** D_2R immunoreactivity in the striatum and **(C)** in the subthalamic nucleus, where mainly neurites and dot-like reactivities are marked. **(D)** Topographical distribution of A_{2A} adenosine receptor in the basal ganglia reveals a marker expression of the receptor in the striatum **(G)** and external globus pallidus, with very mild expression in the internal globus pallidus **(E)**, claustrum **(F)**, thalamus and subthalamic nucleus [evidenced in black, **(H,I)**].

$A_{2A}R$, particularly in the anterior, medial and dorso-lateral STh. According to the morpho-functional subdivision of the STh, the anterior STh, as well as the medial thirds of the central and rostral STh, are functionally related to the limbic circuit, while the dorso-lateral STh is involved in the motor circuits, suggesting for a more prominent purinergic modulation of the limbic and motor STh when compared to the ventral (associative) STh.

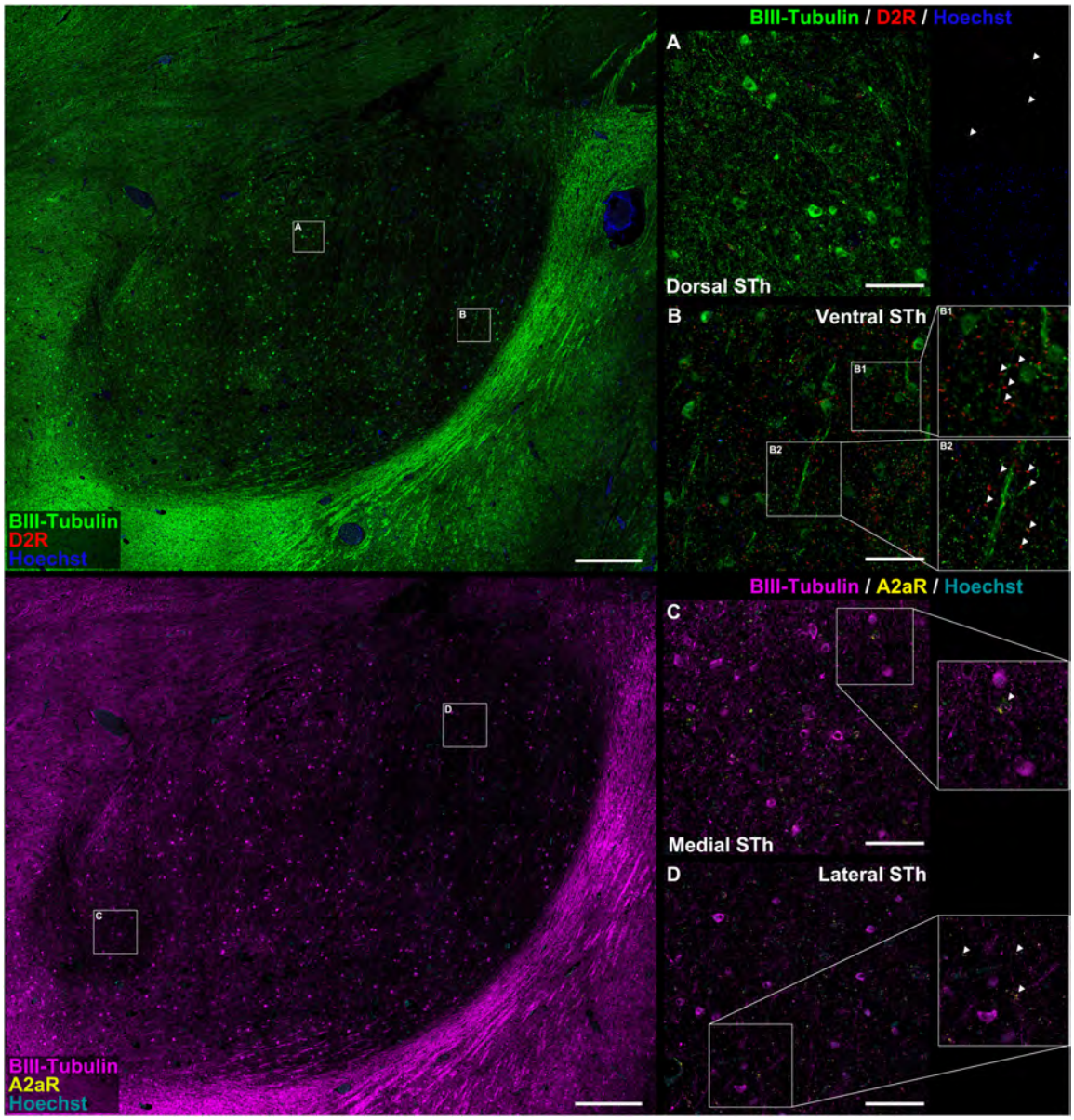

FIGURE 2
Colocalization study between $A_{2A}R$ / D_2R proteins and pan-neuronal marker β-III-tubulin. There appear to be significant differences in the distribution of D2 receptor immunofluorescent signal between the dorsal **(A)** and ventral **(B)** STh. In both instances, immunoreactivities mostly colocalized with β-III-tubulin neuritic structures at the level of dendritic spines [magnification in **(B)**]. In some occasions, D_2R did not colocalize with β-III-tubulin, suggesting for the expression of the receptor also in non-neuronal cells. $A_{2A}R$ can be found as dot-like immunoreactivities colocalizing with β-III-tubulin positive neurites or as rare somatic cytoplasmic reactivities **(C,D)**, even though non-β-III-tubulin colocalizing reactivities were also found.

Similarly, D_2R are known to act as modulators of glutamatergic synapses (Schiffmann et al., 2007). In the STh, we detected D_2R with a similar sub-cellular distribution as $A_{2A}R$, mainly as reactivities on dendritic spines and on sporadic non-neuronal cells. The topography of D_2R within the STh indicates a decreasing gradient between the ventral and medial STh toward the dorsolateral STh. This suggests for a more prominent role of D_2R modulation at the level of the associative (ventral) and limbic (medial) regions of the STh, rather than the motor (dorsal) regions of the STh. Interestingly, Tyrosyne Hydroxylase (TH) staining revealed a conspicuous bundle of cathetcolaminergic fibers originating from the substantia nigra (SN), coursing below the ventral aspect of the STh, and directed laterally toward the Striatum (**Supplementary Figure 1**, passing through the central STh). Sporadic TH+ fibers were found entering the STh from the ventral aspect, likely as collaterals

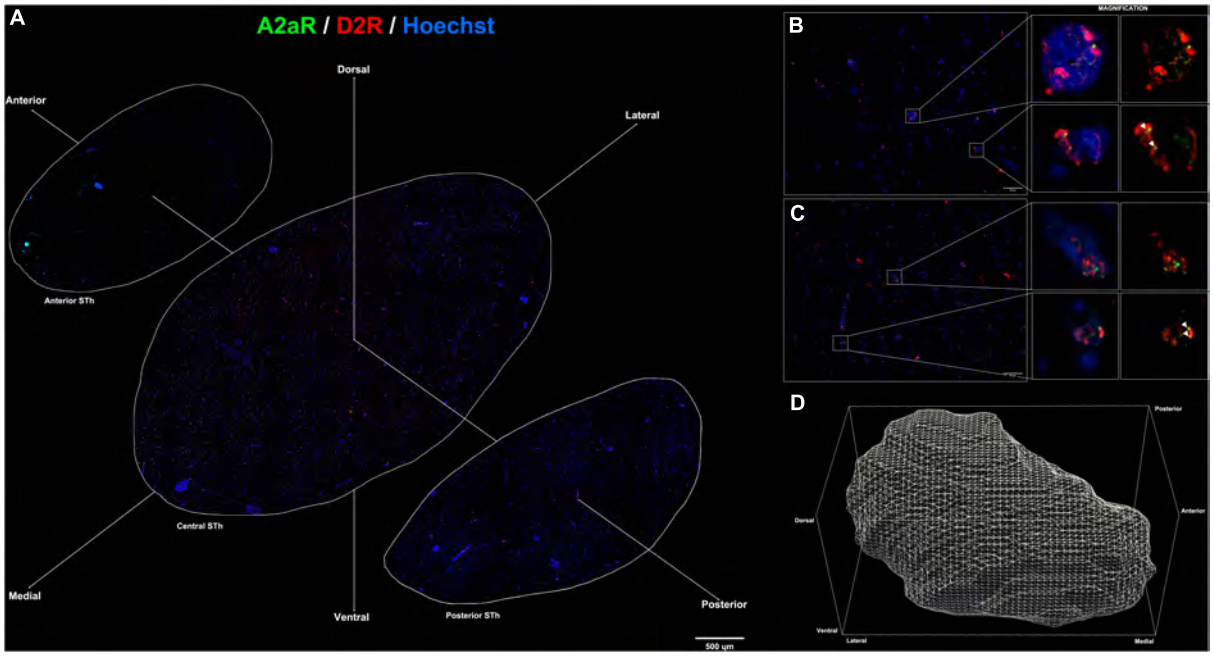

FIGURE 3
(A) Immunofluorescent staining for $A_{2A}R$ (green) and D_2R (red) throughout the rostro-caudal extent of the subthalamic nucleus reveals a peculiar topographical distribution. **(B,C)** colocalization of $A_{2A}R$ and D_2R proteins within the subthalamic nucleus (white arrows). **(D)** 3D representation of the structure of the subthalamic nucleus following reconstruction of serial sections.

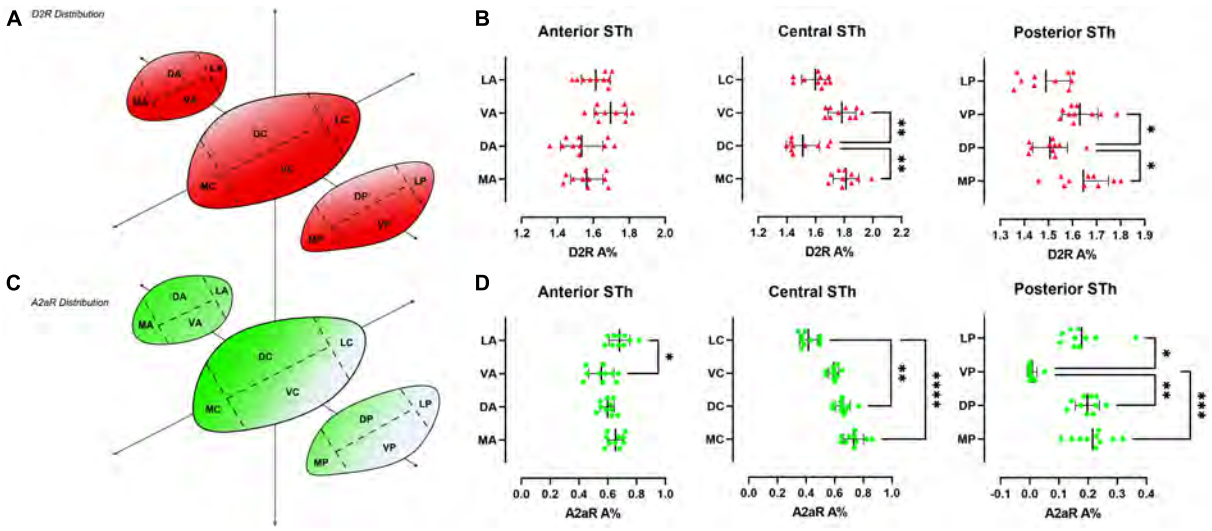

FIGURE 4
Heatmap of the distribution of D_2R **(A)** and $A_{2A}R$ **(C)** throughout the rostro-caudal extent of the STh, indicating a decreasing ventral-to-dorsal gradient for D_2R, and an opposite decreasing dorsomedial-to-ventral gradient for $A_{2A}R$. **(B,D)** Non-parametric ANOVA (Friedman's test) of the different levels of sectioning throughout the STh reveals topographical differences within specific STh subregions.

of the ventrally coursing nigro-striatal fibers, with little-to-no ramifications coursing toward the dorsal aspect of the STh. This is likely associated to the lower density of D_2R in the dorsal-central and -posterior STh.

The detection of colocalizing $A_{2A}R$ and D_2R in topographically defined regions of the STh represents an intriguing finding that requires further investigation, with particular regard to its implication in the modulation

of basal ganglia circuitry in health and disease. *In situ* Proximity Ligation Assay (PLA) (Narváez et al., 2021), as well as co-immunoprecipitation, can be employed to further confirm double-immunofluorescence findings. Interestingly, colocalization between the two receptors appears to be most prominent within the medial and dorsolateral STh. A_{2A} and D_2 receptors are often co-expressed in glutamatergic terminals, where they interact by heterodimerization with an antagonistic relationship, as the activation of a receptor inhibits the action of the other in controlling glutamate release (Guidolin et al., 2020). The antagonistic relationship between $A_{2A}R$ and D_2R leads to reduced D_2R recognition and $G_{i/0}$ coupling (Guidolin et al., 2020) and, consequently, an inhibition of the Ca^{2+} influx over the L-type voltage dependent calcium channels, thus modulating the excitability of these neurons (Fuxe et al., 2010). The detection of colocalizing $A_{2A}R$ and D_2R, particularly in the dorsal STh, may indicate a selective role of receptor heteromers in modulating neuronal activity in the motor regions of the STh.

Given their role in the regulation of motor function within the Basal Ganglia, A_{2A} and D_2 receptors were evaluated as a Parkinson's Disease therapeutic target, basing on the results obtained with co-administration of A_{2A} receptor antagonist and L-DOPA or preferential D_2R antagonists (Ferré et al., 1997). The involvement of $A_{2A}R$ - D_2R heteromers in the pathogenesis of PD appears to be supported by the higher level of expression of heteromers in the Striatum of PD patients (Fernández-Dueñas et al., 2019). In fact, the antagonistic interaction between $A_{2A}R$ and D_2R appears to be increased in the striatum of murine models of Parkinson's disease (Ferré and Fuxe, 1992; Schwarzschild et al., 2006; Fuxe et al., 2010). According to Schiffmann et al. (2007), A_{2A} and D_2R receptors are expressed in striatal GABAergic neurons involved in motor functions with a facilitator and inhibitory role, respectively. Furthermore, the expression of D_2R, $A_{2A}R$ and mGluR5 heteromers, and therefore the interaction between these receptors, within the dendritic spines of dorsal and ventral striato-pallidal GABAergic neurons involved in PD, may suggest an involvement of these receptors in the pathogenesis of PD (Fuxe et al., 2003). The role of $A_{2A}R$ antagonists has been evaluated in several rodent PD models, in which it dose-dependently increases motor activity, when combined with L-DOPA and D_2R agonists at sub-threshold doses; Also, Parkinson-related motor symptoms have been consistently treated in rodents and non-human primates following administration of $A_{2A}R$ antagonists (Ferré and Fuxe, 1992; Tanganelli et al., 2004; Schwarzschild et al., 2006; Fuxe et al., 2007). Fuxe et al. (2010) hypothesize that $A_{2A}R$ antagonists, targeting $A_{2A}R$- D_2R heteromers, increase D_2R signaling. The administration of these antagonists should not have an effect on the expression of heteromers, as they have been found to be constitutive (Canals et al., 2003) and, therefore, present in the absence of their agonists. In the context of PD treatment, the enhancement of $A_{2A}R$ - D_2R heteromers internalization induced by L-DOPA administration causes a compensatory up-regulation of $A_{2A}R$ homomers (Fuxe et al., 2010), which induces an increase in protein phosphorylation including ion channels. This mechanism could eventually stabilize pathological receptors mosaics that tend to form within the transcriptional signaling induced by D_2R excessive activation caused by L-DOPA treatment (Ciruela et al., 2004; Woods et al., 2005). This complex reaction-chain leads, in the end, to an impaired firing pattern in the striato-pallidal GABA pathways which is responsible for dyskinesias (Fuxe et al., 2010). To date Istradefylline is the only approved $A_{2A}R$ antagonist drug. This drug, when combined with L-DOPA or D_2R agonists has been proved by several randomized placebo controlled studies to reduce the off-time and improve motor symptoms, while a worsening in L-dopa long-term treatment-induced dyskinesia has been evidenced, although publication bias does not allow to affirm it with certainty (Sako et al., 2017). Intriguing results have been shown by Collins-Praino et al. (2013), who studied the effect of Deep Brain Stimulation (DBS) in a rodent model of Parkinson's disease which presented dopamine antagonists-induced tremor jaw movements (TJM). DBS induced a significant reduction of TJM, and its effect was dependent on the frequency and intensity of the stimulation. An interesting result was evidenced in a group of rats to which an $A_{2A}R$ antagonist drug (MSX-3) was administered along with DBS. $A_{2A}R$ antagonist treatment enhanced the tremorolytic effect of DBS, allowing to obtain the same clinical results with a lower intensity and frequency of stimulation. Previous studies already proved the synergistic effect of L-DOPA treatment on DBS (Bejjani et al., 2000), but $A_{2A}R$ antagonists may constitute a complementary strategy to prevent levodopa-induced motor complications (Collins-Praino et al., 2013).

Conclusion

Our study describes for the first time the topography and the distribution of A_{2A} adenosine and D_2 dopamine receptors in the human STh. Our findings indicate a peculiar distribution of these receptors throughout the STh, with dopamine D_2R presenting a more diffuse distribution with a decreasing ventral to dorsal gradient, and $A_{2A}R$ presenting a more mild distribution with a distinct dorsal to ventral decreasing gradient. The identification of colocalizations between A_{2A} adenosine and D_2 dopamine receptors in the medial and dorsal STh suggests the presence of receptor-receptor interactions in the form of $A_{2A}R$ -D_2R heteromers.

Data availability statement

The raw data supporting the conclusions of this article will be made available by the authors, without undue reservation.

Ethics statement

Ethical review and approval was not required for the study on human participants in accordance with the local legislation and institutional requirements. The patients/participants provided their written informed consent to participate in this study.

Author contributions

AA, AP, and AE designed the study. RD, AP, and AE sampled the brains. AE and MS performed immunohistochemical staining and the morphometrical evaluation. AE performed the statistical analyses and drafted the figures. AE, AP, DG, AA, and MS drafted the manuscript. All authors reviewed and approved the final version of the manuscript.

Conflict of interest

The authors declare that the research was conducted in the absence of any commercial or financial relationships that could be construed as a potential conflict of interest.

The handling editor declared a past collaboration with the authors, VM, RD, and AP.

Publisher's note

All claims expressed in this article are solely those of the authors and do not necessarily represent those of their affiliated organizations, or those of the publisher, the editors and the reviewers. Any product that may be evaluated in this article, or claim that may be made by its manufacturer, is not guaranteed or endorsed by the publisher.

Supplementary material

The Supplementary Material for this article can be found online at: https://www.frontiersin.org/articles/10.3389/fnins.2022.945574/full#supplementary-material

SUPPLEMENTARY FIGURE 1
Tyrosine hydroxylase (TH) (green) immunofluorescent staining of the subthalamic district reveals a distinct TH+ bundle of axon coursing ventrally to the STh.

References

Alkemade, A., de Hollander, G., Miletic, S., Keuken, M. C., Balesar, R., de Boer, O., et al. (2019). The functional microscopic neuroanatomy of the human subthalamic nucleus. *Brain Struct. Funct.* 224, 3213–3227. doi: 10.1007/s00429-019-01960-1963

Alkemade, A., Schnitzler, A., and Forstmann, B. U. (2015). Topographic organization of the human and non-human primate subthalamic nucleus. *Brain Struct. Funct.* 220, 3075–3086.

Augood, S. J., Hollingsworth, Z. R., Standaert, D. G., Emson, P. C., and Penney, J. B. (2000). Localization of dopaminergic markers in the human subthalamic nucleus. *J. Comp. Neurol.* 421, 247–255.

Bejjani, B. P., Gervais, D., Arnulf, I., Papadopoulos, S., Demeret, S., Bonnet, A. M., et al. (2000). Axial parkinsonian symptoms can be improved: the role of levodopa and bilateral subthalamic stimulation. *J. Neurol. Neurosurg. Psychiatry* 68, 595–600. doi: 10.1136/jnnp.68.5.595

Canals, M., Marcellino, D., Fanelli, F., Ciruela, F., de Benedetti, P., Goldberg, S. R., et al. (2003). Adenosine A2A-Dopamine D2 receptor-receptor heteromerization. *J. Biol. Chem.* 278, 46741–46749. doi: 10.1074/jbc.m306451200

Ciruela, F., Burgueño, J., Casadó, V., Canals, M., Marcellino, D., Goldberg, S. R., et al. (2004). Combining mass spectrometry and pull-down techniques for the study of receptor heteromerization. direct epitope-epitope electrostatic interactions between adenosine A2A and dopamine D2 receptors. *Anal. Chem.* 76, 5354–5363. doi: 10.1021/ac049295f

Collins-Praino, L. E., Paul, N. E., Ledgard, F., Podurgiel, S. J., Kovner, R., Baqi, Y., et al. (2013). Deep brain stimulation of the subthalamic nucleus reverses oral tremor in pharmacological models of parkinsonism: interaction with the effects of adenosine A2A antagonism. *Eur. J. Neurosci.* 38, 2183–2191. doi: 10.1111/ejn.12212

Dawson, T. M., Gehlert, D. R., McCabe, R. T., Barnett, A., and Wamsley, J. K. (1986). D-1 dopamine receptors in the rat brain: a quantitative autoradiographic analysis. *J. Neurosci.* 6, 2352–2365. doi: 10.1523/JNEUROSCI.06-08-02352.1986

Dubois, A., Savasta, M., Curet, O., and Scatton, B. (1986). Autoradiographic distribution of the D1 agonist [3H]SKF 38393, in the rat brain and spinal cord. comparison with the distribution of D2 dopamine receptors. *Neuroscience* 19, 125–137. doi: 10.1016/0306-4522(86)90010-90012

Emmi, A., Antonini, A., Macchi, V., Porzionato, A., and De Caro, R. (2020). Anatomy and connectivity of the subthalamic nucleus in humans and non-human primates. *Front. Neuroanatomy* 14:13. doi: 10.3389/fnana.2020.00013

Emmi, A., Macchi, V., Porzionato, A., Brenner, E., and De Caro, R. (2021a). The academic career of max clara in padova. *Ann. Anatomy - Anatomischer Anzeiger* 236:151697. doi: 10.1016/j.aanat.2021.151697

Emmi, A., Porzionato, A., Contran, M., De Rose, E., Macchi, V., and De Caro, R. (2021b). 3D reconstruction of the morpho-functional topography of the human vagal trigone. *Front. Neuroanatomy* 15:663399. doi: 10.3389/fnana.2021.663399

Emmi, A., Rizzo, S., Barzon, L., Sandre, M., Carturan, E., Sinigaglia, A., et al. (2022a). COVID-19 neuropathology: evidence for SARS-CoV-2 invasion of human brainstem nuclei. *bioRxiv [preprint]* doi: 10.1101/2022.06.29.498117

Emmi, A., Stocco, E., Boscolo-Berto, R., Contran, M., Belluzzi, E., Favero, M., et al. (2022b). Infrapatellar fat pad-synovial membrane anatomo-fuctional unit: microscopic basis for Piezo1/2 mechanosensors involvement in osteoarthritis pain. *Front. Cell Dev. Biol.* 10:886604. doi: 10.3389/fcell.2022.886604

Fernández-Dueñas, V., Gómez-Soler, M., Valle-León, M., Watanabe, M., Ferrer, I., and Ciruela, F. (2019). Revealing adenosine A(2A)-Dopamine D(2) receptor heteromers in Parkinson's disease post-mortem brain through a new alphascreen-based assay. *Int. J. Mol. Sci.* 20:3600. doi: 10.3390/ijms20143600

Ferré, S., and Fuxe, K. (1992). Dopamine denervation leads to an increase in the intramembrane interaction between adenosine A2 and dopamine D2 receptors in the neostriatum. *Brain Res.* 594, 124–130. doi: 10.1016/0006-8993(92)91036-e

Ferré, S., Fuxe, K., Fredholm, B. B., Morelli, M., and Popoli, P. (1997). Adenosine-dopamine receptor-receptor interactions as an integrative mechanism in the basal ganglia. *Trends Neurosci.* 20, 482–487.

Fremeau, R. T. Jr., Duncan, G. E., Fornaretto, M. G., Dearry, A., Gingrich, J. A., et al. (1991). Localization of D1 dopamine receptor mRNA in brain supports a role in cognitive, affective, and neuroendocrine aspects of dopaminergic

neurotransmission. *Proc. Natl. Acad. Sci. U S A.* 88, 3772–3776. doi: 10.1073/pnas.88.9.3772

Fuxe, K., Agnati, L. F., Jacobsen, K., Hillion, J., Canals, M., Torvinen, M., et al. (2003). Receptor heteromerization in adenosine A2A receptor signaling: relevance for striatal function and Parkinson's disease. *Neurology* 61(Suppl. 6), S19–S23. doi: 10.1212/01.wnl.0000095206.44418.5c

Fuxe, K., Marcellino, D., Borroto-Escuela, D. O., Guescini, M., Fernández-Dueñas, V., Tanganelli, S., et al. (2010). Adenosine-dopamine interactions in the pathophysiology and treatment of CNS disorders. *CNS Neurosci. Therapeutics* 16, e18–e42. doi: 10.1111/j.1755-5949.2009.00126.x

Fuxe, K., Marcellino, D., Genedani, S., and Agnati, L. (2007). Adenosine A(2A) receptors, dopamine D(2) receptors and their interactions in Parkinson's disease. *Mov. Disord.* 22, 1990–2017. doi: 10.1002/mds.21440

Galvan, A., Hu, X., Rommelfanger, K. S., Pare, J.-F., Khan, Z. U., Smith, Y., et al. (2014). Localization and function of dopamine receptors in the subthalamic nucleus of normal and parkinsonian monkeys. *J. Neurophysiol.* 112, 467–479. doi: 10.1152/jn.00849.2013

Guidolin, D., Marcoli, M., Tortorella, C., Maura, G., and Agnati, L. F. (2020). Adenosine A(2A)-dopamine D(2) receptor-receptor interaction in neurons and astrocytes: evidence and perspectives. *Prog. Mol. Biol. Transl. Sci.* 169, 247–277. doi: 10.1016/bs.pmbts.2019.11.004

Hedreen, J. C. (1999). Tyrosine hydroxylase-immunoreactive elements in the human globus pallidus and subthalamic nucleus. *J. Comp. Neurol.* 409, 400–410. doi: 10.1002/(sici)1096-9861(19990705)409:3<400::aid-cne5>3.0.co;2-4

Hurd, Y. L., Suzuki, M., and Sedvall, G. C. (2001). D1 and D2 dopamine receptor mRNA expression in whole hemisphere sections of the human brain. *J. Chem. Neuroanat.* 22, 127–137. doi: 10.1016/s0891-0618(01)00122-123

Johnson, A. E., Coirini, H., Källström, L., and Wiesel, F.-A. (1994). Characterization of dopamine receptor binding sites in the subthalamic nucleus. *NeuroReport* 5, 1836–1838. doi: 10.1097/00001756-199409080-199409038

Lévesque, J.-C., and Parent, A. (2005). GABAergic interneurons in human subthalamic nucleus. *Mov. Disord.* 20, 574–584. doi: 10.1002/mds.20374

Mansour, A., Meador-Woodruff, J. H., Zhou, Q., Civelli, O., Akil, H., and Watson, S. J. (1992). A comparison of D1 receptor binding and mRNA in rat brain using receptor autoradiographic and in situ hybridization techniques. *Neuroscience* 46, 959–971. doi: 10.1016/0306-4522(92)90197-a

Matsumoto, M., Hidaka, K., Tada, S., Tasaki, Y., and Yamaguchi, T. (2002). Low levels of mRNA for dopamine D4 receptor in human cerebral cortex and striatum. *J. Neurochem.* 66, 915–919. doi: 10.1046/j.1471-4159.1996.66030915.x

Misgeld, U., Drew, G., and Yanovsky, Y. (2007). Presynaptic modulation of GABA release in the basal ganglia. *Prog. Brain Res.* 160, 245–259. doi: 10.1016/s0079-6123(06)60014-60019

Narváez, M., Crespo-Ramírez, M., Fores-Pons, R., Pita-Rodríguez, M., Ciruela, F., Filip, M., et al. (2021). "Study of GPCR homo- and heteroreceptor complexes in specific neuronal cell populations using the in situ proximity ligation assay," in *Receptor and Ion Channel Detection in the Brain*, eds R. Lujan and F. Ciruela (New York, NY: Springer US), 117–134.

Pelassa, S., Guidolin, D., Venturini, A., Averna, M., Frumento, G., Campanini, L., et al. (2019). A2A-D2 heteromers on striatal astrocytes: biochemical and biophysical evidence. *Int. J. Mol. Sci.* 20:2457. doi: 10.3390/ijms20102457

Porzionato, A., Emmi, A., Contran, M., Stocco, E., Riccetti, S., Sinigaglia, A., et al. (2021a). Case report: the carotid body in COVID-19: histopathological and virological analyses of an autopsy case series. *Front. Immunol.* 12:736529. doi: 10.3389/fimmu.2021.736529

Porzionato, A., Pelletti, G., Barzon, L., Contran, M., Emmi, A., Arminio, A., et al. (2021b). Intravascular large B-cell lymphoma affecting multiple cranial nerves: a histopathological study. *Neuropathology* 41, 396–405. doi: 10.1111/neup.12767

Porzionato, A., Guidolin, D., Emmi, A., Boscolo-Berto, R., Sarasin, G., Rambaldo, A., et al. (2020). High-quality digital 3D reconstruction of microscopic findings in forensic pathology: the terminal pathway of a heart stab wound*. *J. Forensic Sci.* 65, 2155–2159. doi: 10.1111/1556-4029.14497

Porzionato, A., Macchi, V., Stecco, C., Mazzi, A., Rambaldo, A., Sarasin, G., et al. (2012). Quality management of body donation program at the university of padova. *Anat. Sci. Educ.* 5, 264–272. doi: 10.1002/ase.1285

Sako, W., Murakami, N., Motohama, K., Izumi, Y., and Kaji, R. (2017). The effect of istradefylline for Parkinson's disease: a meta-analysis. *Sci. Rep.* 7:18018. doi: 10.1038/s41598-017-18339-18331

Savasta, M., Dubois, A., and Scatton, B. (1986). Autoradiographic localization of D1 dopamine receptors in the rat brain with [3H]SCH 23390. *Brain Res.* 375, 291–301. doi: 10.1016/0006-8993(86)90749-90743

Schiffmann, S. N., Fisone, G., Moresco, R., Cunha, R. A., and Ferré, S. (2007). Adenosine A2A receptors and basal ganglia physiology. *Prog. Neurobiol.* 83, 277–292. doi: 10.1016/j.pneurobio.2007.05.001

Schwarzschild, M. A., Agnati, L., Fuxe, K., Chen, J.-F., and Morelli, M. (2006). Targeting adenosine A2A receptors in Parkinson's disease. *Trends Neurosci.* 29, 647–654. doi: 10.1016/j.tins.2006.09.004

Tanganelli, S., Sandager Nielsen, K., Ferraro, L., Antonelli, T., Kehr, J., Franco, R., et al. (2004). Striatal plasticity at the network level. focus on adenosine A2A and D2 interactions in models of Parkinson's disease. *Parkinsonism Related Disorders* 10, 273–280. doi: 10.1016/j.parkreldis.2004.02.015

Wang, G. J., Volkow, N. D., Logan, J., Pappas, N. R., Wong, C. T., Zhu, W., et al. (2001). Brain dopamine and obesity. *Lancet* 357, 354–357. doi: 10.1016/s0140-6736(00)03643-3646

Woods, A. S., Ciruela, F., Fuxe, K., Agnati, L. F., Lluis, C., Franco, R., et al. (2005). Role of electrostatic interaction in receptor-receptor heteromerization. *J. Mol. Neurosci.* 26, 125–132.